Investigation of signalling involved in maintaining the mutually beneficial association between *Epichloë festucae* and perennial ryegrass

A thesis presented in partial fulfilment of the requirements for the degree of

Doctor of Philosophy
in
Genetics

at Massey University, Palmerston North,
New Zealand.

Carla Jane Eaton

2009

Abstract

In the mutually beneficial association between the fungal endophyte *Epichloë festucae* and perennial ryegrass, fungal growth is highly regulated and coordinated with that of the host. This implies there must be signalling between the fungus and its host to maintain this close association. Recent work has shown a novel role for reactive oxygen species (ROS) in this symbiotic maintenance, with multiple components of the superoxide-producing NADPH oxidase (Nox) complex being essential for normal association. However, the mechanism by which the Nox complex is regulated is unclear.

To identify potential regulators of the *E. festucae* Nox complex, comparisons were made with well-characterised mammalian systems. This search identified three candidate regulators: a stress activated MAP kinase, *sakA*, and the p21-activated kinases, *pakA* and *pakB*. To investigate if these genes were involved in symbiotic maintenance, replacement mutants were generated by homologous recombination. In culture analysis revealed that the Δ*sakA* mutant was hypersensitive to a range of stresses, whereas the pak mutants were hypersensitive to cell wall stress-inducing agents and displayed altered growth and morphology. Examination of perennial ryegrass infected with these mutants revealed drastically altered plant interaction phenotypes for the Δ*sakA* and Δ*pakA* mutants in comparison to the wild-type strain. Δ*sakA*-infected plants were stunted and displayed striking changes in development, with the base of tillers showing loss of anthocyanin pigmentation and disorganisation of host cells below the meristem, resulting in swollen bases. Plants infected with the Δ*pakA* mutant were severely stunted, had no more than two tillers and senesced soon after planting. In contrast, plants infected with the Δ*pakB* mutant were similar to wild-type, with only slight deregulation of growth *in planta*.

Examination of ROS in culture revealed that Δ*sakA* and Δ*pakA* displayed elevated levels of both superoxide and hydrogen peroxide. ROS levels were also elevated around Δ*sakA* hyphae *in planta*. These results support roles for SakA and PakA in Nox regulation. This work highlights the fine balance between mutualism and antagonism, and provides insight into the molecular basis for mutualism.

Acknowledgments

Firstly, I must thank Barry Scott for his excellent supervision. You really were the best supervisor someone undertaking the trials and tribulations of a PhD could ask for. Thank you for your guidance and patience through the good times and the bad times. Your faith in me kept me going during the times when it felt like nothing was working and I questioned whether I could ever finish. To my co-supervisor Jerry Hyams, thanks for your expert guidance with the *S. pombe* work and for your humour, which was like a breath of fresh air during the trying times of this PhD.

Thanks to the New Zealand Tertiary Education Commission for funding this project through a Top Achievers Doctoral Scholarship, and to the Lincoln Bioprotection CoRE for additional funding. Thanks to Chris Schardl for provision of *E. festucae* 2368 genomic sequence through grant EF-0523661 from the US National Science Foundation.

To Isabelle Jourdain, without your help with the *S. pombe* work and *E. festucae* microscopy much of the results presented in this thesis could not have been achieved. I have valued your help, advice and most importantly your friendship. You were a listening ear when I needed to vent my problems and most of the time could even offer a solution. Without your support all this would not have been possible.

Thanks to all past and present members of the Scottbase lab, you all helped me in so many ways. Special thanks to Michelle Bryant for your support, advice and friendship, especially at the start of my PhD; to Matt Nicholson, for answering my endless questions and helping to 'problem-solve' when things just did not seem to work. Thanks also to Yvonne Rolke for your advice and support, especially during the writing phase, and to Matthias Becker for helping dissect meristems and for the top quality SEM images. To Aiko, Daigo, Sanjay, Kim and Sarah for helpful advice and suggestions. A big thanks to Milena Mitic, Emma Brasell, Gemma Cartwright and Ruth Wrenn for your great friendship throughout my PhD and for helping me to smile during the tough times.

Many thanks to everyone at AgResearch who helped me during this project, especially Mike Christensen for advice and help with analysing the *in planta* phenotypes, Anouck

de Bonth for developing my many immunoblots during the arduous infection experiments, and Wayne Simpson for together with Anouck taking good care of my plants. Thanks to everyone at the Manawatu Microscopy and Imaging Centre, particularly Doug Hopcroft for your top quality sample preparation and advice to help me get the best images possible. Thanks also to Barbara Ambrose for advice and help with plant tissue preparation, sectioning and staining.

Special thanks are due to Ann Truter and Cynthia Cresswell. You two are like the guardian angels of IMBS and I'm sure without you things would fall to pieces – I know I would have, especially during poster printing times! Thanks for all your help with so many things throughout my PhD.

A big thank-you to John O'Sullivan for your support and help during the writing of this thesis. I will forever be grateful to you for introducing me to the wonder of biology all those long years ago. The phrase 'a good teacher makes all the difference' could not be any truer. Your passion for biology inspired me - who knew it would lead me to this point.

Lastly, my deepest thanks must go to my family. Mum, without your support and love none of this would have been possible. Thank you for enduring many hours as an audience for me to practice my presentations to, and for all your advice on the layout and design of presentations and posters. Thanks to my sister and sister-in-law Debbie and Anne-Marie for enduring many "practice presentations" even though you probably have no real interest in grass, fungus or any of those other things I rambled on about. Debbie, your faith in me being able to achieve whatever I set my mind to has meant more to me than you realise. To my brother Shane – thanks for bringing me back to earth when my head gets lost in the world of science! To my nephews and nieces James, Caleb, Tyler, Cassandra, Bailey, Riley and Maia. You have kept me anchored in reality by being able to brighten my mood even on those days when nothing seemed to be going right, and loving me whether or not my experiments were working. Tyler, thank you for always being interested in my work, and for listening to my presentations and asking some pretty good questions – I may make a scientist out of you yet! Dad and Sherree, I love you and miss you and wish you could be here to share this moment with me, but I know you would have been proud.

Table of contents

Abbreviations

A	Adenine
AD	Activation domain
Ade	Adenine
Amp	Ampicillin
Amp^R	Ampicillin resistant
ABC	ATP-binding cassette
ANS	Anthocyanin synthase
ASS	Active site signature
ATP	Adenine triphosphate
BD	Binding domain
BLAST	Basic local alignment search tool
BLASTn	Nucleotide database search using a nucleotide query
BLASTp	Protein database search using a protein query
BLASTx	Protein database search using a translated nucleotide query
bp	Base pair(s)
BSA	Bovine serum albumin
˚C	Degrees celsius
CCD	Charged couple device
cDNA	Complementary DNA
CDS	Coding sequence
CFW	Calcofluor white
Cgfp	C-terminal green fluorescent protein tag
CHM	Cla4-homologue *Magnaporthe*
CHS	Chalcone synthase
CIAP	Calf intestinal alkaline phosphatase
Comp	Complemented
CRIB	Cdc42/Rac interactive binding
cv	Cultivar
DAB	3-3'Diaminobenzidine
DAG	Diacylglycerol
DAPI	4',6-diamidino-2-phenylindole

dATP	Deoxyadenine triphosphate
DBD	DND binding domain
dCTP	Deoxycytosine triphosphate
DIC	Differential interference contrast
DEPC	Diethylpyrocarbonate
DMSO	Dimethyl sulfoxide
DNA	Deoxyribose nucleic acid
dNTP	Deoxynucleotide triphosphate
DSPTP	Dual specificity protein tyrosine phosphatase
Ec	Ectopic
EC	Enzyme commission
ECM	Extracellular matrix
EDTA	Ethylene diamine tetra-acetic acid
EGFP	Enhanced green fluorescent protein
EGTA	Ethylene glycol tetraacetic acid
EMM	Edinburgh minimal medium
FAA	Formaldehyde acetic acid
FAD	Flavin adenine dinucleotide
Fg	*Fusarium graminearum*
FGI	Fungal Genome Initiative
Flu	Fludioxonil
g	Gram
GAP	GTPase-activating protein
GDI	Guanine dissociation inhibitor
gDNA	Genomic DNA
GDP	Guanosine Diphosphate
GEF	Guanine nucleotide-exchange factor
Gen^R	Geneticin resistant
GFP	Green fluorescent protein
GO	Gene ontology
GST	Glutathione S-transferase
GTP	Guanosine triphosphate
h	Hour(s)
H	Histidine

H_2O_2	hydrogen peroxide
HA	Hemagglutinin
HCT	Hydroxycinnamoyl transferase
Hepes	4-2-hydroxyethyl-1-piperazineethanesulfonic acid
His	Histidine
HOG	High osmolarity glycerol
Hph	Hygromycin phosphotransferase
HRP	Horse-radish peroxidase
Hyg^R	Hygromycin resistant
IAA	Indole-3-acetic acid
ID	Identity
IDA	Inferred direct assay
IDI	Inferred direct interaction
IGI	Inferred genetic interaction
IMP	Inferred mutant phenotype
iNOS	Inducible nitric oxide synthase
IPTG	Isopropyl α-D-1-thiogalactopyranoside
IS	Intercellular space(s)
kb	Kilobases
KIND	Kinase non-catalytic C-lobe domain
KO	Knock-out
LB	Luria-Bertaini broth
L	Leucine
Leu	Leucine
Lys	Lysine
M	Molar
MAP	Mitogen activated protein
MAPK	Mitogen activated protein kinase
MAPKK	Mitogen activated protein kinase kinase
MFS	Major facilitator superfamily
min	Minute(s)
μg	Micro-gram
mg	Milli-gram
Mg	*Magnaporthe grisea*

µL	Micro-litre
mL	Milli-litre
µM	Micro-molar
mM	Milli-molar
mm	Milli-metre
MOPS	3-(N-morpholino)-propanesulfonic acid
mRNA	Messenger ribonucleic acid
MSO	Murashige and Skoog medium
MST	*Magnaporthe* Ste20
NA	Numerical aperture
NADH	Nicotinamide adenine dinucleotide (reduced form)
NADPH	Nicotinamide adenine dinucleotide phosphate (reduced form)
NBT	Nitroblue tetrazolium
Nc	*Neurospora crassa*
NCBI	National centre for biotechnology information
NEB	New England Biolabs
ng	Nano-gram
Nh	*Nectria haematococca*
nmt	No message in thiamine
NO	Nitric oxide
Nox	NADPH oxidase
Npt	Neomycin Phosphotransferase
OD	Optical density
P	Plant cell
pak	p21-activated kinase
PASS	Phosphatase active site signature
PBD	p21-Rho binding domain
PCR	Polymerase chain reaction
pcw	Plant cell wall
PD	Potato dextrose
PEG	Polyethylene glycol
PH	Pleckstrin homology
Phox	Phagocyte oxidase
PKC	Protein kinase C

pmol	Picomole
PMSF	Phenylmethylsulphonyl fluoride
PTP	Protein tyrosine phosphatase
PVP	Polyvinylpyrolidone
PX	Phox homology
RA	Ras-associating
RCA	Reviewed computational analysis
RG	Regeneration
RNA	Ribonucleic acid
RNase	Ribonuclease
RO	Reverse osmosis
ROS	Reactive oxygen species
rpm	Revolutions per minute
RT	Room temperature
RT	Reverse transcriptase
RT-PCR	Reverse transcriptase-polymerase chain reaction
Sak	Stress-activated kinase
SAM	Sterile α motif
SD	Synthetic dropout
SDS	Sodium dodecyl sulphate
SE	Standard error
SEM	Scanning electron microscopy
Ser	Serine
SH	Src homology
SLS	Sodium lauroyl sarcosine
SOD	Superoxide dismutase
Sorb	Sorbitol
SSC	Sodium-sodium citrate
Sty	Suppressor of tyrosine phosphatase
T	Thiamine
TAS	Traceable author statement
TAT	Tubulin antibody
TBE	Tris-boric acid-EDTA
tBLASTn	Translated nucleotide database search using a protein query

tBLASTx	Translated nucleotide database search using translated nucleotide query
TEM	Transmission electron microscopy
Thi	Thiamine
Tr	*Trichoderma reesei*
tRNA	Transfer RNA
Trp	Tryptophan
Tub	Tubulin
Ura	Uracil
UTR	Untranslated region
UV	Ultra-violet
v	Vacuole
V	Volts
v/v	Volume/volume ratio
WT	Wild-type
w/v	Weight/volume ratio
X-gal	5-bromo-4-chloro-3-indolyl-β-D-galactopyranoside
YE	Yeast extract
YPAD	Yeast extract-peptone-adenine-dextrose

List of figures

List of tables

1. Introduction

1.1. Plant-microbe associations

In order to survive the variety of harsh environmental conditions they are faced with, many plants have developed the ability to form beneficial associations or symbioses with microbes, which provides these plants with ecological advantage. Perhaps the best described example of this is the rhizobia-legume association, in which bacteria of the genus *Rhizobium* associate with the roots of leguminous plants, forming nitrogen-fixing nodules that provide the host with access to otherwise unutilisable nitrogen (Cooper, 2007). Another example is found between mycorrhizal fungi and the roots of a variety of plant species, in which the fungus greatly increases the supply of water and nutrients to the host, and in return is provided with plant-fixed carbon (Parniske, 2008). However, not all associations between plants and microbes are beneficial. Indeed, symbioses span a broad continuum from mutualism to antagonism. In mutualistic or mutually beneficial associations, such as those described above, both host and symbiont benefit from the association. In contrast, in antagonistic associations one partner, usually the symbiont, benefits at a cost to the other partner, in many cases resulting in its eventual death.

1.2. Plant-fungal associations

The associations between plants and fungi are particularly well documented, with some of the best-known fungal symbionts being major pathogens of crop plants. Fungal pathogens are classified as biotrophs, hemibiotrophs or necrotrophs, depending on whether they grow on living or dead tissue. Biotrophs grow exclusively on living tissues, so have evolved strategies to avoid inducing death of their host. Hemibiotrophs, in comparison, grow on living tissue but will continue to grow once the host tissue has died. In contrast, necrotrophs employ a variety of enzymes and toxins to induce host death so they can grow on the dead tissue. One example of a biotroph is the corn smut fungus, *Ustilago maydis*. This dimorphic fungus can grow as yeast-like and filamentous forms, with infection exclusively caused by the filamentous form (Morrow and Fraser, 2009). The rice blast fungus *Magnaporthe oryzae* displays a hemibiotrophic lifestyle,

characterised by a long biotrophic phase followed, late in infection, by a switch to necrotrophic growth (Wilson and Talbot, 2009). The importance of this pathogen is highlighted by the fact that between 2001-2005 it was responsible for the loss of 5.7 million hectares of rice in China (Wilson and Talbot, 2009). The necrotroph *Botrytis cinerea* is the causal agent of grey mould disease across a broad range of hosts. *B. cinerea* induces death of its host by a combination of toxins, production of reactive oxygen species (ROS) and through induction of the host's own oxidative burst defense response (Choquer et al., 2007).

1.3. Endophyte associations with cool-season grasses

Perhaps one of the most agriculturally important mutualistic plant-fungal associations is that formed between endophytes of the *Epichloë* and *Neotyphodium* species (family *Clavicipitaceae*) and cool season grasses (family *Poaceae*). These associations have a long history, exemplified by their co-divergence (Schardl et al., 2008).

1.3.1. Endophyte diversity and lifecycle

Epichloë endophytes are taxonomically classified as two main groups based on the means by which they reproduce (Fig. 1.1). Endophytes of the genus *Epichloë* are able to reproduce both sexually and asexually. In comparison, those of the genus *Neotyphodium* are strictly asexual (Glenn et al., 1996). In the asexual lifecycle, the host remains asymptomatic and the fungus is transmitted vertically via the colonisation of host seeds. The sexual lifecycle of some *Epichloë* species is induced in response to the start of host flowering, causing these fungi to deviate from their mutualistic lifecycle and become antagonistic. Hyphae start to proliferate over the surface of the leaves surrounding the host inflorescence, forming a stroma that prevents opening of the inflorescence, a phenomenon known as 'choke' (Schardl et al., 2004). The sexual cycle then initiates on the stroma, facilitated by *Botanophila* flies, which transfer spermatia between the two mating types (Bultman et al., 1995). The stromata then mature and eject their ascospores, resulting in horizontal transmission when the ejected ascospores land and

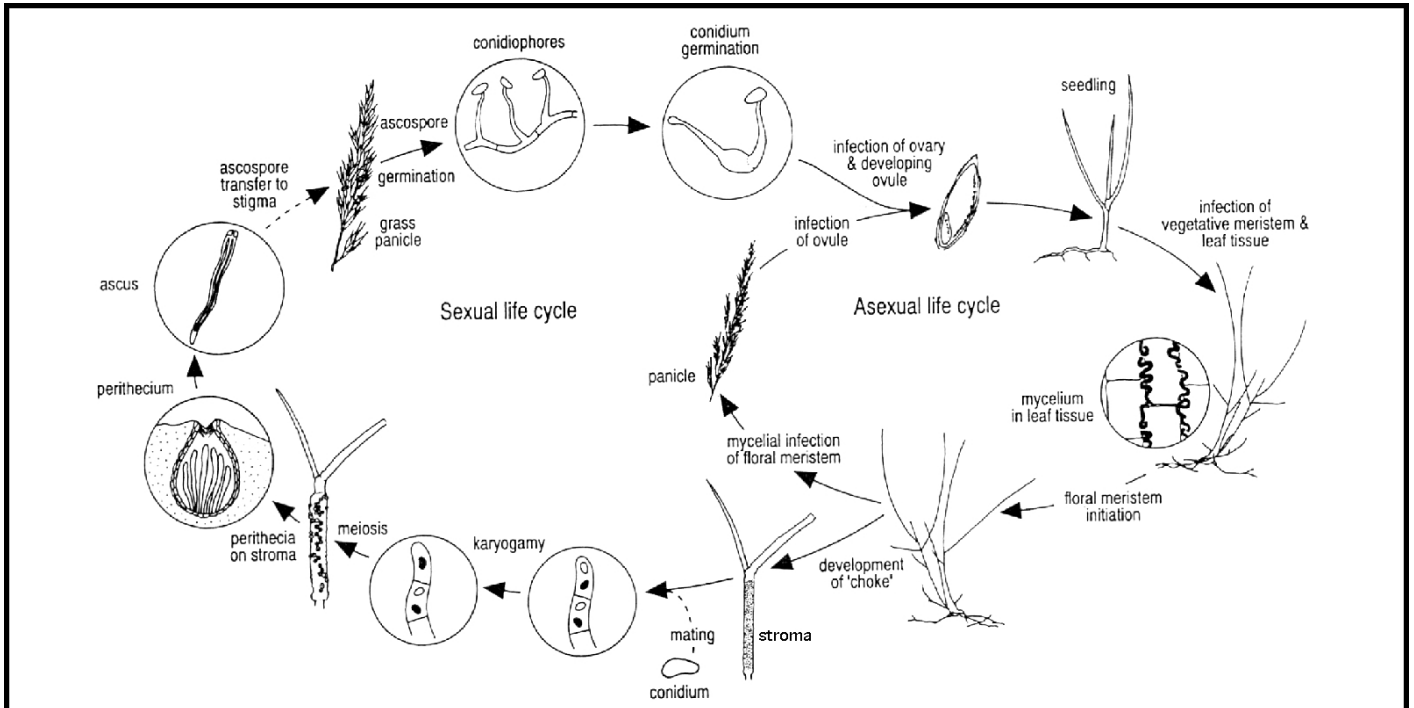

Figure 1.1 Life-cycle of endophyte-grass associations
Schematic representation of the life-cycle of *Epichloë* and *Neotyphodium* endophytes within their host grass. *Epichloë* species show both asexual and sexual life-cycles, whereas *Neotyphodium* species are strictly asexual. In the asexual life-cycle, hyphae are vertically transmitted via colonisation of host seed, and the host remains asymptomatic. In the sexual life-cycle, the onset of host flowering induces the endophyte to ramify over the developing inflorescence, forming a stroma that prevents the inflorescence opening - a phenomenon known as 'choke'. Hyphae are horizontally transmitted via a three organism-interaction where spermatia produced by the endophyte on the surface of the stroma are transferred to stroma of opposite mating types by Botanophila flies. Ascospores then develop and mature on the stroma. Ejected ascospores then germinate on the surface of new grass florets, grow into the ovule and colonise the seed. Reproduced from Scott & Schardl (1993). Trends Microbiol. 5:196-200.

germinate on the surface of a grass floret, colonise the ovule and enter the seed (Schardl, 2001).

1.3.2. Benefits of association

Apart from 'choke' displayed by some *Epichloë* species, endophyte-grass associations are generally mutually beneficial. In these associations the fungus is provided with nutrients, protection and a means of reproductive transmission via colonisation of host seeds (Schardl et al., 2004). In return, the fungus enhances the tolerance of the host to a number of biotic and abiotic stresses. Increased tolerance to biotic stresses is mediated by the production of a four classes of toxic alkaloids: indole-diterpenes, ergot alkaloids, lolines and peramine (Schardl, 2001). The most well known indole-diterpene produced by the epichloë endophytes is lolitrem B, a potent mammalian neurotoxin and the causal agent of ryegrass staggers (Gallagher et al., 1984). Production of this toxin requires 10 genes that are highly expressed *in planta* and organised in a complex cluster interspersed with transposon relics (Young et al., 2006). The ergot alkaloids also act as potent mammalian toxins, causing ergot poisoning of grazing livestock (Bacon et al., 1986). Similar to the lolitrem B biosynthetic genes, genes involved in the biosynthesis of the ergot alkaloid ergovaline are also found within a cluster interspersed with transposon relics and are highly expressed *in planta* (Fleetwood et al., 2007). The other two classes of alkaloids, the lolines and peramine, act as insect feeding deterrents (Schardl, 2001). Genes required for biosynthesis of the loline alkaloids are also arranged in a gene cluster (Spiering et al., 2005). In contrast, the *perA* gene, encoding a non-ribosomal peptide synthetase, is both necessary and sufficient for peramine biosynthesis, and greatly enhances resistance to herbivory by the Argentine stem weevil (Tanaka et al., 2005). Endophyte infection also enhances tolerance to abiotic stresses such as drought stress (Arechavaleta et al., 1989; Hahn et al., 2008), and enhances growth on phosphorus-deficient soils (Malinowski and Belesky, 1999).

1.3.3. Endophyte growth *in planta*

Growth of epichloë endophytes *in planta* is highly regulated. Hyphae have never been reported within host cells but rather grow in the host intercellular spaces, aligned parallel to the leaf axis and seldom branching (Christensen et al., 2002). Hyphal growth is also tightly coordinated with that of the host plant as hyphae only grow whilst the leaves grow, and when the leaves stop growing hyphal growth ceases, resulting in similar concentrations of hyphae in both old and young leaves (Tan et al., 1997; Christensen et al., 2002). However, this pattern of growth is inconsistent with the dogma that fungi grow mainly by polarised tip growth (Harris and Momany, 2004). Instead, Christensen et al. (2008) proposed that these epichloë endophytes grow by a novel mechanism – intercalary division and extension. These authors proposed a model in which hyphae initially grow by tip growth in the host shoot apical meristem, forming a highly branched network. From here hyphae enter the developing leaf primordia. The host cells in the leaf primordium then divide and enlarge, causing the hyphae to stretch. To avoid being sheared, hyphae switch to intercalary extension and cell division, keeping pace with the rapid leaf growth of more than 1 cm a day (Christensen et al., 2008). Above the leaf expansion zone, hyphae stop expanding but remain metabolically active (Tan et al., 2001). Hyphal colonisation of the host grass is systemic throughout all aerial tissues of the plant, with higher concentrations of hyphae present in the leaf sheath tissue than in the blade (Christensen et al., 1997). In some associations epiphyllous hyphae are also seen on the surface of infected plant tissues (Christensen et al., 1997; Moy et al., 2000). However, hyphae are seldom found within root tissues and in host vascular bundles (Christensen et al., 1997; Schardl, 2001).

1.3.4. Role of reactive oxygen species in maintenance of association

The highly regulated and coordinated pattern of hyphal growth *in planta* implies there must be signalling between the fungus and its host in order to maintain this intimate, mutualistic association. To investigate the genetic basis of this signalling, Scott et al. (2007) have developed the *Epichloë festucae*-perennial ryegrass (*Lolium perenne*) symbiosis as a model experimental system. This is a good system for studying these endophyte

associations as *E. festucae* is haploid, grows relatively fast in culture compared to other epichloë endophytes, and has much higher rates of homologous recombination than other strains (Scott et al., 2007). In addition, it is relatively easy to inoculate into perennial ryegrass seedlings, with infection rates of 80-90% for the wild-type strain, and forms a stable symbiosis (Scott et al., 2007). Using insertional mutagenesis as a forward genetics approach, Tanaka et al. (2006) generated *E. festucae* mutants, which were screened for any disruption of the mutualistic symbiotic interaction. This resulted in the identification of a mutant that was unable to form a mutualistic association with perennial ryegrass, instead forming an antagonistic association in which the host lost apical dominance, was severely stunted and displayed precocious senescence. Fungal growth *in planta* was also drastically altered, with hyphae appearing hyper-branched and no longer aligned to the leaf axis. In addition, fungal biomass *in planta* was significantly greater than in wild-type associations. This dramatic plant interaction phenotype was caused by disruption of the *noxA* gene, which encodes a key catalytic component of the NADPH oxidase (Nox) complex. The multi-subunit Nox complex is best characterised in mammalian systems where its role in the oxidative burst response of neutrophils to invading pathogens is well established. This complex is comprised of integral membrane proteins and cytosolic regulatory subunits that associate with the membrane bound subunits in response to an activating signal (Sumimoto et al., 2005). The enzymatic function of this complex is to catalyse the conversion of molecular oxygen to the reactive oxygen species superoxide. This is achieved via an NADPH-dependent reaction in which electrons are extracted from intracellular NADPH and transferred via FAD and two haem cofactors to molecular oxygen, generating superoxide on the extra-cellular face of the plasma membrane (Sumimoto et al., 2005). The superoxide anions are then rapidly dismutated into hydrogen peroxide either spontaneously or via superoxide dismutase (SOD) (Bedard and Krause, 2007).

The *E. festucae* genome also contains a second Nox isoform, *noxB*. However, targeted disruption revealed that this gene is not required for normal association with perennial ryegrass (Tanaka et al., 2006). In contrast, targeted disruption of two predicted cytosolic regulatory components, *noxR* and *racA*, resulted in a similarly defective plant interaction phenotype to the *noxA* mutant (Takemoto et al., 2006; Tanaka et al., 2008a).

1.4. Role of NADPH oxidase (Nox) complexes in fungal symbioses

1.4.1. The mammalian Nox complex as a model

As detailed above, the Nox complex is well characterised in mammalian systems. In humans, six unique membrane-bound Nox isoforms have been identified (Lambeth, 2004). *E. festucae* NoxA (and NoxB) appears to be most similar to the Nox2 isoform, also known as gp91phox, the oxidase found in phagocytes. gp91phox contains six transmembrane α helices which anchor it in the membrane, and contain binding sites for FAD, NADPH and two haem groups, which are essential co-factors for the electron transfer reaction (Vignais, 2002). gp91phox is also extensively glycosylated, with more than one third of its mass being carbohydrate (Vignais, 2002). In the membrane, gp91phox associates with p22phox, forming the flavocytochrome b558 complex, the catalytic core for the electron transfer reactions (Groemping and Rittinger, 2005). p22phox is likely involved in recruiting the cytosolic components of the Nox complex via a proline rich region in its C-terminus, and is a target for phosphorylation by a number of protein kinases (Sumimoto et al., 1992; Regier et al., 2000). The gp91phox complex contains four cytosolic regulatory components, three of which are proposed to form a trimeric complex in the cytoplasm under non-activated conditions and are recruited together upon activation (Groemping and Rittinger, 2005). This trimeric regulatory complex consists of p67phox (homologous to *E. festucae* NoxR), p47phox and p40phox. p67phox is referred to as the Nox activator due to the presence of an activation domain, which interacts with gp91phox, aiding in electron transfer (Han et al., 1998). p67phox binds directly to p47phox, p40phox and the additional cytosolic regulatory component Rac1 (homologous to *E. festucae* RacA), and is also a target for phosphorylation by a number of protein kinases (Dang et al., 2003). p47phox is known as the Nox organiser protein as its main role is to facilitate translocation of the trimeric regulatory complex to the membrane and position it correctly with respect to the flavocytochrome b558 complex via interaction with p22phox (Groemping and Rittinger, 2005). p47phox is also the most highly phosphorylated component, and it is thought that the majority of Nox complex regulation is mediated through phosphorylation of this subunit (El Benna et al., 1996). p40phox appears to play a less important role in the Nox complex and is not essential for superoxide production (Abo

et al., 1992). The final cytosolic component is the small GTPase, Rac1, which is essential for superoxide production (Abo et al., 1991). To date only homologues of gp91phox (NoxA and NoxB), p67phox (NoxR) and Rac1 (RacA) have been identified in fungi. The apparent lack of p40phox and p47phox homologues in fungi is consistent with findings of Takemoto et al. (2006), who showed that the domains involved in p40phox and p47phox binding by p67phox are absent in the fungal homologue NoxR. This led Takemoto et al. (2007) to propose a model for the fungal Nox complex, as shown in Figure 1.2.

1.4.2. Roles of the Nox complex in other fungi

Nox genes have been identified in a number of phytopathogenic fungi in which they play essential roles in virulence. In the rice blast fungus, *Magnaporthe grisea*, mutation of *NOX1* (homologous to *E. festucae noxA*), or *NOX2* (homologous to *E. festucae noxB*) results in complete loss of pathogenicity (Egan et al., 2007). These mutants still form appressoria but are unable to penetrate the host cuticle and cause disease. However, Δ*nox1* and Δ*nox1*Δ*nox2* mutants are still unable to cause disease on wounded tissue, suggesting *nox1* is essential for growth *in planta* (Egan et al., 2007). In the ergot fungus *Claviceps purpurea*, Δ*nox1* mutants can penetrate the host surface but are greatly impaired in colonisation (Giesbert et al., 2008). In *B. cinerea* both *noxA* and *noxB* are required for the formation of sclerotia and for normal pathogenicity (Segmüller et al., 2008). Δ*noxA* mutants can penetrate host tissues but show greatly reduced colonisation. In comparison, Δ*noxB* mutants are impaired in the formation of penetration structures. Δ*noxA*Δ*noxB* mutants showed defects in both penetration and colonisation and are almost non-pathogenic. Δ*noxR* mutants appear similar to Δ*noxA*Δ*noxB* mutants, suggesting NoxR activates NoxA and NoxB in *B. cinerea* (Segmüller et al., 2008).

1.4.3. Possible mechanisms of Nox regulation in fungi

Insights for possible regulation of the fungal Nox complex can be gained by considering what is known for mammalian systems. A number of studies have demonstrated a link between the stress-activated MAP kinase p38 and the Nox complex. Indeed, p38

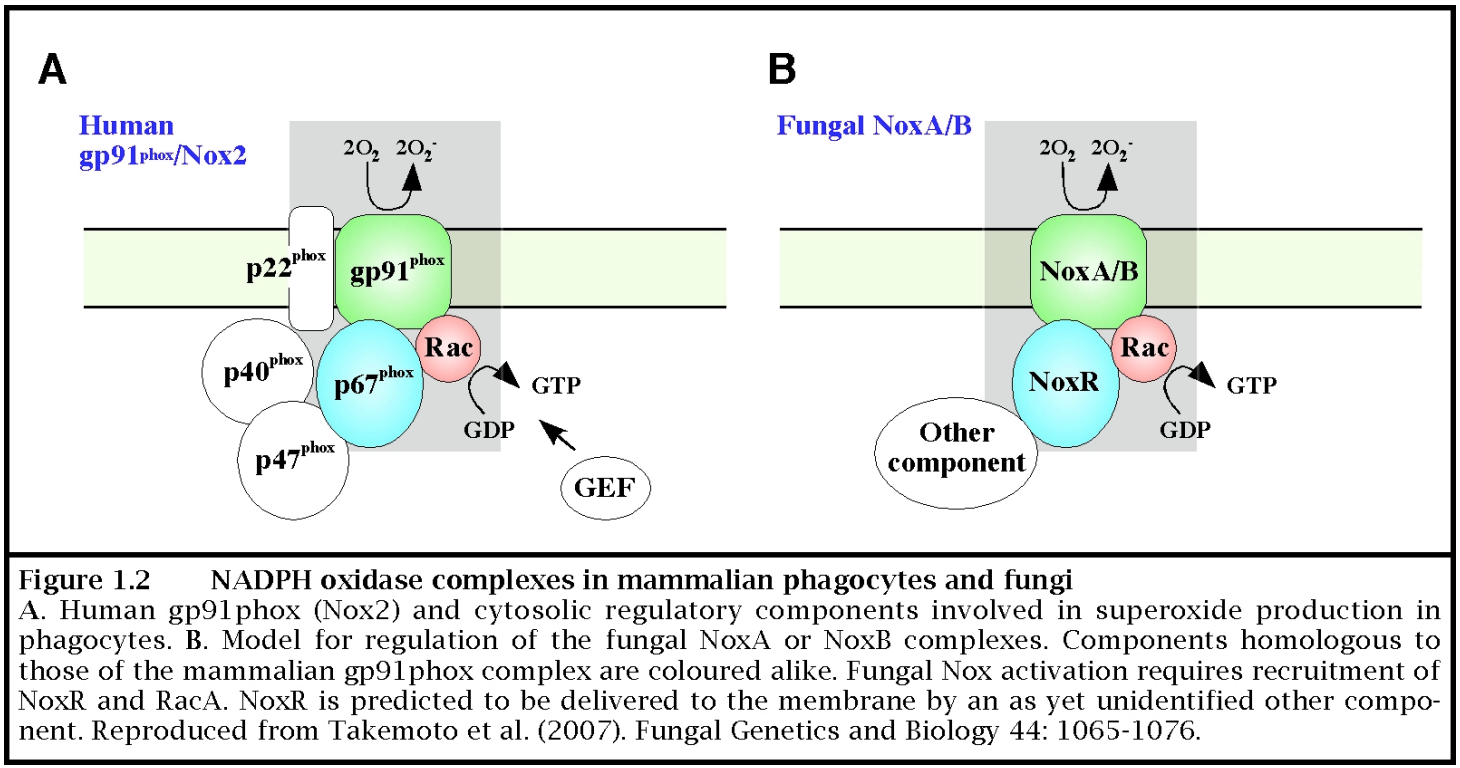

Figure 1.2 NADPH oxidase complexes in mammalian phagocytes and fungi
A. Human gp91phox (Nox2) and cytosolic regulatory components involved in superoxide production in phagocytes. B. Model for regulation of the fungal NoxA or NoxB complexes. Components homologous to those of the mammalian gp91phox complex are coloured alike. Fungal Nox activation requires recruitment of NoxR and RacA. NoxR is predicted to be delivered to the membrane by an as yet unidentified other component. Reproduced from Takemoto et al. (2007). Fungal Genetics and Biology 44: 1065-1076.

MAPK phosphorylates p67phox *in vitro* and *in vivo*, likely triggering a change to an active conformation (Dang et al., 2003). Brown et al. (2004) demonstrated that p38 MAPK is involved in both priming and activation of the mammalian Nox2 complex. p38 MAPK also regulates production of peroxynitrite ($ONOO^-$) by regulating both the Nox complex and the inducible nitric oxide synthase (iNOS) (Yoo et al., 2008). Peroxynitrite is formed by the reaction of nitric oxide (NO) with superoxide ($O_2^{\bullet-}$). Yoo et al. (2008) showed that inhibition of p38 MAPK or use of dominant negative p38 MAPK resulted in decreased peroxynitrite levels due to downregulation of iNOS expression and suppression of Nox activity. These studies all suggest a role for p38 MAPK in activation of the Nox complex. However, in the model filamentous fungus *Aspergillus nidulans*, the p38 MAPK homologue, SakA, has been shown to repress expression of *noxA* (Lara-Ortíz et al., 2003) suggesting that in fungi, regulation of the Nox complex may occur differently than in mammalian systems.

Another group of enzymes, the p21-activated kinases (paks), are also involved in regulation of the Nox complex in mammalian systems. Pak activity has been shown to be essential for the efficient production of superoxide by mammalian neutrophils (Martyn et al., 2005). In addition, Pak translocates to the membrane in response to a Nox activating signal, colocalising with p47phox and p22phox (Martyn et al., 2005). Pak also phosphorylates several serine residues within p47phox. However, it does not bind directly to p47phox but rather to p22phox (Martyn et al., 2005). Paks may also regulate Nox activity via the Rac GTPase. Bovine Pak1 activates Rac1 by inducing its release from RhoGDI (guanine dissociation inhibitor) (DerMardirossian et al., 2004). Whether paks are involved in Nox regulation in fungi remains to be determined.

1.5. MAP kinase signalling

1.5.1. The MAP kinase cascade

Mitogen activated protein (MAP) kinase pathways are perhaps some of the most conserved and crucial signalling pathways possessed by eukaryotes, and are found in all

eukaryotic kingdoms from animals to fungi. These pathways translate diverse physical or chemical signals detected at the cell surface into changes in gene expression via a phosphorylation (MAP kinase) cascade consisting of three highly conserved protein kinases – the MAP kinase kinase kinase (MAPKK kinase), MAP kinase kinase (MAPK kinase) and MAP kinase (Fig. 1.3). Cells possess multiple MAP kinase pathways for responses to a range of stimuli from pheromones to stress signals. The activating stimulus is detected at the cell surface, usually by a membrane receptor. The signal is then transmitted to the first component of the MAP kinase cascade, the MAPKK kinase, either directly or via an adapter module composed of additional protein kinases which act as signal transducers and primary kinases (Banuett, 1998; Dean et al., 2005). The activated MAPKK kinase then activates the MAPK kinase via phosphorylation, which in turn phosphorylates the MAP kinase on two closely spaced threonine and tyrosine residues (Thr-X-Tyr, where X = proline, glycine or glutamine) on the MAPK kinase, resulting in its activation. The MAP kinase then phosphorylates target proteins, including but not limited to transcription factors, facilitating changes in gene expression in response to the activating stimulus (Banuett, 1998).

1.5.2. MAP kinase pathways in fungi

In the model yeast, *Saccharomyces cerevisiae*, four MAP kinase pathways are involved in normal vegetative growth, with roles in pheromone response (Fus3 pathway), filamentation/invasion (Kss1 pathway), high osmolarity growth (Hog1 pathway) and cell integrity (Slt2 pathway). A fifth pathway (Smk1 pathway) involved in spore wall assembly is active only during sporulation (Gustin et al., 1998). Most filamentous fungi possess only three MAP kinase pathways. However, in the *Aspergilli*, the number of MAP kinases has been expanded with *Aspergillus fumigatus* and *A. nidulans* possessing four, and *A. oryzae* possessing five due to redundancy of the Hog1-like MAP kinase (Kobayashi et al., 2007). In pathogenic fungi MAP kinase pathways have been found to play important roles in virulence (Román et al., 2007). For example, in *M. grisea* two of the three MAP kinase pathways have been adapted to roles in virulence with the MPS1 pathway (homologous to *S. cerevisiae* Slt2 pathway) involved in penetration peg formation, and the PMK1 pathway (homologous to *S. cerevisiae* Fus3 and Kss1 pathways) involved in appressorium formation (Dean et al., 2005). The third pathway (OSM1 pathway

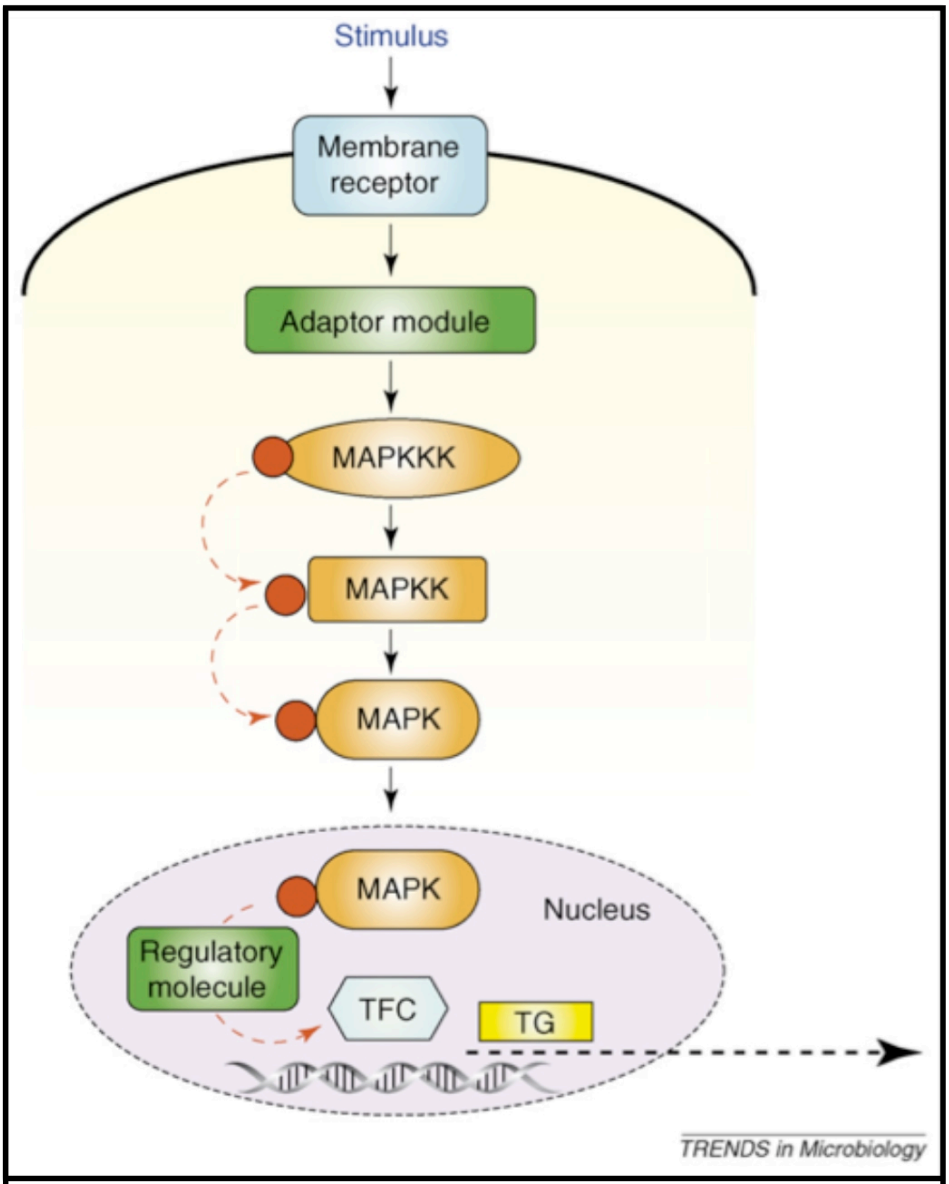

Figure 1.3 General scheme of a MAPK pathway
An external stimulus is perceived at the plasma membrane by a specific receptor protein. This receptor then transmits the signal through a two-component system and/or adaptor molecules to the core MAP kinase phosphorylation cascade. This cascade is composed of three highly conserved protein kinases, the MAP kinase kinase kinase (MAPKKK), MAP kinase kinase (MAPKK) and MAP kinase (MAPK). These kinases are sequentially phosphorylated and activated. Upon phosphorylation, the MAPK generally translocates to the nucleus where it activates target transcription factor complexes (TFC), leading to changes in target gene (TG) expression. The MAPK may also phosphorylate other regulatory molecules such as repressor complexes, relieving the repression of gene expression. Reproduced from Román et al. (2007). Trends in Microbiology 4: 181-190.

homologous to *S. cerevisiae* Hog1 pathway) is involved in the hyper-osmotic response (Dean et al., 2005).

1.5.3. Yeast stress-activated MAP kinase pathways

The best-characterised fungal MAP kinase pathway is the Hog1 pathway involved in the osmotic stress response. The Hog1 MAP kinase was identified in a screen for mutants unable to grow under conditions of high osmolarity (Brewster et al., 1993). The name Hog1 (high osmolarity glycerol) derives from the fact that mutants not only display reduced growth under high osmolarity but also have a greatly reduced glycerol response (Brewster et al., 1993). These mutants also display altered cell morphology on high osmolarity media, forming large multinucleated cells with multiple elongated buds (Brewster et al., 1993).

The stress-activated MAP kinase from the model fission yeast, *S. pombe*, was independently discovered three times and hence has three names, *sty1/spc1/phh1* (suppressor of tyrosine phosphatase/suppressor of phosphatase 2C/*pombe* homologue of *hog1*) (Millar et al., 1995; Shiozaki and Russell, 1995a; Kato et al., 1996). In comparison to Hog1p, which responds to only osmotic stress, the *S. pombe* MAP kinase is more like the mammalian p38 MAP kinase, being involved in responses to a number of stresses including osmotic, temperature, oxidative and UV (Millar et al., 1995; Shiozaki and Russell, 1995a; Kato et al., 1996). The *S. pombe* MAP kinase is also involved in cell cycle control, with mutants displaying a delay in the G2 phase of mitosis, resulting in increased cell length (Millar et al., 1995; Shiozaki and Russell, 1995b).

1.5.4. Role of the stress-activated MAP kinase pathway in filamentous fungi

Stress-activated MAP kinases have been characterised in a number of filamentous fungi, ranging from saprobes to plant and animal pathogens (Rispail et al., 2009). This has revealed that these proteins are often involved in more than just responses to stress conditions.

1.5.4.1. Saprotrophic fungi

In the model filamentous fungus *Neurospora crassa*, the stress-activated MAP kinase Os-2 is required not only for growth under conditions of osmotic stress, but also for sensitivity to phenylpyrrole fungicides (Zhang et al., 2002), an observation that will be discussed further in Section 1.5.4.4. Interestingly, the *N. crassa* Os-2 MAP kinase pathway appears to be regulated by the circadian clock (Vitalini et al., 2007). The clock rhythmically activates Os-2, and it is predicted that this allows *N. crassa* to prepare for osmotic stress that will occur at sunrise (Vitalini et al., 2007). The role of the *A. nidulans* stress-activated MAP kinase SakA has been independently characterised twice, with some unexpected results (Han and Prade, 2002; Kawasaki et al., 2002). Despite being able to complement the osmosensitivity defect of an *S. pombe sty1*Δ mutant, SakA was not required for growth of *A. nidulans* under osmotic stress conditions unless grown at lower than optimal temperature, suggesting an alternative pathway regulates the osmotic stress response in *A. nidulans* (Han and Prade, 2002; Kawasaki et al., 2002). Rather, it appears that SakA has been adapted to a role in repression of sexual development, with Δ*sakA* mutants displaying premature sexual development, and spore survival, with mutant conidiospores being sensitive to oxidative and heat stresses and losing viability when stored (Kawasaki et al., 2002). Altered chitin deposition in these mutants also suggests a possible role in cell wall biogenesis (Han and Prade, 2002).

1.5.4.2. Animal and insect pathogens

Candida albicans, an opportunistic human pathogen, is a dimorphic fungus, growing as both yeast and filamentous forms. This morphogenetic switching is regulated by the Hog1 MAP kinase, with *hog1*Δ mutants switching to filamentous growth under conditions in which this transition is repressed in the wild-type strain (Alonso-Monge et al., 1999). In contrast, *HOG1* was found to act as an inducer of chlamydospore formation, with mutants being unable to produce these structures (Alonso-Monge et al., 2003). *C. albicans HOG1* is also predicted to be involved in cell wall metabolism, with mutants displaying increased resistance to chemicals that interfere with the cell wall (Alonso-Monge et al., 1999). Additionally, Munro et al. (2007) demonstrated a link between the *C. albicans* HOG, PKC (protein kinase C), and calcineurin signalling

pathways in promotion of chitin synthase expression and activity, with *hog1*Δ mutants having significantly less chitin in their cell wall than the wild-type strain. Perhaps most importantly, *C. albicans* Δ*hog1* mutants display reduced virulence in a mouse model, possibly due to the fact that they display increased sensitivity to oxidative stress, thereby making them unable to cope with the host oxidative burst response (Alonso-Monge et al., 1999; Alonso-Monge et al., 2003).

In the human basidiomycete pathogen *Cryptococcus neoformans*, the HOG pathway has been adapted to a role in regulation of morphological differentiation and production of virulence factors in the highly virulent serotype A H99 clinical isolate, but not in the less virulent laboratory-generated serotype D strain JEC21 (Bahn et al., 2005). *hog1*Δ mutants of both serotype A and D strains are hypersensitive to osmotic and UV stresses. However, only the serotype A *hog1*Δ mutant displays increased sensitivity to temperature and oxidative stresses. Similar to the *C. albicans* mutant, the serotype A *hog1*Δ mutant has reduced virulence compared to the wild-type strain (Bahn et al., 2005).

As mentioned earlier (Section 1.5.2), the *Aspergilli* display redundancy of their stress-activated MAP kinases (Kobayashi et al., 2007; Miskei et al., 2009). The opportunistic human pathogen *A. fumigatus*, for example, contains the *HOG1* homologue *sakA* and an additional gene, *mpkC*, which does not have an *S. cerevisiae* homologue but is most similar to *HOG1* (Xue et al., 2004; Reyes et al., 2006). SakA and MpkC were shown to play important roles in growth under poor nitrogen and carbon conditions respectively. SakA and MpkC also display different responses to stress, with *sakA* expression induced by osmotic stress, and *mpkC* expression induced by oxidative stress. Consistent with this observation, the Δ*sakA* mutant is sensitive to osmotic stress, whereas the Δ*mpkC* mutant is not. However, despite being induced by oxidative stress, *mpkC* was not required for growth under oxidative stress conditions (Xue et al., 2004; Reyes et al., 2006). Whether *sakA* and *mpkC* are involved in virulence of *A. fumigatus* remains to be determined.

In the mycoparasite *Trichoderma harzianum*, *hog1* is required for growth under osmotic stress but plays only a secondary role in the oxidative stress response, with mutants only slightly more sensitive to oxidative stress than the wild-type strain (Delgado-Jarana et al., 2006). However, *hog1* was found to be involved in regulating antagonistic interactions of

T. harzianum with other fungi, with the *hog1*-silenced mutant being less able to antagonise the plant pathogens *Colletotrichum acutatum* and *Phoma betae* (Delgado-Jarana et al., 2006).

1.5.4.3. Plant pathogens

The involvement of stress-activated MAP kinases in virulence of plant pathogens appears to be highly variable. In many fungi the stress-activated MAP kinase is essential for normal virulence. For example, in the dimorphic fungus *Mycosphaerella graminicola*, the causal agent of septoria tritici leaf blotch on wheat, *Hog1* is required for the switch to filamentous growth, and for growth under osmotic stress conditions (Mehrabi et al., 2006). Given the filamentous form is required for infection, mutants are consequently non-pathogenic (Mehrabi et al., 2006). In the chestnut blight fungus *Cryphonectria parasitica* the stress-activated MAP kinase *cpmk*1 is also required for optimal virulence, although this is complicated by the involvement of a mycovirus that specifically targets *cpmk1* (Park et al., 2004). The stress-activated MAP kinase also appears to be important for virulence of necrotrophs. For example, in *Cochliobolus heterostrophus*, the causal agent of southern corn leaf blight, *hog1* mutants produce smaller appressoria than the wild-type strain and cause reduced disease symptoms on maize, possibly due to the smaller appressoria (Igbaria et al., 2008). *hog1* mutants are also sensitive to osmotic stress and oxidative stress, possibly contributing to the reduced virulence. These mutants also appear to age more rapidly than the wild-type strain, with cells abruptly losing viability, turning brown and staining with the cell death indicator trypan blue (Igbaria et al., 2008). Loss of *B. cinerea sak1* also results in reduced virulence, with mutants unable to penetrate host tissue and displaying reduced colonisation of wounded tissue (Segmüller et al., 2007). Mutants are also sensitive to osmotic stress and oxidative stress induced by hydrogen peroxide but not menadione (Segmüller et al., 2007). However, only a subset of the typical oxidative stress response genes are regulated by SAK1, suggesting that similar to *T. harzianum*, another pathway is also involved in the *B. cinerea* oxidative stress response (Segmüller et al., 2007).

In contrast, the stress-activated MAP kinase is dispensable for virulence in a number of other fungi. For example, in the rice blast fungus *M. grisea*, deletion of *OSM1* increased sensitivity to osmotic stress, altered hyphal morphology under osmotic stress conditions

and reduced conidiation (Dixon et al., 1999). However, Δ*osm1* mutants still produce functional appressoria and are fully pathogenic (Dixon et al., 1999). Similarly, in *Bipolaris oryzae*, the causal agent of brown leaf spot disease of rice, Δ*srm1* mutants are sensitive to osmotic stress, hydrogen peroxide and UV but remain fully pathogenic (Moriwaki et al., 2006). Loss of *Colletotrichum lagenarium osc1* also has no effect on pathogenicity, although mutants are sensitive to osmotic stress (Kojima et al., 2004).

1.5.4.4. Role in fungicide sensitivity

Phenylpyrrole fungicides are broad spectrum fungicides used to control a variety of plant-pathogenic fungi (Gehmann et al., 1990). The two most common of these are fenpiclonil (4-(2,3-dichlorophenyl)-1H-pyrrole-3-carbonitrile; CGA142705) and fludioxonil (4-(2,2-difluoro-1,3-benzodioxol-4-yl)pyrrole-3-carbonitrile; CGA173506), which are derived from the antibiotic pyrrolnitrin (Nevill et al., 1988; Gehmann et al., 1990). Two historical observations had alluded to a possible role of the stress-activated MAP kinase pathway in mediating sensitivity to these fungicides (Jespers et al., 1993; Jespers and De Waard, 1995). Firstly, treatment of *Fusarium sulphureum* with fenpiclonil induced the accumulation of glycerol and mannitol, common compatible solutes. Secondly, a number of fungal mutants that were resistant to these fungicides were also sensitive to high osmolarity. This led researchers of fungal stress-activated MAP kinase pathways to investigate fungicide sensitivity in their mutants.

In *N. crassa*, loss of the *os-2* MAP kinase confers resistance to fludioxonil and fenpiclonil (Zhang et al., 2002). In addition, treatment with fludioxonil and fenpiclonil was found to increase Os-2 phosphorylation, suggesting Os-2 is a direct target of these fungicides (Irmler et al., 2006). In *C. lagenarium* loss of the *OSC1* MAP kinase also confers fludioxonil resistance, and in wild-type *C. lagenarium* fludioxonil treatment induces translocation of OSC1 to the nucleus (Kojima et al., 2004). Interestingly, in *A. fumigatus*, the Δ*sakA* mutant is resistant to fludioxonil whereas the Δ*mpkC* mutant is not, suggesting fungicide signalling acts through SakA, not MpkC (Xue et al., 2004; Reyes et al., 2006). Another interesting case is that of *B. cinerea* in which the Δ*sak1* mutant is not resistant to fludioxonil, but a mutant in the upstream histidine kinase *bos1* is resistant, suggesting

that in *B. cinerea*, Bos1 regulates fungicide sensitivity independently of Sak1 (Segmüller et al., 2007; Liu et al., 2008).

1.6. p21-activated kinase signalling

The p21-activated kinases (paks), as the name suggests, are serine/threonine protein kinases that are activated by the p21 GTPase proteins Rac and Cdc42 (Manser et al., 1994). However, paks can also be activated via GTPase-independent mechanisms (Bokoch, 2003). These proteins are involved in a variety of cellular processes including cytoskeletal dynamics and polarised growth, MAP kinase signalling, and cell-cycle control (Bokoch, 2003). Paks contain a highly conserved C-terminal catalytic kinase domain and an N-terminal regulatory (or p21-binding) domain (Bokoch, 2003). Within the p21-binding domain (PBD) is a CRIB (Cdc42/Rac interactive binding) motif to which Cdc42 and Rac bind (Chong et al., 2001). The PBD overlaps an auto-inhibitory region that interacts with the kinase domain preventing pak activity (Lei et al., 2000). Binding of Rac or Cdc42 to the CRIB motif induces a conformational change in the pak, allowing it to auto-phosphorylate the kinase and N-terminal regulatory domains, leading to activation (Lei et al., 2000) (Fig. 1.4). Once activated the pak is able to release the GTPase and remain active (Manser et al., 1994). The N-terminal regulatory domain also contains proline-rich (PxxP) motifs that act as potential binding sites for SH3 domain proteins, such as *S. cerevisiae* Bem1 (Daniels and Bokoch, 1999; Winters and Pryciak, 2005).

1.6.1. The Rho GTPase molecular switches

The small Rho GTPase proteins play a number of crucial roles within cells and are referred to as molecular switches due to the on/off mechanism by which they are regulated. Activity of these proteins is regulated by two distinct cycles: GDP/GTP exchange and membrane/cytosol cycling (DerMardirossian et al., 2004). The GDP/GTP cycle is facilitated by guanine nucleotide-exchange factors (GEFs) and GTPase-activating proteins (GAPs). GTPases are only active when in their GTP-bound

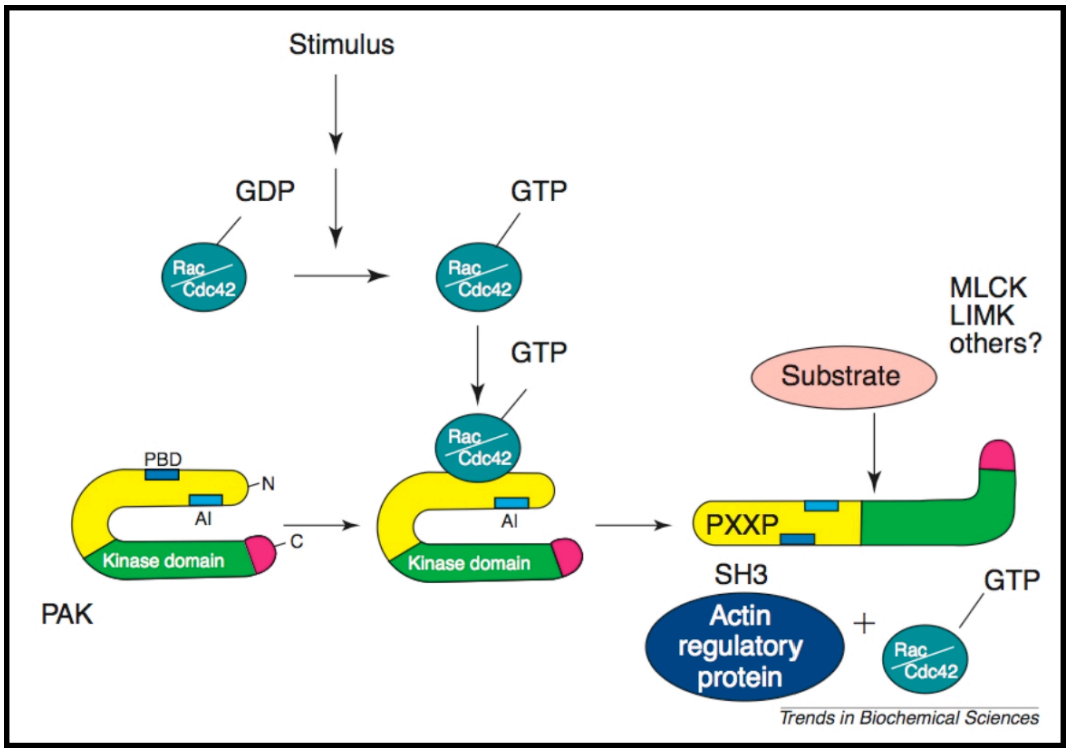

Figure 1.4 Model showing activation of mammalian p21-activated kinases (Paks) by the GTPases Cdc42 and Rac
Under non-activated conditions Paks are kept inactive due to interaction of an autoinhibitory (AI) region with the catalytic kinase domain. Binding of Cdc42 or Rac to the p21-binding domain (PBD) induces a conformational change within the Pak, allowing autophosphorylation of the kinase and N-terminal regulatory domains, resulting in Pak activation. Activated Pak can then phosphorylate its substrates including lim kinase (LIMK) and myosin regulatory light chain kinase (MLCK). Proline-rich (PXXP) motifs within the N-terminus are also free to interact with SH3-domain proteins such as actin regulatory proteins. Reproduced from Daniels & Bokoch (1999). Trends in Biochemical Sciences 24: 350-355.

form. GAPs act as negative regulators of GTPase activity by enhancing the hydrolysis of GTP to GDP. In contrast, GEFs promote GTPase activity by exchanging GDP for GTP, thereby activating the GTPase (DerMardirossian et al., 2004). The membrane/cytosol cycle refers to the location of the GTPase within the cell. In order to activate their targets, GTPases generally must localise to the membrane where their targets reside. Both these cycles of GTPase regulation are affected by the guanine dissociation inhibitors (RhoGDIs).

1.6.1.1. The tripartite role of RhoGDI

RhoGDIs perform three separate functions in regulation of Rho GTPases. Firstly, they prevent dissociation of GDP from the GTPases by preventing interaction with GEFs due to an overlap in the GEF and RhoGDI binding sites. Secondly, they interact with activated GTP-bound GTPases preventing intrinsic and GAP-catalysed GTP hydrolysis. Thirdly, they regulate membrane/cytosol cycling (Dransart et al., 2005). Rho GTPases contain an isoprenyl lipid at their C-terminus, which inserts into the membrane. RhoGDI prevents GTPase binding to the membrane by binding directly to this isoprenyl moiety via its hydrophobic pocket (DerMardirossian and Bokoch, 2005). RhoGDI can also extract GTPases out of the membrane, possibly in order to terminate GTPase signalling (DerMardirossian and Bokoch, 2005). For example, RhoGDI from the ectomycorrhizal fungus *Tuber borchii* was able to solubilise Cdc42 out of the membrane in a translocation assay (Menotta et al., 2008), and the *S. cerevisiae* Rdi1 RhoGDI was shown to extract both Cdc42 and Rho1 from membranes (Tiedje et al., 2008). However, RhoGDI is also hypothesised to play a positive role in GTPase signalling by acting as a shuttle to target GTPases to the correct membrane site for signalling (Lin et al., 2003).

1.6.2. The pak conundrum

As detailed above, the Rac and Cdc42 GTPases activate the p21-activated kinases. However, bovine Pak1 has also been shown to be involved in activation of the Rac GTPase by triggering its release from the RhoGDI (Fig. 1.5) (DerMardirossian et al.,

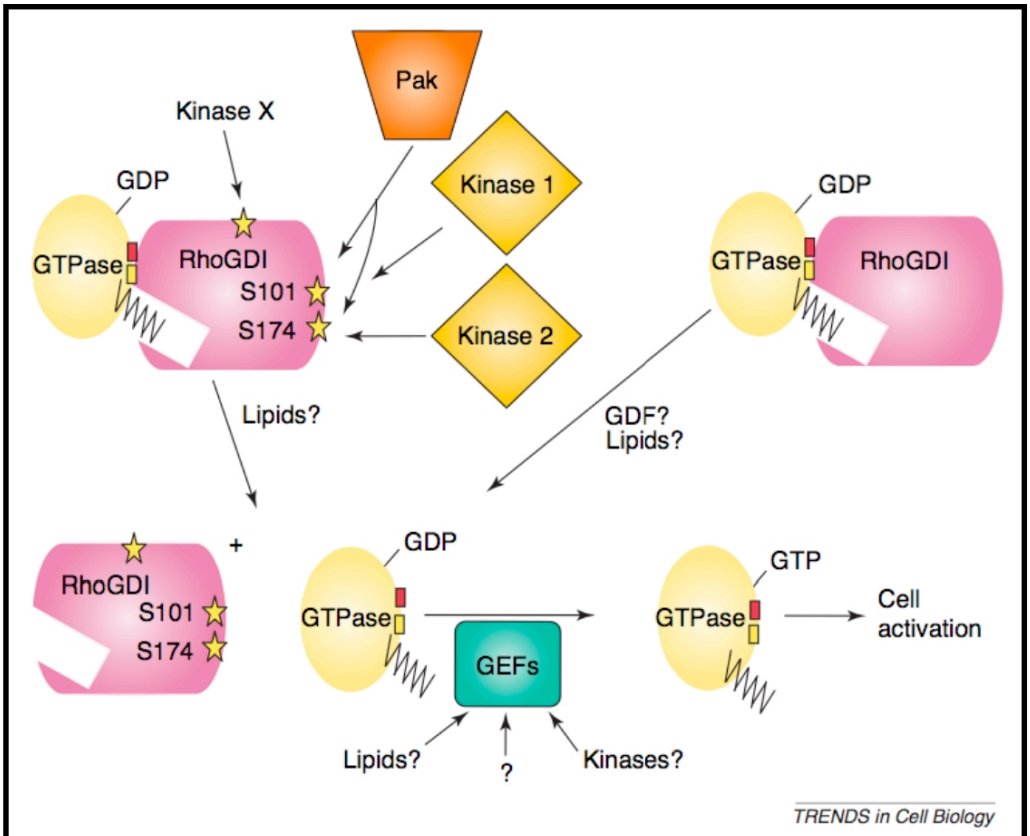

Figure 1.5 Model showing regulation of RhoGTPases by RhoGDI and a p21-activated kinase (Pak)
Under non-activated conditions GTPases are held inactive in the cytoplasm by interaction with the inhibitor protein RhoGDI. Targeted phosphorylation of RhoGDI on two closely spaced serine residues, Ser101 and Ser174, induces specific release of the Rac GTPase. Phosphorylation of only one of these serine residues, or on alternative serine residues by other kinases is insufficient to induce release of Rac. Released Rac is then activated by guanine exchange factors which replace GDP with GTP. Activated Rac can then take part in cell activation processes. Reproduced from DerMardirossian & Bokoch (2005). Trends in Cell Biology 7: 356-363.

2004). Pak1 phosphorylates RhoGDI on two serine residues (Ser^{101} and Ser^{174}), which border the hydrophobic pocket of RhoGDI. This is predicted to induce a conformation change that destabilises binding of the Rac isoprenyl group. However, binding of RhoA and Cdc42 is unaffected. In contrast, the *S. cerevisiae* p21-activated kinase Cla4 was found to disrupt binding between RhoGDI and both Rho1 and Cdc42 (Tiedje et al., 2008). Given Pak is both activated by and potentially activates Rac/Cdc42 this suggests there may be a positive-feedback mechanism in play, in which a small pool of activated Rac/Cdc42 activates Pak, which in turn activates more Rac/Cdc42 by triggering its release from the RhoGDI (Dransart et al., 2005). However, it is important to note that the negative regulation of RhoGDI/GTPase binding by p21-activated kinases may also reduce GTPase signalling due to loss of targeting of the GTPase by RhoGDI.

1.6.3. Role of the p21-activated kinases in yeast

Fungal p21-activated kinases are best characterised in the model yeast *S. cerevisiae*, which possesses three paks – Cla4, Ste20 and Skm1. In addition to the catalytic and p21-binding domains detailed earlier, Cla4 and Skm1 contain a putative membrane-binding pleckstrin homology (PH) domain at their N terminus, a feature unique to paks from lower eukaryotes (Hofmann et al., 2004). This PH domain can specifically bind to phosphoinositides in cell membranes and is thought to play an important role in regulating pak function (Lemmon et al., 1997). *S. cerevisiae* Ste20 is involved in activation of the pheromone response, filamentation/invasion and high osmolarity growth MAP kinase pathways (Hofmann et al., 2004). It also plays important roles in polarised growth and actin organisation (Eby et al., 1998; Goehring et al., 2003). *S. cerevisiae* Cla4 is also involved in polarised growth, and actin organisation, with important roles in budding and cytokinesis (Cvrcková et al., 1995). Additionally, both Ste20 and Cla4 are involved in regulation of vacuole inheritance (Bartholomew and Hardy, 2009). Skm1 shows no redundancy with Ste20 or Cla4 and appears dispensable for growth (Martin et al., 1997).

In *S. pombe*, the Ste20 homologue Shk1 (Ste20 homologous kinase), also known as Pak1, is involved in establishment of cell polarity and mating, and is essential for viability (Marcus et al., 1995; Qyang et al., 2002). The Cla4 homologue Shk2, also known as

Pak2, is not essential for viability and appears to function redundantly with Shk1 (Sells et al., 1998; Yang et al., 1998).

1.6.4. Roles in filamentous fungi

The p21-activated kinases of filamentous fungi play diverse roles in fungal development and are often involved in virulence-associated processes. In *M. grisea*, for example, disruption of the *CLA4* homologue *CHM1* resulted in reduced growth, cellular compartment length and conidiation, whereas disruption of the *STE20* homologue, *MST20*, resulted in reduced aerial hyphae and conidiation. Interestingly, whilst *MST20* was dispensable for pathogenicity, *CHM1* mutants were found to display reduced virulence. These mutants produced few appressoria, and those that were produced were unable to penetrate, although these mutants were able to colonise through wounds (Li et al., 2004). Disruption of *C. purpurea cla4* resulted in a similar phenotype of reduced growth, cellular compartment length, conidiation and virulence, with mutants unable to penetrate host tissues (Rolke and Tudzynski, 2008). Interestingly, the *C. purpurea* Δ*cla4* mutant had an identical phenotype to the *C. purpurea* Δ*rac* mutant (Rolke and Tudzynski, 2008). In *Ustilago maydis*, *cla4* mutants are also non-pathogenic and display defective budding and delocalised chitin deposition along their cell wall, suggesting possible roles for Cla4 in regulating cell polarity and chitin localisation (Leveleki et al., 2004). Interestingly, disruption of the *U. maydis ste20* homologue *smu1* (Ste20p affecting mating in *Ustilago*) also had an impact on pathogenicity, with mutants displaying reduced virulence, but were still able to cause disease (Smith et al., 2004). These mutants also displayed a delayed mating response, suggesting a role for Ste20 in regulating mating. Both *C. neoformans* paks, *PAK1* and *STE20*, are also required for normal mating and virulence (Wang et al., 2002; Nichols et al., 2004). The Cla4 homologue, unfortunately named Ste20, is involved in maintenance of polarity in the mating filament, whilst the Ste20 homologue, Pak1, is involved in cell fusion (Nichols et al., 2004). In the cotton pathogen *Ashbya gossypii*, disruption of *CLA4* blocks hyphal maturation, the developmental switch from slow-growing young hyphae to fast-growing mature hyphae (Ayad-Durieux et al., 2000). *A. gossypii cla4* also appears to play an important role in septation, with mutants being unable to form actin and chitin rings properly (Ayad-

Durieux et al., 2000). Whether *CLA4* is required for virulence of *A. gossypii* remains to be determined.

1.7. Aims

The biological question at the heart of this research is: how is the mutually beneficial association between *E. festucae* and perennial ryegrass regulated? To address this question, two key aims were formulated based on the possible Nox regulators described in Section 1.4.3 and their proposed mode of action as summarised in Figure 1.6 (Scott and Eaton, 2008).

The first aim of this research was to determine whether the stress-activated MAP kinase is involved in regulating the association with perennial ryegrass. This aim was split into four main objectives:

1. Determine if the *sakA* gene encodes a functional stress-activated MAP kinase.

In this objective the *E. festucae sakA* gene was transformed into an *S. pombe sty1*Δ mutant to determine whether *sakA* is able to functionally complement for *sty1*, and therefore rescue the mutant from its osmosensitivity and cell cycle defects.

2. Determine if *sakA* is required for growth of *E. festucae* in axenic culture.

In this objective an *E. festucae* Δ*sakA* mutant was generated by homologous recombination. The growth and morphology of this mutant was then examined under a range of conditions in culture.

3. Investigate whether *sakA* is required for maintenance of the beneficial association with perennial ryegrass.

In this objective the Δ*sakA* mutant was inoculated into perennial ryegrass seedlings and the resulting plant interaction phenotype analysed, both at the whole plant and sub-cellular levels using a range of microscopy techniques.

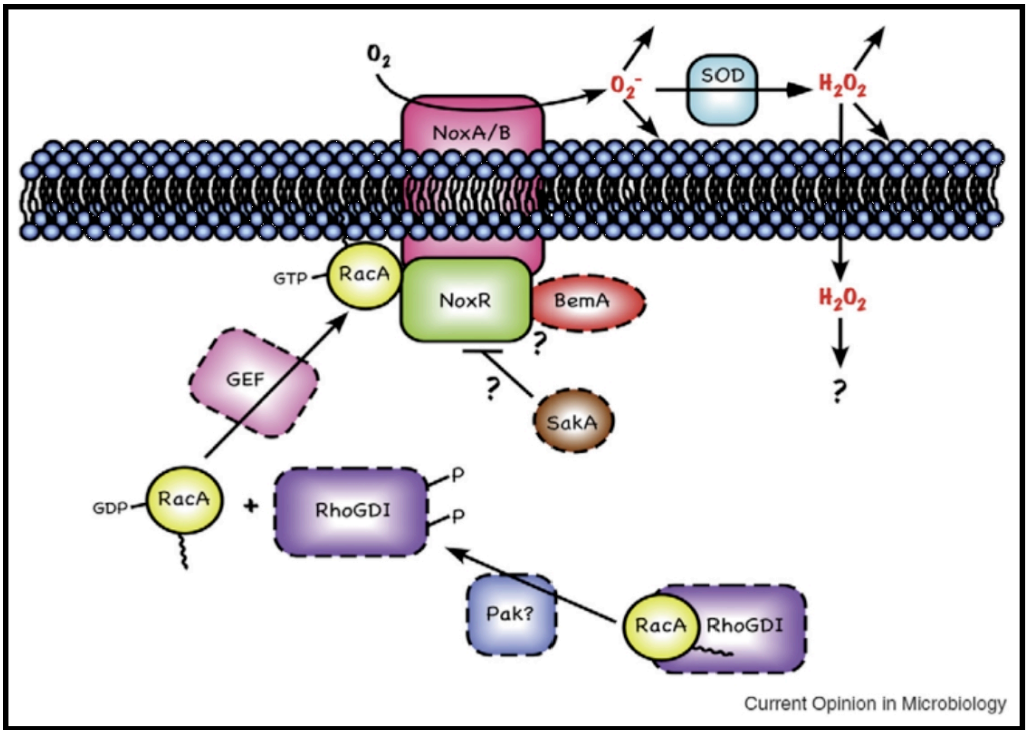

Figure 1.6 Hypothesised regulation of the fungal Nox complex
A proposed scheme for regulation of the fungal NoxA and NoxB complexes. In response to an activating signal, the cytosolic regulatory components RacA and NoxR are recruited to the membrane and associate with the catalytic subunit NoxA or NoxB, activating production of superoxide from molecular oxygen. Superoxide is then rapidly converted to hydrogen peroxide either spontaneously by the superoxide dismutase (SOD). Dashed boxes show predicted regulators of the Nox complex based on analogy with mammalian Nox2 regulation. The adapter protein BemA, is predicted to be a functional analogue of mammalian p40phox and may be involved in recruitment of NoxR. The stress-activated MAP kinase, SakA, may regulate the Nox complex via interaction with NoxR, as is seen for mammalian p38 MAPK and the NoxR homologue p67phox. A p21-activated kinase (Pak) may regulate the Nox complex by triggering release of RacA from the inhibitory RhoGDI protein, allowing RacA to then be activated by guanine exchange factors (GEFs) and associate with the Nox complex. A Pak may also interact directly with components of the Nox complex as is seen for mammalian Pak1. Reproduced from Scott & Eaton (2008). Current Opinion in Microbiology 11:488-493.

4. Investigate whether *sakA* is involved in regulation of the Nox complex.

In this objective the Δ*sakA* mutant was screened for any change in the production of ROS in culture and *in planta*. Possible regulation of *nox* gene expression by *sakA* was examined using RT-PCR.

The second aim of this research was to determine whether the p21-activated kinases (paks) are involved in regulating the association with perennial ryegrass. This aim was split into two main objectives:

1. Determine if the p21-activated kinases are required for growth of *E. festucae* in axenic culture.

In this objective mutants were generated for the two *E. festucae* paks using homologous recombination. The growth and morphology of these mutants was then examined at the whole colony and sub-cellular levels using a range of microscopy techniques.

2. Determine whether the paks are required for maintenance of the mutualistic association with perennial ryegrass.

In this objective the Δ*pakA* and Δ*pakB* mutants were inoculated into perennial ryegrass seedlings. The resulting plant interaction phenotypes were then analysed using a range of microscopy techniques.

In addition to the two aims detailed above, a third aim of this research was to use bioinformatic analyses to identify and characterise key components of the three *E. festucae* MAP kinase pathways. This aim will aid in annotation of the recently released *E. festucae* genome.

2. Materials and Methods

2.1. Biological material

Bacterial and fungal strains and plant material used in this study are listed in Table 2.1. Plasmids and cosmids are listed in Table 2.2.

Table 2.1: Bacterial strains, fungal strains and plant material

Strain	Relevant Characteristics	Source or Reference
Fungal Strains		
E. festucae		
PN2278	Wild-type Fl1	Young et al. (2005)
PN2656	Δ*sakA*; Fl1/Δ*sakA*::P*trpC-hph*; Hyg^R (T1-3)	Eaton et al. (2008)
PN2657	PN2278/pCE12; Hyg^R (T25-2)	Eaton et al. (2008)
PN2658	Δ*sakA*/*sakA*; PN2656/pCE1; pII99; Hyg^R; Gen^R (C5-2)	Eaton et al. (2008)
PN2660	Δ*pakA*; Fl1/Δ*pakA*::P*trpC-hph*; Hyg^R	This study
PN2661	Δ*pakB*; Fl1/Δ*pakB*::P*trpC-hph*; Hyg^R	This study
PN2697	Δ*pakA*/*pakA*; PN2660/pCE43; Hyg^R; Gen^R	This study
PN2698	Δ*pakB*/*pakB*; PN2661/pCE42; Hyg^R; Gen^R	This study
PN2327	Δ*noxA*; Fl1/Δ*noxA*::P*trpC-hph*; Hyg^R	Tanaka et al. (2006)
PN2479	Δ*noxR*; Fl1/Δ*noxR*::P*trpC-hph*; Hyg^R	Takemoto et al. (2006)
S. pombe		
PN2578 (WT)	WT; 972 h-	Eaton et al. (2008)
PN2580 (JM1745)	*sty1*Δ; *sty1*::*ura4 leu1.32 ura4-D18*, h-	J. Millar, UK
PN2582	PN2580/pREP81	Eaton et al. (2008)
PN2584	PN2580/pF37	Eaton et al. (2008)
PN2585	PN2580/pCE22	Eaton et al. (2008)
PN2586	PN2580/pCE23	Eaton et al. (2008)
PN2606	PN2580/pREP81-Cgfp	Eaton et al. (2008)
PN2607	PN2580/pCE30	Eaton et al. (2008)
***E. coli* Strains**		
XL-1 Blue	*supE*44, *hsdR*17, *recA*1, *endA*1, *gyrA*46, *thi*, *relA*1, *lac*$^-$, F' [*pro*AB$^+$, *lac*I^q, *lac*ZΔM15, Tn10 (Tet^R)]	Bullock et al. (1987)
Mach1	Δ*recA*1398, *endA*1, *tonA*Φ81, *lac*ZΔM15, ΔlacX74, *hsdR*(r_k^- m_k^+)	Invitrogen

TOP10	F⁻, *mcrA*, Δ(*mrr-hsdRMS-mcrBC*), ϕ80*lacZ*ΔM15, Δ*lacX74*, *deoR*, *recA1*, *araD139*, Δ(*ara-leu*)7697 *galU*, *galK*, *rpsL*(Str^R), *endA1*, *nupG*	Invitrogen
DH5α	F⁻, ϕ80*lacZ*, ΔM15, Δ(*lacZYA-argF*), U169, *recA1*, *endA1*, *hsdR17* (r_k^-, m_k^-), *phoA*, *supE44*, λ⁻, *thi-1*, *gyrA96*, *relA1*	Invitrogen
PN1908	Mach1/pCE1	Eaton et al. (2008)
PN1952	XL-1 Blue/pCE12	Eaton et al. (2008)
PN1972	XL-1 Blue/pCE22	Eaton et al. (2008)
PN1973	XL-1 Blue/pCE23	Eaton et al. (2008)
PN4020	XL-1 Blue/pCE30	Eaton et al. (2008)
PN1932	XL-1 Blue/pF37	Eaton et al. (2008)
PN1933	XL-1 Blue/pREP81	Eaton et al. (2008)
PN4019	XL-1/pREP81-Cgfp	Eaton et al. (2008)
PN4047	DH5α/pCE35	This study
PN4048	DH5α/pCE36	This study
PN4050	DH5α/pCE37	This study
PN4051	DH5α/pCE38	This study
PN4052	DH5α/pCE40	This study
PN4053	DH5α/pCE41	This study
PN4081	TOP10/pCE42	This study
PN4082	TOP10/pCE43	This study

Plant Material

Δ*sakA* infection analysis

Round 1

G2869	*L. perenne* cv. Samson/PN2278; WT Fl1	This study
G2870	*L. perenne* cv. Samson/PN2656 ; Δ*sakA*	This study
G2871	*L. perenne* cv. Samson/PN2657	This study
G2872	*L. perenne* cv. Samson/PN2658 ; Δ*sakA*/*sakA*	This study

Round 2

G3214, 3217, 3220, 3223, 3226	*L. perenne* cv. Samson/PN2278; WT Fl1	This study
G3215, 3218, 3221, 3224, 3227	*L. perenne* cv. Samson/PN2656 ; Δ*sakA*	This study
G3216, 3219, 3222, 3225, 3228	*L. perenne* cv. Samson/PN2658 ; Δ*sakA*/*sakA*	This study

Round 3

G3309	*L. perenne* cv. Samson/PN2278; WT Fl1	This study
G3310-3312	*L. perenne* cv. Samson/PN2656 ; Δ*sakA*	This study

G3313	*L. perenne* cv. Samson/PN2658 ; Δ*sakA/sakA*	This study
Round 4		
G3765-67; 3809-11	*L. perenne* cv. Samson/PN2278; WT Fl1	This study
G3774-76; 3818-20	*L. perenne* cv. Samson/PN2656 ; Δ*sakA*	This study
G3777-79; 3821-23	*L. perenne* cv. Samson/PN2658 ; Δ*sakA/sakA*	This study
	Δ*pakA* survival analysis	
G3756-58; 3765-67; 3780-82; 3809-11; 3284-26	*L. perenne* cv. Samson/PN2278; WT Fl1	This study
G3759-61; 3768-70; 3783-85; 3812-14; 3827-29	*L. perenne* cv. Samson/PN2660; Δ*pakA*	This study
G3762-64; 3771-73; 3786-88; 3815-17; 3830-32	*L. perenne* cv. Samson/PN2661; Δ*pakB*	This study
	Grown under sterile conditions	
M59-63, 134-145	*L. perenne* cv. Samson/PN2278; WT Fl1	This study
M39-58, 146-174	*L. perenne* cv. Samson/PN2656 ; Δ*sakA*	This study
M64-68	*L. perenne* cv. Samson/PN2658 ; Δ*sakA/sakA*	This study

Table 2.2: Plasmids and cosmids

Name	Relevant characteristics	Source/reference
Cosmid		
44D6	pMO-cosX clone Fl1 genomic DNA cosmid library containing the *sakA* gene	Eaton et al. (2008)
24B3	pMO-cosX clone Fl1 genomic DNA cosmid library containing the *pakA* gene	This study
9H6	pMO-cosX clone Fl1 genomic DNA cosmid library containing the *pakB* gene	This study
Plasmid		
pCE1	12 kb *Bam*HI fragment ex cosmid clone 44D6 in pUC118, Amp^R	Eaton et al. (2008)
pCE12	3.2 kb *Eco*RI fragment ex pCE1 and 1.5 kb sak22/sak23 PCR fragment in pSF15.15	Eaton et al. (2008)
pCE22	1.7 kb sak24/sak39 PCR fragment in pREP81	Eaton et al. (2008)
pCE23	1.1 kb sak24/sak39 cDNA fragment in pREP81	Eaton et al. (2008)
pCE30	1.1 kb sak24/sak57 cDNA fragment in pREP81-Cgfp	Eaton et al. (2008)
pCE35	2 kb pak3/pak4 PCR fragment in pSF15.15	This study
pCE36	2.1 kb pak1/pak2 PCR fragment in pCE35	This study
pCE37	1.6 kb pak7/pak8 PCR fragment in pSF15.15	This study
pCE38	3 kb pak5/pak6 PCR fragment in pCE37	This study
pCE42	8.3 kb *Bgl*II fragment ex 9H6 in pSF17.8	This study
pCE43	4.9 kb pak22/pak23 PCR fragment in pCR4-Topo	This study
pF37	pREP81-*sty1* HA6H	J. Millar, UK
pREP81	Amp^R; *LEU2*	D. Mulvihill, UK
pREP81-Cgfp	pREP81 with C-terminal GFP tag	I. Hagan, UK
pPN83	pBlueScriptII® KS(+) with P*gpd*-EGFP-T*trpC*; Amp^R	Takemoto et al. (2006)
pII99	P*trpC-nptII*-T*trpC* ; Amp^R/Gen^R	Namiki et al. (2001)
pSF15.15	Amp^R; Hyg^R	S. Foster
pSF17.8	Amp^R; Gen^R	S. Foster
pUC118	Amp^R	Vieira & Messing (1987)
pGEM-T Easy	Amp^R	Promega
pCR4-Topo	Kan^R	Invitrogen
pAN7-1	Amp^R/Hyg^R (P*trpC-hph*)	Punt et al. (1987)

2.2. Medium and growth conditions

All media were prepared with milli-Q water and sterilised at approximately 121°C for 15-20 min unless otherwise stated.

2.2.1. *Escherichia coli*

E. coli strains were grown at 37°C overnight on LB agar plates or in LB broth, shaking at 200 rpm. For antibiotic selection, ampicillin or kanamycin was added to a final concentration of 100 μg/mL or 50 μg/mL respectively. For blue-white selection of transformants, IPTG and X-gal were added to final concentrations of 0.1 mM and 40 μg/mL respectively. Cultures were stored at -80°C in 50% (v/v) glycerol.

2.2.1.1. Luria-Bertani medium (LB)

LB medium (Miller, 1972) contained 0.5% (w/v) NaCl, 1% (w/v) tryptone and 0.5% (w/v) yeast extract; pH 7.0 – 7.5. LB agar was prepared by addition of agar to a final concentration of 1.5% (w/v).

2.2.1.2. SOC medium

SOC medium (Dower et al., 1988) contained (per L) 10 mM NaCl, 2.5 mM KCl, 10 mM $MgCl_2$, 10 mM $MgSO_4.7H_2O$, 20 mM glucose, 2% (w/v) tryptone and 0.5% (w/v) yeast extract.

2.2.2. *Schizosaccharomyces pombe*

S. pombe strains were grown at 25°C on EMM agar for 7 days, YE agar for 5 days, or in EMM or YE broth shaking at 200 rpm for 2 days. Expression from the thiamine-

repressible *nmt1* promoter was repressed by addition of thiamine to a final concentration of 30 μM.

2.2.2.1. Edinburgh minimal medium (EMM)

EMM contained (per L) 14.7 mM potassium hydrogen phthalate, 1.5 mM Na_2HPO_4, 93.5 mM ammonium chloride, 2% (w/v) glucose, 20 mL salts solution (50x), 1 mL vitamins solution (1000x) and 0.1 mL minerals solution (10,000x). EMM agar was prepared by addition of agar to a final concentration of 2% (w/v).

2.2.2.1.1. Salts solution

Salts solution (50x) contained 0.26 M $MgCl_2.6H_2O$, 4.99 mM $CaCl_2.2H_2O$, 0.67 M KCl and 14.1 mM Na_2SO_4.

2.2.2.1.2. Vitamins solution

Vitamins solution (1000x) contained 4.20 mM pantothenic acid, 81.2 mM nicotinic acid, 55.5 mM *myo*-inositol and 40.8 μM biotin.

2.2.2.1.3. Minerals solution

Minerals solution (10,000x) contained: 80.9 mM boric acid, 23.7 mM $MnSO_4$, 13.9 mM $ZnSO_4.7H_2O$, 7.40 mM $FeCl_2.6H_2O$, 2.47 mM Molybdic acid, 6.02 mM KI, 1.60 mM $CuSO_4.5H_2O$ and 47.6 mM citric acid.

2.2.2.2. Yeast extract medium (YE)

YE medium contained 0.5% (w/v) yeast extract and 3.0% (w/v) glucose. YE agar was prepared by addition of agar to a final concentration of 2% (w/v).

2.2.2.3. Growth tests

To assess the ability of various *S. pombe* strains to grow under stress conditions in culture, single colonies were re-suspended in liquid EMM and 2 μL streaked onto plates containing the stress agent. For osmotic stress induction EMM was supplemented with 0.1 M NaCl, 0.6 M KCl or 1.5 M sorbitol. For oxidative stress induction EMM was supplemented with 0.6 mM hydrogen peroxide. Plates containing hydrogen peroxide were incubated in the dark to prevent decomposition of the hydrogen peroxide.

2.2.3. *Epichloë festucae*

E. festucae strains were grown at 22°C on PD agar for 5-8 days or in PD broth, shaking at 150 rpm for 5-7 days. Protoplasts were regenerated on RG medium for 10-14 days or until colonies grew through the antibiotic overlay. Cultures were stored at -80°C in 15% (v/v) glycerol and working stocks maintained at 4°C.

2.2.3.1. Potato dextrose medium (PD)

PD broth contained 2.4% (w/v) potato dextrose broth (Difco), pH adjusted to 6.5. PD agar was made by addition of agar to a final concentration of 1.5% (w/v). For antibiotic selection, hygromycin or geneticin was added to final concentrations of 150 μg/mL and 200 μg/mL respectively.

2.2.3.2. Regeneration medium (RG)

RG medium contained (per L) 2.4% (w/v) potato dextrose broth (Difco) and 0.8 M sucrose, pH adjusted to 6.5. RG agar was made by addition of agar to a final concentration of 1.5% (w/v) for plates or 0.8% (w/v) for overlays.

2.2.3.3. Growth tests

To assess the ability of *E. festucae* strains to grow under stress conditions in culture, 28 mm^2 plugs of mycelia were inoculated onto PD plates containing various stress agents. Osmotic stress was induced by addition of 0.3 M NaCl, 0.3 M KCl or 0.7 M sorbitol. Oxidative stress was induced by addition of hydrogen peroxide to 7 mM. For induction of temperature stress, cultures were incubated at 30°C. To examine sensitivity to phenyl-pyrrole fungicides, fludioxonil was added to 100 μg/mL. To assess the cell wall integrity of *E. festucae* strains, mycelial plugs were inoculated onto PD medium supplemented with either 100 μg/mL calcofluor white (CFW) or 0.01% (w/v) SDS. Plates containing hydrogen peroxide and CFW were stored and incubated in the dark to prevent decomposition of the additives.

2.2.4. *Lolium perenne*

2.2.4.1. Murashige and Skoog (MSO)-Phytoagar

For growth of *L. perenne* seedlings under sterile conditions, two weeks after inoculation seedlings were transferred to sterile bottles containing MSO-Phytoagar and incubated at 20°C for up to three months. MSO-Phytoagar contained (per L) 0.75% (w/v) phytoagar and 0.43% (w/v) MSO.

2.2.4.2. Maintenance of plants in the greenhouse

Plants not required to be grown under sterile conditions were planted in root trainers containing potting mix two weeks after inoculation. Approximately two months later plants were repotted in larger pots and Confidor® Insecticide (Bayer) pellets added to the potting mix. Plants were regularly watered and when required sprayed with insecticide and fungicides.

2.3. DNA isolation

2.3.1. Plasmid DNA

For isolation of plasmid DNA, cells were grown overnight at 37°C in 5 mL LB broth supplemented with appropriate antibiotic. Cells were harvested from 3-5 mL of culture by centrifugation at 13,000 rpm for 1 min. Plasmid DNA was then isolated using the High Pure™ plasmid isolation kit (Roche Diagnostics) according to manufacturer's instructions.

2.3.2. Cosmid DNA

For isolation of cosmid DNA, cells were grown overnight as for plasmid isolation (Section 2.3.1). Cells were harvested from 5 mL of culture by centrifugation at 13,000 rpm for 1 min. Cells were then resuspended in 200 µL ice cold Solution I (50 mM glucose, 25 mM Tris-HCl, 10 mM EDTA; pH 8.0). Cell lysis was induced by addition of 0.5 mg lysozyme and incubation at RT for 5 min, followed by addition of 300 µL fresh Solution II (0.4 N NaOH, 2% SDS (w/v)) and incubation on ice for 5 min. The solution was then neutralised by addition of 300 µL ice cold Solution III (3 M potassium acetate, 11.5% (v/v) glacial acetic acid) and incubation on ice for a further 5 min. Cellular debris was pelleted by centrifugation at 13,000 rpm for 10 min. RNaseA (Sigma-Aldrich) was then added to the supernatant to a final concentration of 20 µg/mL and the mixture incubated at 37°C for 20 min to remove contaminating RNAs.

The supernatant was then purified by two chloroform extractions. An equal volume of isopropanol was added to the aqueous phase to precipitate the DNA, which was then pelleted by centrifugation at 13,000 rpm for 10 min. The pellet was then washed with 70% ethanol, air-dried and resuspended in 32 µL milli-Q water. To obtain sequencing quality DNA, a further PEG purification step was performed. NaCl and PEG 8000 were added to the DNA to final concentrations of 0.4 M and 6.5% (w/v) respectively. The DNA was precipitated on ice for 20 min then pelleted by centrifugation at 13,000 rpm for 15 min at 4˚C. The pellet was then washed with 70% ethanol, air-dried and resuspended in 50 µL milli-Q water.

2.3.3. Fungal genomic DNA

E. festucae genomic DNA was isolated from freeze-dried mycelia using the method of Byrd et al. (1990). 10-20 mg of mycelia was ground to a fine powder in liquid nitrogen and resuspended in 800 µL extraction buffer (150 mM EDTA, 50 mM Tris-HCl, 1% SLS; pH 8.0). Proteinase K was added to a final concentration of 2 mg/mL and samples incubated at 37°C for 20 min. Samples were then centrifuged at 13,000 rpm for 10 min to pellet the cellular debris. The aqueous phase was then extracted three times with equal volumes of a 1:1 phenol-chloroform mix. The aqueous phase was then extracted with an equal volume of chloroform and centrifuged at 13,000 rpm for 10 min. Isopropanol was added to the aqueous phase and incubated at RT for 10 min, or -20°C for 1-2 h, to precipitate the DNA. The DNA was then pelleted by centrifugation at 13,000 rpm for 10 min, washed with 70% ethanol, air dried and resuspended in milli-Q water. If the DNA pellet appeared sticky due to the presence of polysaccharide it was resuspended in an equal volume of 1 M NaCl, incubated at RT for 10 min then centrifuged at 13,000 rpm for 10 min to pellet the polysaccharide. The DNA was then ethanol precipitated, pelleted, air-dried and resuspended in milli-Q water as described above.

2.4. DNA manipulation

2.4.1. Quantification

All DNA and RNA samples, with the exception of *E. festucae* genomic DNA, were quantified using a Nanophotometer (Implen) as per the manufacturer's instructions. *E. festucae* genomic DNA was quantified using the DyNA Quant 200 Fluorometer (Hoefer) as per the manufacturer's instructions. For quantification by agarose gel electrophoresis (Section 2.4.6) an aliquot of the DNA sample was separated with a range of standard DNA solutions of known concentration on a 0.7% agarose (w/v) gel at 90 V for ~1 h. Gels were stained with ethidium bromide and the intensity of the sample band compared to those of the standards. This quantification approach also gave an indication of the DNA quality, with degraded DNA producing a smear on the gel.

2.4.2. Restriction endonuclease digestion

Generally, plasmid DNA was digested at 37°C for 1 h and cosmid DNA for 2 h per 1 μg of DNA. Digestions were performed in 10-20 μL final volumes with 3 units of enzyme/μg of DNA, and in the commercial buffer provided with the enzyme. Fungal genomic DNA for Southern blot analysis was digested overnight at 37°C, in a final volume of 50 μL containing 1.1 μg DNA, 30 units of enzyme and the commercial buffer provided with the enzyme. A 100 ng aliquot was checked for complete digestion by gel electrophoresis on a 0.7% (w/v) agarose gel (Section 2.4.6).

2.4.3. DNA purification

To inactivate and/or remove enzymes or other impurities, DNA samples were purified by phenol/chloroform extraction or column purification. For phenol/chloroform extraction, samples were extracted with 0.5 volumes phenol and 0.5 volumes chloroform and centrifuged at 13,000 rpm for 3 min. The aqueous phase was then extracted with an equal volume of chloroform and centrifuged at 13,000 rpm for 3 min.

The DNA was then ethanol precipitated as described in Section 2.4.4. Column purification was performed using the Wizard® SV Gel and PCR Clean-up System (Promega). An equal volume of membrane binding solution was added to the DNA sample, the solution mixed then transferred to an SV mini-column and incubated at RT for 1 min. The DNA was then column purified as per the manufacturer's instructions.

2.4.4. DNA concentration by ethanol precipitation

Low concentration DNA samples were concentrated by ethanol precipitation. 2.5 volumes of 95% ethanol and 0.1 volumes of 3 M Na acetate were added to the sample and the DNA precipitated at -20°C for 2 h. The DNA was then pelleted by centrifugation at 13,000 rpm for 10 min, washed with 70% ethanol, air-dried and resuspended in milli-Q water.

2.4.5. Sub-cloning

Generally, PCR products containing A-overhangs were ligated into pGEM-T easy or pCR4-Topo, sequenced to confirm error-free sequence and sub-cloned into expression or replacement vectors.

2.4.5.1. A-tailing

To facilitate cloning of PCR products amplified with proof-reading enzymes into pGEM-T easy or pCR4-Topo, A-residues were added to the ends of the PCR products via an A-tailing reaction. For addition of A-residues directly after amplification, 1.5 units of Taq DNA polymerase (Roche Diagnostics) were added to the PCR reaction and incubated at 72°C for 10 min. For addition of A-residues to purified PCR products, 200 ng of purified product was incubated at 72°C for 10 min in a 10 μL mixture containing 5 units of Taq DNA polymerase, 1 x Taq DNA polymerase buffer, and 200 nM dATP.

2.4.5.2. Calf intestinal alkaline phosphatase (CIAP) treatment of vectors

To prevent vector re-ligation after restriction endonuclease digestion, samples were treated with Calf intestinal alkaline-phosphatase (CIAP; Roche Diagnostics). Generally, 2-5 μg digested vector was incubated with 1 unit of CIAP per picomole of DNA ends, in a total volume of 50 μL containing the dephosphorylation buffer supplied with the enzyme. Samples were incubated at 37°C for 60 min, then the DNA purified by column purification (Section 2.4.3).

2.4.5.3. Gel extraction

To isolate specific fragments after restriction endonuclease digestion, digests were separated by gel electrophoresis on a low percentage agarose gel (Section 2.4.6). Bands were excised under low wavelength UV light and DNA extracted using the Wizard® SV Gel and PCR Clean-up System (Promega) according to the manufacturer's instructions.

2.4.5.4. PCR product purification

PCR products were purified using the Wizard® SV Gel and PCR Clean-up System (Promega) according to the manufacturer's instructions.

2.4.5.5. Ligation

For ligation of A-tailed PCR fragments into pCR4-Topo (Invitrogen), 4 μL PCR product was incubated with 10 ng pCR4-Topo and 1 μL salt solution (1.2 M NaCl, 0.06 M $MgCl_2$) in a total volume of 10 μL, at RT for 30 min. For ligation of A-tailed PCR fragments into pGEM-T easy (Promega), 50 ng pGEM-T easy was incubated at RT for 2-3 h with 1 unit T4 DNA ligase, an appropriate amount of insert to give a 3 insert:1 vector ratio, and buffer supplied with the enzyme. Ligations into CIAP-treated expression or replacement vectors were performed overnight at RT in a reaction mixture containing 50 ng vector DNA, an appropriate amount of insert DNA to give a

3 insert:1 vector ratio, 1 unit T4 DNA ligase (NEB) and the buffer supplied with the enzyme.

2.4.5.6. *E. coli* transformation

Chemically competent XL-1 Blue or DH5α *E. coli* cells were transformed by heat shock transformation. 100 µL cells were mixed with 2-5 µL ligation mixture or 1 ng control plasmid and incubated on ice for 20 min. Cells were heat shocked at 42°C for 60s then 900 µL SOC added. Cells were then incubated on a shaker at 37°C for 1 h before plating on LB plates supplemented with ampicillin or kanamycin. Chemically competent One Shot® TOP10 cells were transformed with TOPO cloning reactions by heat shock transformation. 50 µL of cells were mixed with 2 µL ligation mixture and incubated on ice for 20-30 min. Cells were then heat shocked at 42°C for 30 sec. 250 µL SOC was then added and the mixture incubated on a shaker at 37°C for 1 h. Cells were then spread on LB plates containing kanamycin.

2.4.5.6.1. Cracking analysis of transformants

To determine if *E. coli* transformants contained insert DNA, a crude cracking analysis was performed. Colonies were picked and swirled in cracking buffer (50 mM NaOH, 0.05% (w/v) SDS, 5 mM EDTA) to lyse the cells. Samples were then heated to 70°C for 5 min to aid in cell lysis and reduce viscosity. 2-5 µL SDS loading dye was then added and the samples analysed by gel electrophoresis (Section 2.4.6). By comparison of banding patterns produced by vector only control samples to ligation samples the presence of insert was detected by a reduction in band mobility.

2.4.6. Agarose gel electrophoresis

Samples for gel electrophoresis were mixed with 0.1 volumes 10 x SDS loading dye (20% (w/v) sucrose; 5 mM EDTA; 1% (w/v) SDS; 0.2% (w/v) bromophenol blue; pH 8.0). Gels were prepared by dissolving agarose (Roche Diagnostics) in 1 x TBE

buffer (89 mM Tris; 89 mM boric acid; 2.5 mM Na_2EDTA, pH 8.2) in a microwave. The percentage of agarose in the gel was varied depending on the size of DNA fragments to be separated.

Table 2.3: Separation range for agarose gels

Percentage of Agarose (w/v)	Approximate Fragment Separation Range (kb)
0.7	2 – 25
1.0	0.5 – 10
1.6	0.2 – 4

The agarose solution was allowed to equilibrate to 55˚C before pouring. Electrophoresis was then performed in 1 x TBE buffer. Separation of plasmid digests and PCR reactions were performed at 90-100 V for 1-2 h. Separation of genomic DNA digests for Southern blotting was performed at 30 V overnight on 0.8% agarose gels. After electrophoresis, gels were stained with ethidium bromide (1 μg/mL in milli-Q water, prepared weekly) for 15-20 min. Bands were visualised and photographed using a UV transilluminator Gel Documentation system (Bio-Rad).

2.4.6.1. Electrophoresis of RNA

Electrophoresis of RNA samples to check quality and concentration was performed on SDS-agarose gels (1.4 % (w/v) agarose, 0.3% (w/v) SDS). RNA samples were mixed with 0.1 volumes of 10 x SDS loading dye and run at 90-100 V for 1-1½ h. Gels were stained and visualised as described in Section 2.4.6.

2.4.7. Southern blotting

E. festucae genomic digests were transferred to positively charged nylon membranes using a modification of the method of Southern (1975). Digestions were separated by gel electrophoresis on a 0.8% agarose gel overnight at 30 V. The gel was then stained with ethidium bromide and visualised as described in Section 2.4.6. Gels were then prepared

for blotting as follows: depurination by 15 min gentle agitation in blotting solution 1 (0.25 M HCl); denaturation by 45 min gentle agitation in blotting solution 2 (0.5 M NaOH, 0.5 M NaCl); and neutralisation by 45 min gentle agitation in blotting solution 3 (2.0 M NaCl, 0.5 M Tris, pH7.4). The gel was then washed for 2 min in 2 x SSC (0.3 M NaCl, 0.03 M trisodium citrate) and assembled onto a blotting stand prepared as follows: 2 x 3MM paper wicks soaked in 20 x SSC (3 M NaCl, 0.3 M trisodium citrate); covered with plastic wrap with a hole slightly smaller than the gel; gel placed on top and overlayed with the nylon membrane; 2 x 3MM paper pre-soaked in 2 x SSC; 2 x dry 3MM sheets, followed by a stack of paper towels and an evenly positioned weight. The DNA was then transferred to the membrane overnight. The membrane was then washed in 2 x SSC and the DNA crosslinked to the membrane using an Ultraviolet crosslinker Cex-800 (120,000 lJ/cm2) (Ultra-Lum Inc.).

2.4.7.1. Radioactive hybridisation

The PCR amplified replacement fragments used to replace *sakA*, *pakA* and *pakB* were used as probes to screen the corresponding transformants. 30 ng of each of these fragments was made single stranded by boiling for 3 min then placing directly on ice. These fragments were then radioactively labelled with [α-^{32} P]dCTP (3,000 Ci/mmol; Amersham Biosciences) using the High Prime kit (Roche Diagnostics) as per the manufacturer's instructions. Hybridisation was performed in glass hybridisation tubes (Amersham Biosciences). The membrane was first prehybridised in 10 x Denhardt's solution (0.4 M Hepes buffer (pH7.0), 3 x SSC, 0.02 mg/mL *E. coli* tRNA, 0.1% (w/v) SDS, 0.2% (w/v) ficoll, 0.2% (w/v) BSA, 0.2% (w/v) PVP, 0.0018% (w/v) phenol-extracted herring DNA). The labelled probe DNA was then denatured by boiling and added to the pre-hybridised membrane. After hybridisation, membranes were washed and hybridisation detected by exposure to X-ray film (Fuji) at -80°C. Length of exposure varied depending on signal intensity. Film was developed using a 100Plus™ automatic X-ray processor (All-Pro Imaging Corp.)

2.4.7.2. Stripping of radioactive membranes

Hybridised membranes were stripped using boiling 0.1% (w/v) SDS. The membrane was covered with the boiling SDS solution and left to agitate until the solution had cooled to RT. This process was then repeated a minimum of three times to ensure all radioactive probe DNA was removed from the membrane. The membrane was then checked using a Geiger counter to ensure all radioactive DNA had been removed.

2.4.8. Screening the cosmid library

To probe the cosmid library, small fragments of *sakA*, *pakA* and *pakB* were amplified with sak1/2, pak9/10 and pak11/12 primer sets respectively and radioactively labeled as for described in Section 2.4.7.1. Cosmid library filters were pre-hybridised in hybridisation buffer (1 mM EDTA, 7% (w/v) SDS, 1% (w/v) BSA (Invitrogen), 0.36 M Na_2HPO_4, 65 mM NaH_2PO_4, pH 8.0, 4˚C). for 2 h at 65˚C. Denatured probe was added to the buffer and hybridised overnight at 65˚C. The filter was then washed in wash buffer (0.1 x SSC; 0.1% (w/v) SDS) three times for 30 min at 65˚C. Filters were then exposed to X-ray film and developed as described in Section 2.4.7.1. Hybridised filters were then stripped as described in Section 2.4.7.2.

2.5. RNA isolation and manipulation

2.5.1. RNA isolation

Total RNA was extracted from *E. festucae* mycelium using TRIzol® reagent (Invitrogen). For isolation of *E. festucae* RNA, ~1 g of mycelia was ground in liquid nitrogen using a mortar and pestle pre-treated with RNase-away (Molecular BioProducts). Samples were then resuspended in 4 mL of TRIzol and centrifuged at 10,700 rpm for 10 min at 4°C. The supernatant was incubated at RT for 5 min before addition of 0.2 volumes of chloroform. The solution was then mixed for 15 s before incubation at RT for 3 min, followed by centrifugation at 10,700 rpm for 15 min at 4°C. RNA was precipitated by addition of isopropanol to the aqueous phase and incubation at RT for 10 min. The

RNA was then pelleted by centrifugation at 10,700 rpm for 10 min at 4°C, washed with 75% ethanol, air-dried and resuspended in DEPC-treated water.
Total RNA was isolated from *S. pombe* using the FastRNA® Pro Red kit (Qbiogene). Cells were grown in 5 mL EMM for 2 days, then cells harvested by centrifugation at 4,400 rpm for 2 min. RNA was isolated according to the manufacturer's instructions.

2.5.2. RT-PCR

5 μg of *S. pombe* total RNA or 1 μg *E. festucae* total RNA was heat denatured and reverse transcribed using SuperScript™ II RT (Invitrogen) according to the manufacturer's instructions. Specific amplification of *sakA*, *tubB* (ß-tubulin), *noxA* and *noxR* cDNAs were performed using the primer pairs sak24/sak39, T1.1/T1.2, noxAr/noxAf2 and Efp67-F1/Efp67-R1 respectively, using Platinum® *Pfx* DNA polymerase.

2.6. DNA sequencing and bioinformatics

2.6.1. DNA sequencing

DNA sequencing was performed by the Allan Wilson Centre Genome Service facility at Massey University using the BigDye™ Terminator (version 3.1) Ready Reaction Cycle Sequencing Kit (Applied Biosystems). Samples for sequencing contained 250 ng plasmid DNA and 3.2 pmol primer. Sequencing results were analysed using MacVector™ Assembler (Accelrys) or SEQUENCHER version 4.5 (Gene Codes).

2.6.2. Sequence comparison and domain characteristics

Comparison of *E. festucae* sequences to other sequences was performed at the National Centre for Biotechnology Information (NCBI) site (http://www.ncbi.nlm.nih.gov/) using the BLASTn, BLASTp and BLASTx algorithms (Altschul et al., 1997). Amino acid sequence similarity was assessed using MacVector™ ClustalW. Predicted intron/exon boundaries were analysed by Fgenesh at the Softberry site

(http://www.softberry.com/berry.phtml). Predicted protein domain structures were analysed using ExPASy PROSITE (http://au.expasy.org/prosite/).

2.6.3. Synteny analysis

Conserved micro-synteny between *E. festucae* and other Sordariomycetes was examined using the Fungal Genome Initiative (FGI) site (http://www.broad.mit.edu/) and *E. festucae* genome site (http://csurs.csr.uky.edu/biodb-testbed/). Synteny maps were prepared using MacVector™. *F. verticillioides*, *Fusarium graminearum*, *N. crassa* and *M. grisea* sequences were obtained from the FGI site. *T. reesei* sequences were obtained from the DOE Joint Genome Institute site (http://www.jgi.doe.gov/). *P. anserina* sequences were obtained from the *Podospora* Genome site (http://www.podospora.igmors.u-psud.fr/).

2.6.4. Bioinformatic analysis of MAP kinase cascades

Filamentous fungal homologues of *S. cerevisiae* proteins involved in MAP kinase signalling pathways were identified by BLASTp against the NCBI fungal database. The filamentous fungal sequence (generally from *M. grisea*) was then compared against the *E. festucae* genome (http://www.genome.ou.edu/fungi.html) using tBLASTn. This analysis identified the contig on which the *E. festucae* homolog was located. The corresponding gene on that contig was then identified by BLASTp comparison of the predicted polypeptide sequences for all genes on that contig against the fungal database at NCBI. The amino acid sequence similarity between the predicted *E. festucae* polypeptide and other filamentous fungal homologues was then analysed using MacVector™ ClustalW. Domain structures of predicted *E. festucae* polypeptides were analysed using ExPASy PROSITE.

2.6.5. Statistical analysis

The statistical significance of differences between wild-type *E. festucae* and mutant strains were analysed using the *t*-test. *p*-values were calculated using R (version 2.9.2) (http://www.r-project.org/). For comparisons between wild-type and mutant strains, or mutant and complemented strains, one-tailed calculations were performed based on the

assumption that the mutant would be less than the other strains. For comparisons of the wild-type and complemented strains two-tailed calculations were performed.

2.7. PCR analysis

Primers used in this study are listed in Table 2.4.

Table 2.4: Primers used in this study

Name	Sequence (5' – 3')	Used for
sak1	TGCGAYTTGAAGATYTGCGA	Degenerate PCR
sak2	TCDGCRTCRTTGAARCTCCA	Degenerate PCR
sak22	GGATCCTCAATGACGCCGACCTGC	KO construct preparation
sak23	AAGCTTACCTCGCTATCTGGTGGCC	KO construct preparation
sak24	CATATGGCTGAATTCGTGCGTGCCC	Translational fusion PCR
sak39	GGATCCATGCTGTCGCTGTCTTTCGC	Translational fusion PCR
sak40	GCTTACGCCTTGGAAATAGG	KO screening
sak41	GAGGGTCTTGGATTCTTGCC	KO screening
sak57	GGATCCTTGTCCATTGAAATCTTGGCC	Translational fusion PCR
sak60	GAATTCATGGCTGAATTCGTGC	Translational fusion PCR
pak1a	AAGATYGGHCARGGTGCNTCYGG	Degenerate PCR
pak1b	TCCATRWAYTCCATDACNACCC	Degenerate PCR
pak1	GGTACCAGCAGTCGTTAGACAATACCG	KO construct preparation
pak2	GAATTCAACGAAGAACCAGACACACCC	KO construct preparation
pak3	CTGCAGATACTTACTGGTGGAGGTGGC	KO construct preparation
pak4	GGATCCATCCTGTTAGTCCAAGGGTTG	KO construct preparation
pak5	CTCGAGAATGAGGGATGGCTTGTTCTG	KO construct preparation
pak6	GGATCCCTGTCCTTTCTGGTTTGGTGC	KO construct preparation
pak7	GGTACCCAACTTCTATCTCGTTAGCCG	KO construct preparation
pak8	AGATCTTCATAGAGGGCATAGAGACCG	KO construct preparation
pak9	GGTTGGGCATCAGTCAAGGAG	KO screening
pak10	TGGGTTTTCGGCTCTCTTAGC	KO screening
pak11	CATCCTGCTGTTTCTCAGTGG	KO screening
pak12	GATTGGCTTCTTTTGTGACCC	KO screening

pak13	GGACGACTAAACCAAAATAGG	KO screening
pak14	TTCCTCTCTCATCCAACGCCC	KO screening
pak15	TCTCTCACGGAGTCTCTTACG	KO screening
pak16	CACGAGCAGGGGTGAAAATCG	KO screening
pak17	ATTGACGGCGGTTATTCTTGC	KO screening
pak22	GAAAAATGGCGTGCTCAGTTGTTAC	*pakA* complementation
pak23	ACGCCTCCCAGCCGCTAGATGAA	*pakA* complementation
pUChph6	ACTTCGAGCGGAGGCATC	KO screening
pII99-2	TTGAGTGAGCTGATACCG	KO construct amplification
pII99-3	GGCTGGCTTAACTATGCG	KO construct amplification
T1.1	GAGAAAATGCGTGAGATTGT	β-tubulin expression analysis
T1.2	TGGTCAACCAGCTCAGCACC	β-tubulin expression analysis
noxAr	TGCAGAGGAGCATGACATGT	*noxA* expression analysis
noxAf2	CAACAGAAATTACCATGGCG	*noxA* expression analysis
Efp67-F1	CTGGCTCGATATGATAAC	*noxR* expression analysis
Efp67-R1	TGAAGAGTACTTCGCACG	*noxR* expression analysis

2.7.1. Standard PCR

Standard PCR amplification was performed with Taq DNA polymerase (Roche Diagnostics) using 1 ng plasmid DNA or 10 ng *E. festucae* genomic DNA template.

2.7.2. Extract-N-Amp PCR

Crude PCR analysis of *E. festucae* transformants was performed using the Extract-N-Amp Plant PCR kit (Sigma-Aldrich) according to the manufacturer's instructions with slight modifications to account for the use of a plant PCR kit with fungal tissue. For DNA extraction, a small piece of mycelium just big enough to cover the tip of a scalpel blade was scraped from fresh fungal colonies. This was placed into a tube with 50 μL extraction solution, vortexed, then incubated at 95°C for 10 minutes. Tubes were then placed on ice and 50 μL cold dilution buffer added. Samples were briefly vortexed and the DNA extract stored at 4°C until required for PCR. PCR reactions recommended by the manufacturer were scaled to a quarter reaction containing 2.5 μL Extract-N-Amp PCR reaction mixture, 20 μM of each primer and 0.5 μL of the DNA extract.

2.7.3. High fidelity enzymes

PCR products to be expressed were amplified using proof-reading enzymes Platinum® *Pfx* DNA polymerase (Invitrogen) or Expand HiFi (Roche Diagnostics) according to the manufacturer's instructions with 1 ng plasmid DNA or 1 μL cDNA as template. Primers contained restriction endonuclease recognition site overhangs to facilitate cloning. PCR products were A-tailed (Section 2.4.5.1), ligated into pCR4-TOPO and sequenced to confirm the absence of polymerase-induced errors. Products were then sub-cloned using the appropriate restriction endonucleases into the expression vector.

2.8. Fungal transformations

2.8.1. *E. festucae*

2.8.1.1. Protoplast preparation

Wild-type *E. festucae* protoplasts were prepared as previously described (Young et al., 2005). Ground mycelium was used to inoculate 50 mL of PD broth and cultures were then grown at 22°C for 7 days. Mycelia were then harvested, washed three times with sterile milli-Q water and once with OM buffer (1.2 M $MgSO_4.7H_2O$, 10 mM Na_2HPO_4, pH adjusted to 5.8 with 100 mM $NaH_2PO_4.2H_2O$). The mycelia were then weighed and an appropriate volume of 10 mg/mL filter-sterilised glucanex (Chemcolour) added to give ~10 mL per 1.2 g of mycelia (wet weight). Mycelia were digested at 30°C for 4-5 h, shaking at ~80 rpm. Samples were filtered through a nappy liner to remove undigested mycelia. Protoplasts were then harvested from the filtrate by overlaying with 2 mL ST buffer (0.6 M sorbitol, 100 mM Tris-HCl, pH 8) and centrifuging at 4,000 rpm for 10 min. Protoplasts formed a band at the glucanex-ST interface. This band was removed and the protoplasts washed with STC buffer (1 M sorbitol, 50 mM $CaCl_2$, 50 mM Tris-HCl, pH 8). The protoplasts were then pelleted by centrifugation at 4,000 rpm for 10 min. The pellet was resuspended in 5 mL STC and centrifuged at 4,000 rpm for 10 min. This washing step was repeated a further 1-2 times

before the protoplasts were resuspended in STC to a final concentration of 1.25 x 10^8 protoplasts/mL. For long term storage 80 µL protoplast aliquots were mixed with 20 µL PEG buffer (40% PEG 4000, 50 mM $CaCl_2$, 1 M sorbitol, 50 mM Tris-HCl, pH 8) and stored at -80°C.

Given the osmosensitive nature of Δ*sakA*, protoplast preparation for complementation of Δ*sakA* was slightly modified. Mycelia were incubated with glucanex for 2 h to avoid prolonged exposure to the high osmolarity buffer. For isolation of Δ*pakA* protoplasts, two wash steps were performed to reduce the loss of small protoplasts during washing. The protoplast band at the glucanex-ST interface was washed with STC and the protoplasts pelleted by centrifugation. The pellet was then washed once with STC before being resuspended to a final concentration of 1.25 x 10^8 protoplasts/mL.

2.8.1.2. Transformation

Protoplasts were transformed using the method of Itoh et al. (1994). 5 µL heparin (5 mg/mL), 2 µL spermidine (50 mM) and 5 µg DNA were added to 80 µl protoplasts (or 80 µl protoplasts + 20 µl PEG buffer). Samples were then mixed gently and incubated on ice for 30 min, 900 µL PEG buffer then added, gently mixed and incubated for a further 15-20 min on ice. 330 µL aliquots were then added to 3.5 mL molten 0.8% (w/v) RG medium and the mixture spread on RG plates. After incubation at 22°C for ~24 h plates were overlayed with 5 mL molten 0.8% (w/v) RG containing hygromycin or geneticin to give final concentrations of 150 µg/mL and 200 µg/mL respectively. Plates were then incubated at 22°C for a further 10-14 days. Transformants that grew through the overlay were sub-cultured onto PD medium containing hygromycin or geneticin. Transformants were nuclear purified by a minimum of three rounds of sub-culturing on PD medium containing antibiotic. For replacement of *sakA*, *pakA* and *pakB* protoplasts were transformed with 5 µg linear PCR product amplified using the Expand Long Template PCR system (Roche Diagnostics) from pCE12, pCE36 and pCE38 respectively using primers pII99-2 and pII99-3. For complementation of Δ*sakA*, protoplasts were transformed with 5 µg circular pCE1 and pII99. For complementation of Δ*pakA*, protoplasts were transformed with 5 µg circular pCE43 and pII99, and for complementation of Δ*pakB*, protoplasts were transformed with 5 µg circular pCE42.

2.8.2. *S. pombe* lithium-acetate/PEG transformation

S. pombe cells were grown to log phase (1-4 x 10^6 cells/mL) and pelleted by centrifugation at 3,000 rpm for 3 min. The cells were washed with lithium acetate (0.1 M, pH 4.9), then resuspended in 100 μL lithium acetate per transformation reaction and incubated at 25°C for 1 h to permeabilise the cell membranes. The mixture was then vortexed and 100 μL added to 100 μL PEG containing 3-5 μg of the DNA to be transformed. The cells were incubated with the DNA at 25°C for 1 h, then heat shocked by incubation at 42°C for 10 min. The cells were pelleted by centrifugation at 13,000 rpm for 2 min, then resuspended in 100 μL milli-Q water, spread on EMM agar plates and incubated at 25°C for 7-10 days. Transformants were then screened for their ability to grow in the absence of leucine by streaking on unsupplemented EMM.

2.9. Plant inoculation and growth analysis

2.9.1. Seed sterilisation

Endophyte free *L. perenne* (cultivar Samson) seeds were surface sterilised by immersion in 50% sulfuric acid for 30 min, followed by three washes with milli-Q water then immersion in 50% bleach for 20 min. The sterilised seeds were then washed three times with sterile milli-Q water and allowed to air-dry.

2.9.2. Seedling germination and inoculation

Surface sterilised *L. perenne* seeds were germinated on water agar plates (3% agar (w/v)) incubated at 22°C in the dark for 7 days. The seedlings were then inoculated using the method of Latch and Christensen (1985), and incubated for a further 7 days in the dark at 22°C. The seedlings were then transferred to light conditions and incubated for a further 7 days at 22°C. The seedlings were then transferred to the AgResearch greenhouse and planted in root trainers containing potting mix.

2.9.3. Immunoblotting

To determine if inoculated seedlings were systemically infected with endophyte, they were immunoblotted 4-6 weeks after planting. Tillers were cut close to their base, dead outer leaf sheaths removed and the cut end of the tiller pressed onto nitrocellulose membrane. The membrane was then soaked in blocking solution at RT for a minimum of 2 h. The membrane was then transferred to fresh blocking solution containing primary antibody (1:1000 dilution) and incubated at 4°C overnight. Several washes with fresh blocking solution were then performed to remove unbound primary antibody from the membrane. The membrane was then transferred to blocking solution containing secondary antibody (1:2000 dilution) and incubated at RT for 2 h. Unbound secondary antibody was then washed off by several washes with fresh blocking solution. The membrane was then transferred to fresh chromogen solution (a mixture of 12.5 mg Fast red in 12.5 mL Tris buffer and 12.5 mg naphthol AS-MX phosphate in 12.5 mL Tris buffer) and incubated at RT for 15 min to develop the colour. The membrane was then rinsed with water to remove excess chromogen, and allowed to dry.

2.9.4. Aniline blue staining

To detect fungal hyphae *in planta*, epidermal peels were taken from the inner surface of the outer leaf sheath. Peels were mounted in aniline blue stain (lactic acid 88%, glycerol 50%, aniline blue 0.1% (w/v)), covered with a coverslip and heated briefly to aid stain penetration and remove air bubbles. Samples were observed by light microscopy.

2.10. Plant sectioning and staining

2.10.1. Tissue fixation and wax embedding

Tissue for wax embedding was fixed in fresh FAA (3.7% (v/v) formaldehyde, 5% (v/v) glacial acetic acid, 50% ethanol). Samples were vacuum infiltrated for ~15 min or until

the tissue sunk and bubbles ceased to rise to the surface. Samples were then left in FAA for 4 h at RT. The tissue was then incubated in 70% ethanol overnight at 4°C. Samples were then dehydrated through a graded ethanol series at RT as follows: 2 h in 85% and 95% ethanol, then 2 x 2 h in 100% ethanol. The tissue was then incubated in 100% ethanol overnight at 4°C. Next the ethanol was replaced with Histoclear (National Diagnostics) by passage through a graded Histoclear:ethanol series. Samples were incubated for 1 h at RT in: 25% histoclear:75% ethanol, 50% histoclear:50% ethanol, 75% histoclear:25% ethanol, 3 x 100% Histoclear. The Histoclear was then gradually replaced with Paraplast X-tra (McCormick Scientific). The tissue was transferred to 50% Histoclear:50% molten Paraplast X-tra. The samples were then incubated at 60°C until the Paraplast X-tra melted. The tissue was then transferred to 100% Paraplast X-tra and incubated at 60°C overnight. A minimum of six 3 h incubations in fresh Paraplast X-tra at 60°C were performed before the tissue was finally embedded in moulds containing Paraplast X-tra. 10-12 μm sections were then prepared from the wax embedded samples using a Leica RM 2145 Rotary Microtome and mounted onto slides.

2.10.2. Alcian blue/safranin O Staining

Slides were incubated in Histoclear for 2 x 10 min to remove the Paraplast X-tra from the samples. The Histoclear was then replaced with isopropanol and the slides incubated for 2 x 5 min to dehydrate the samples. The slides were then air-dried for ~1 h. Samples were then stained with Alcian blue/Safranin O (1% (w/v) Alcian blue 8GX, 1% (w/v) safranin O, 50% (v/v) isopropanol, 2.5% (v/v) glacial acetic acid, 0.08% (v/v) formalin pH5.0) for 15 min, dipped in milli-Q water to remove excess stain and air-dried on a slide warmer at 42°C for 20-30 min. 22x60 mm coverslips were then mounted onto the slides in Entellan (Merck).

2.11. Microscopy

For microscopic observation of *E. festucae* strains, cultures were grown on slide plates. Approximately 20 mL of PD agar was poured into Petri dishes and allowed to set.

Sterile slides were then placed on top of the PD agar and overlayed with 8-10 mL of PD agarose (2% w/v). Cultures were then inoculated adjacent to the slide and incubated at 22°C for ~7 days or until the colonies started to grow across the slide. Fluorescence and DIC microscopy was performed using an Olympus IX71 microscope with a ×63 or a ×100 oil immersion objective, NA = 1.4. Photographs were taken with a Hamamatsu ORCA- ER C4742-80 digital CCD camera (Hamamatsu Corporation) and analysed using Metamorph software (Molecular Devices Corporation). Confocal microscopy was performed using a Leica TCS SP5 confocal microscope. Bright field microscopy was performed using a Zeiss Axiophot light microscope and images recorded using a Leica DCF320 digital camera.

2.11.1. Light microscopy

To quantify changes in *S. pombe* cell length, cells were observed by DIC (differential interference contrast) microscopy 19, 22, 25 and 27 h following release of thiamine repression at a density of 2-4 x 10^6 cells/mL. At least 100 cells were measured for each sample and average lengths calculated. Results are representative of three independent experiments. Growth of *E. festucae* strains in culture was examined using DIC microscopy. Superoxide production by *E. festucae* strains was visualised by bright field microscopy of NBT stained samples. *In planta* samples stained with Alcian blue/safranin O, aniline blue, toluidine blue, or Lactophenol trypan blue were also observed by light microscopy.

2.11.2. Fluorescence microscopy

Samples for fluorescence microscopy were kept in the dark after staining to prevent photobleaching.

2.11.2.1. GFP

GFP localisation in *S. pombe* was performed in an imaging chamber (CoverWell, 20 mm diameter, 0.5 mm deep) (Molecular Probes) filled with 800 μL of 2% agarose in EMM

and sealed with a 22x22 mm glass coverslip. Cells were observed under UV light, and for osmotic stress induction, the EMM agarose was supplemented with 0.6 M KCl.

2.11.2.2. FM4-64

For visualisation of vacuoles in *E. festucae* strains, samples were stained with FM4-64. 4-5 x 1 μL aliquots of FM4-64 (stock concentration 1.64 mM in DMSO, diluted to 16.4 μM with milli-Q prior to use; Invitrogen) were spotted around the edge of the colony. A sterile coverslip was then mounted on the colony and incubated at 22°C for ~28 h. Fluorescence was then observed under UV light.

2.11.2.3. Calcofluor white (CFW)

For visualisation of chitin deposits, samples were stained with calcofluor white by spotting 4-5 x 1 μL aliquots of 3 μg/mL CFW (Fluorescent brightener 28; Sigma) around the edge of the colony then mounting a coverslip. Samples were incubated at RT for 2-5 min then fluorescence observed under UV light. Cell compartment lengths were then measured as the distance between septa using Metamorph software. The width of cell compartments was measured at the septa.

2.11.3. Confocal microscopy

Calcofluor white stained fungal hyphae and EGFP-expressing hyphae growing *in planta* were examined using a Leica SP5 DM6000B Confocal microscope. For examination of fungal growth *in planta*, whole leaf sheathes were mounted in water and optical sections taken at 2 μm intervals through 50 μm depth.

2.11.4. Transmission electron microscopy

For examination of hyphal structure, small pieces (0.5-1 mm thick) of pseudostem tissue from endophyte-infected plants were fixed in 3% glutaraldehyde and 2% formaldehyde

in 0.1 M phosphate buffer, pH7.2 for 1 h and then transverse sections prepared for light microscopy and TEM as described by Spiers and Hopcroft (1993). For light microscopy, the sections were stained with toluidine blue as described by Christensen et al. (2002). A Philips CM10 transmission electron microscope was used to examine hyphal structure and images were recorded using a SIS Morada digital camera.

2.11.4.1. Cerium chloride staining for ROS

To detect hydrogen peroxide *in planta*, a modified cytochemical method was used (Briggs et al., 1975; Bestwick et al., 1997). Approximately 3-4 mm sections from the meristematic zone of endophyte-infected plants were vacuum-infiltrated with 5 mM $CeCl_3$ solution buffered with 50 mM 3-(N-morpholino)-propanesulfonic acid (MOPS), pH 7.2 or MOPS only. Samples were then fixed in 3% glutaraldehyde buffered with 0.1 M cacodylate buffer, pH 7.2 for 1 h. Samples were then incubated in 1% osmium tetroxide at RT for 30 min – 1 h, followed by dehydration through an acetone series and infiltration and embedding in Procure 812 epoxy resin. Samples were prepared for TEM as described by Shinogi et al. (2001), observed with a Philips CM10 transmission electron microscope and images recorded using a SIS Morada digital camera.

2.11.5. Scanning electron microscopy

For examination of epiphyllous hyphae by scanning electron microscopy (SEM), plants were inoculated with the *E. festucae* strains then grown under sterile conditions on MSO-phytoagar to prevent surface contamination by other fungi. Blade and sheath samples were incubated in fixative (3% glutaraldehyde and 2% formaldehyde in 0.1 M phosphate buffer, pH 7.2) for a minimum of 24 h at room temperature. Samples were then washed three times with 0.1 M phosphate buffer (pH 7.2) before being dehydrated by passage through a graded ethanol series. Samples were then critical point dried using liquid CO_2. Dried samples were mounted onto aluminium specimen support stubs, sputter-coated with gold, and observed using an FEI Quanta 200 SEM.

2.12. Protein isolation and analysis

2.12.1. Protein isolation from *S. pombe*

Total protein was isolated from 50 mL *S. pombe* culture as previously described (Daga et al., 2003). Cells were pelleted by centrifugation at 3,000 rpm for 2 min. The pellet was then resuspended in 100 µL ice-cold extraction buffer (50 mM Hepes, 50 mM NaF, 50 mM Na-β-glycerophosphate, 5 mM EGTA pH 8, 5 mM EDTA pH 8, 0.2% (w/v) Triton-X-100, 1 mM PMSF and protease inhibitor cocktail). The cells were mixed with glass beads by vortexing and ribolysed in a FastPrep® Cell Disrupter (Qbiogene, Inc) at 4°C for 20 s at power 6.5. Extra extraction buffer was added to cool the sample, which was vortexed and placed on ice. The supernatant was then snap frozen in liquid nitrogen and stored at -80°C. Protein concentrations were determined by the Bradford Assay (Bradford, 1976).

2.12.2. Western blotting

For western blotting, 50 µg of each protein sample was separated on an 8% SDS-polyacrylamide gel. The gel was soaked briefly in transfer buffer (369 mM Tris, 390 mM glycine, 20% (v/v) isopropanol), assembled onto a semi-dry transfer machine (Bio-Rad) and the proteins transferred to nitrocellulose membrane at 10V for 30 min. After transfer, the membrane was stained with Ponceau red (0.2% (w/v) Ponceau red, 1% (v/v) glacial acetic acid) for 5 min to allow visualisation of transferred proteins. The membrane was then destained with 1% (v/v) glacial acetic acid. Excess glacial acetic acid was removed by several washes in blocking solution. The membrane was then incubated with anti-Hog1 antibody (Santa Cruz Biotechnologies sc-9079) (1:200 dilution), and TAT-1 anti-tubulin antibody (obtained from K. Gull, Oxford, UK) (1:1000) as an internal loading control. The membrane was incubated with secondary horseradish peroxidase (HRP) conjugated anti-rabbit antibody (Promega) (1:2500) and HRP-conjugated anti-mouse antibody (Promega) (1:2500). Binding of the secondary antibodies was detected using the Super Signal Kit (Pierce).

2.13. Colony staining

2.13.1. Diaminobenzidine

Cultures were stained with freshly prepared DAB (1 mg/mL in milli-Q water, ~pH 3.2; Sigma-Aldrich) in the dark at RT for ~24 h then 4°C for ~24 h or until brick-red precipitate formed.

2.13.2. Nitroblue tetrazolium

Cultures were stained with NBT (0.05% in 50 mM sodium phosphate buffer, pH 7.5; Sigma-Aldrich) for ~5 h at RT. The reaction was terminated by flooding with 100% ethanol, and precipitate formation examined by light microscopy.

2.14. Host defense response analysis

2.14.1. Lactophenol-trypan blue staining

For examination of any potential host defense response induced by the Δ*sakA* mutant, blade and pseudostem tissue were stained with Lactophenol trypan blue as previously described (Koch and Slusarenko, 1990). Plants were grown on MSO-phytoagar under sterile conditions to prevent surface contamination. Blade and pseudostem samples were cleared by incubation in methanol for at least 24 h. Tissue was then transferred to Lactophenol trypan blue (33% (v/v) lactic acid, 33% (v/v) glycerol, 0.03% (w/v) trypan blue, 33% (w/v) phenol) and boiled for 5 min. The tissue was then transferred to fixation solution (50 g chloral hydrate in 50 mL milli-Q water) and allowed to clear for at least 2 h while gently shaking. Samples were then viewed by light microscopy.

3. Role of *sakA* in Maintenance of Symbiosis

3.1. Isolation of the *E. festucae* stress-activated MAP kinase

PCR amplification of *E. festucae* genomic DNA using degenerate primers, sak1 and sak2, designed to amplify fungal stress-activated MAP kinases, but not other classes of MAP kinases, generated a 660bp product which was used to screen an *E. festucae* cosmid library (Tanaka et al., 2005; Eaton et al., 2008). Cosmid clone 44D6 was isolated and a 12kb *Bam*HI fragment containing the putative stress MAP kinase gene sub-cloned into pUC118 and sequenced (Eaton, 2005). Analysis of this sequence identified a 1,672 bp coding region, designated *sakA*. Sequencing of the full-length cDNA confirmed the presence of eight introns. Conceptual translation of the *sakA* gene gives rise to a 358 amino acid polypeptide which shares considerable sequence identity with other fungal stress MAP kinases (Fig. 3.1). For example, *E. festucae* SakA shows 95% amino acid identity (ID) to FgHog1 from *F. graminearum*, 93% ID to Os-2 from *N. crassa* and OSM1 from *M. grisea* and 81% ID to Sty1 from *S. pombe*. Analysis of the predicted SakA polypeptide using ExPASy PROSITE identified multiple domains characteristic of MAP kinases (Fig. 3.2). These include a highly conserved TXY lip (X=glycine) between amino acids 171–173, the target site for dual phosphorylation by the upstream MAPKK, an ATP binding region between amino acids 26–50, and a serine/threonine protein kinase catalytic domain between amino acids 19–299 (Hanks and Hunter, 1995).

3.2. The *sakA* locus displays conserved micro-synteny

Comparison of the *E. festucae sakA* (44D6-6) locus with stress-activated MAP kinase loci from *F. verticillioides*, *F. graminearum*, *T. reesei*, *N. crassa*, *P. anserina*, and *M. grisea* revealed significant conservation of micro-synteny (Fig.3.3; Table 3.1). All species examined contain genes encoding a carbohydrate phosphorylase (44D6-5) and a conserved hypothetical protein (44D6-3) at this locus. With the exception of *N. crassa*, all these species also contain a linked G-protein alpha subunit-encoding gene (44D6-4). In *N. crassa*, this gene is adjacent to genes encoding a cullin-like protein (44D6-2) and

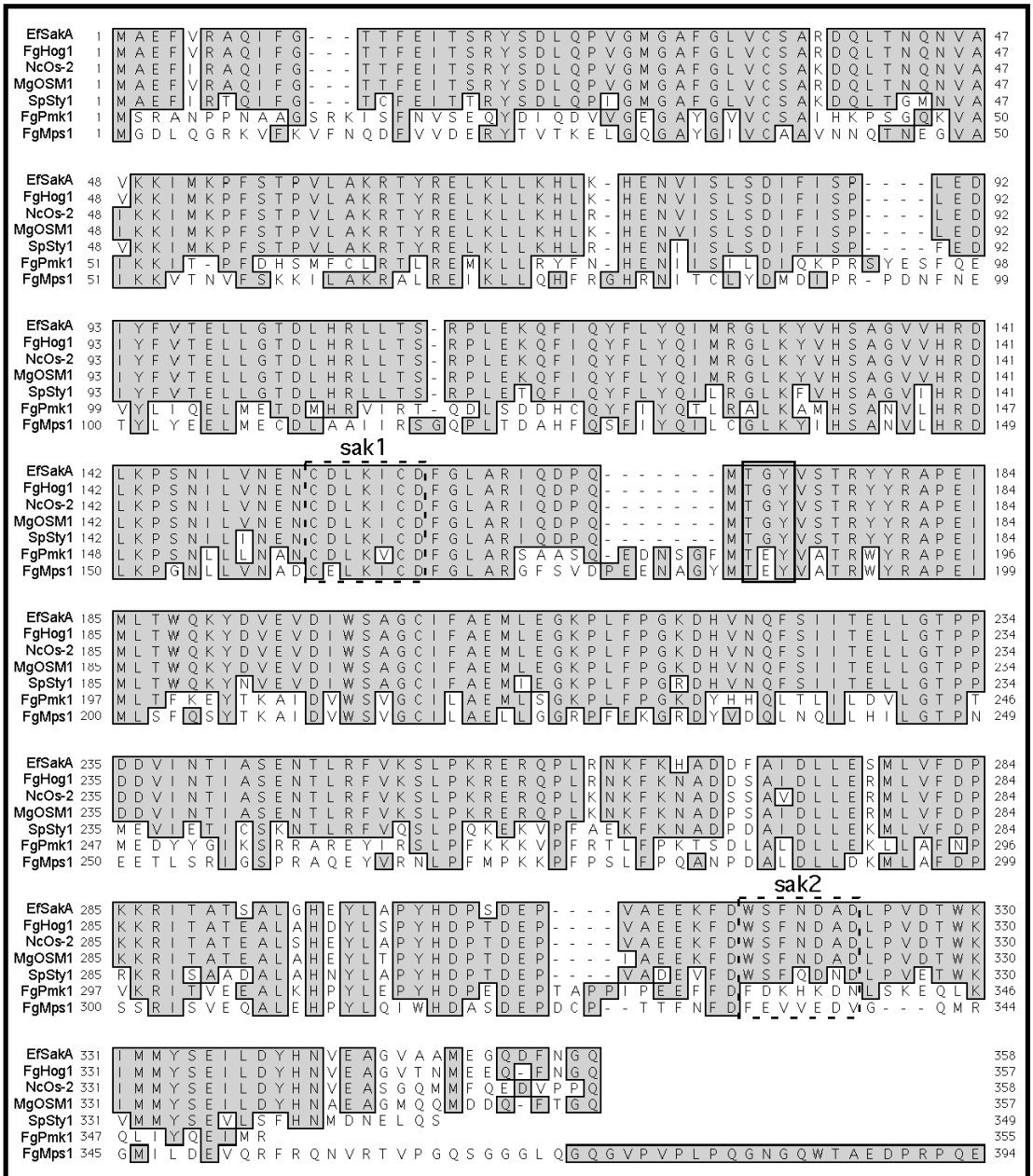

Figure 3.1 Amino acid sequence alignment of fungal MAP kinases
The predicted amino acid sequence of *E. festucae* SakA (EfSakA) is aligned with stress MAP kinases from *F. graminearum* (FgHog1), *N. crassa* (NcOs-2), *M. grisea* (MgOSM1), and *S. pombe* (SpSty1); and two non-stress activated MAP kinases from *F. graminearum* (FgPmk1 and FgMps1). Dashed black boxing indicates regions to which degenerate primers sak1 and sak2 were designed. Solid boxing indicates the position of the highly conserved TGY lip. Adapted from Eaton (2005). In Institute of Molecular BioSciences.

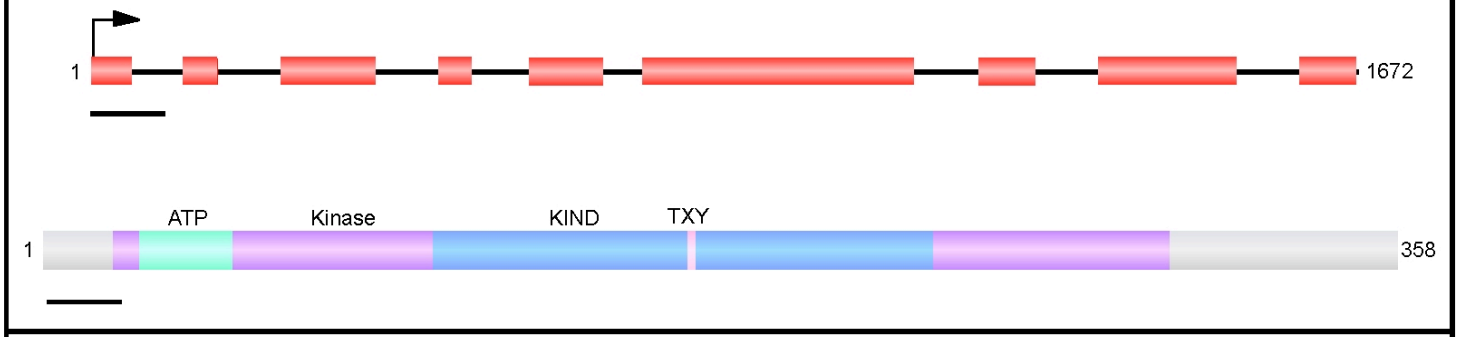

Figure 3.2 Organisation of the *E. festucae sakA* gene and predicted polypeptide
The *sakA* gene is 1672 bp and contains nine exons (red boxes) separated by eight introns whose positions were confirmed by sequencing full length cDNA. The predicted SakA polypeptide is 358 amino acids in length and contains a serine/threonine protein kinase catalytic domain (purple); protein kinase non-catalytic C-lobe domain (KIND, blue); ATP binding signature (green); and a highly conserved TXY lip (pink). Bar = 100 bp and 20 aa for *sakA* gene and predicted polypeptide respectively.

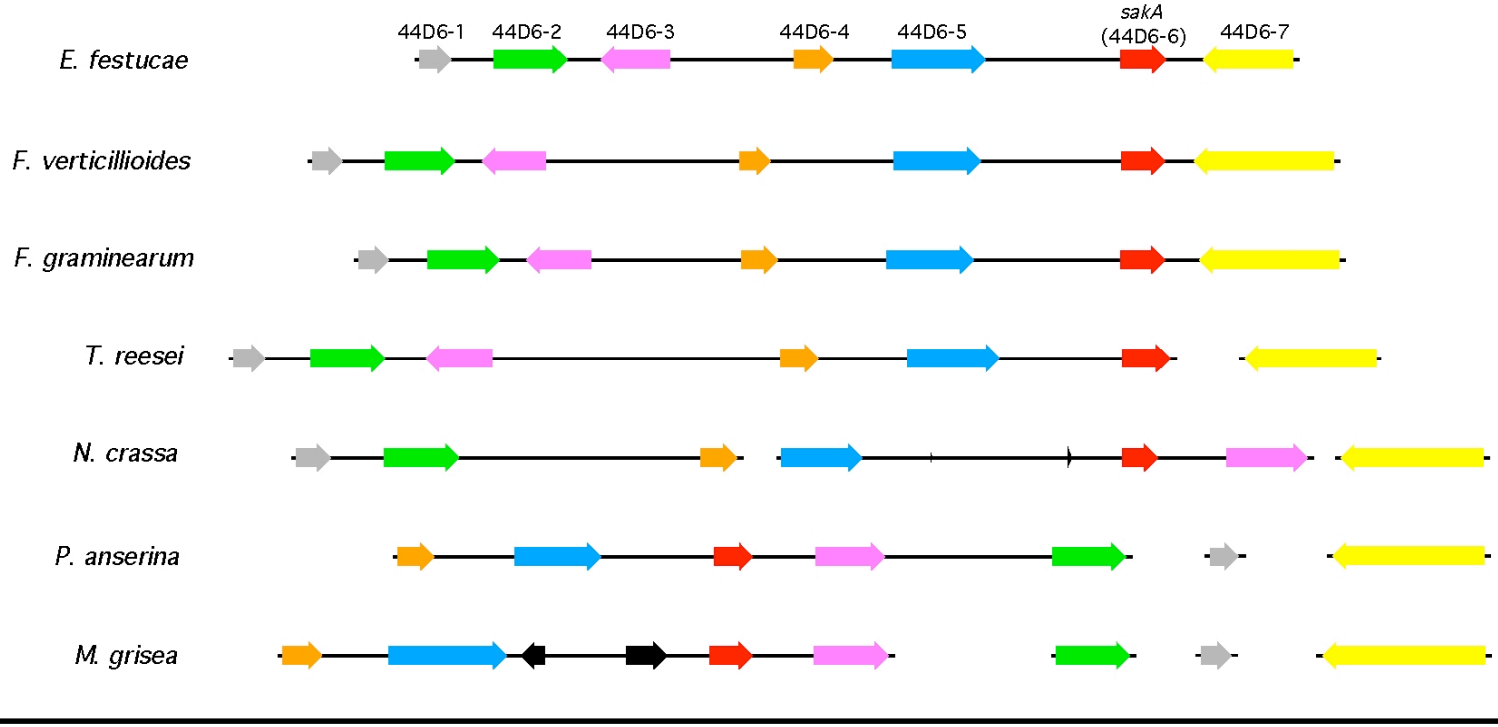

Figure 3.3 Conserved micro-synteny at the *sakA* locus
The *E. festucae sakA* locus displays conserved synteny with *Fusarium verticillioides*, *F. graminearum*, *Trichoderma reesei*, *N. crassa*, *Podospora anserina* and *M. grisea*. *E. festucae* genes are numbered based on position in the 44D6 cosmid clone (refer Table 3.1). Matching coloured arrows represent orthologous genes. Non-conserved genes are represented in black.

Table 3.1 Description of genes displaying conserved synteny at the stress-activated MAP kinase locus

		Annotated/autocalled gene in fungal genome database											
		F. verticillioides		*F. graminearum*		*T. reesei*		*N. crassa*		*P. anserina*		*M. grisea*	
Gene	Putative function	Annotation	E-value	Annotation	E-value	Annotation[a]	E-value	Annotation	E-value	Annotation[b]	E-value	Annotation	E-value
44D6-1	Conserved hypothetical protein	FVEG_04173	0	FG09617	2e-110	74932	8e-89	NCU05203	3e-79	Pa_1_23900	7e-71	MG06053	2e-59
44D6-2	Cullin	FVEG_04172	0	FG09616	0	55706	0	NCU05204	0	Pa_1_23890	0	MG07145	0
44D6-3	Conserved hypothetical protein	FVEG_04171	0	FG09615	2e-127	26151	0	NCU07023	2e-105	Pa_1_23920	1e-108	MG01823	3e-84
44D6-4	G protein alpha subunit	FVEG_04170	0	FG09614	8e-173	21505	0	NCU05206	5e-158	Pa_1_23950	1e-149	MG01818	2e-167
44D6-5	Carbohydrate phosphorylase	FVEG_04169	0	FG09613	0	120198	0	NCU07027	0	Pa_1_23940	0	MG01819	0
44D6-6	Stress-activated MAP kinase	FVEG_04168	0	FG09612	0	45018	0	NCU07024	0	Pa_1_23930	0	MG01822	0
44D6-7	ABC transporter	FVEG_04167	9.8e-38	FG09611	0	55747	0	NCU06382	2e-165	Pa_2_6480	1e-38	MG06024	3e-60

a. Protein ID numbers from the DOE Joint Genome Institute site (http://www.jgi.doe.gov/)
b. Annotation from the *Podospora* genome site (http://podospora.igmors.u-psud.fr/)
c. Annotation from the Fungal Genome Initiative site (http://www.broad.mit.edu/)

another conserved hypothetical protein (44D6-1). This cullin-like gene is found at the stress MAP kinase locus in all other species examined except *M. grisea*, and the conserved hypothetical gene is linked in all other species examined except *M. grisea* and *P. anserina*. *E. festucae* and the two *Fusarium* species examined also contain an ABC transporter-encoding gene (44D6-7) at this locus.

3.3. SakA is a functional orthologue of *S. pombe* Sty1

To determine if the *E. festucae sakA* gene encodes a functional stress-activated MAP kinase, complementation of the stress sensitivity and cell cycle defects of a *S. pombe sty1*Δ mutant was tested. *S. pombe* rather than *S. cerevisiae* was used because of the greater level of amino acid identity between SakA and Sty1 (81%) compared to HOG1 (65%). Expression constructs containing either the 1.7 kb *sakA* gene (gDNA) or 1.1 kb full length *sakA* coding sequence were prepared by cloning these fragments as translational fusions with the *S. pombe* thiamine repressible *nmt1* promoter of the pREP81 vector (Basi et al., 1993), generating pCE22 and pCE23 respectively. pREP81 vector alone, and a construct containing 6×His and HA tagged *S. pombe sty1* in pREP81 were also included in the complementation experiments.

3.3.1. Complementation of stress sensitivity

To determine whether *sakA* can complement the stress sensitivity defects of the *sty1*Δ mutant, the complementation constructs were transformed into *sty1*Δ cells and tested for their ability to grow under conditions of osmotic and oxidative stress (Fig. 3.4). All strains grew equally well on unsupplemented EMM, whereas only wild-type *S. pombe* and *sty1*Δ strains containing *sty1* or *sakA* cDNA displayed significant growth on EMM under conditions of osmotic or oxidative stress. This suggests *sakA* cDNA is able to functionally complement the stress sensitivity defect of the *S. pombe sty1*Δ mutant, whereas *sakA* gDNA is not.

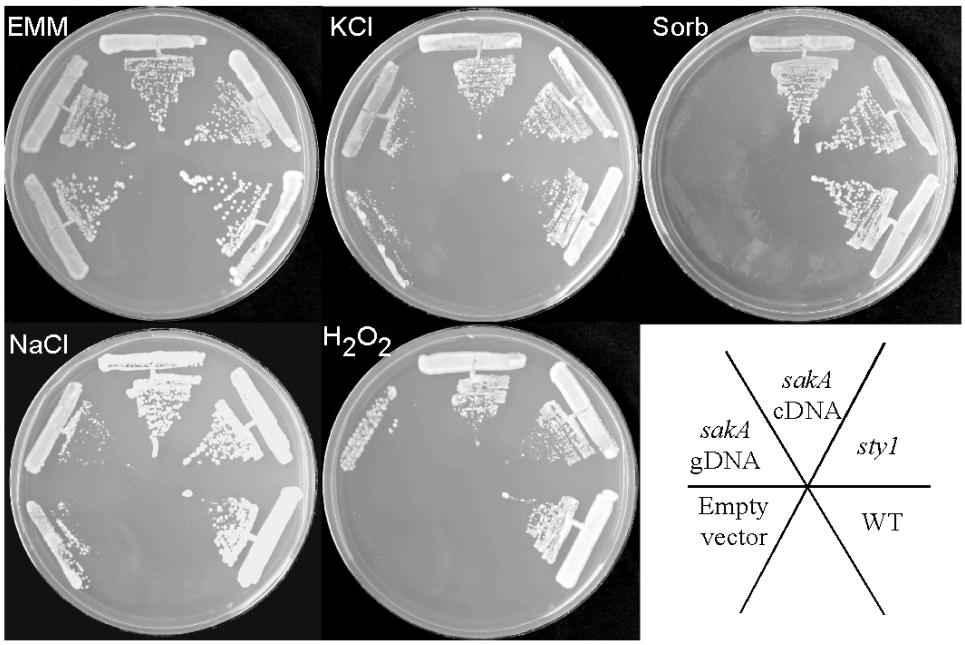

Figure 3.4 Complementation of *S. pombe sty1*Δ stress sensitivity
Wild-type (WT) *S. pombe* and the *sty1*Δ mutant carrying empty pREP81 vector or plasmids expressing the *E. festucae sakA* gene (*sakA* gDNA), *sakA* cDNA or *S. pombe sty1* were streaked onto EMM containing no stress agents (EMM), 0.6 M KCl, 1.5 M sorbitol (sorb), 0.1 M NaCl, or 0.6 mM hydrogen peroxide (H_2O_2) and incubated at 25˚C.

3.3.2. Complementation of cell morphology defect

To determine whether *sakA* was also able to rescue the cell cycle defect of *sty1*Δ, the morphology of the various transformants was observed by microscopy (Fig. 3.5A). A key morphological indicator of the *sty1*Δ cell cycle defect is increased cell length due to delayed entry into mitosis (Shiozaki and Russell, 1995b). Transformants were observed at multiple times after induction of expression of SakA or Sty1 and average cell lengths compared with each other and with those of cells grown under repressed conditions (Fig. 3.5A and B). In *sty1*Δ transformants containing *sty1* or *sakA* cDNA under non-repressed conditions, average cell length showed a significant reduction over the course of the experiment, indicating rescue from the *sty1*Δ phenotype. No reduction was seen in any strain under repressed conditions, or in strains containing *sakA* gDNA or empty vector under non-repressed conditions, indicating they are non-functional and cannot rescue the *sty1*Δ phenotype. No difference was seen for wild-type under repressed or non-repressed conditions. Total protein samples from the *sty1* and *sakA* cDNA transformants taken at 19 and 27 hours were analysed by western blotting to determine whether the length reduction seen in these transformants was due to increased SakA or Sty1 protein levels. Western blotting using an anti-Hog1 antibody showed that SakA and Sty1 protein levels increased dramatically from 19 to 27 h in the absence of thiamine, with SakA levels noticeably greater than Sty1 levels at 27 h (Fig. 3.5C). No SakA or Sty1 protein was observed in the presence of thiamine. Wild-type Sty1 protein levels were constant under all conditions examined. Together the results of the stress sensitivity and cell length analyses indicate that *E. festucae sakA* does encode a functional homologue of *S. pombe* Sty1.

3.3.3. *S. pombe* is unable to splice *E. festucae* introns

To determine why *sakA* gDNA was unable to complement the stress sensitivity and cell morphology defects of the *sty1*Δ mutant, mRNA was isolated from the *sty1*Δ strain expressing the *sakA* gDNA and analysed by RT-PCR. One major and two minor products were detected after gel electrophoresis (Fig. 3.6). Sequencing revealed that all are the result of mis-splicing. The major (651 bp) product contains exons 1, 7, 8 and

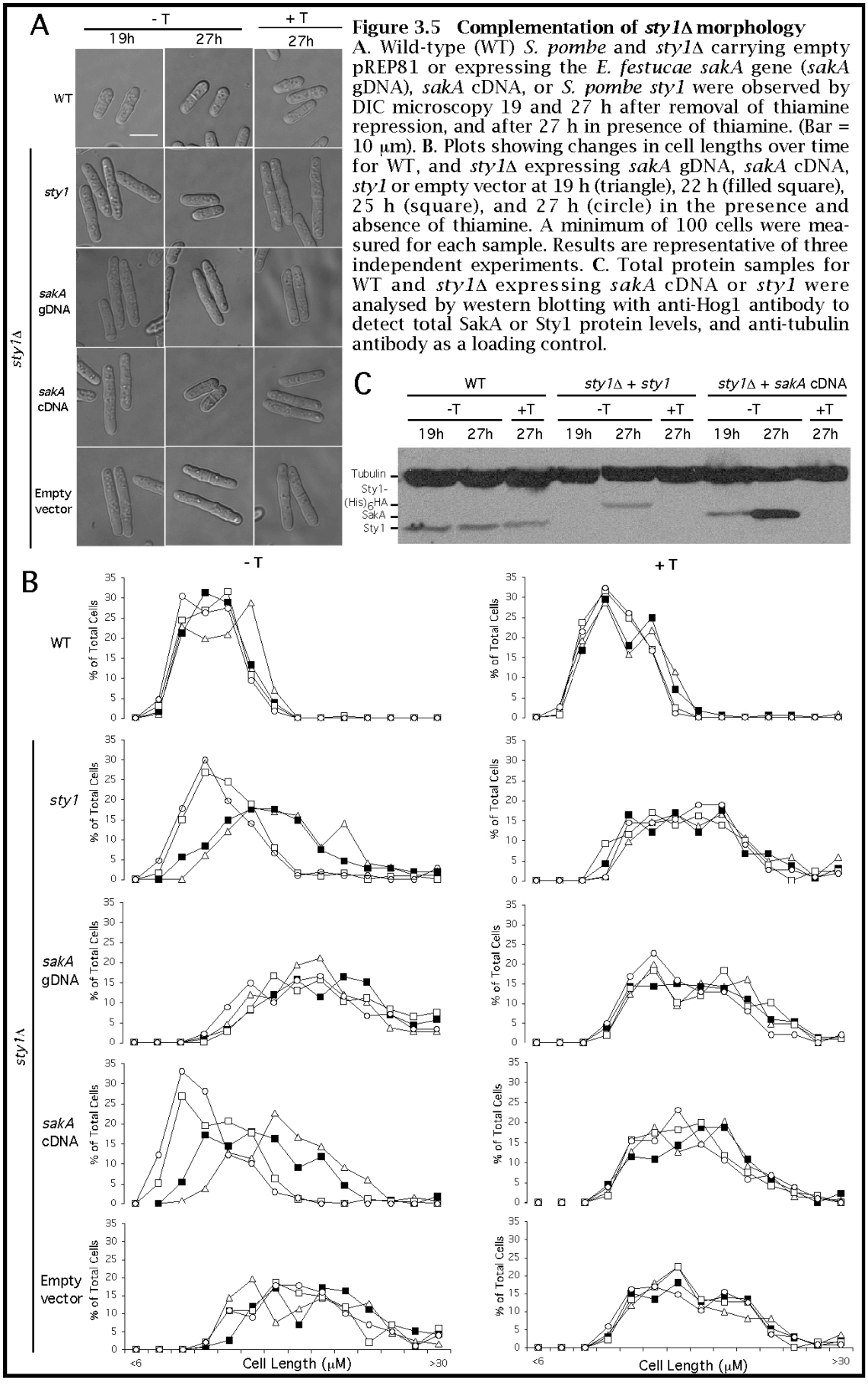

Figure 3.5 Complementation of *sty1*Δ morphology
A. Wild-type (WT) *S. pombe* and *sty1*Δ carrying empty pREP81 or expressing the *E. festucae sakA* gene (*sakA* gDNA), *sakA* cDNA, or *S. pombe sty1* were observed by DIC microscopy 19 and 27 h after removal of thiamine repression, and after 27 h in presence of thiamine. (Bar = 10 μm). **B.** Plots showing changes in cell lengths over time for WT, and *sty1*Δ expressing *sakA* gDNA, *sakA* cDNA, *sty1* or empty vector at 19 h (triangle), 22 h (filled square), 25 h (square), and 27 h (circle) in the presence and absence of thiamine. A minimum of 100 cells were measured for each sample. Results are representative of three independent experiments. **C.** Total protein samples for WT and *sty1*Δ expressing *sakA* cDNA or *sty1* were analysed by western blotting with anti-Hog1 antibody to detect total SakA or Sty1 protein levels, and anti-tubulin antibody as a loading control.

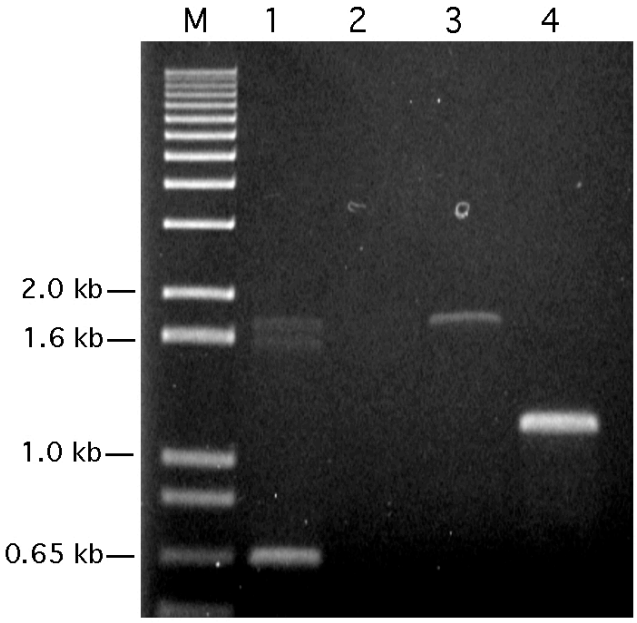

Figure 3.6 Agarose gel electrophoresis of *sakA* RT-PCR products RT-PCR amplification with primers sak24 and sak39 was performed on cDNA isolated from *sty1*Δ expressing *sakA* gDNA (lane 1), no RT control (lane 2), *E. festucae* genomic DNA (lane 3) and *E. festucae* cDNA (lane 4). M, 1 kb plus ladder (Invitrogen).

some intronic sequence. One of the minor products (1619 bp) contains all exons and six introns, whereas the other product (1762 bp) corresponds to unspliced *sakA*. This suggests that the inability of *sakA* gDNA to complement for *sty1* is due to mis-splicing of the *E. festucae* introns by *S. pombe*.

3.4. Translocation of SakA to the nucleus is induced by stress

To determine whether SakA relocates from the cytoplasm to the nucleus in response to osmotic stress, the C-terminus of SakA was fused to GFP (*sakA*-GFP), and expressed in *S. pombe sty1*Δ under conditions of osmotic stress. Whereas GFP fluorescence was detected predominantly in the cytoplasm in control cells, cells exposed to 0.6 M KCl fluoresced predominantly in the nucleus (Fig. 3.7). Prolonged exposure to the UV light source under non-stressed conditions also resulted in a shift of the GFP fluorescence from the cytoplasm to the nucleus (data not shown). These results suggest that SakA relocalises to the nucleus in response to both osmotic and UV stresses. The SakA-GFP construct used for these experiments was shown to complement the osmotic stress sensitivity defect of the *sty1*Δ mutant, indicating that this fusion protein is still able to perform its normal function (Fig. 3.8).

3.5. Deletion of *sakA* alters growth and stress responses in culture

To investigate the role of *sakA* in growth of *E. festucae* in axenic culture, a replacement construct, pCE12, was prepared and a PCR-generated linear fragment of this plasmid (Fig. 3.9A) recombined into the *E. festucae* genome. Given the predicted osmosensitive nature of the Δ*sakA* mutant, special consideration was given to the transformation procedure since protoplasts need to be kept in the presence of high salt or high sugar until a cell wall forms to prevent bursting. A modified method, based on the method used by Dixon et al. (1999) for generation of the *M. grisea* Δ*osm1* mutant, in which transformed protoplasts were incubated in liquid RG medium overnight, then plated onto PD plates was performed in parallel with transformations performed using the

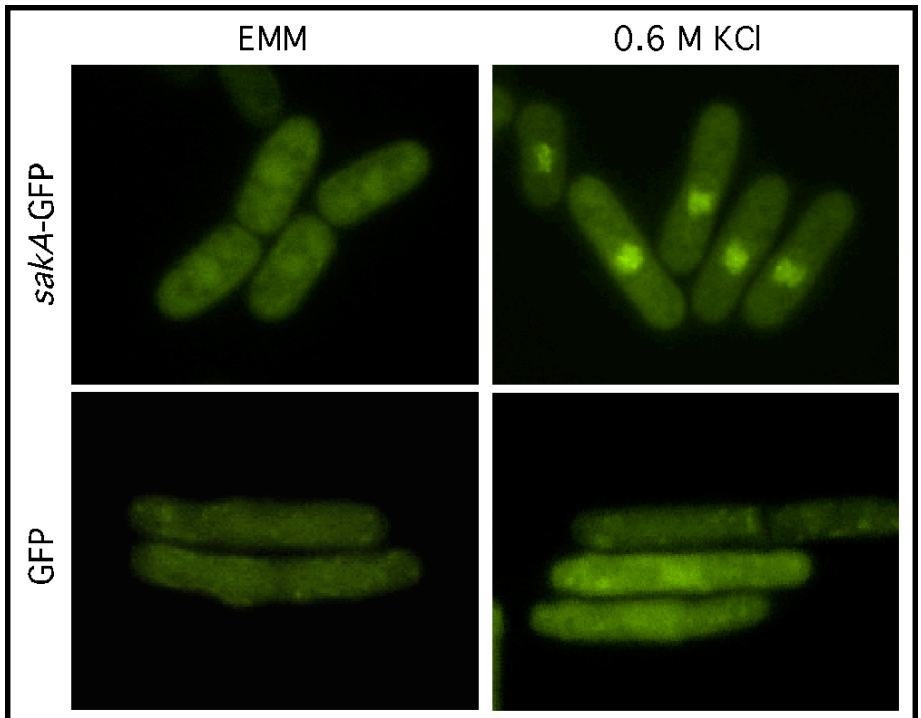

Figure 3.7 Fluorescence microscopy showing GFP localisation of SakA in *S. pombe sty1Δ* mutant cells under osmotic stress
*S. pombe sty1*Δ mutant cells expressing GFP or an *E. festucae sakA* cDNA-GFP fusion (SakA-GFP) were grown in EMM and observed under osmotic stress (0.6 M KCl) and non-stressed conditions (EMM).

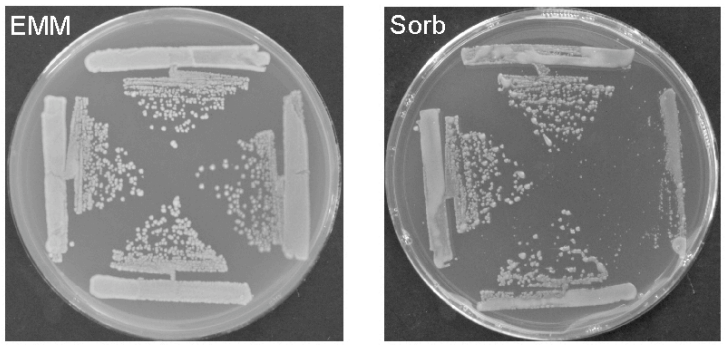

Figure 3.8 Complementation of *S. pombe sty1*Δ osmosensitivity with a *sakA* C-terminal GFP fusion protein
Wild-type *S. pombe* (WT) and the *sty1*Δ mutant carrying pREP81-GFP or *sakA*-GFP were streaked onto EMM containing no stress agents (EMM) or 1.5 M sorbitol (sorb).

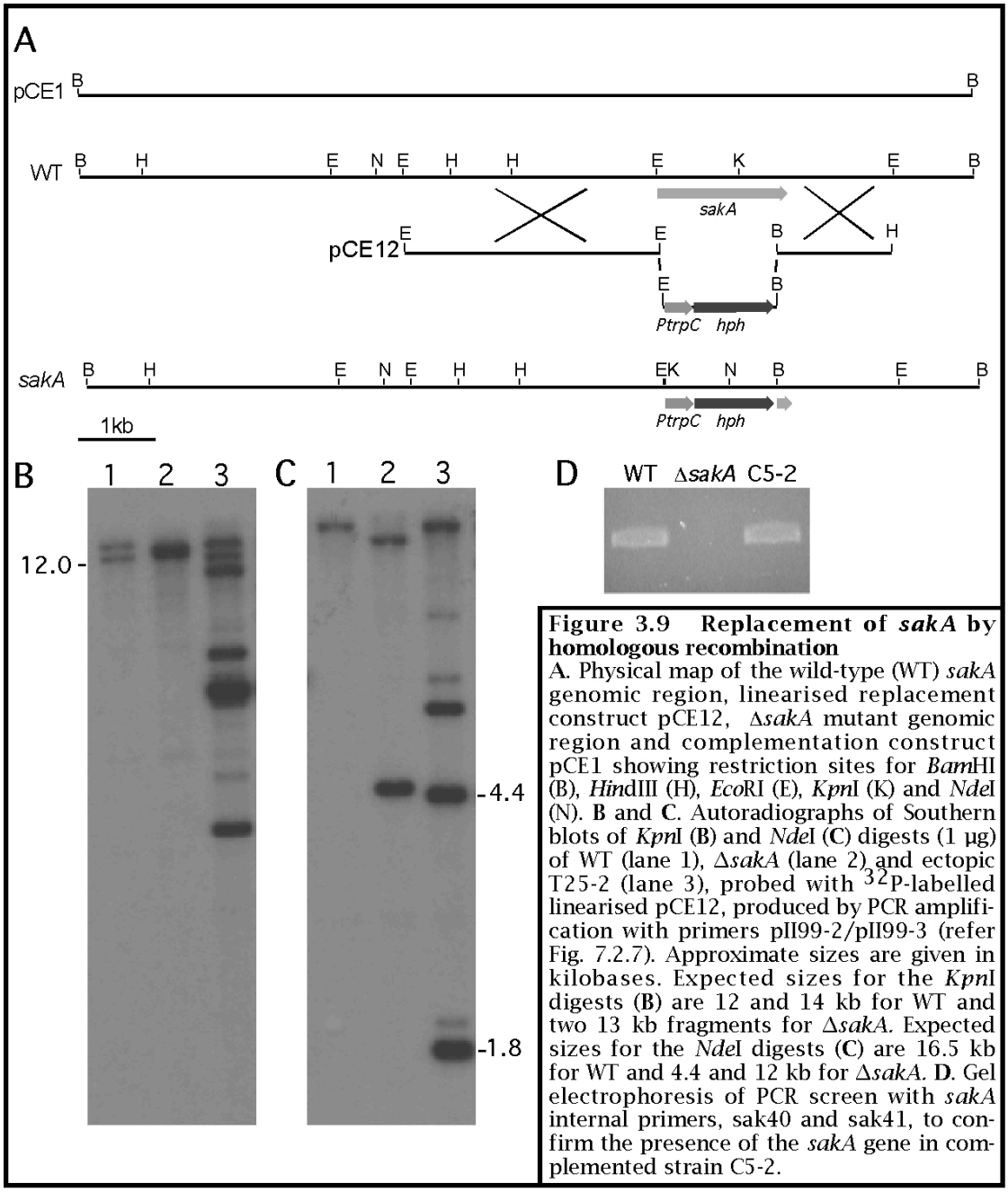

Figure 3.9 Replacement of *sakA* by homologous recombination
A. Physical map of the wild-type (WT) *sakA* genomic region, linearised replacement construct pCE12, Δ*sakA* mutant genomic region and complementation construct pCE1 showing restriction sites for *Bam*HI (B), *Hin*dIII (H), *Eco*RI (E), *Kpn*I (K) and *Nde*I (N). **B** and **C**. Autoradiographs of Southern blots of *Kpn*I (**B**) and *Nde*I (**C**) digests (1 µg) of WT (lane 1), Δ*sakA* (lane 2) and ectopic T25-2 (lane 3), probed with ^{32}P-labelled linearised pCE12, produced by PCR amplification with primers pII99-2/pII99-3 (refer Fig. 7.2.7). Approximate sizes are given in kilobases. Expected sizes for the *Kpn*I digests (**B**) are 12 and 14 kb for WT and two 13 kb fragments for Δ*sakA*. Expected sizes for the *Nde*I digests (**C**) are 16.5 kb for WT and 4.4 and 12 kb for Δ*sakA*. **D.** Gel electrophoresis of PCR screen with *sakA* internal primers, sak40 and sak41, to confirm the presence of the *sakA* gene in complemented strain C5-2.

normal method. However, no transformants grew on the PD plates, suggesting overnight incubation was not long enough for cell walls to form. Two different transformant types were observed on the RG plates – a filamentous form and a raised, glossy form. Approximately 100 of each of these types were sub-cultured onto PD plates with hygromycin. Surprisingly, the raised, glossy colonies grew like the wild-type strain on PD medium, suggesting their altered growth was due to the high sugar RG medium. Screening on PD medium containing 0.3 M NaCl to identify osmosensitive transformants produced an almost perfect correlation between osmosensitive transformants and those that grew raised and glossy on RG. Based on the results of this screening, osmosensitive transformants were chosen for PCR analysis. This confirmed that all these transformants were Δ*sakA* mutants. Selected transformants were then analysed using Southern blotting to determine the copy number of the replacement construct and whether any ectopic integrations were also present. Southern blot analysis showed that transformant T1-3 (henceforth referred to as Δ*sakA*) contains a single copy of the replacement construct at the *sakA* locus and no ectopic integrations, and that transformant T25-2 contains a tandem, non-homologous insertion of the replacement construct at an ectopic locus (Fig. 3.9B). These two transformants were used in all subsequent analyses.

Comparison of the growth of the Δ*sakA* mutant with the wild-type and ectopic strains revealed that the Δ*sakA* mutant shows increased sensitivity to both temperature and salt (NaCl) (Fig. 3.10A). The Δ*sakA* mutant also showed resistance to the phenyl-pyrrole fungicide fludioxonil, consistent with observations for other stress-activated MAP kinase mutants from filamentous fungi. Surprisingly, the Δ*sakA* mutant showed no increased sensitivity to oxidative stress induced by hydrogen peroxide. No difference in colony morphology or growth rate was observed when grown under normal conditions. However, when grown under nutrient-limiting conditions such as on thin layer agar or when grown for extended periods a marked difference was seen in comparison to the wild-type strain. Under these conditions, the wild-type strain was found to produce spherical or elliptical structures at the hyphal tip (Fig. 3.11). These structures appeared static but only loosely attached to the hyphae, as flooding with media or stain detached them. The tip of the hypha bearing these structures stained intensely with calcofluor white (CFW), whereas the structures themselves stained less intensely. These structures

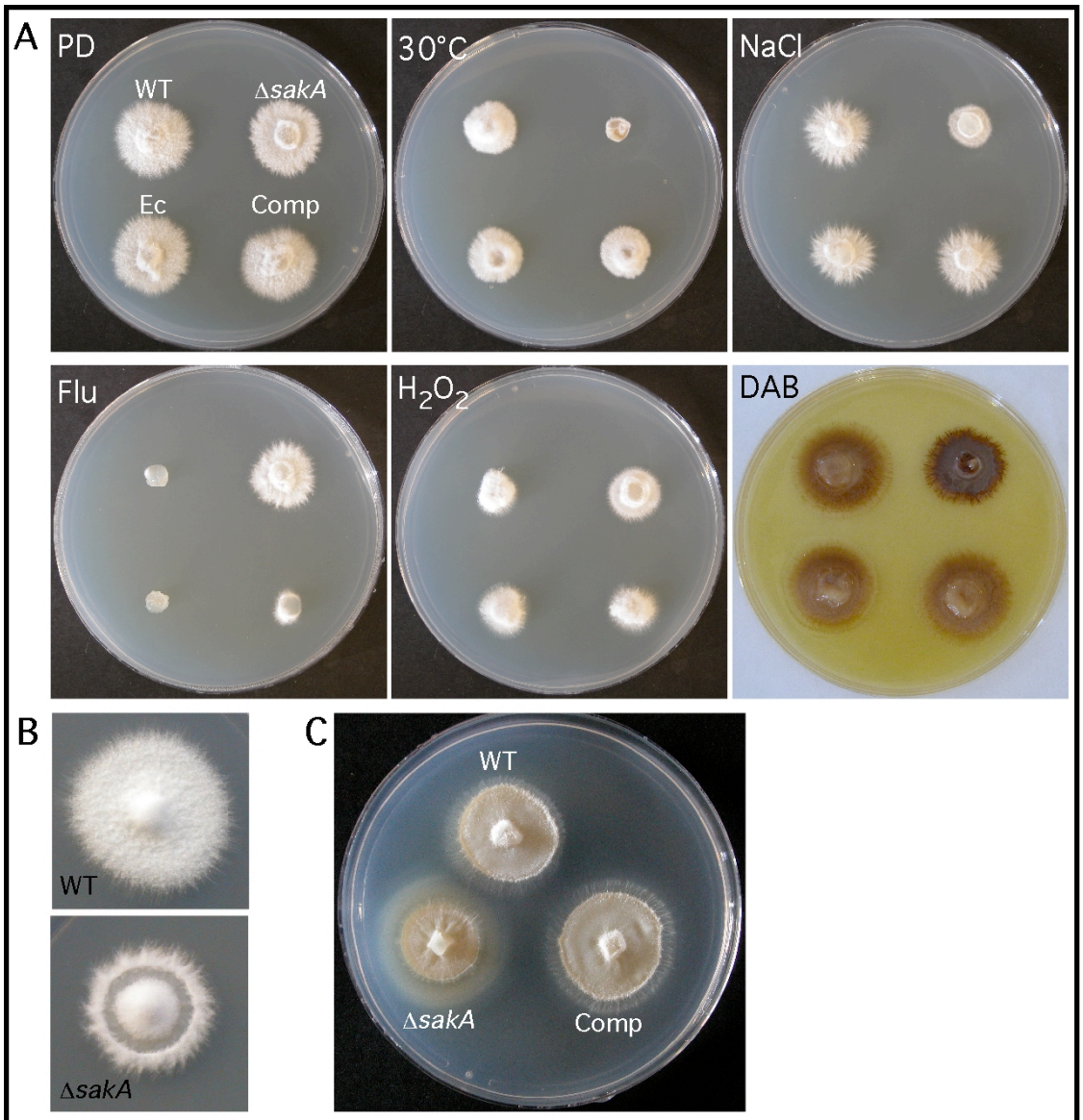

Figure 3.10 Culture phenotype of the Δ*sakA* mutant
A. Wild-type *E. festucae* (WT), the Δ*sakA* mutant, ectopic integration strain T25-2 (Ec) and complemented strain C5-2 (Comp) were tested for sensitivity to temperature stress on PD media incubated at 30˚C; sensitivity to osmotic stress on PD media containing 0.3 M NaCl; resistance to phenyl-pyrrole fungicide on PD media containing 100 μM fludioxonil (Flu), and sensitivity to oxidative stress on PD media containing 7 mM H_2O_2. Growth was compared to that under normal conditions of PD media at 22˚C. H_2O_2 production was analysed by incubation with DAB (3, 3‘ diaminobenzidine) for 40 h. In the presence of H_2O_2 a brick red precipitate forms. Colony labelling shown in panel 1 applies to all other panels. **B**. Photographs of 10 day old colonies of WT and the Δ*sakA* mutant grown on PD medium at 22˚C. The Δ*sakA* mutant displays symptoms of senescence with loss of aerial hyphae in the middle of the colony. **C**. Colonies of WT, the Δ*sakA* mutant and complemented strain (comp) were grown on PD medium for 7 days then stored at 4˚C for approximately 3 months. A halo of exudate can be seen around the Δ*sakA* mutant colony.

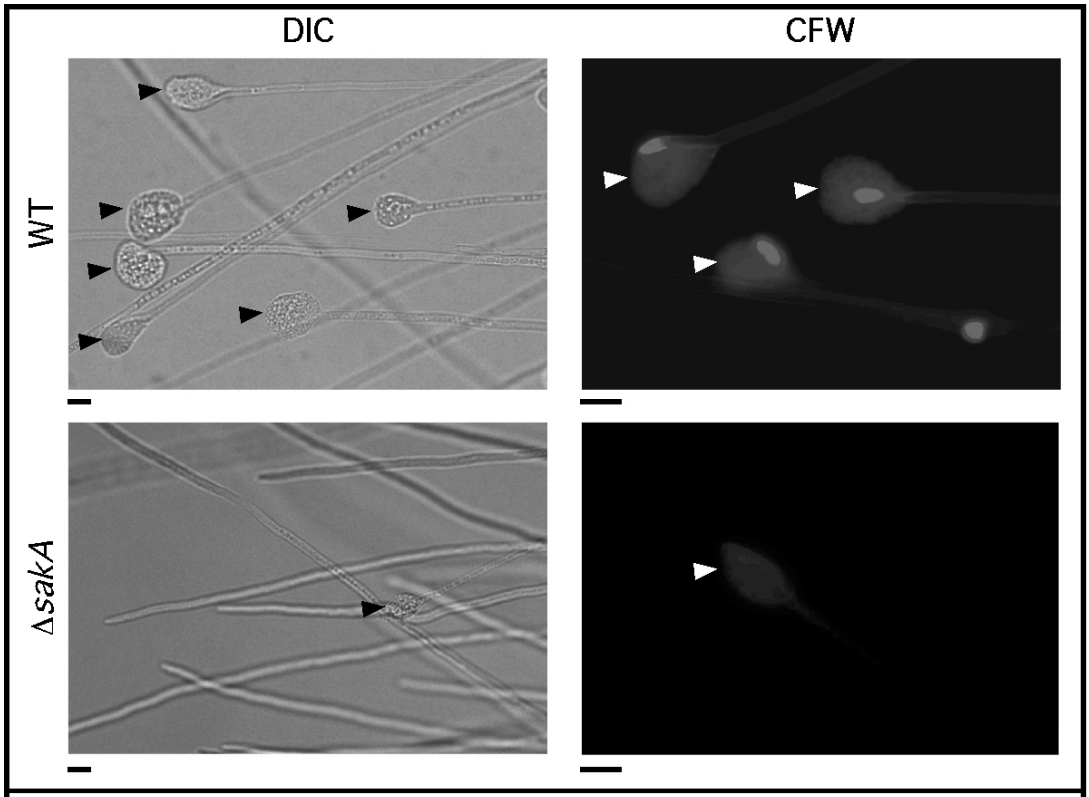

Figure 3.11 Examination of structures at the hyphal tip by DIC and fluorescence microscopy
Differential interference contrast (DIC) and calcofluor white (CFW) fluorescence micrographs showing spherical/elliptical structures at the hyphal tips of wild-type *E. festucae* (WT) and the Δ*sakA* mutant. Intense CFW staining can be seen at the tip of WT hyphae bearing these structures. Very few of these structures are seen in the Δ*sakA* mutant. Those which are seen appear misshapen and no CFW staining can be seen at the tips of the hyphae bearing these abnormal structures. Arrows indicate the positions of these structures. Bar = 10 μm.

were seldom seen in the Δ*sakA* mutant, and those that were seen appeared small, misshapen, and the hypha bearing them did not stain intensely with CFW.

Examination of CFW stained hyphae also revealed that the Δ*sakA* mutant displays altered branching, with branches frequently growing back inwards towards the body of the colony instead of growing outwards (Fig. 3.12). The localisation of CFW staining was also altered in the Δ*sakA* mutant with the hyphal tip staining poorly compared to those of the wild-type strain. However, many Δ*sakA* mutant hyphae stained brightly with CFW along their entire length. When viewed by DIC these hyphae were found to be dead or dying, often with cytoplasmic aggregations or obvious ruptures. The presence of dead hyphae within the Δ*sakA* mutant colony is consistent with observations that under nutrient-limiting conditions the Δ*sakA* mutant appears to senesce, losing aerial hyphae in the centre of the colony, leaving a smooth, wettable central zone (Fig. 3.10B). When stored for extended periods at 4°C the Δ*sakA* mutant also exudes a yellow substance into the media (Fig. 3.10C). This is only seen for wild-type colonies stored for much longer periods and is predicted to be associated with aging, suggesting the Δ*sakA* mutant may have accelerated aging.

3.5.1. Complementation of the Δ*sakA* mutant

To confirm that the altered culture phenotypes seen for the Δ*sakA* mutant were solely due to loss of the *sakA* gene, the gene was ectopically re-inserted back into the mutant, generating complemented strain C5-2. PCR with *sakA* internal primers, sak40 and sak41, confirmed the presence of the gene in strain C5-2 (Fig. 3.9D). This strain displayed wild-type growth and morphology under all conditions tested (Fig. 3.10A).

3.6. The *sakA* mutant has increased ROS levels in culture

To determine if ROS production was altered in the Δ*sakA* mutant, colonies were incubated with 3, 3'-diaminobenzidine (DAB), which forms a brick red precipitate with hydrogen peroxide (Fig. 3.10A). This revealed that the Δ*sakA* mutant has much higher

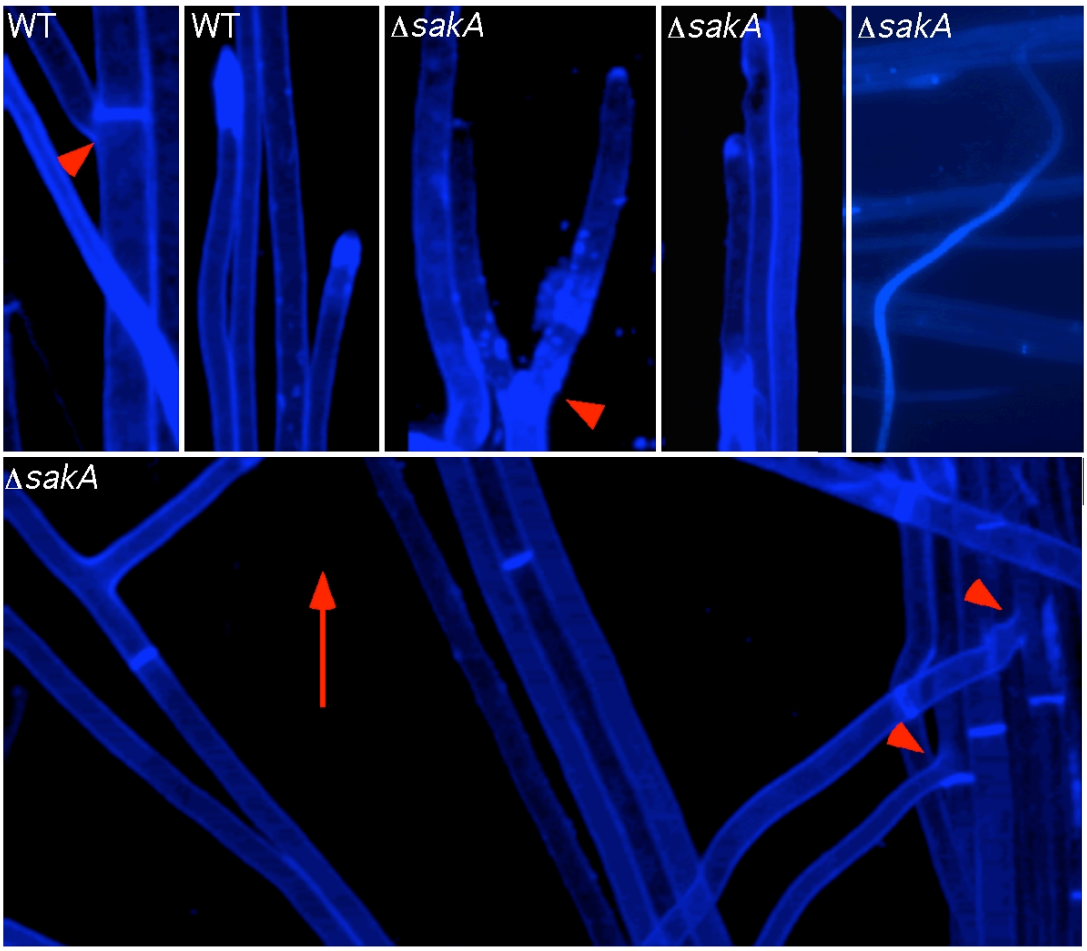

Figure 3.12 Calcofluor white (CFW) staining of hyphal growth in culture
Fluorescence micrographs showing CFW-stained hyphae of wild-type *E. festucae* (WT) and the Δ*sakA* mutant. WT hyphal tips stain brightly with CFW and branches form adjacent to the tip-proximal septa. In the Δ*sakA* mutant hyphal tips stain poorly with CFW. Branching is also altered with the formation of tip bifurcations and branching back in towards the centre of the colony. Extended CFW staining at some tip-distal regions is also observed due to frequent cell death throughout the colony. The arrow points towards the outside of the colony. Arrowheads indicate the positions of branches.

levels of hydrogen peroxide throughout the entire colony than the wild-type or ectopic strains, but wild-type levels are restored by complementation with the *sakA* gene. To determine whether this increased ROS is still highly localised to the hyphal tip as is seen for the wild-type strain, cultures were incubated with nitroblue tetrazolium (NBT) and visualised by microscopy. NBT forms a dark blue water insoluble formazan precipitate with superoxide anions. In wild-type associations the formazan precipitate is highly localised to the hyphal tip indicating a gradient of superoxide anions at the tip (Tanaka et al., 2006). In the Δ*sakA* mutant the formazan precipitate was no longer localised to the hyphal tip but was found back from the hyphal tip, suggesting ROS production is no longer localised to the hyphal tip (Fig. 3.13). In addition, many more Δ*sakA* mutant hyphae contained the formazan precipitate than in wild-type, suggesting an increase in the levels of ROS in this mutant.

3.7. SakA does not regulate *nox* expression

To determine whether the difference in ROS production observed in the Δ*sakA* mutant is due to changes in expression of the *nox* genes, RT-PCR was used to examine expression of *noxA* and *noxR* in the Δ*sakA* mutant compared to wild-type *E. festucae* (Fig. 3.14). No major differences were observed between the levels of *noxA* or *noxR* expression in the Δ*sakA* mutant in comparison to wild-type *E. festucae*, as was also the case for the constitutively expressed ß-tubulin (*tubB*) gene. This indicates that SakA is likely not involved in major transcriptional regulation of the *nox* genes in *E. festucae*.

3.8. *sakA* is required for normal association with perennial ryegrass

To determine if *sakA* has a role in regulating the growth of *E. festucae in planta*, the Δ*sakA* mutant was inoculated into *L. perenne* seedlings. After 4-6 weeks, plants were screened for infection, revealing that the Δ*sakA* mutant had much lower rates of infection than the wild-type strain (Fig. 3.15A). However, due to the way in which the seedlings are inoculated, this cannot be attributed to reduced ability to infect perennial ryegrass but

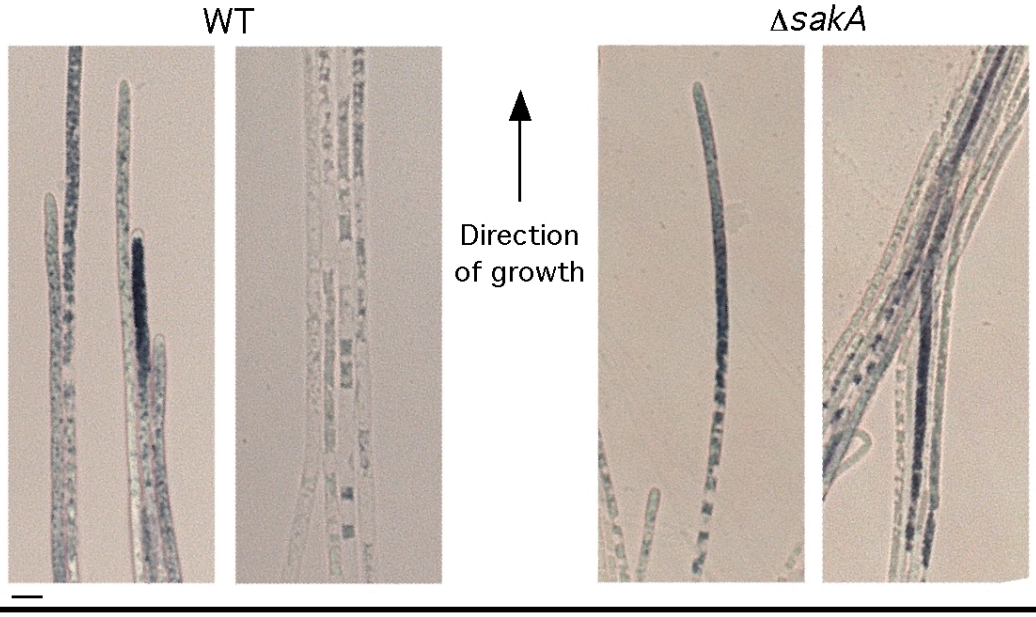

Figure 3.13 Nitroblue-tetrazolium (NBT) detection of superoxide anion production by *E. festucae*
Wild-type (WT) and Δ*sakA* mutant colonies were grown across PD-agarose covered slides for 5-7 days at 22˚C. Colonies were then incubated with 0.05% (w/v) NBT for 5 h at 22˚C. Reduction of NBT to dark-blue, water-insoluble formazan by superoxide anions was detected by light microscopy. In WT, reduced NBT is localised to the hyphal tip. In the Δ*sakA* mutant reduced NBT is found delocalised back from the tip. Bar = 5 μm.

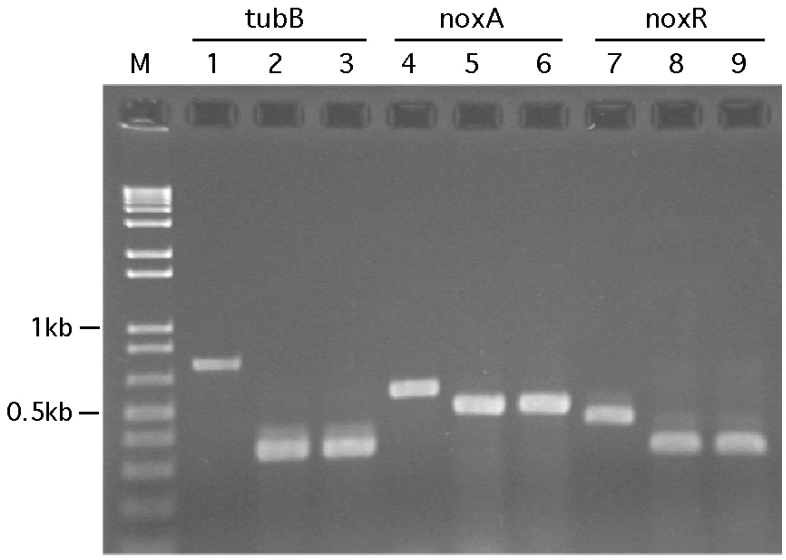

Figure 3.14 *nox* expression analysis
Total RNA was isolated from wild-type (WT) *E. festucae* (lanes 2, 5 and 8) and Δ*sakA* mutant (lanes 3, 6 and 9) mycelia grown in axenic culture for 7 days and used for cDNA synthesis. 30 cycle RT-PCR was performed with primers specific for *E. festucae* β-tubulin (T1.1 and T1.2), *noxA* (noxAr and noxAf2) and *noxR* (Efp67-F1 and Efp67-R1). Wild-type genomic DNA (gDNA) (lanes 1, 4 and 7) was used as a control for DNA contamination. Approximate fragment sizes are given in kilobases. M, 1 kb plus ladder (Invitrogen).

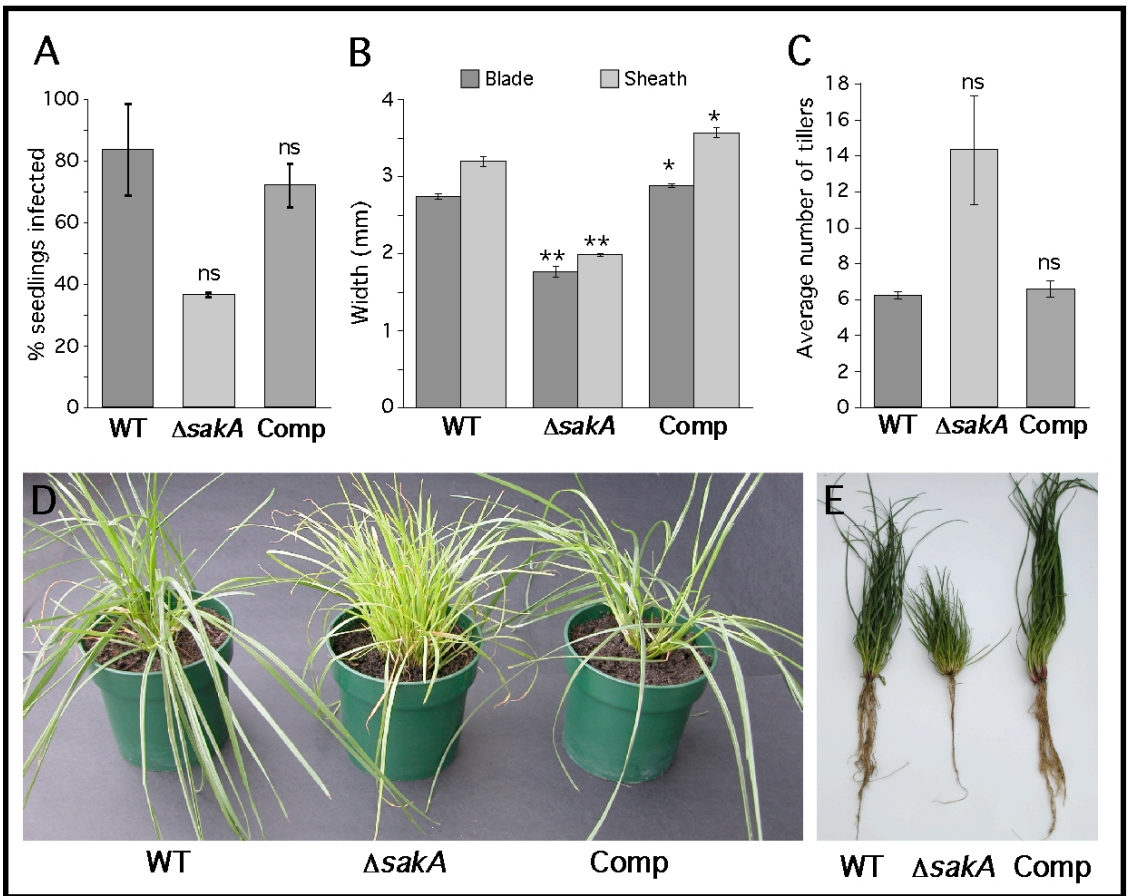

Figure 3.15 Symbiotic Phenotype of the *E. festucae* Δ*sakA* mutant
A. Infection rate analysis for perennial ryegrass inoculated with *E. festucae* wild-type (WT), the Δ*sakA* mutant, and complemented strain (Comp). Bars are ± SE for two independent experiments (n = 47, 60, and 61 for WT, Δ*sakA* and comp strains respectively). **B** and **C**. Tiller width and number of plants infected with WT, Δ*sakA*, and comp strains. Measurements were taken just above the ligule on the blade (dark shading) and just below the ligule on the sheath (light shading). Bars are ± SE for two independent experiments (For width analysis n = 50 for all strains; for tiller number n = 11, 9 and 10 for WT, Δ*sakA* and comp strains respectively). Statistical significance in comparison to the wild-type strain was determined using the Student's *t*-test where *p*-value < 0.05 is significant (* = 0.05-0.01, ** = 0.01-0.001, ns = non-significant) (refer Section 7.4). **D** and E. Tiller and root phenotypes of perennial ryegrass infected with WT, Δ*sakA*, and comp strains. These photographs were taken 12 weeks after inoculation. Yellowing of Δ*sakA* mutant-infected tillers indicates the onset of premature senescence.

rather to reduced ability to establish systemic infection from the site of inoculation. In addition, due to the variability of infection rates with the wild-type strain this difference cannot be deemed statistically significant. Examination of plants where Δ*sakA* mutant infection was established revealed a dramatically altered plant interaction phenotype. These plants appeared to display an increase in the production of tillers but these were much thinner than seen in wild-type associations and the overall growth of these plants was significantly stunted (Fig. 3.15B-D). These plants also had poorly developed root systems (Fig. 3.15E), and prematurely senesced 2-3 months after inoculation. In wild-type associations, infected plants will stay alive indefinitely if well maintained.

3.8.1. Growth *in planta*

Microscopic examination of fungal growth *in planta* using aniline blue to stain the fungal cytoplasm revealed a marked change in the growth of the Δ*sakA* mutant compared to the wild-type strain (Fig. 3.16A). In wild-type associations, hyphae grow within the host intercellular spaces, parallel to the leaf axis, seldom branch and stain intensely with aniline blue. However, in Δ*sakA* mutant associations hyphae appeared hyper-branched, seldom grew parallel to the leaf axis, stained poorly with aniline blue, and had a substantial increase in biomass. These mutant hyphae were also found within host vascular bundles, a region never colonised by wild-type hyphae (Fig. 3.16B). The increased fungal biomass in Δ*sakA* mutant associations was also seen by transmission electron microscopy (TEM) (Fig. 3.17). In wild-type associations, generally only one or two hyphae occupy a single intercellular space. However, in Δ*sakA* mutant associations, intercellular spaces often contained three or more hyphae. The Δ*sakA* hyphae were also often much more irregular in size and shape and often much larger than wild-type hyphae. The Δ*sakA* hyphae were also highly vacuolated, in comparison to wild-type hyphae, which rarely contain vacuoles *in planta*. Generally, the presence of large vacuoles in hyphae is an indicator that the fungus is stressed. To determine if the host induced the increased vacuolation, vacuoles were examined in culture using FM4-64, which stains the vacuolar membrane red. As vacuoles are highly variable in size and shape depending upon the width of the hypha and the distance from the hyphal tip (Shoji et al., 2006), to achieve a fair comparison of the two strains, vacuoles at the

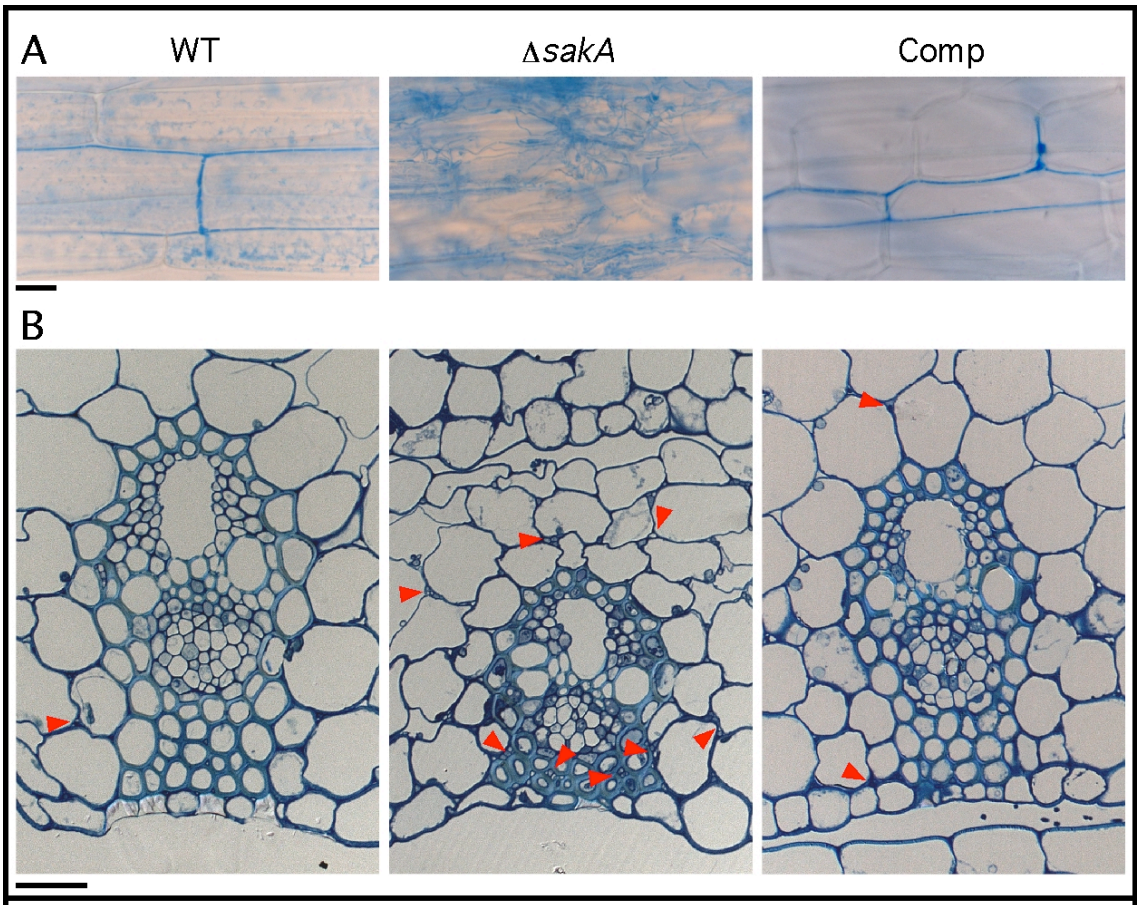

Figure 3.16 Growth of the Δ*sakA* mutant *in planta*
A. Light micrographs of aniline blue-stained hyphae growing in the leaf sheaths of 8 week old perennial ryegrass plants infected with *E. festucae* wild-type (WT), the Δ*sakA* mutant, and complemented strain (Comp). Bar = 30 µm. **B.** Light micrographs of toluidine blue-stained transverse sections showing vascular bundles in the pseudostem of WT, Δ*sakA* and complemented strain-infected perennial ryegrass. Δ*sakA* mutant hyphae can be seen within the vascular bundle complex. Arrows indicate the position of fungal hyphae. Bar = 20 µm.

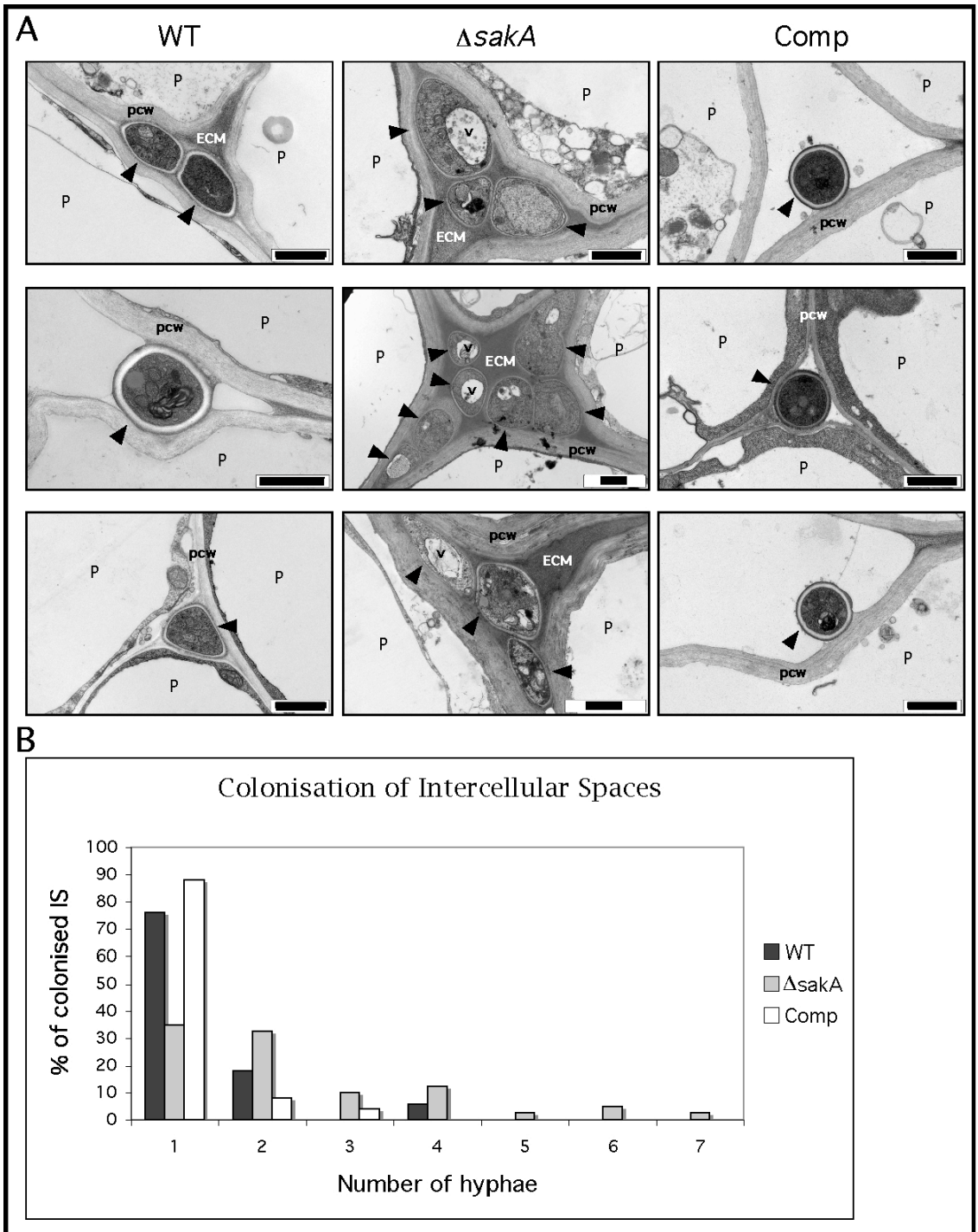

Figure 3.17 Examination of hyphal morphology and density *in planta* by TEM
A. Transmission electron micrographs of cross-sections showing *E. festucae* hyphae growing in the intercellular spaces of host pseudostem tissue. Arrows, fungal hyphae; P, plant cell; ECM, extracellular matrix; v, vacuole; pcw, plant cell wall. Bar = 1 μm. **B.** Graph showing number of hyphae in intercellular spaces (IS) colonised by the wild-type (WT), Δ*sakA* and complemented (Comp) strains.

hyphal tip were compared. However, no obvious differences were seen between the wild-type and Δ*sakA* mutant strains suggesting that these large vacuoles *in planta* are induced by the host (Fig. 3.18). TEM also showed that the intercellular spaces surrounding the Δ*sakA* mutant hyphae appeared very electron dense as compared to the relatively light space seen around wild-type hyphae (Fig. 3.17). Electron dense intercellular space is thought to be an indicator of a host defence response. However, as Δ*sakA* mutant-infected plants take 2-3 months to senesce it is unlikely that this is due to host defence response as this is generally much more rapid. Complementation with the *sakA* gene restored the wild-type host interaction phenotype (Fig. 3.15-3.17).

3.8.2. The Δ*sakA* mutant does not induce a host defense response

To confirm that the premature senescence displayed by the Δ*sakA* mutant-infected plants was not due to a host defense response, infected blade and pseudostem tissues were stained with lactophenol trypan blue, which stains localised areas of cell death dark blue. No clusters of dead plant cells were observed in either the wild-type or Δ*sakA* mutant infected plant samples. The Δ*sakA* mutant-infected tissue samples did appear considerably darker overall than the wild-type samples (Fig. 3.19). However, this increased staining was not of individual cells but rather was diffuse and particularly prominent surrounding the host vascular bundles. This increased staining is likely due to increased permeability of the Δ*sakA* mutant-infected tissue to the stain. During the staining process, samples are first cleared with methanol and it was noted that the mutant infected tissue cleared more rapidly than the wild-type-infected tissue. The Δ*sakA* mutant-infected samples also took up the stain more readily than wild-type-infected samples. This suggests leaves of Δ*sakA* mutant-infected plants are more permeable than wild-type-infected plants, possibly due to the onset of senescence.

3.8.3. The Δ*sakA* mutant induces branching of the host vascular tissues

When samples stained with lactophenol trypan blue were examined by microscopy it was observed that blade tissue infected with the Δ*sakA* mutant showed much more frequent branching between the host vascular bundles than is seen in wild-type associations (Fig. 3.20). However, the difference between wild-type and Δ*sakA* mutant

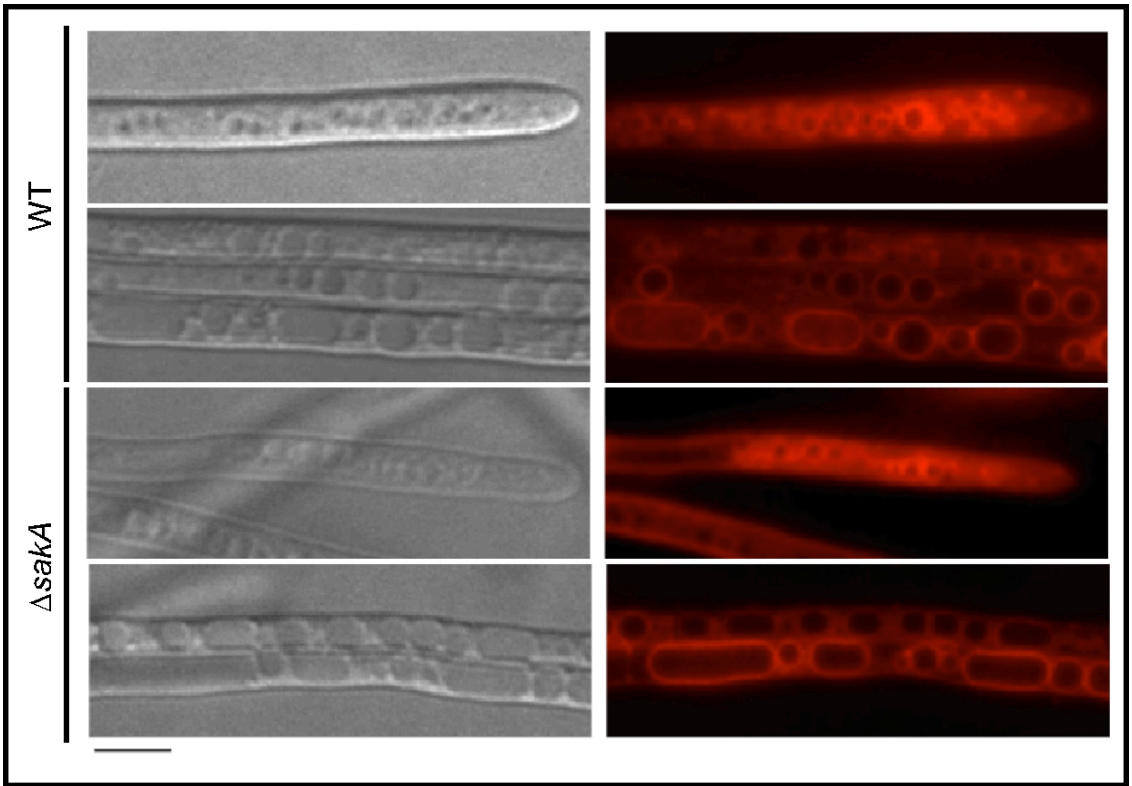

Figure 3.18 Fluorescence micrographs of FM4-64 stained vacuoles in culture
FM4-64 selectively stains the vacuolar membrane red and can be observed by fluorescence microscopy. No difference is seen between vacuoles at the hyphal tips in wild-type (WT) or the Δ*sakA* mutant. Vacuoles in regions distant from the tip are highly variable in size but no obvious difference is observed between WT and the Δ*sakA* mutant. Bar = 5 μm.

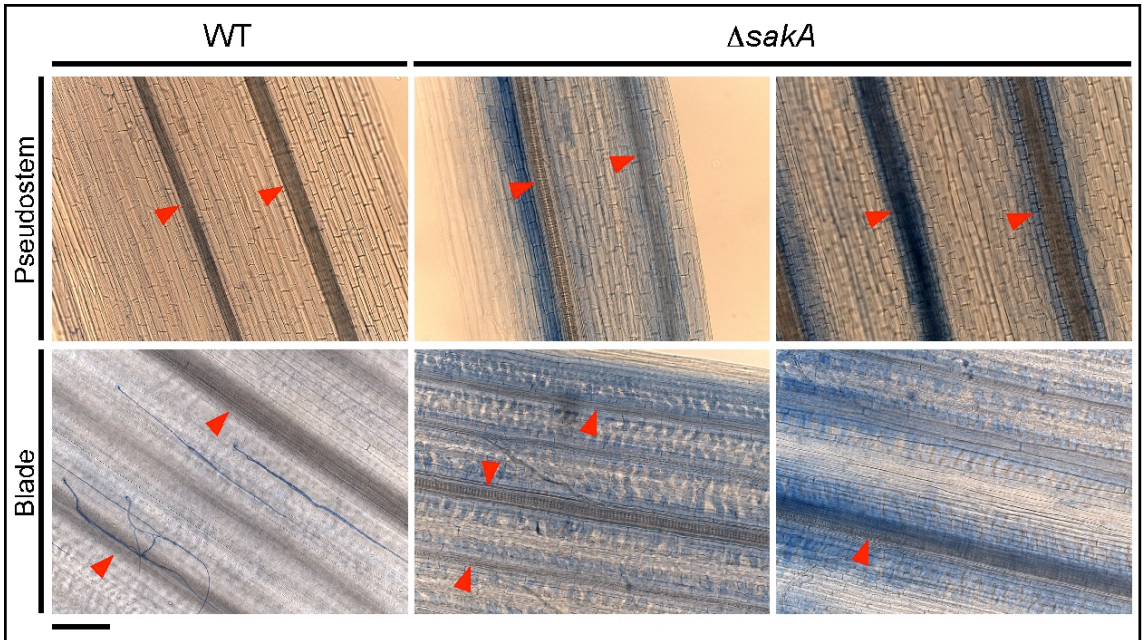

Figure 3.19 Analysis of host defense responses by lactophenol trypan blue staining
Light micrographs showing sections from the pseudostem and blade tissue infected with wild-type *E. festucae* (WT) and the Δ*sakA* mutant. Plants infected with the Δ*sakA* mutant show diffuse staining throughout the tissue, particularly surrounding the host vascular bundles. This is likely due to increased permeability of Δ*sakA*-infected tissue to the stain due to the onset of premature senescence. No localised areas of intense staining, indicative of localised plant cell death can be seen in WT or Δ*sakA*-infected tissue. Epiphyllous hyphae can be seen on the surface of WT-infected blade tissue but not Δ*sakA*-infected tissue. Arrowheads indicate the positions of host vascular bundles. Bar = 100 μm.

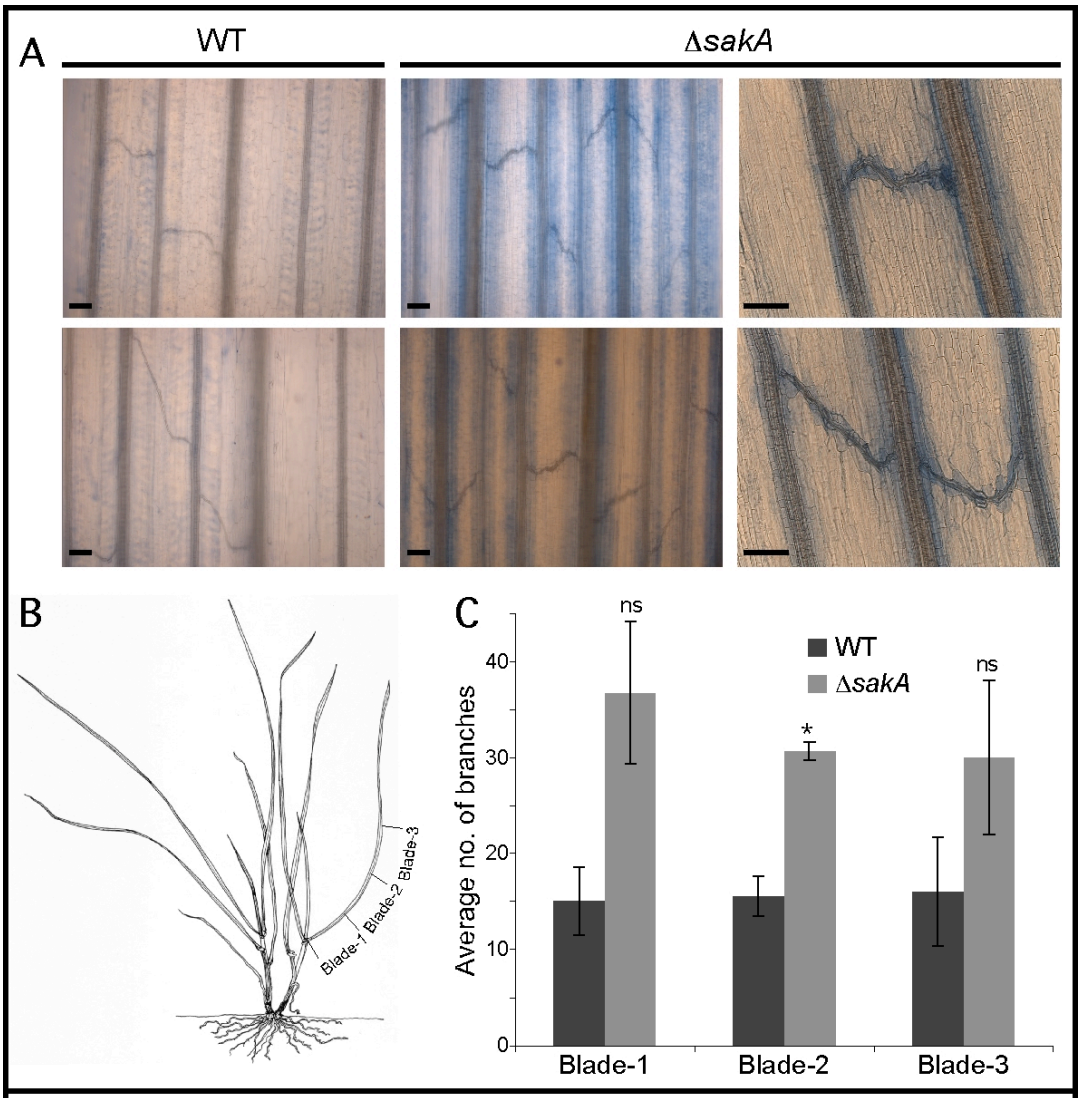

Figure 3.20 Branching of perennial ryegrass vasculature
A. Light micrographs of perennial ryegrass blade tissue showing branching between the vasculature of plants infected with wild-type *E. festucae* (WT) and the Δ*sakA* mutant. Bar = 100 μm. **B**. Schematic representation showing the positions of sections taken from infected blade tissue. Blade segment 1 (blade-1) was taken from the ligule to 1 cm up the blade. Segment 2 (blade-2) was taken from 1 cm to 2 cm above the ligule. Segment 3 (blade-3) was taken from 2 cm to 3 cm above the ligule. **C**. Quantification of vasculature branching in plants infected with the WT and Δ*sakA* mutant strains. Sections were taken from a minimum of six tillers from two independent plants. Statistical significance in comparison to the wild-type strain was determined using the Student's *t*-test where *p*-value < 0.05 is significant (* = 0.05-0.01, ns = non-significant) (refer Section 7.4).

associations is only statistically significant between 1-2 cm away from the ligule. Above this point the number of branches is more variable in Δ*sakA*-infected plants, and there is no significant difference to the number present in wild-type associations. This suggests there has been an alteration in the signalling that leads to the increased formation of these branches close to the ligule.

3.8.4. Epiphyllous growth

Wild-type *E. festucae* is also known to produce epiphyllous hyphae on leaf sheath and blade tissues. Examination of blade tissue from plants grown under sterile conditions using scanning electron microscopy, and light microscopy of lactophenol trypan blue-stained tissue, revealed that in comparison to the wild-type association, few epiphyllous hyphae were seen in Δ*sakA* mutant associations (Fig. 3.21A and E). Those Δ*sakA* mutant epiphyllous hyphae that were seen frequently contained swollen compartments, seldom seen in wild-type associations (Fig. 3.21B). In contrast, these Δ*sakA* mutant epiphyllous hyphae appeared unable to produce the coil-like hyphal structures frequently seen in wild-type associations (Fig. 3.21B). Δ*sakA* mutant hyphae also often appeared convoluted in comparison to the relatively straight hyphae of the wild-type strain (Fig. 3.21C). Interestingly, the Δ*sakA* mutant appeared unable to penetrate through the host cuticle, as opposed to wild-type associations where hyphae puncture through the cuticle to grow on the surface. Instead, Δ*sakA* mutant hyphae grow out through host guard cells, a situation that is seldom seen in wild-type associations (Fig. 3.21D). It is likely that the Δ*sakA* mutant is unable to penetrate the host cuticle and so the only way it can exit the host tissues is via guard cells, thereby limiting epiphyllous growth.

3.9. The Δ*sakA* mutant alters development of its grass host

Close examination of the base of plants infected with the Δ*sakA* mutant revealed a dramatic change in the development of the host plant, with the formation of bulbs and reduced anthocyanin pigmentation (Fig. 3.22). In wild-type associations, tillers are

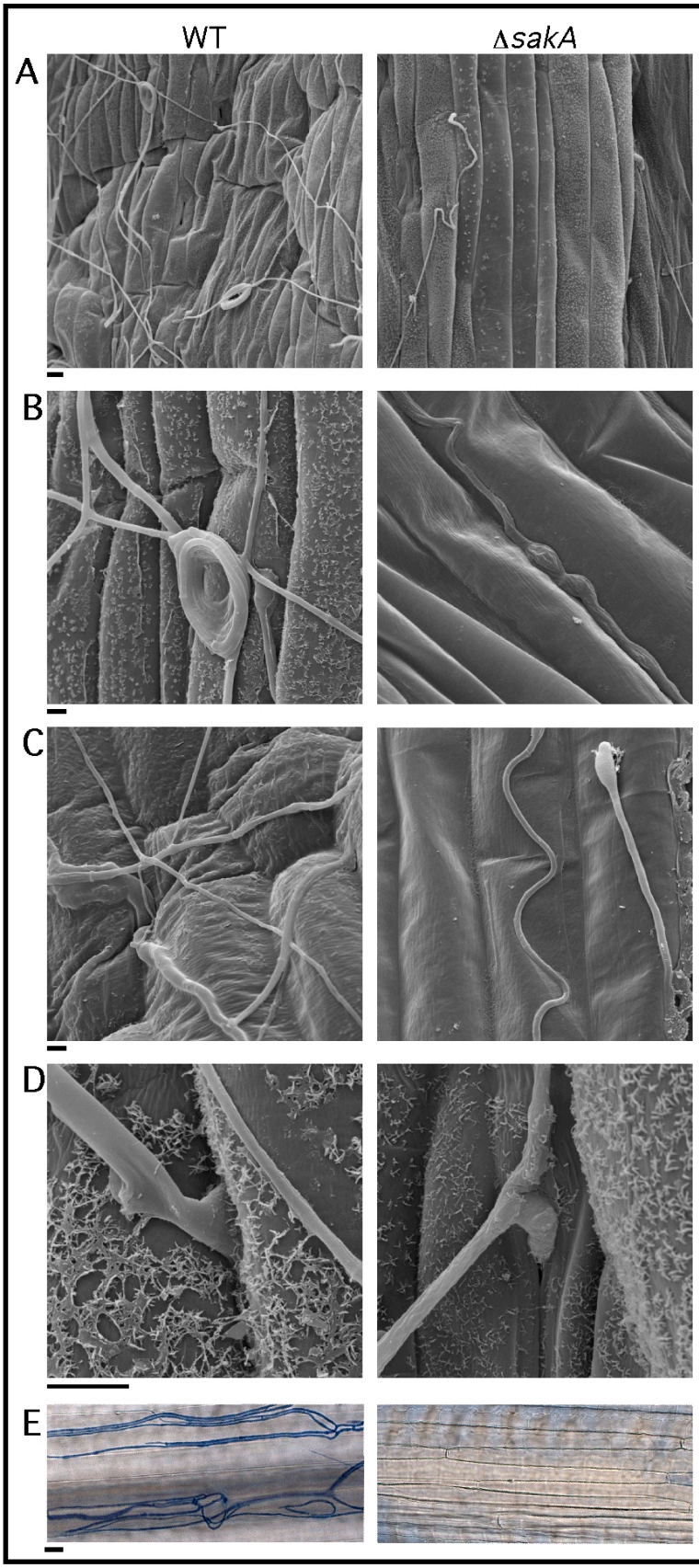

Figure 3.21 Examination of epiphyllous hyphal growth

A-D. Scanning electron micrographs showing epiphyllous hyphae of wild-type (WT) *E. festucae* and the Δ*sakA* mutant growing on the surface of infected perennial ryegrass blade tissue grown under sterile conditions. Photographs were taken nine weeks after inoculation. **A.** Micrographs showing the reduced epiphyllous growth of the Δ*sakA* mutant. Bar = 10 μm. **B.** Micrographs showing swellings within Δ*sakA* mutant hyphae and the absence of hyphal coil-like structures seen in WT associations. Bar = 10 μm. **C.** Micrographs showing convoluted hyphae frequently seen in the Δ*sakA* mutant in comparison to the relatively straight hyphae of WT. Bar = 10 μm. **D.** Micrographs showing a WT hypha growing out through the host cuticle and a Δ*sakA* mutant hypha growing out through a host stoma. Bar = 5 μm. **E.** Light micrographs showing lactophenol trypan blue-stained epiphyllous hyphae of WT *E. festucae* on infected perennial ryegrass blade tissue grown under sterile conditions. No epiphyllous hyphae of the Δ*sakA* mutant were seen by light microscopy. Photographs were taken 10 weeks after inoculation. Bar = 20 μm.

SEM images courtesy M. Becker.

Figure 3.22 Altered development of Δ*sakA*-infected perennial ryegrass
Photographs were taken of the base of perennial ryegrass plants infected with wild-type *E. festucae* (WT), Δ*sakA* mutant and complemented strain (comp) 10 weeks after inoculation. Photographs of Δ*noxA* and Δ*noxR*-infected plants were taken eight weeks after inoculation, just before these plants senesced. The highly stunted nature of these Δ*noxA* and Δ*noxR*-infected plants is reflected in their reduced tiller number. The boxed region of the Δ*sakA*-infected plant was removed and is magnified in the lower panel. Bulges can be seen at the bases of Δ*sakA*- and Δ*noxA*-infected tillers. There is almost complete loss of anthocyanin pigmentation in Δ*sakA*-infected plants. The lack of pigmentation in Δ*noxA*- and Δ*noxR*-infected plants is mostly due to senescence of the pigment-containing outer leaf sheaths, which have been removed.

straight at their base and do not form bulbs, whereas most Δ*sakA* mutant-infected tillers were swollen at their base and appeared more like spring onions or scallions. Complementation with the *sakA* gene restored normal host development. In Δ*noxA* mutant associations, mild swelling is seen in some tillers but the majority of tillers are not swollen, and in Δ*noxR* mutant associations, tillers are not swollen (Fig. 3.22). A slight reduction in anthocyanin pigmentation is seen in both Δ*noxA* and Δ*noxR* mutant associations. While this is much less severe than in Δ*sakA* mutant associations, it appears as severe due to senescence of the anthocyanin-containing outer leaf sheaths (Fig 3.22). Production of photoprotective anthocyanin pigments at the base of tillers is characteristic of perennial ryegrass and is seen in wild-type associations and endophyte free plants. The almost complete loss of anthocyanin pigmentation in Δ*sakA* mutant-associations suggests a major change in biosynthesis or breakdown of these pigments.

Microscopic examination of the swollen region in Δ*sakA* mutant infected plants revealed that the cells below the shoot apical meristem are much less organised than in wild-type associations and no longer form linear cell files (Fig. 3.23). The disordered packing of these cells is one possible cause of this swelling, as they will occupy more space. In addition, many of the cells below the meristem appeared irregular in size and shape, thereby contributing further to the swollen phenotype.

3.10. *In planta* ROS levels are increased in Δ*sakA* mutant associations

Given the Δ*sakA* mutant produces elevated levels of hydrogen peroxide and superoxide in culture, it was important to determine whether ROS levels were also elevated *in planta*. To examine this phenotype, a modified TEM method, in which hydrogen peroxide is reacted with cerium ions to form electron dense cerium perhydroxide precipitates, was employed. To obtain a fair comparison between wild-type and Δ*sakA* mutant associations, the region just below the shoot apical meristem was examined, as samples from this region will be at a similar developmental stage. Precipitates indicative of the presence of hydrogen peroxide were detected in the fungal extracellular matrix (ECM) and along the plant cell walls surrounding hyphae in both wild-type and Δ*sakA* associations (Fig. 3.24). However, quantification of the number of

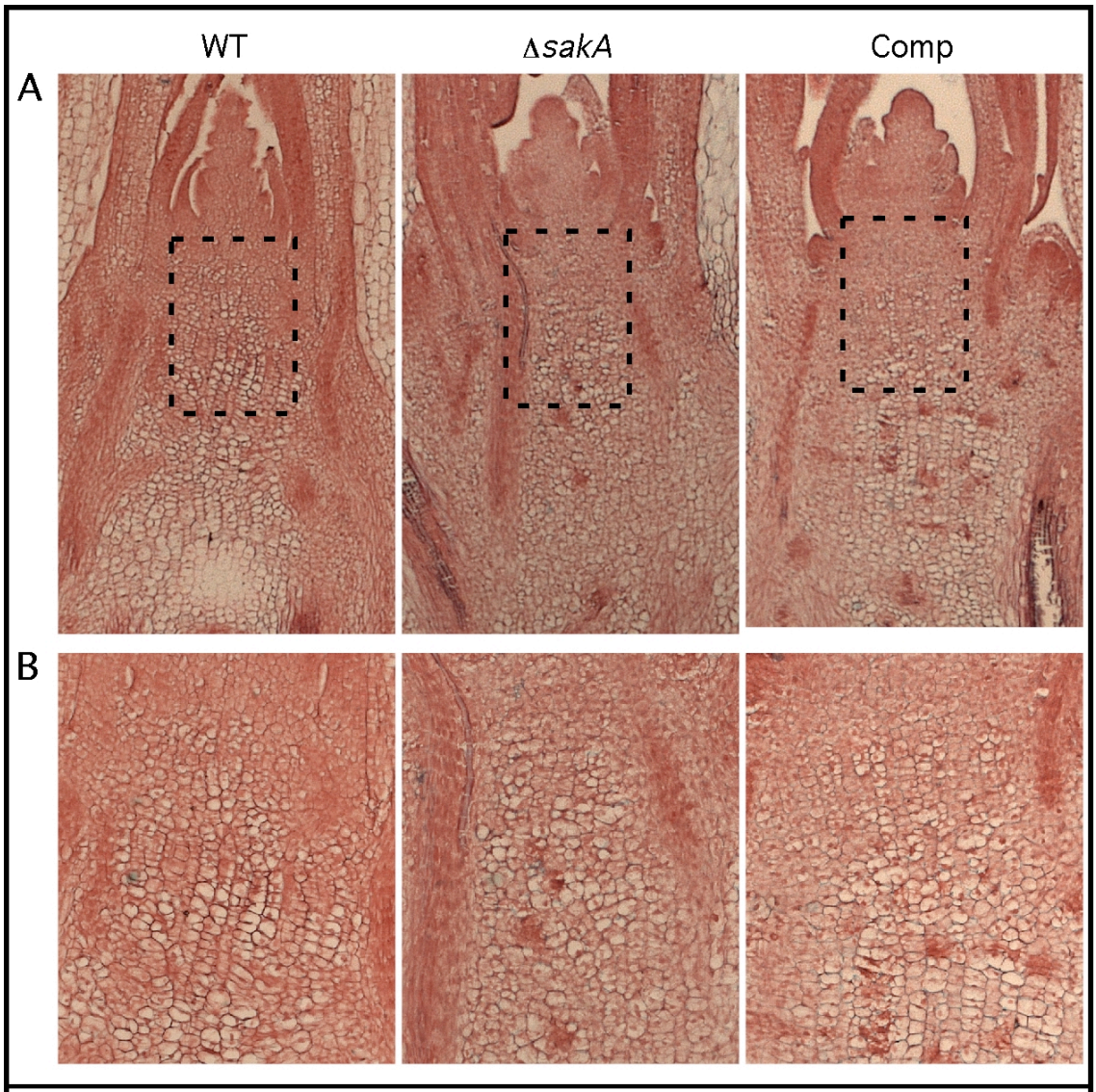

Figure 3.23 Alteration of cell organisation below the shoot apical meristem
A. Light micrographs of alcian-blue/safranin O stained longitudinal sections through the meristem region of tillers infected with *E. festucae* wild-type (WT), the Δ*sakA* mutant and complemented strain. Cells below the shoot apical meristem in Δ*sakA* mutant associations do not form linear cell files and appear disorganised and less uniform in size and shape compared to cells from the same region in wild-type associations. B. Enlargement of boxed regions in micrographs above.

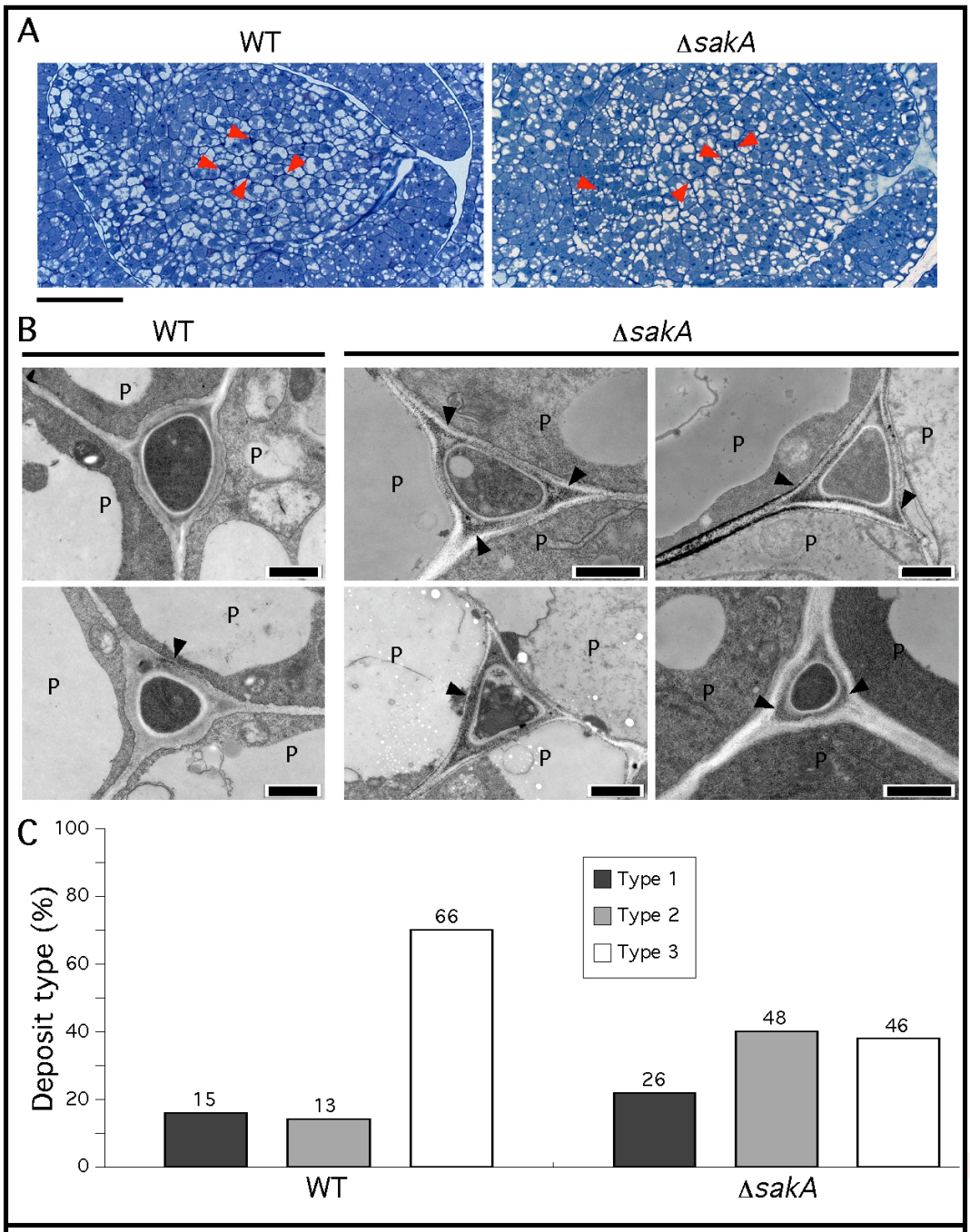

Figure 3.24 Elevated ROS levels in the Δ*sakA* mutant association
A. Light micrographs of toluidine blue-stained transverse sections through the meristem region of wild-type (WT) and Δ*sakA*-infected plants showing the region where H_2O_2 localisation was examined. Arrows indicate positions of hyphae. Bar = 50 mm. **B.** Transmission electron micrographs showing H_2O_2 localisation in meristematic tissue infected with WT or the Δ*sakA* mutant. Cerium chloride-reactive deposits indicative of H_2O_2 production are indicated by arrows. P, plant cell; bar = 1 mm. **C.** Distribution of cerium chloride-reactive deposits in meristematic tissue infected with WT or the Δ*sakA* mutant. Type 1, deposits in the fungal extracellular matrix (ECM); Type 2, deposits in the fungal ECM and host cell wall; Type 3, no deposits detected. The number of intercellular spaces of each type is given above each column.

infected intercellular spaces with either precipitate in the fungal ECM, precipitate in the fungal ECM and host cell wall, or no precipitate, revealed that in Δ*sakA* mutant associations the majority of infected intercellular spaces contain precipitate in the fungal ECM or both the fungal ECM and host cell wall. In comparison, in wild-type associations the majority of infected intercellular spaces contain no precipitate. This confirms that in Δ*sakA* mutant associations, more hydrogen peroxide is found around the fungal hyphae than in wild-type associations, suggesting *sakA* may regulate ROS production *in planta*. However, it is important to note that we cannot rule out the possibility that the host produces some, or all, of the ROS seen *in planta*. Complementation with the *sakA* gene restored wild-type ROS levels. Interestingly, in contrast to that seen in the pseudostem, where multiple Δ*sakA* hyphae occupy single intercellular spaces, generally only one Δ*sakA* mutant hyphae was found in any given intercellular space in the meristem region (Fig. 3.24).

4. Analysis of the p21-Activated Kinases

4.1. Isolation and characterisation of the *E. festucae pak* genes

The second aim of this study was to investigate the potential role of the p21-activated kinases (paks) in growth of *E. festucae* in culture and its association with perennial ryegrass. Filamentous fungi contain two paks classified as Cla4- and Ste20-type kinases based on their homology to *S. cerevisiae* Cla4 and Ste20. This chapter describes the isolation and functional analysis of the two p21-activated kinase genes from *E. festucae*.

4.1.1. Identification of the *E. festucae pak* genes

To identify the *E. festucae pak* genes, degenerate primers were designed to regions conserved in both Ste20- and Cla4-type kinases based on alignments of sequences from *F. graminearum*, *Trichoderma reesei*, *Nectria haematococca*, *N. crassa* and *M. grisea* (Section 7.1.1). Given *N. crassa* and *M. grisea* are phylogenetically more distant from *E. festucae* than the other species, primer design was biased towards the more closely related species. Amplification with the resulting pak1a/paklb primer set produced a 269 bp and a 221 bp product (Fig. 4.1). Sequencing followed by tBLASTx analysis of these products confirmed that the 269 bp product was most similar to Cla4-type kinases, whereas the 221 bp product was most similar to Ste20-type kinases. To determine which *E. festucae* genes these fragments corresponded to, the sequences were compared to the *E. festucae* genome database (http://csurs.csr.uky.edu/biodb-testbed/) using BLASTn. The Cla4-type sequence mapped to gene A.3.65 on contig 1082 whereas the Ste20-type sequence mapped to gene A.4.2646 on contig 806. Gene A.3.65 was found to have a 3013 bp CDS with three introns and was designated *pakA*. Conceptual translation gave rise to an 848 amino acid polypeptide, which is predicted by ExPASy PROSITE analysis to contain a protein kinase domain (PS50011) between amino acids 560-828, pleckstrin homology (PH) domain (PS50003) between amino acids 80-188, p21-binding domain (PBD; PF00786) between amino acids 192-250, and within this an N-terminal Cdc42/Rac-interactive binding (CRIB) motif (PS50108) between amino acids 193-206 (Fig. 4.2A) (Burbelo et al., 1995; Leberer et al., 1997). Comparison of the amino acid sequence to other Cla4-type kinases using ClustalW revealed that the predicted

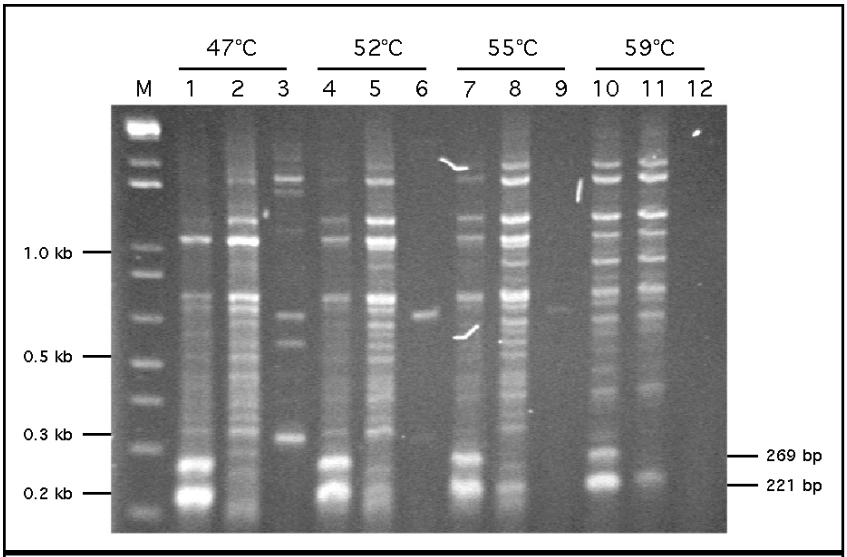

Figure 4.1 Degenerate PCR amplification of the *E. festucae* p21-activated kinases
Degenerate primers were designed to amplify an ~270 bp region from *cla4*-type kinases and an ~220 bp region from *ste20*-type kinases. Amplification from *E. festucae* genomic DNA was performed over a range of annealing temperatures from 47ºC to 59ºC. Lanes 1, 4, 7 and 10 contain primers pak1a and pak1b. Lanes 2, 5, 8 and 11 contain just primer pak1a. Lanes 3, 6, 9 and 12 contain just primer pak1b. Approximate fragment sizes are given in kilobases (kb) and base pairs (bp). M, 1 kb plus ladder (Invitrogen).

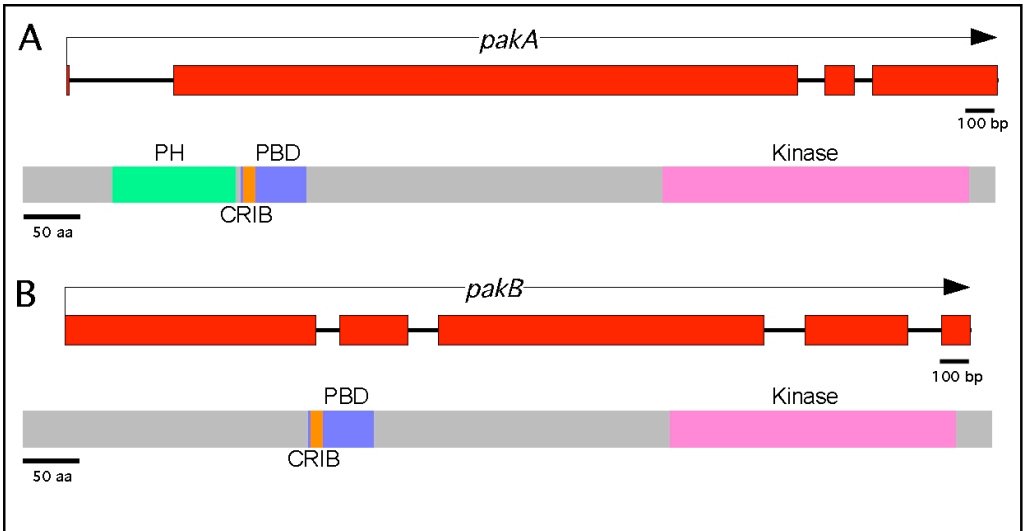

Figure 4.2 Organisation of the *E. festucae* p21-activated kinase genes and predicted polypeptides
A. The *pakA* gene is 3013 bp and contains four exons (red boxes) separated by three introns, based on conceptual translation. The predicted PakA polypeptide is 848 amino acids in length and contains a protein kinase domain (purple); pleckstrin homology domain (PH, green); p21-binding domain (blue), and within this a Cdc42/Rac interactive binding (CRIB) motif (orange). Bar = 100 bp and 50 amino acids for the *pakA* gene and predicted polypeptide respectively. **B.** The *pakB* gene is 2932 bp and contains five exons based on conceptual translation. The predicted PakB polypeptide is 846 amino acids in length and contains a protein kinase domain; p21-binding domain and CRIB motif. Scale bars are as in A.

E. festucae PakA polypeptide shares 78% identity (ID) to the *F. graminearum* homologue, 69% ID to the *N. crassa* homologue and 73% ID to CHM1 from *M. grisea* (Fig. 4.3).

Gene A.4.2646 was found to have a 2932 bp CDS with four introns and was designated *pakB*. Conceptual translation gave rise to an 846 amino acid polypeptide that was predicted to contain a PBD domain between amino acids 251-309, and within this the N-terminal CRIB motif between amino acids 252-265. PakB is also predicted to contain a kinase domain between amino acids 567-818 (Fig. 4.2B). Comparison of the amino acid sequence to other Ste20-like kinases revealed that the predicted PakB polypeptide shares 54% ID to the *F. graminearum* homologue, 55% ID to the *N. crassa* homologue and 59% to MST20 from *M. grisea* (Fig. 4.4).

4.1.2. Conserved microsynteny and genomic rearrangement at the *pak* loci

Comparison of the sequences flanking the *pak* loci in *E. festucae*, *F. graminearum*, *N. crassa* and *M. grisea* revealed a rearrangement of gene organisation in *E. festucae* and *F. graminearum* in comparison to *N. crassa* and *M. grisea* (Fig. 4.5, Table 4.1). The *N. crassa* cla4-type pak locus contains genes encoding a methyltransferase (NCU00401, = *E. festucae* A.16.2560), glucose dehydratase (NCU00403, = *E. festucae* A.18.2560), Brix domain protein (NCU00404, = *E. festucae* A.19.2560), and tRNA synthetase (NCU00405, = *E. festucae* A.4.65). A similar gene arrangement is seen in *M. grisea* except that the methyltransferase gene is not linked to the *pakA* homologue (*CHM1*) but rather an RNA binding protein-encoding gene (MGG_06318, = *E. festucae* A.1.65) is found at this locus. In comparison, in the *E. festucae* sequenced strain 2368 and *F. graminearum*, these genes are split across two contigs, with the *pakA* homologue only being linked to the genes encoding the tRNA synthetase and RNA binding protein. However, the other three genes remain linked to each other in these species. This arrangement suggests these two sets of genes were separated in the lineage leading to *E. festucae* and *F. graminearum*. In *F. graminearum* these two sets of genes are found on separate chromosomes, with the *pakA* locus located on chromosome 4 and the locus containing the other three genes located on chromosome 3, indicating significant reorganisation of these genes. Interestingly, *pakA* and the two genes adjacent to it in *E. festucae*, A.4.65 and

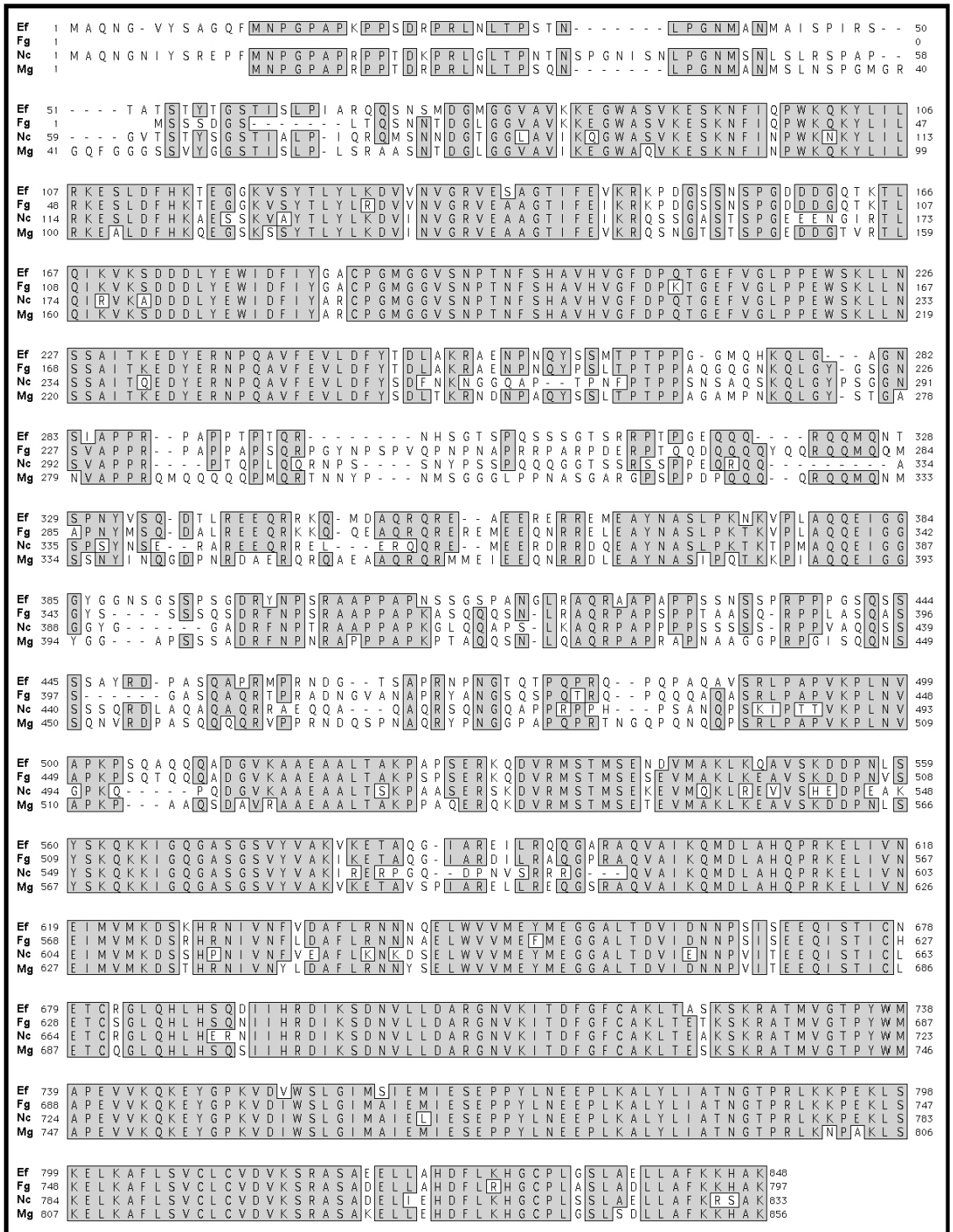

Figure 4.3 Amino acid sequence alignment of fungal Cla4 homologues
The predicted amino acid sequence of *E. festucae* PakA (Ef) is aligned with Cla4 homologues from *F. graminearum* (Fg), *N. crassa* (Nc) and *M. grisea* (Mg). PakA displays 78% amino acid identity to the *F. graminearum* homologue, 69% identity to the *N. crassa* homologue and 73% identity to the *M. grisea* homologue.

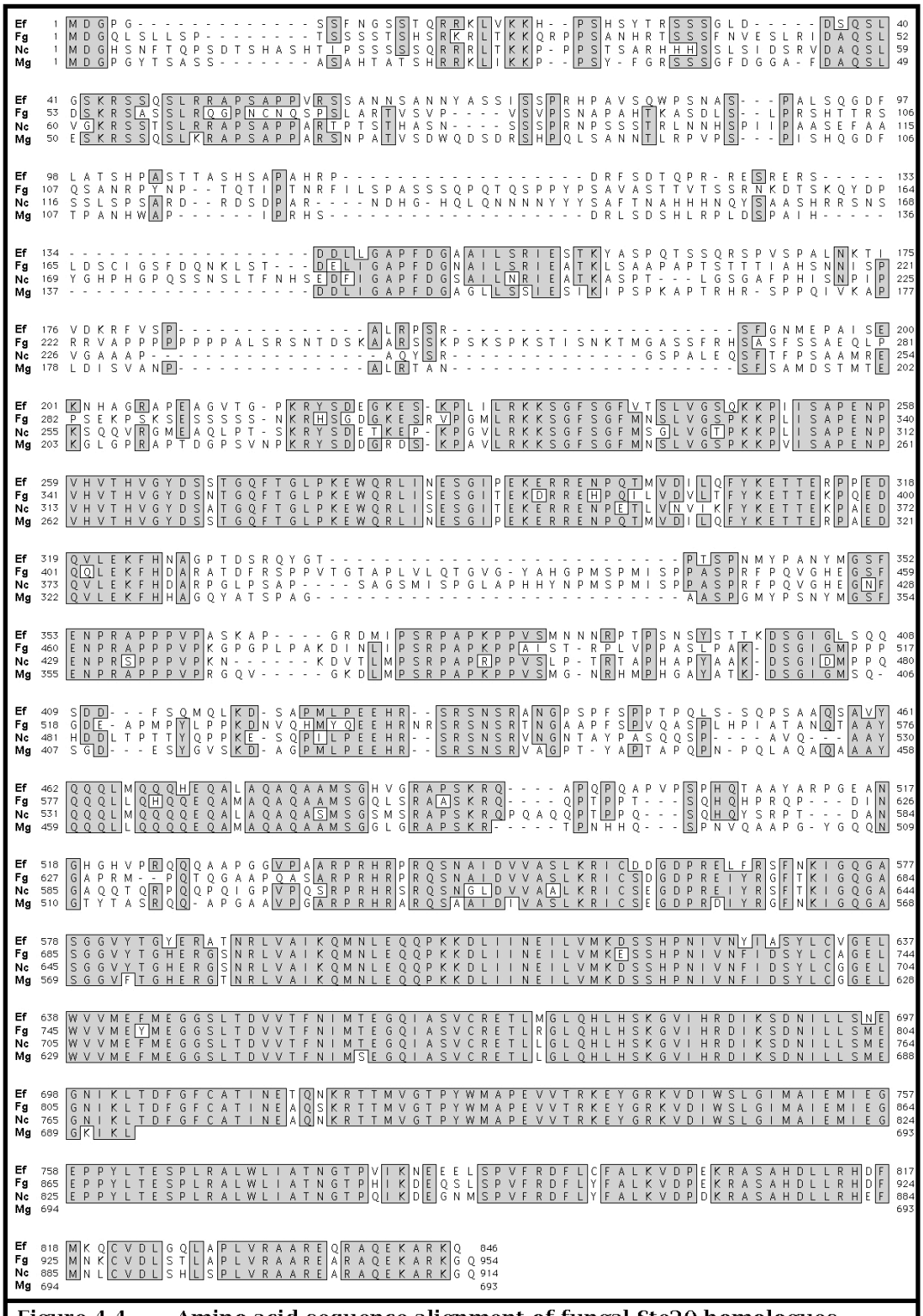

Figure 4.4 Amino acid sequence alignment of fungal Ste20 homologues
The predicted amino acid sequence of *E. festucae* PakB (Ef) is aligned with Ste20 homologues from *F. graminearum* (Fg), *N. crassa* (Nc) and *M. grisea* (Mg). PakB displays 54% amino acid identity to the *F. graminearum* homologue, 55% identity to the *N. crassa* homologue and 59% identity to the *M. grisea* homologue.

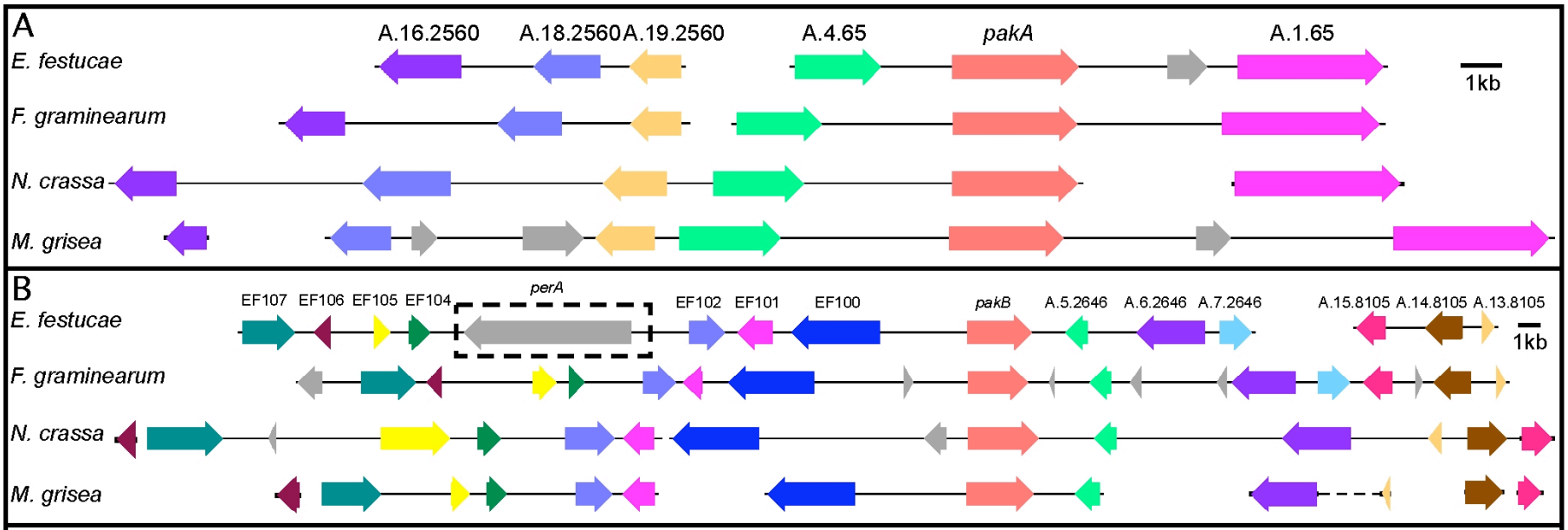

Figure 4.5 Conserved micro-synteny and genomic rearrangement at the *pak* loci
A. Genes located at the *pakA* loci in *N. crassa* and *M. grisea* have undergone rearrangement in *E. festucae* and *F. graminearum*. *E. festucae* genes A.16.2560-A.19.2560 and A.4.65-A.1.65 are numbered based on annotations of contigs 7 and 1082 respectively in the *E. festucae* genome database (http://csurs.csr.uky.edu/biodb-testbed/). Matching coloured arrows represent orthologous genes. Non-conserved genes are represented in grey. Full gene descriptions are listed in Table 4.1. B. The *E. festucae pakB* locus displays conserved synteny with *F. graminearum*, *N. crassa* and *M. grisea*. In the sequenced *E. festucae* strain 2368 EF104 and EF102 are found on two separate contigs (718 and 806 respectively). However, in strain Fl1 these contigs are linked by the *perA* gene, as indicated by the dashed black box. This gene is interupted by a transposon relic in strain 2368, likely preventing linkage of contigs 718 and 806. Genes EF100-107 are numbered based on Tanaka et al. (2005). Genes A.5.2646-A.7.2646 and A.13.8105-A.15.8105 are numbered based on 806 and 385 respectively in the *E. festucae* genome database. Full gene descriptions are listed in Table 4.2.

Table 4.1 Description of genes found at the *pakA* loci

		Annotated/autocalled gene in fungal genome database					
		F. graminearum[b]		*N. crassa*[b]		*M. grisea*[b]	
Gene[a]	Putative function	Annotation	E-value	Annotation	E-value	Annotation	E-value
A.16.2560	S-adenosylmethionine-dependent methyltransferase	FGSG_05468	5e-95	NCU00401	4e-71	MGG_07964	2e-31
A.18.2650	dtdp-glucose 4,6-dehydratase	FGSG_05467	4e-107	NCU00403	4e-78	MGG_06324	3e-109
A.19.2650	Brix domain protein	FGSG_05466	4e-177	NCU00404	9e-117	MGG_06322	1e-144
A.4.65	Glycyl-tRNA synthetase	FGSG_06958	0	NCU00405	0	MGG_06321	0
pakA (A.3.65)	p21-activated kinase	FGSG_06957	0	NCU00406	0	MGG_06320	0
A.1.65	Puf family RNA-binding protein	FGSG_13028	0	NCU06199	0	MGG_06318	0

a. Annotation from the *E. festucae* genome database (http://csurs.csr.uky.edu/biodb-testbed/)
b. Annotation from the Fungal Genome Initiative site (http://www.broad.mit.edu/)

A.1.65, appear more highly conserved at the amino acid level across the fungi examined than the other three genes. BLASTp of *E. festucae* A.4.65, A.1.65 and *pakA* sequences identified the homologues from *F. graminearum*, *N. crassa* and *M. grisea* all with E-values of 0. In comparison, BLASTp with A.16.2560, A.18.2560 and A.19.2560 sequences identified the *F. graminearum*, *N. crassa* and *M. grisea* homologues with E-values greater than 0. This suggests the A.4.65, A.1.65 and *pakA* genes may be under stronger selection pressure than the other three genes.

In *F. graminearum* the Ste20 locus contains genes encoding a GTPase binding protein (FGSG_09486, = *E. festucae* EF107), methyltransferase (FGSG_09487, = *E. festucae* EF106), conserved hypothetical proteins (FGSG_09488, = *E. festucae* EF105; FGSG_09496, = *E. festucae* A.7.2646; FGSG_09497, = *E. festucae* A.15.8105), ubiquinol cytochrome C reductase hinge protein (FGSG_09489, = *E. festucae* EF104), MFS transporter (FGSG_09490, = *E. festucae* EF102), ketosteroid reductase (FGSG_13596, = *E. festucae* EF101), RNA binding effector protein (FGSG_09491, = *E. festucae* EF100), short chain dehydrogenase (FGSG_09494, = *E. festucae* A.5.2646), chromatin remodelling complex subunit (FGSG_09495, = *E. festucae* A.6.2646), stromal membrane associated protein (FGSG_09499, = *E. festucae* A.14.8105) and peptide methionine sulfoxide reductase (FGSG_09500, = *E. festucae* A.13.8105) (Fig. 4.5; Table 4.2). In the sequenced *E. festucae* strain 2368 these genes are split across three contigs (385, 806 and 718) but the gene order and orientation is the same as in *F. graminearum*. It is likely that these three contigs are linked as genes A.7.2646 and A.15.8105 are found at the ends of their contigs. In addition, in *E. festucae* strain Fl1 EF104 and EF102 are linked with the *perA* gene between them, as indicated in the dashed black box in Figure 4.5 (Tanaka et al., 2005). In strain 2368 a transposon relic flanks the 5' untranslated region (UTR) of an inactive *perA* gene (D. Fleetwood, personal communication), which is probably why these two contigs (718 and 806) have not been linked in this strain. In *N. crassa* genes encoding the RNA binding effector protein (NCU03897, = *E. festucae* EF100), short chain dehydrogenase (NCU03893, = *E. festucae* A.5.2646), chromatin remodelling complex subunit (NCU03892, = *E. festucae* A.6.2646), stromal membrane associated protein (NCU03890, = *E. festucae* A.14.8105), peptide methionine sulfoxide reductase (NCU03891, = *E. festucae* A.13.8105), and conserved hypothetical protein (NCU03888, = *E. festucae* A.15.8105) are linked to *pakB*. Genes encoding the GTPase binding protein (NCU05987, = *E. festucae* EF107), conserved

Table 4.2 Description of genes found at the *pakB* loci

		Annotated/autocalled gene in fungal genome database					
		F. graminearum[b]		*N. crassa*[b]		*M. grisea*[b]	
Gene[a]	Putative function	Annotation	E-value	Annotation	E-value	Annotation	E-value
EF107	GTPase binding protein	FGSG_09486	0	NCU05987	2e-174	MGG_01308	0
EF106	Methyltransferase	FGSG_09487	6e-79	NCU02941	4e-18	MGG_03293	6e-19
EF105	Conserved hypothetical protein	FGSG_09488	7e-111	NCU05988	4e-29	MGG_01306	3e-43
EF104	Ubiquinol cytochrome C reductase hinge protein	FGSG_09489	2e-36	NCU05989	2e-29	MGG_01305	2e-22
EF102	MFS transporter	FGSG_09490	0	NCU05990	9e-145	MGG_01304	8e-134
EF101	Ketosteroid reductase	FGSG_13596	0	NCU05991	5e-102	MGG_01303	2e-72
EF100	RNA-binding effector protein	FGSG_09491	0	NCU03897	0	MGG_06496	0
pakB (A.4.2646)	p21-activated kinase	FGSG_09492	0	NCU03894	0	MST20	0
A.5.2646	Short chain dehydrogenase	FGSG_09494	3e-175	NCU03893	1e-143	MGG_06494	2e-146
A.6.2646	Chromatin remodeling complex subunit	FGSG_09495	0	NCU03892	0	MGG_02493	0
A.7.2646	Conserved hypothetical protein	FGSG_09496	4e-11	-	-	-	-
A.15.8105	Conserved hypothetical protein	FGSG_09497	4e-175	NCU03888	1e-151	MGG_02506	1e-111
A.14.8105	Stromal membrane associated protein	FGSG_09499	2e-175	NCU03890	4e-144	MGG_04954	2e-167
A.13.8105	Peptide methionine sulfoxide reductase	FGSG_09500	4e-65	NCU03891	5e-63	MGG_02496	6e-64

a. Annotation from the *E. festucae* genome database (http://csurs.csr.uky.edu/biodb-testbed/) and Tanaka et al. (2005)
b. Annotation from the Fungal Genome Initiative site (http://www.broad.mit.edu/)

hypothetical protein NCU05988 (= *E. festucae* EF105), ubiquinol cytochrome C reductase hinge protein (NCU05989, = *E. festucae* EF104), MFS transporter (NCU05990, = *E. festucae* EF102) and ketosteroid reductase (NCU05991, = *E. festucae* EF101) are found linked to each other but are located elsewhere in the genome. The methyltransferase-encoding gene NCU02941 (= *E. festucae* EF106) is not linked to any of the genes described above. No *N. crassa* homologue could be identified for conserved hypothetical protein A.7.2646. In *M. grisea* only the RNA binding effector protein (MGG_06496, = *E. festucae* EF100) and short chain dehydrogenase (MGG_06494, = *E. festucae* A.5.2646) encoding genes are linked to *pakB*. Genes encoding the GTPase binding protein (MGG_01308, = *E. festucae* EF107), conserved hypothetical protein MGG_01306 (= *E. festucae* EF105), ubiquinol cytochrome C reductase hinge protein (MGG_01305, = *E. festucae* EF104), MFS transporter (MGG_01304, = *E. festucae* EF102) and ketosteroid reductase (MGG_01303, = *E. festucae* EF101) remain linked to each other. In comparison, genes encoding the chromatin remodelling complex subunit (MGG_02493, = *E. festucae* A.6.2646), peptide methionine sulfoxide reductase (MGG_02496, = *E. festucae* A.13.8105), stromal membrane associated protein (MGG_04954, = *E. festucae* A.14.8105) and conserved hypothetical protein MGG_02506 (= *E. festucae* A.15.8105) are not linked to any of genes detailed above. Similar to *N. crassa, M. grisea* does not contain a homologue of conserved hypothetical protein A.7.2646.

4.2. Targeted replacement of the *pakA* and *pakB* genes

To determine if the *pak* genes are important for growth of *E. festucae* in culture or in regulating its association with perennial ryegrass, gene replacement mutants were generated by homologous recombination.

4.2.1. Preparation of *pakA* and *pakB* replacement constructs

The *pakA* replacement construct, pCE36, was prepared by PCR as no suitable restriction fragments were found (refer Section 2.7.3). PCR amplification from cosmid

24B3 generated a 2 kb pak1/2 fragment from close to the 3' end of *pakA* which was ligated into pCR4-TOPO, sequenced then sub-cloned upstream of the hygromycin resistance cassette *hph* in the pII99-based vector pSF15.15. A 2kb pak3/4 fragment from close to the 5' end of *pakA* was similarly amplified from cosmid 24B3 and cloned downstream of *hph*, generating the final replacement construct (Fig. 4.6A). The *pakB* replacement construct, pCE38, was also prepared by PCR. A 3 kb pak5/6 fragment from close to the 5' end of *pakB* was PCR amplified from cosmid 9H6, ligated into pCR4-TOPO, sequenced then sub-cloned downstream of *hph* in pSF15.15. A 1.6 kb pak7/8 fragment from close to the 3' end of *pakB* was similarly amplified from cosmid 9H6 and cloned upstream of *hph*, generating the final replacement construct (Fig. 4.6B). The *pakA* and *pakB* flanking regions were directionally cloned in such a way that they face in the opposite direction to the *hph* cassette to avoid potential read through, as the *hph* cassette contains no terminator sequence. PCR amplification using the primers described above was performed from cosmid DNA as amplification from *E. festucae* genomic DNA was unsuccessful. Cosmid clones containing the *pakA* and *pakB* genes were isolated from the *E. festucae* cosmid library (Tanaka et al., 2005). The 269 bp *pakA* fragment and 221 bp *pakB* fragments detailed earlier (Section 4.1.1) were radioactively labelled and used to screen an *E. festucae* Fl1 cosmid library. Cosmid DNA was isolated for clones showing the strongest hybridisation signals. Based on comparison of restriction patterns produced by these clones with patterns expected based on *E. festucae* genomic sequence analysis two clones, 24B3 and 9H6, which contain extensive flanking sequence either side of the *pakA* and *pakB* genes respectively were selected as templates for amplification of the fragments for generation of the replacement constructs. Primers used in amplification of these fragments contained mismatches to generate restriction site overhangs to facilitate cloning into pSF15.15 (Table 2.4). For transformation of protoplasts, the replacement constructs were amplified using the Expand Long Template PCR system with primers pII99-2 and pII99-3 to generate a linear construct. Transformation with linear DNA greatly reduces the frequency of non-homologous integration, as two recombination events are required for integration rather than just one when circular DNA is used.

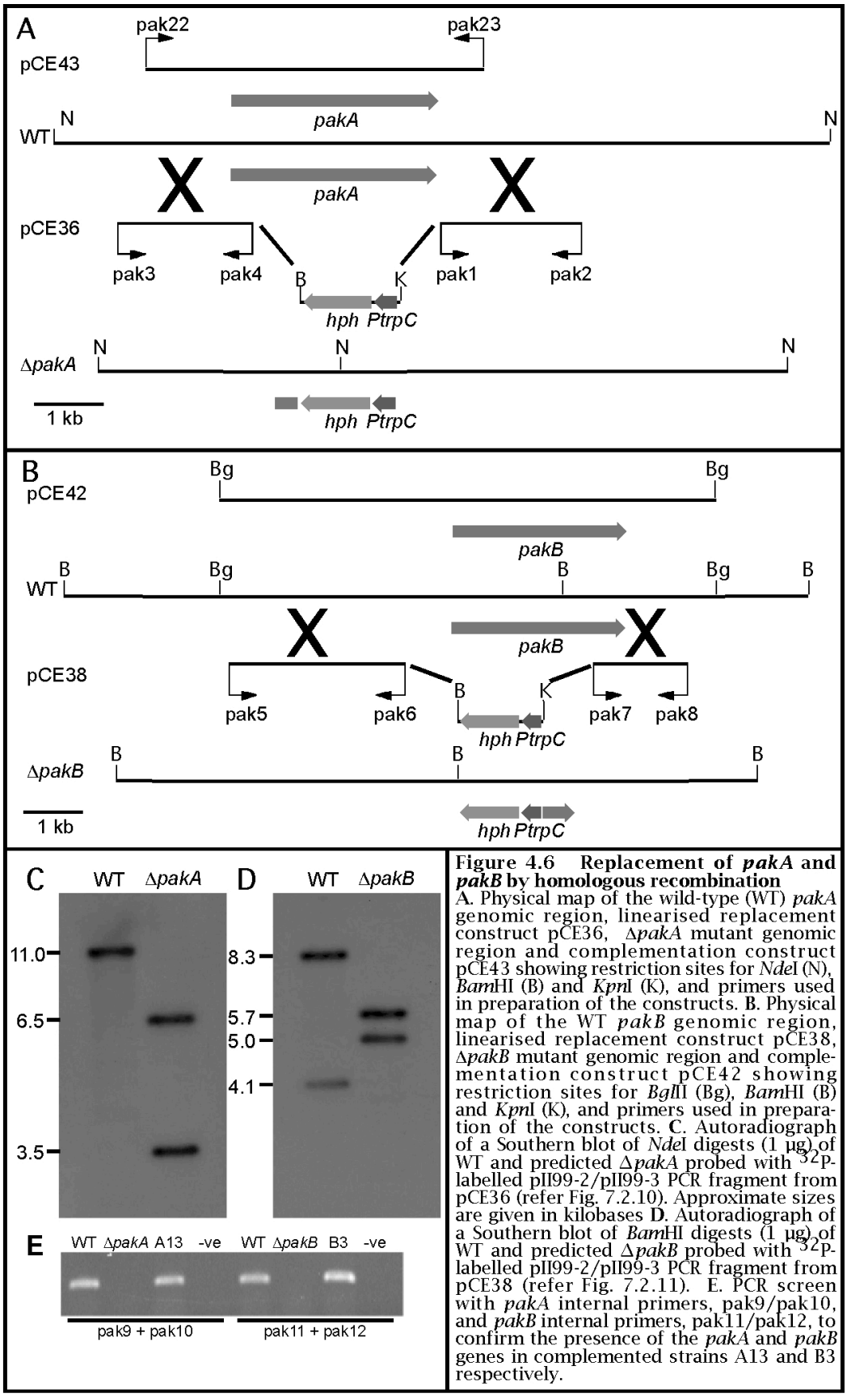

Figure 4.6 Replacement of *pakA* and *pakB* by homologous recombination
A. Physical map of the wild-type (WT) *pakA* genomic region, linearised replacement construct pCE36, Δ*pakA* mutant genomic region and complementation construct pCE43 showing restriction sites for *Nde*I (N), *Bam*HI (B) and *Kpn*I (K), and primers used in preparation of the constructs. **B.** Physical map of the WT *pakB* genomic region, linearised replacement construct pCE38, Δ*pakB* mutant genomic region and complementation construct pCE42 showing restriction sites for *Bgl*II (Bg), *Bam*HI (B) and *Kpn*I (K), and primers used in preparation of the constructs. **C.** Autoradiograph of a Southern blot of *Nde*I digests (1 µg) of WT and predicted Δ*pakA* probed with ^{32}P-labelled pII99-2/pII99-3 PCR fragment from pCE36 (refer Fig. 7.2.10). Approximate sizes are given in kilobases **D.** Autoradiograph of a Southern blot of *Bam*HI digests (1 µg) of WT and predicted Δ*pakB* probed with ^{32}P-labelled pII99-2/pII99-3 PCR fragment from pCE38 (refer Fig. 7.2.11). **E.** PCR screen with *pakA* internal primers, pak9/pak10, and *pakB* internal primers, pak11/pak12, to confirm the presence of the *pakA* and *pakB* genes in complemented strains A13 and B3 respectively.

4.2.2. Screening for *pakA* and *pakB* replacement mutants

Transformants were sub-cultured a minimum of three times onto media containing hygromycin in order to achieve nuclear purification. *pakA* transformants were then selected for further screening based on the altered colony morphology of a sub-set of transformants, which displayed reduced radial growth and appeared fluffy due to an increase in aerial hyphae. These transformants together with a selection of transformants displaying wild-type growth were screened by PCR. A crude Extract-N-Amp (Sigma-Aldrich) screen was performed first using primer set pak9/10 which produce a 525 bp *pakA* internal fragment only in wild-type and ectopic integration strains (Fig. 4.7A). Based on the results of this screen nine transformants that did not produce a band were selected for further analysis using purified genomic template. Two PCR screens using primer sets pak14/pUChph6 and pak13/15 which produce 2.7 kb and 2.4 kb fragments respectively only from *pakA* replacement strains were performed (Fig. 4.7A). This confirmed that four of the nine transformants had complete integration of the replacement construct at the *pakA* locus, replacing *pakA* with the *hph* cassette. Southern blotting was then used to determine whether these transformants contain single or multiple integrations of the replacement construct at the *pakA* locus. This revealed that only strain 43-3 contained a single integration of the construct, whereas the other three strains contained multiple copies of the replacement construct at the *pakA* locus. The Southern blot result for strain 43-3, henceforth referred to as the Δ*pakA* mutant, is shown in Figure 4.6.

In comparison to the *pakA* transformants, the *pakB* transformants did not display any obvious morphological differences to the wild-type strain. Thus 20 strains were arbitrarily chosen for crude Extract-N-Amp analysis using primer set pak11/12 which produces a 522 bp *pakB* internal fragment only in wild-type and ectopic integration strains (Fig. 4.7B). However, even after multiple attempts Extract-N-Amp proved unsuccessful. The transformants were then examined more closely to try and identify more subtle differences in morphology. This revealed that a number of transformants appeared flatter and less fluffy than the wild-type strain due to a reduction in aerial hyphae. Based on this subtle difference 10 transformants were chosen for further PCR analysis from purified genomic template. Two PCR screens using primer sets

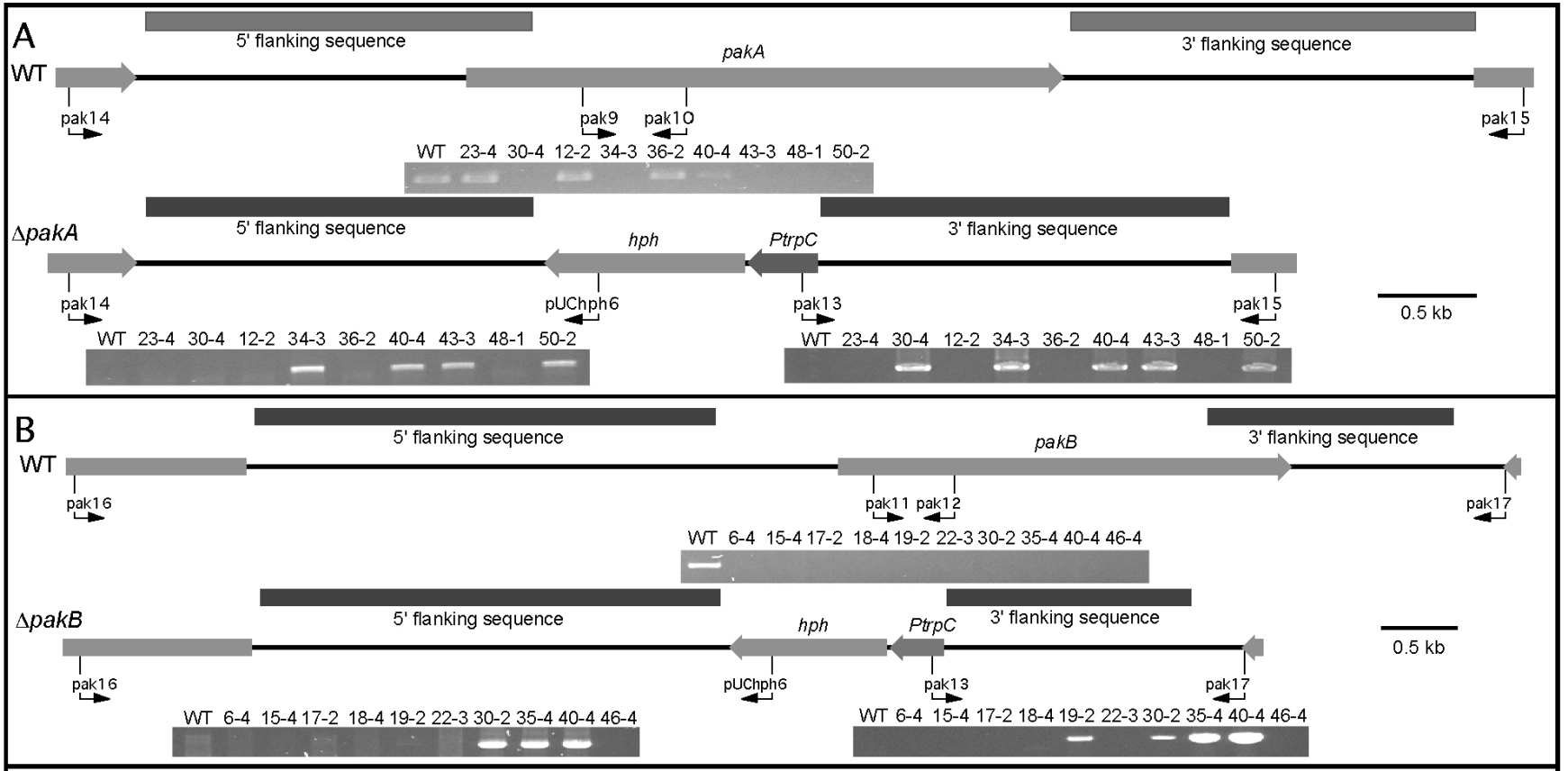

Figure 4.7 PCR screen to identify *pakA* and *pakB* replacement mutants
A. Genomic maps of the *pakA* locus in wild-type *E. festucae* (WT) and the Δ*pakA* mutant showing positions of primers used in screening for replacement mutants. Products produced by pak9/10, pak14/pUChph6 and pak13/15 primer sets are shown below the corresponding primer binding sites on each genomic map. pak9/10 products are only generated from WT and ectopic integration strains. pak14/pUChph6 and pak13/15 products are only generated from Δ*pakA* replacement strains. B. Genomic maps of the pakB locus in WT and the Δ*pakB* mutant showing positions of primers used in screening for replacement mutants. Products produced by pak11/12, pak16/pUChph6 and pak13/17 primer sets are shown below the corresponding primer binding sites on each genomic map. pak11/12 products are only generated from WT and ectopic integration strains. pak16/pUChph6 and pak13/17 products are only generated from Δ*pakB* replacement strains.

pak16/pUChph6 and pak13/17 which produce 4.5 kb and 2 kb fragments respectively only from *pakB* replacement strains were performed (Fig. 4.7B). This identified three transformants that had complete integration of the replacement construct at the *pakB* locus, replacing *pakB* with the *hph* cassette. Southern blotting was used to determine whether these transformants contained single or multiple integrations of the replacement construct at the *pakB* locus. This revealed that strain 35-4 contained a single integration of the construct at the *pakB* locus. The Southern blot result for strain 35-4, henceforth referred to as the Δ*pakB* mutant, is shown in Figure 4.6.

4.2.3. Complementation of the Δ*pakA* and Δ*pakB* mutants

To confirm that any phenotypic differences observed between the pak mutants and wild-type *E. festucae* were solely due to the loss of the *pak* gene, the Δ*pakA* and Δ*pakB* replacement mutants were complemented with the *pakA* and *pakB* genes respectively. The *pakA* complementation construct pCE43 was prepared by PCR amplification using the proof-reading enzyme Expand HiFi, of a 4.9 kb pak22/23 fragment containing the entire *pakA* gene with 1.2 kb upstream and 650 bp downstream for inclusion of promoter and terminator sequences (Fig. 4.6). The PCR product was then cloned into pCR4-TOPO and DNA from 12 independent clones pooled to maximise the possibility of obtaining transformants that contain error free sequence. This pooled DNA was co-transformed into Δ*pakA* protoplasts with pII99, which contains the geneticin resistance cassette *npt*II. The *pakB* complementation construct, pCE42, was prepared by sub-cloning an 8.3 kb *Bgl*II fragment from cosmid clone 9H6 into the pII99-based vector pSF17.8, which contains the *npt*II cassette. pCE42 was then transformed into Δ*pakB* protoplasts. *pakA* and *pakB* transformants were sub-cultured twice on media containing geneticin to achieve nuclear purification. Δ*pakA* transformants that displayed increased radial growth in comparison to the Δ*pakA* mutant, and a random selection of Δ*pakB* transformants were screened by Extract-N-Amp analysis. Primer sets pak9/10 and pak11/12 for *pakA* and *pakB* respectively were used to confirm the presence or absence of the *pakA* and *pakB* genes in these strains (Fig. 4.6). One complemented strain each for *pakA* and *pakB* were selected for further analysis. These strains will henceforth be referred to as A13 and B3 for *pakA* and *pakB* respectively.

4.3. *pakA* and *pakB* are essential for normal growth in culture

To determine whether the *E. festucae pak* genes are required for normal growth in culture, mutants were examined for any change in their growth both at the whole colony and microscopic levels.

4.3.1. Growth in culture

As detailed above, the Δ*pakA* and Δ*pakB* mutants displayed altered colony morphology under normal growth conditions, with Δ*pakA* mutant colonies having reduced radial growth and appearing fluffy due to increased aerial hyphae and Δ*pakB* mutant colonies appearing flatter due to reduced aerial hyphae (Fig. 4.8). The pak mutants also displayed increased sensitivity to cell wall-stressing agents. The Δ*pakA* mutant displayed increased sensitivity to both CFW and sodium dodecyl sulphate (SDS). In comparison, the Δ*pakB* mutant was slightly more sensitive to CFW than the wild-type strain but no more sensitive to SDS. Transformation of the Δ*pakA* mutant with pCE43, which contains the *pakA* gene, and the Δ*pakB* mutant with pCE42, which contains the *pakB* gene, restored wild-type growth both under normal and cell wall-stressing conditions.

4.3.2. Changes at the microscopic level

Examination of the growth of the pak mutants using DIC microscopy revealed a number of key differences in comparison to the wild-type strain (Fig. 4.9). The Δ*pakA* mutant displayed significant changes in branching with hyphae appearing hyperbranched and tip bifurcations frequently present. Many hyphae also appeared convoluted in comparison to the relatively straight hyphae of the wild-type strain. In the Δ*pakB* mutant, tip bifurcations were also frequently observed. Branch positioning and direction were also altered with branches growing both outwards and inwards from the edge of the colony, and many branches arising from close to the middle of the hyphal compartment rather than adjacent to the tip-proximal septa as in wild-type. In addition, these hyphae also contained numerous swellings and were often kinked or bent. The

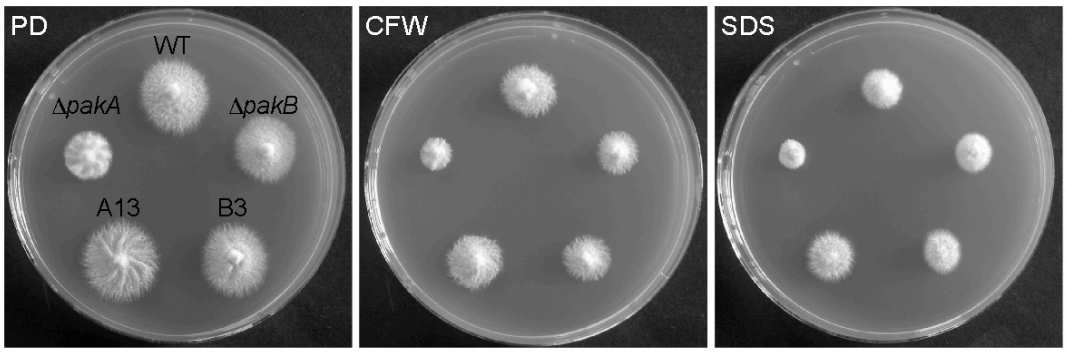

Figure 4.8 Culture phenotype of the pak mutants
Growth of wild-type *E. festucae* (WT), Δ*pakA*, Δ*pakB* and complemented strains A13 and B3 were examined under normal conditions of PD at 22°C and under conditions of cell wall stress induced by 0.01% SDS and 100 μg/ml CFW. On unsupplemented PD the Δ*pakA* mutant displays reduced radial growth and appears fluffy due to increased aerial hyphae. The Δ*pakB* mutant appears flatter due to a reduction in aerial hyphae, particularly obvious at the colony edge. On media containing CFW and SDS growth of the Δ*pakA* mutant is reduced further than that of WT due to increased sensitivity to these agents. The Δ*pakB* mutant is slightly more sensitive to CFW than WT, but is no more sensitive to SDS than WT. *pakA* complemented strain A13 displays WT growth on PD and WT sensitivity to CFW and SDS. *pakB* complemented strain B3 shows WT growth on PD and in the presence of CFW. Colony labeling shown in panel one applies to all panels.

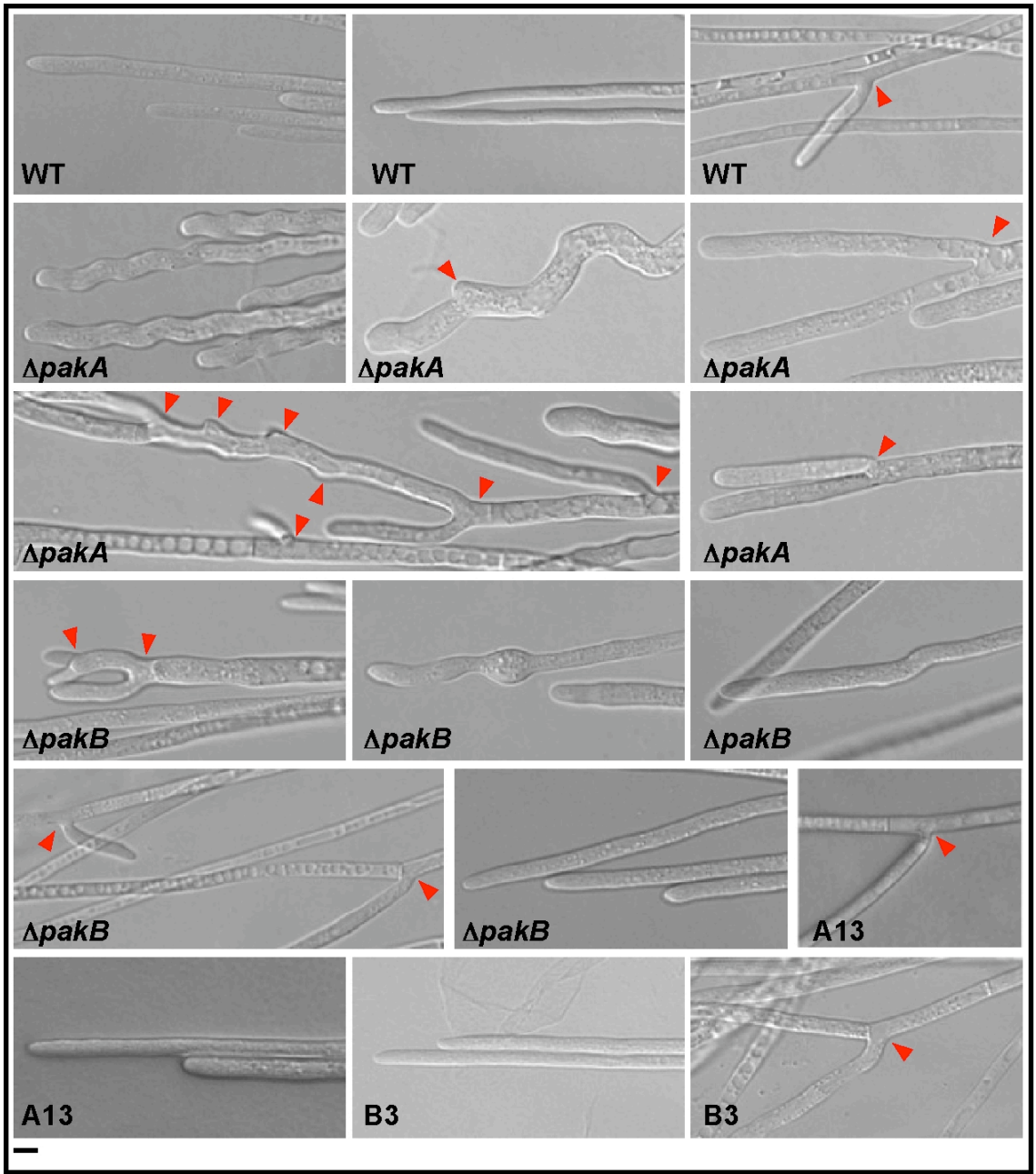

Figure 4.9 Growth of the pak mutants in culture
Differential interference contrast (DIC) micrographs showing growth of wild-type *E. festucae* (WT), Δ*pakA*, Δ*pakB* and complemented strains A13 and B3 on PD medium. Tips of the WT strain appear straight and branches form adjacent to the tip-proximal septa. In the Δ*pakA* mutant the hyphal tips appear convoluted. Branching is also altered with the hyphae appearing hyperbranched with frequent tip bifurcations. In the Δ*pakB* mutant tip bifurcations are also obvious. Hyphae often contain swellings or appear bent. Branches are also observed to grow back towards the centre of the colony. In *pakA* complemented strain A13 and *pakB* complemented strain B3 hyphal tip appearance and branching is restored back to that of the WT strain. Arrowheads indicate the position of branch points.

Δ*pakA* complemented strain A13, and Δ*pakB* complemented strain B3 displayed wild-type growth and morphology.

4.3.2.1. The Δ*pakA* mutant displays altered cell compartment size

Given that pak mutants from other filamentous fungi often display changes in cellular compartment size, the width and length of Δ*pakA* and Δ*pakB* mutant cells were examined. Colonies were stained with CFW to allow visualisation of the septa, and the distance between septa measured to determine the average cell length for wild-type *E. festucae*, the Δ*pakA* and Δ*pakB* mutants, and complemented strains A13 and B3 (Fig. 4.10). Hyphal width was measured at the septum to achieve an accurate comparison as hyphal width may vary across a compartment. Using this approach the Δ*pakA* mutant cell compartments were found to be both significantly shorter and wider than those of wild-type. In comparison, the Δ*pakB* mutant cells were slightly shorter on average than those of wild-type but of a similar width. Complemented strains A13 and B3 displayed lengths and widths similar to those of the wild-type strain. Staining with CFW also revealed that the Δ*pakA* mutant showed extended CFW staining at the hyphal tip in comparison to the wild-type strain.

4.3.2.2. The Δ*pakA* mutant displays increased vacuole size

When examining the pak mutants by DIC it became obvious that the Δ*pakA* mutant contained much larger vacuoles than the wild-type strain. To examine this more closely colonies were incubated with FM4-64, which stains the vacuolar membrane red (Fig. 4.11). This confirmed that vacuoles in the Δ*pakA* mutant were much larger than those of the wild-type strain and are visible much closer to the hyphal tip. In contrast, vacuoles in the Δ*pakB* mutant and Δ*pakA* complemented strain A13 appeared similar to those of the wild-type strain.

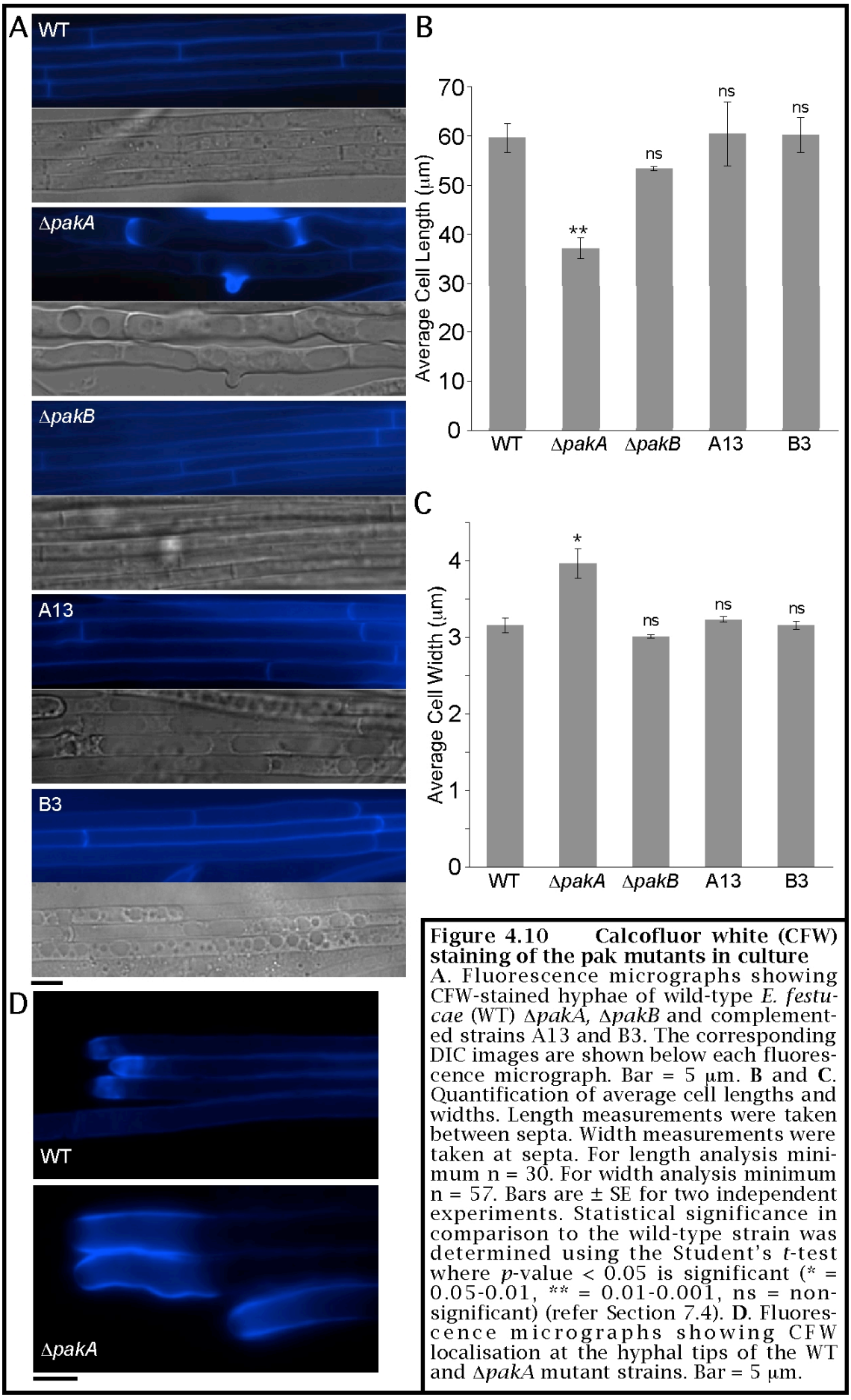

Figure 4.10 Calcofluor white (CFW) staining of the pak mutants in culture
A. Fluorescence micrographs showing CFW-stained hyphae of wild-type *E. festucae* (WT) Δ*pakA,* Δ*pakB* and complemented strains A13 and B3. The corresponding DIC images are shown below each fluorescence micrograph. Bar = 5 μm. **B** and **C.** Quantification of average cell lengths and widths. Length measurements were taken between septa. Width measurements were taken at septa. For length analysis minimum n = 30. For width analysis minimum n = 57. Bars are ± SE for two independent experiments. Statistical significance in comparison to the wild-type strain was determined using the Student's *t*-test where *p*-value < 0.05 is significant (* = 0.05-0.01, ** = 0.01-0.001, ns = non-significant) (refer Section 7.4). **D.** Fluorescence micrographs showing CFW localisation at the hyphal tips of the WT and Δ*pakA* mutant strains. Bar = 5 μm.

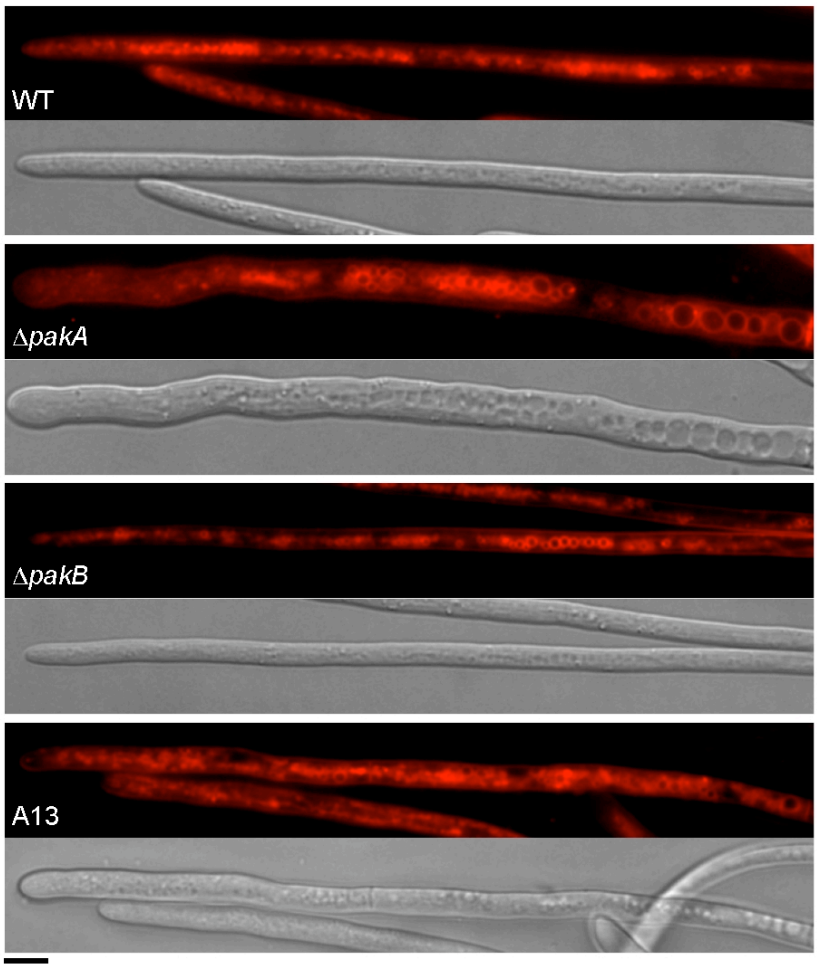

Figure 4.11 Fluorescence microscopy showing FM4-64 stained vacuoles in culture
Fluorescence micrographs showing FM4-64 stained hyphae of wild-type (WT), Δ*pakA*, Δ*pakB* and *pakA* complemented strain A13. FM4-64 selectively stains the vacuolar membrane red. In the Δ*pakA* mutant vacuoles can be seen closer to the hyphal tip than in WT, Δ*pakB* and the *pakA* complemented strain. Vacuoles in the Δ*pakA* mutant are also much larger than in the other strains. The corresponding DIC image is shown below each fluorescence micrograph. Vacuoles can also be seen in these micrographs. Bar = 10 μm.

4.3.2.3. Structures at the hyphal tip

Examination of the pak mutants by DIC also revealed that the Δ*pakA* mutant did not develop the structures seen at the tips of wild-type hyphae under conditions of nutrient stress or after extended growth (refer Section 3.5) (Fig. 4.12). In contrast, the Δ*pakB* mutant appeared to overproduce these structures, with nearly every hypha containing these structures at their tip. The density of these structures in the Δ*pakB* mutant prevented examination by fluorescence microscopy, as when stained with calcofluor white (CFW) the fluorescence from the colony periphery was too intense for individual hyphae to be visualised. However, this does suggest that these structures stain with CFW in the Δ*pakB* mutant.

4.4. The Δ*pakA* mutant displays increased ROS levels in culture

Given the potential role of a pak in activation of the Nox complex it was important to determine whether ROS levels were altered in either of the *E. festucae* pak mutants. Both hydrogen peroxide and superoxide levels were examined using DAB and NBT respectively. Incubation with DAB resulted in formation of a dark red ring of staining around the periphery of the Δ*pakA* mutant colony (Fig. 4.13A). In comparison, the wild-type and Δ*pakB* mutant strains displayed only background staining. ROS produced by the Δ*sakA* mutant were shown to be delocalised back from the hyphal tip, evidenced both by the dark red staining of the entire colony with DAB and by microscopic examination of colonies incubated with NBT (Fig. 3.10A and 3.13). The appearance of staining only around the edge of the Δ*pakA* mutant colony suggested that the ROS was still localised to the hyphal tip. This was confirmed by incubation with NBT, which showed that the formazan precipitate was still highly localised to the hyphal tip (Fig. 4.13B). However, in comparison to wild-type *E. festucae* where only a subset of hyphal tips contained formazan precipitate, nearly every Δ*pakA* mutant tip contained the precipitate. This indicates that ROS levels are elevated in the Δ*pakA* mutant, but this ROS is still highly localised to the hyphal tip. The Δ*pakA* complemented strain A13

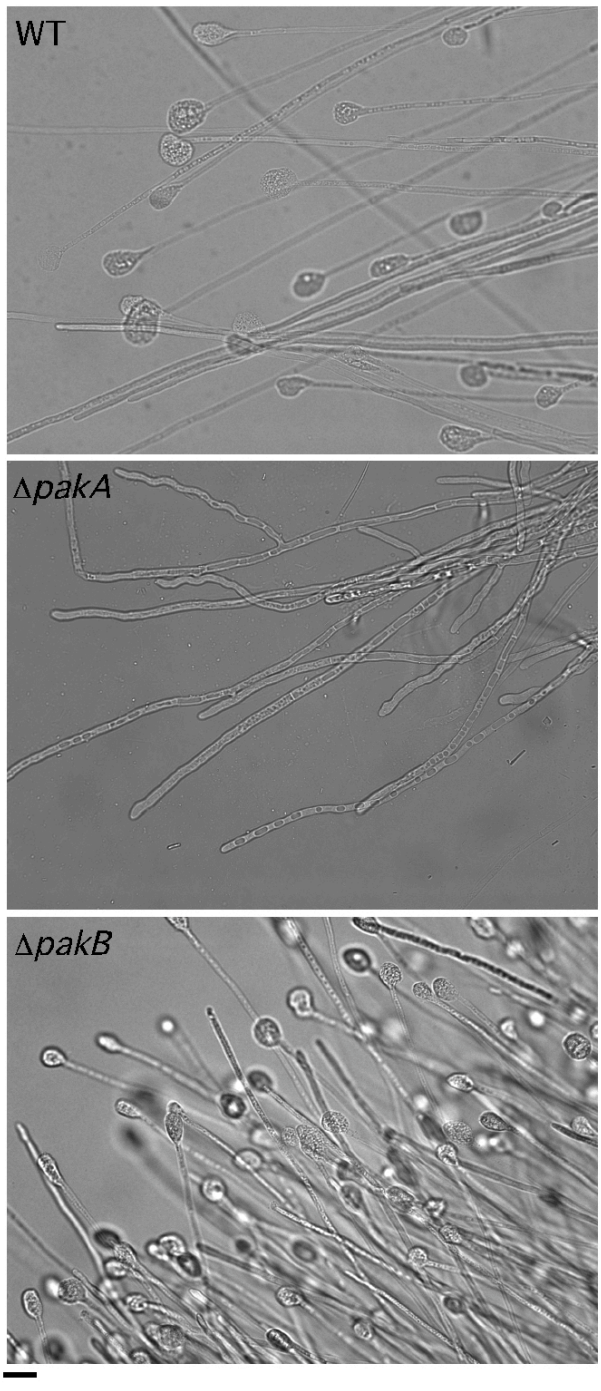

Figure 4.12 Examination of structures at the hyphal tip by DIC microscopy
Differential interference contrast (DIC) micrographs showing spherical/elliptical structures at the hyphal tips of wild-type *E. festucae* (WT) and the Δ*pakB* mutant. These structures are seen at the end of nearly every hypha in the Δ*pakB* mutant, but are not seen in the Δ*pakA* mutant. Cultures were grown on thin layer PD agarose for 7-10 days to induce nutrient-stressed conditions. Bar = 20 μm.

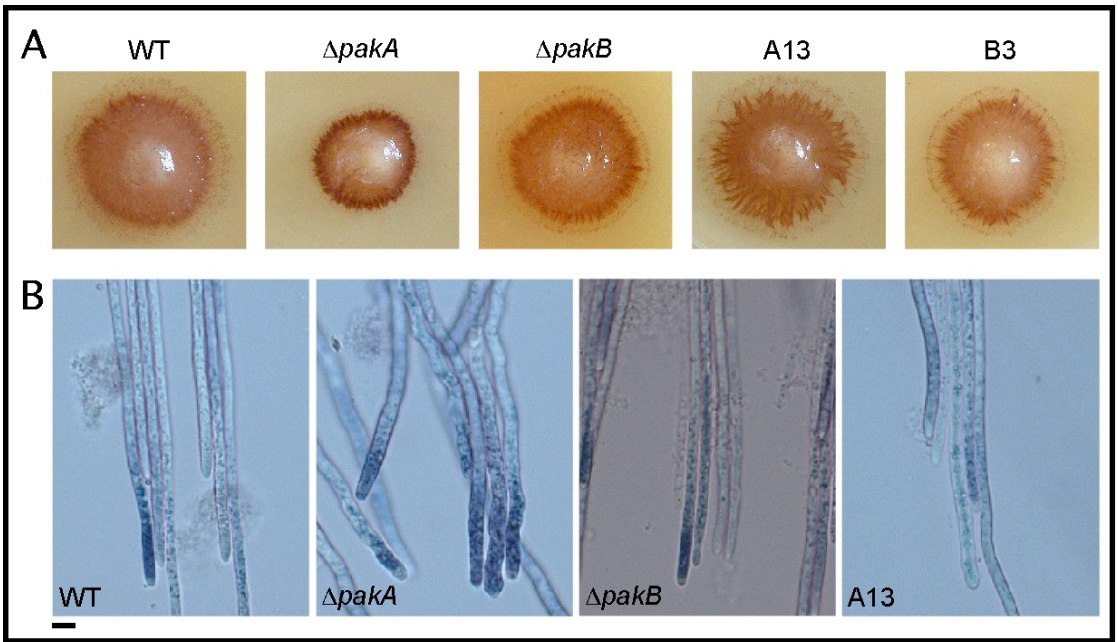

Figure 4.13 Examination of reactive oxygen species (ROS) levels in culture
A. Detection of hydrogen peroxide (H_2O_2) using 3, 3'diaminobenzidine (DAB) which forms a brick-red precipitate by reaction with H_2O_2. Colonies of wild-type (WT), Δ*pakA,* Δ*pakB, pakA* complemented strain A13 and *pakB* complemented strain B3 were grown on PD medium for 7 days at 22˚C, then incubated with DAB for 24 h at 22˚C then 20 h at 4˚C. **B.** Colonies of WT, Δ*pakA,* Δ*pakB* and A13 were grown across PD-agarose covered slides for 5-7 days at 22˚C. Superoxide levels were then detected by incubation with nitroblue tetrazolium (NBT) for 5 h at 22˚C. NBT forms a dark-blue, water-insoluble formazan precipitate on reaction with superoxide anions. Colonies were then examined by light microscopy. Bar = 5 μm.

displayed wild-type levels of hydrogen peroxide, and only slightly elevated levels of superoxide in comparison to wild-type *E. festucae* (Fig. 4.13).

4.5. *pakA* is required for symbiotic maintenance

To determine whether the *pak* genes play a role in regulating the association of *E. festucae* with perennial ryegrass, seedlings were inoculated with the replacement mutants and the survival and growth of the inoculated plants monitored.

4.5.1. The Δ*pakA* mutant reduces host survival and induces severe stunting

Observation of the survival of seedlings inoculated with the Δ*pakA* and Δ*pakB* mutants revealed that seedlings inoculated with the Δ*pakA* mutant had a much lower rate of survival than those inoculated with the wild-type or Δ*pakB* mutant strains (Fig. 4.14A). By 51 days post planting, only 40% of the seedlings inoculated with the Δ*pakA* mutant were alive compared to 79% and 76% for the wild-type and Δ*pakB* mutant strains respectively. By the time seedlings were large enough to be screened for infection, only 7% of plants inoculated with the Δ*pakA* mutant were still alive compared to around 60% for the wild-type and Δ*pakB* mutant strains (Fig. 4.14B). These Δ*pakA*-infected plants were severely stunted, failed to develop more than two tillers and died within eight weeks after planting (Fig. 4.14C). The stunting displayed by these plants was the most severe seen for any *E. festucae* symbiotic mutants identified to date. In comparison, growth of plants infected with the Δ*pakB* mutant was indistinguishable from wild-type. Surprisingly, strain A13, the Δ*pakA* mutant containing pCE43, displayed a similar phenotype to the Δ*pakA* mutant, with 80% of inoculated seedlings dying within six weeks of planting and the remaining 20% being uninfected. Indeed, plants infected with A13 appeared to be even more severely affected than those infected with the Δ*pakA* mutant as the A13 infected plants died sooner and did not grow larger than one tiller. This suggests that transformation with pCE43 did not rescue the symbiotic phenotype of the Δ*pakA* mutant, but rather may have exacerbated the Δ*pakA* mutant host phenotype. However, this needs to be repeated to confirm this result.

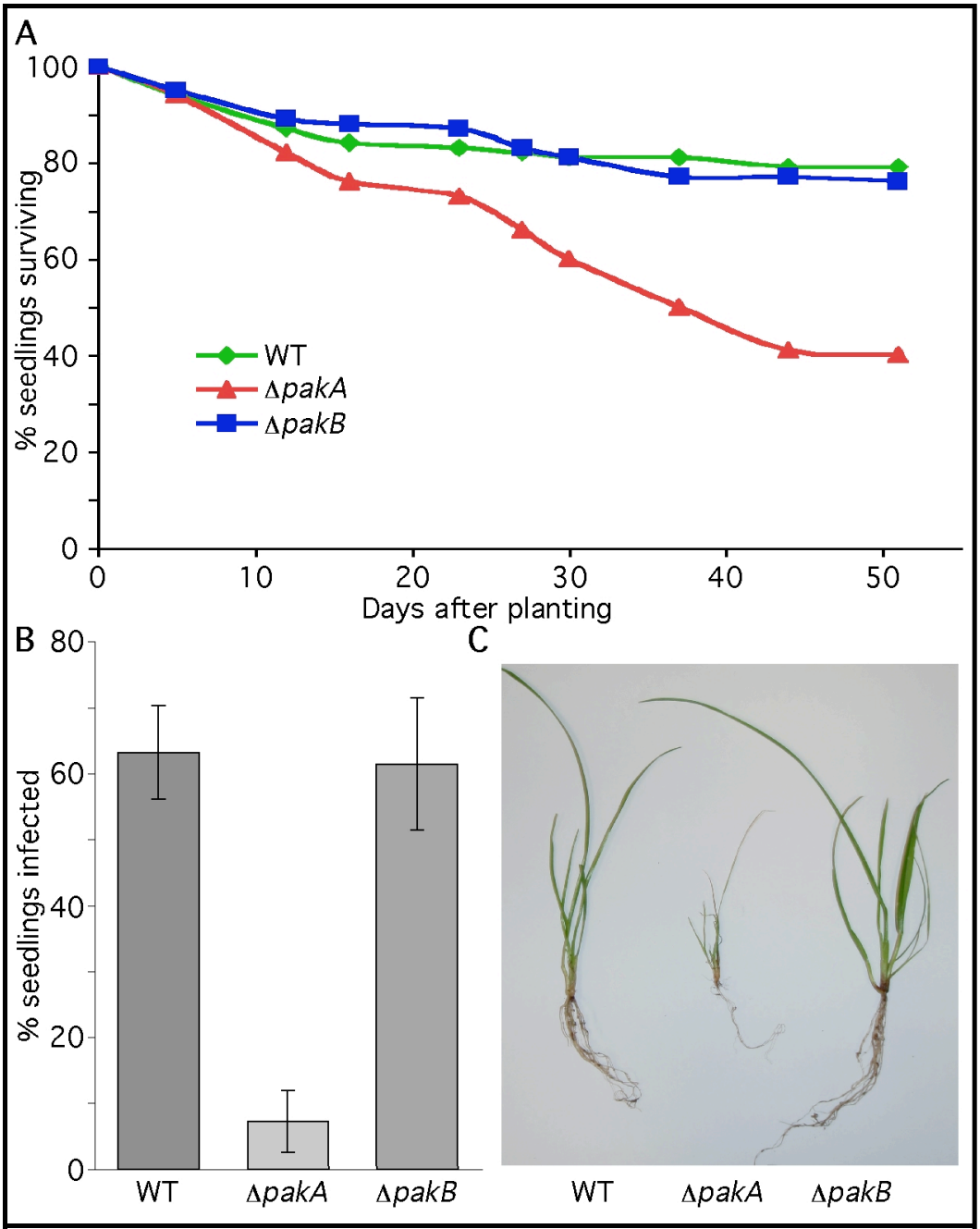

Figure 4.14 Symbiotic phenotype of the *E. festucae* pak mutants
A. Survival analysis of perennial ryegrass seedlings inoculated with *E. festucae* wild-type (WT), the Δ*pakA* mutant, and Δ*pakB* mutant. Survival of seedlings was monitored for 51 days after planting. **B.** Infection rate analysis for perennial ryegrass inoculated with WT, Δ*pakA,* and Δ*pakB* strains. Bars are ± SE for five independent experiments (n = 37, 20, and 36 for WT, Δ*pakA* and Δ*pakB* strains respectively). The low sample number for Δ*pakA* inoculated plants was due to most of these plants having died before they were large enough to be screened for infection. **C.** Tiller phenotypes of perennial ryegrass infected with WT, Δ*pakA*, and Δ*pakB* strains. These photographs were taken six weeks after inoculation.

4.5.2. The pak mutants display deregulated growth *in planta*

To determine why the Δ*pakA* mutant induced such severe stunting of the host, fungal growth *in planta* was examined (Fig. 4.15). The Δ*pakA* and Δ*pakB* mutants were transformed with a construct that constitutively expresses enhanced GFP (EGFP) and their growth *in planta* examined using confocal microscopy (Fig. 4.15A and B). This revealed that growth of the Δ*pakA* mutant *in planta* was deregulated, with substantial hyphal hyper-branching and the formation of hyphal networks. The hyphae also appeared highly vacuolated, and there was an increase in autofluorescence of the host chloroplasts. In contrast, growth of the Δ*pakB* mutant was only slightly less regulated than that of the wild-type strain, with mildly increased branching, frequent tip branching, and an apparent increase in fungal biomass. A similar result was seen for both Δ*pakA* and Δ*pakB* mutants when infected plant tissue was stained with aniline blue and examined by light microscopy (Fig. 4.15C). Plants infected with strain A13 died before they were large enough to be examined for fungal growth *in planta.* Surprisingly, growth of strain B3, the Δ*pakB* mutant containing pCE42, appeared even more deregulated than that of the Δ*pakB* mutant, with increased branching and formation of hyphal networks seldom seen in the Δ*pakB* mutant (Fig. 4.16). This suggests that similar to the results seen for strain A13, transformation of the Δ*pakB* mutant with pCE42 exacerbated the abnormal plant interaction phenotype. However, this needs to be repeated to confirm this unexpected result.

4.5.2.1. The Δ*pakA* mutant colonises host vascular bundles

To determine whether the pak mutants colonise the host vascular tissues as seen for the Δ*sakA* mutant (Fig. 3.16), toluidine blue-stained transverse sections through the pseudostem were examined by light microscopy (Fig. 4.15D). This revealed dramatic colonisation of the host vasculature by the Δ*pakA* mutant. Colonisation was so extensive that the vascular bundles were expanded to almost twice their normal size, and many of the host cells appeared distorted. This extensive colonisation was a likely contributing factor for the premature senescence displayed by these plants, as the hyphal load would

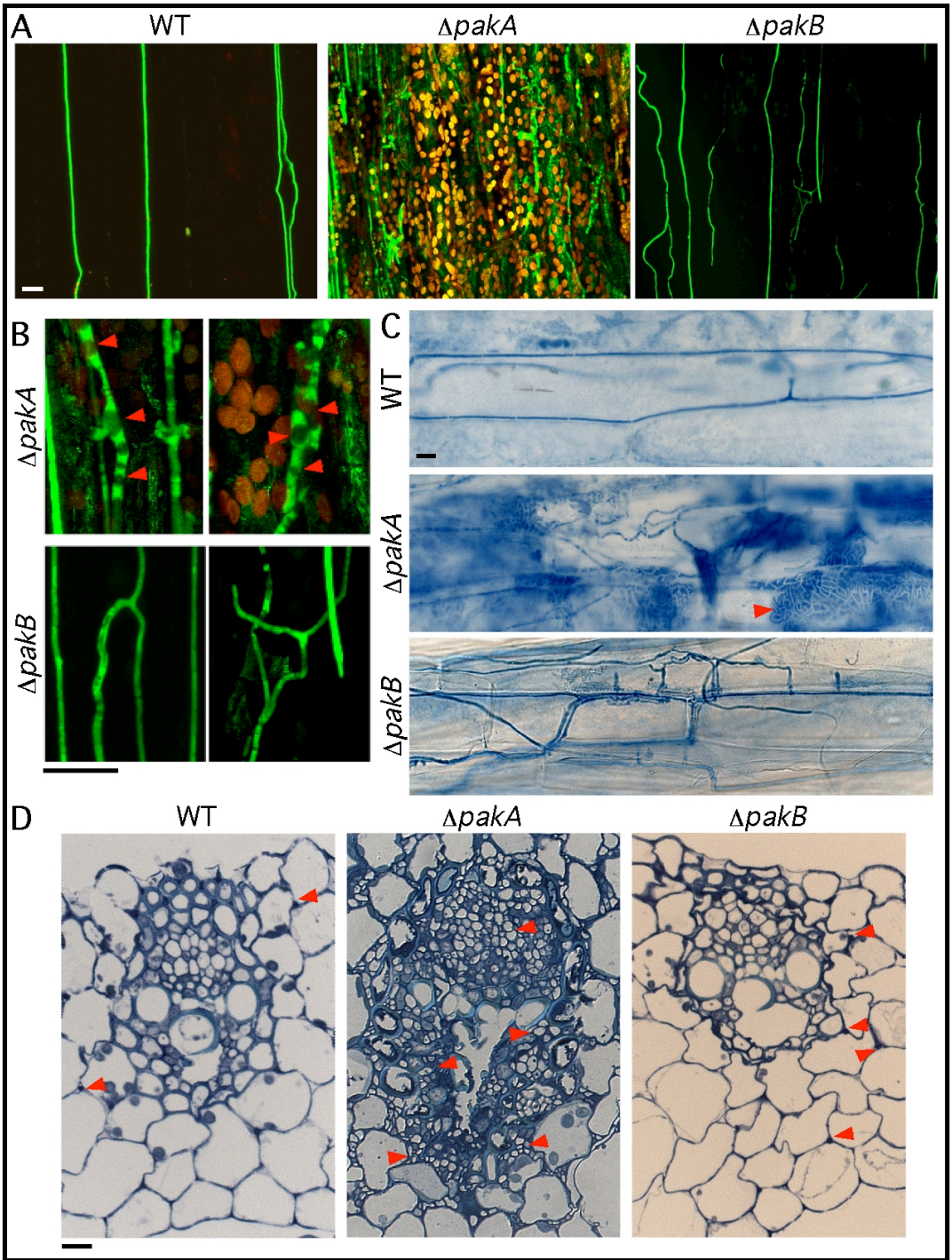

Figure 4.15 Growth of the pak mutants *in planta*
A and **B.** Confocal depth series images of hyphal growth of wild-type *E. festucae* (WT), the Δ*pakA* mutant, and Δ*pakB* mutant expressing enhanced GFP in the leaf sheath of perennial ryegrass. Vacuoles can be seen within Δ*pakA* mutant hyphae and frequent tip branching is seen in the Δ*pakB* mutant. Arrows indicate vacuoles. Bar = 20 μm. **C.** Light micrographs of aniline blue-stained hyphae of WT, Δ*pakA* and Δ*pakB* in the leaf sheath of perennial ryegrass. Arrows indicate hyphal networks. Bar = 10 μm. **D.** Light micrographs of toluidine blue-stained transverse sections showing vascular bundles in the pseudostem of WT, Δ*pakA* and Δ*pakB*-infected perennial ryegrass. Arrows indicate hyphae. Bar = 10 μm. All photographs were taken 8 weeks after inoculation.

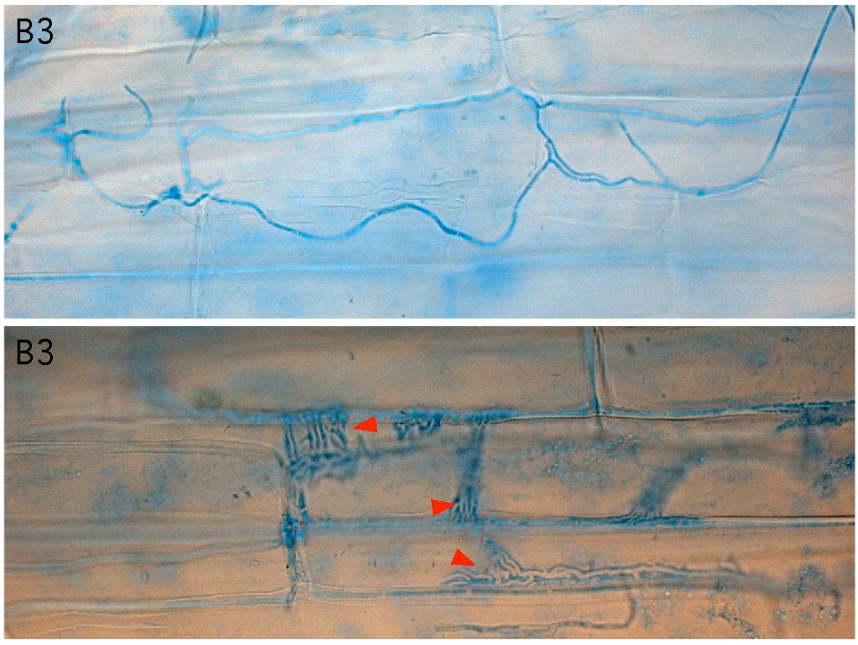

Figure 4.16 Growth of strain B3 *in planta*
Light micrographs of aniline blue-stained epidermal peels from perennial ryegrass infected with the strain B3, the Δ*pakB* mutant containing pCE42. Hyphae appear hyper-branched and hyphal networks are frequently seen. Arrow indicates hyphal network. Photographs were taken 8 weeks after inoculation. Bar = 10 μm.

greatly hamper the transport of water and nutrients by the host. Similar to the wild-type strain, the Δ*pakB* mutant did not colonise the host vascular bundles.

4.5.3. Δ*pakA* mutant hyphae display altered morphology *in planta*

To determine whether the morphology of the Δ*pakA* and Δ*pakB* mutant hyphae was altered *in planta*, pseudostem sections were examined by TEM (Fig. 4.17). This revealed a number of key differences between the Δ*pakA* mutant and wild-type strain. Firstly, many more hyphae colonised the host intercellular spaces than in wild-type associations. In some cases there were so many hyphae packed into individual intercellular spaces that the spaces merged into each other, linked by networks of fungal hyphae. These hyphae were also often much larger than wild-type hyphae and were irregular in shape. Similar to the Δ*sakA* mutant (Figure 3.17), the Δ*pakA* mutant hyphae also contained large vacuoles *in planta*. However, this is perhaps unsurprising given the Δ*pakA* mutant has large vacuoles in culture. Also, similar to Δ*sakA* mutant associations, the extracellular matrix surrounding the Δ*pakA* mutant was electron dense. In comparison, Δ*pakB* mutant hyphae had wild-type appearance, were circular in shape, evenly sized and contained electron dense cytoplasm with no visible vacuoles. Generally only one or two Δ*pakB* mutant hyphae were found within individual host intercellular spaces. However, more intercellular spaces appeared to be occupied by the Δ*pakB* mutant than is seen in wild-type associations, suggesting the Δ*pakB* mutant displayed increased biomass in comparison to the wild-type strain. This supports the confocal microscopy results (Section 4.5.2) which suggested that growth of the Δ*pakB* mutant was slightly less regulated than that of the wild-type strain.

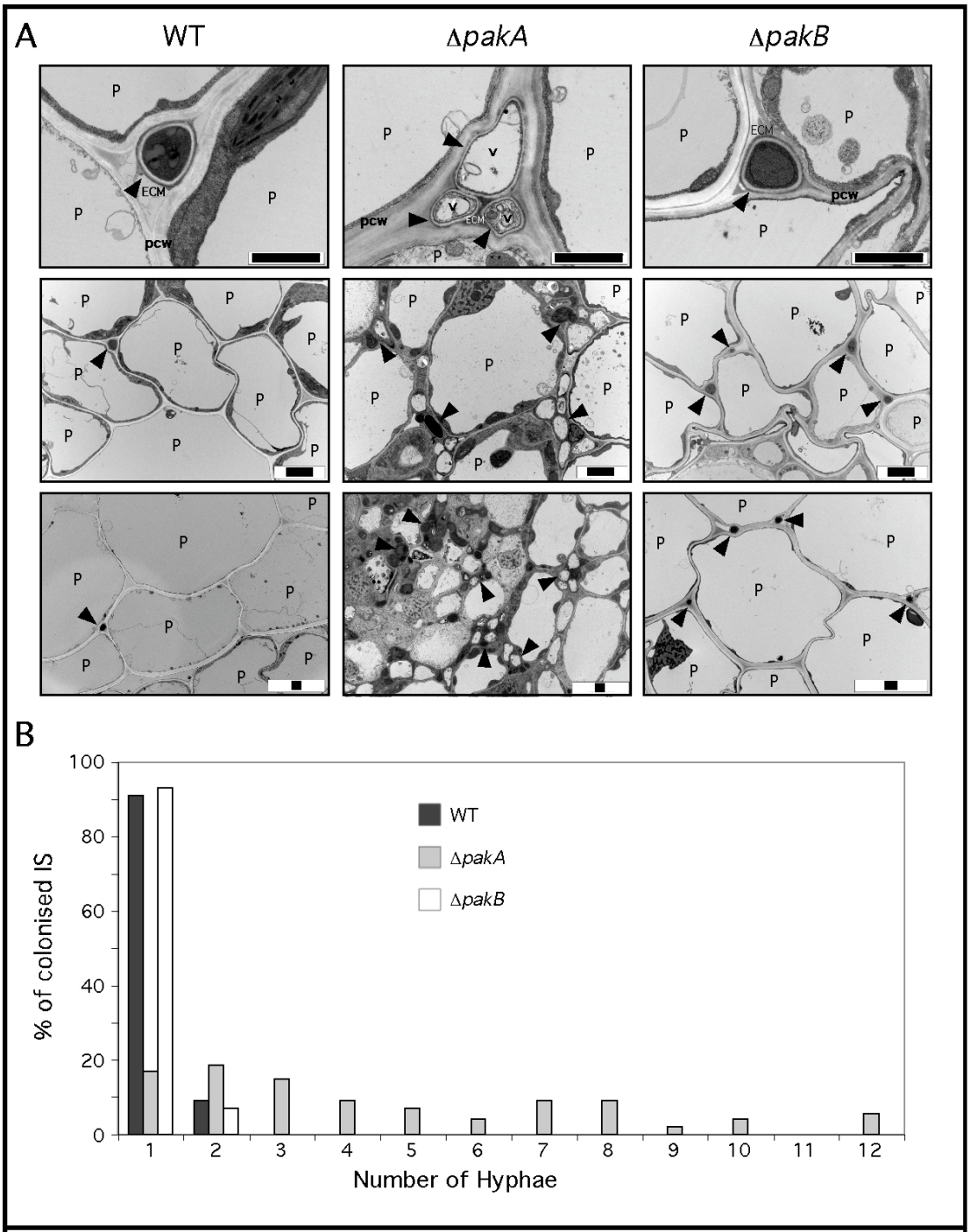

Figure 4.17 Examination of hyphal morphology and density *in planta* by TEM
A. Transmission electron micrographs of cross-sections showing *E. festucae* hyphae growing in the intercellular spaces of host pseudostem tissue. Arrows, fungal hyphae; P, plant cell; ECM, extracellular matrix; v, vacuole; pcw, plant cell wall. Bar = 2 μm. **B**. Graph showing number of hyphae in intercellular spaces (IS) colonised by the wild-type (WT), Δ*pakA* and Δ*pakB* strains.

5. Bioinformatic Analysis of MAP Kinase Pathways

5.1. Analysis of *E. festucae* MAP kinase pathways

Multiple MAP kinase pathways exist in fungi to facilitate detection of and responses to a variety of environmental cues, including pheromones, osmolarity and temperature. These pathways are highly conserved across the fungal kingdom and are best characterised in the model budding yeast *S. cerevisiae*. Given the importance of these pathways in fungal growth and development, and the recent release of the *E. festucae* genome, components of the three *E. festucae* MAP kinase pathways were characterised using bioinformatics. However, given the diversity of the receptors, signal transducers and targets of the MAP kinase pathways across different fungi, only the primary kinases, components of the MAP kinase cascade (MAPKK kinase, MAPK kinase and MAP kinase), and phosphatases were characterised. Candidates were selected for analysis based on Figure 3 published in the *M. grisea* genome paper by Dean et al. (2005) (Fig. 5.1).

5.1.1. Search approach

To identify components of the *E. festucae* MAP kinase pathway, the corresponding *S. cerevisiae* gene was used to search the fungal database at NCBI (http://blast.ncbi.nlm.nih.gov/Blast.cgi) using BLASTp. The filamentous fungal protein displaying the greatest E value was then used to search the *E. festucae* genome (http://www.genome.ou.edu/blast/ef_blastall.html) using tBLASTn. The *E. festucae* protein sequence was then searched back against NCBI to confirm it was the true homologue. The *E. festucae* amino acid sequence was compared to homologues from *F. graminearum*, *N. crassa* and *M. grisea* using ClustalW. Amino acid identities are listed in Table 5.2. Domain structure was analysed using ExPASy PROSITE (http://au.expasy.org/prosite/) and InterProScan (http://www.ebi.ac.uk/Tools/InterProScan/). For enzymatic components of the pathways Enzyme Commission (EC) numbers were obtained from the ENZYME nomenclature database at ExPASy (http://au.expasy.org/enzyme/) and Panther Classification System (http://www.pantherdb.org/). Gene Ontology (GO) annotations were obtained for

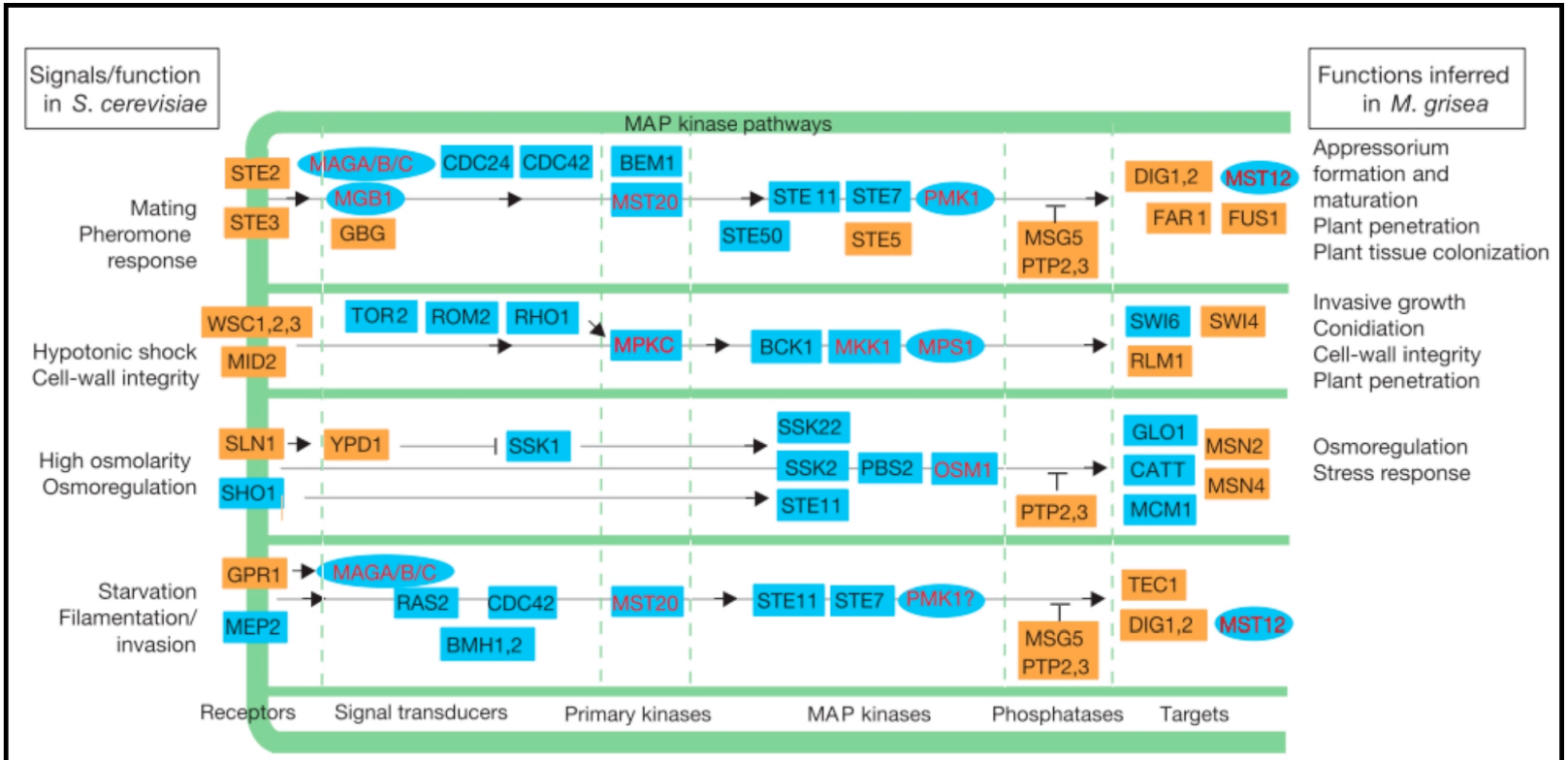

Figure 5.1 Comparison of MAP kinase signalling pathways between *S. cerevisiae* and *M. grisea*
The core components of MAP kinase signalling pathways are conserved; however, receptors and downstream targets are less conserved. Names in red indicate previously identified *M. grisea* homologues; *S. cerevisiae* protein names are in black. The coloured boxing indicates the degree of conservation between *M. grisea* and *S. cerevisiae* based on BLASTp analysis: blue, e-value $<1 \times 10^{-10}$; orange, e-value $>1 \times 10^{-10}$. Ovals indicate *M. grisea* homologues required for pathogenicity. Reproduced from Dean et al. (2005). Nature 434: 980-986.

S. cerevisiae and *M. grisea* proteins from the GO database (http://amigo.geneontology.org/cgi-bin/amigo/search.cgi). *E. festucae* GO annotations were based on predictions inferred from sequence similarity (ISS) using InterProScan. For *E. festucae* SakA and PakB annotations were also manually determined based on the results presented in chapters 3 and 4. Predicted functions for *S. cerevisiae* proteins were obtained from the *Saccharomyces* Genome Database (http://www.yeastgenome.org/).

5.2. The stress-activated MAP kinase pathway

Components of the *E. festucae* stress-activated MAP kinase pathway are illustrated in Figure 5.2. GO annotations for selected stress-activated MAP kinase pathway components from *S. cerevisiae*, *M. grisea* and *E. festucae* are presented in Table 5.1. Amino acid conservation analyses are summarised in Table 5.2.

5.2.1. Primary kinases

No primary kinases have been identified for the stress-activated MAP kinase pathway in filamentous fungi.

5.2.2. The MAP kinase cascade

5.2.2.1. Ssk2p/22p

In *S. cerevisiae*, multiple MAPKK kinases are involved in signalling for the stress-activated Hog1 pathway. Two of these proteins, Ssk2p and Ssk22p, are functionally redundant and homologous to each other (EC 2.7.11.25). Analysis of the *E. festucae* homologues of these proteins revealed that filamentous fungi contain only one Ssk2p/Ssk22p-like protein. Both *SSK2* and *SSK22* are most similar to the *E. festucae* gene A.2.6421 on contig 1286, and the FGSG_00408, NCU03071 and MGG_00183 genes from *F. graminearum*, *N. crassa* and *M. grisea* respectively. Amino acid alignment of the

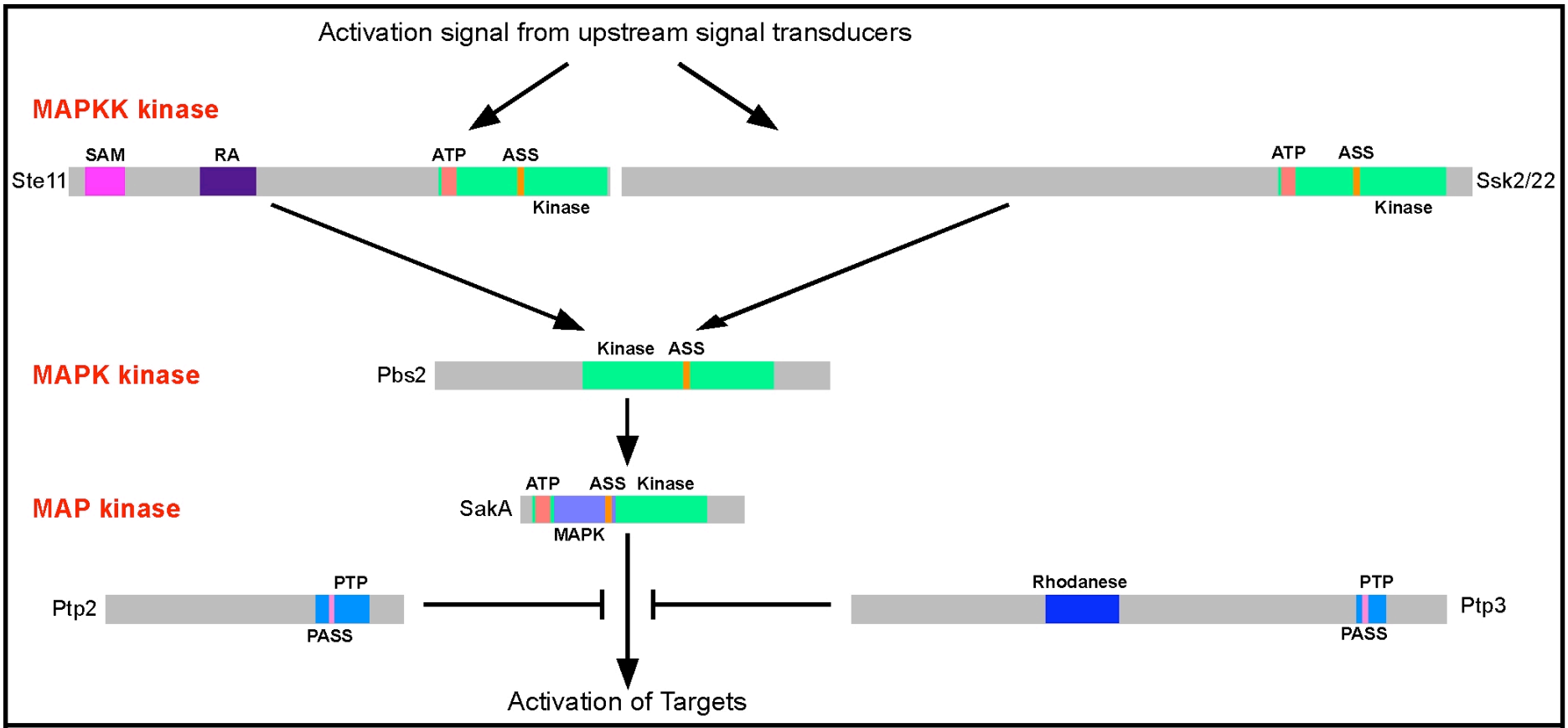

Figure 5.2 The *E. festucae* stress-activated MAP kinase pathway
Schematic illustrating domain structures of key components of the *E. festucae* stress-activated MAP kinase pathway - the MAPKK kinases Ste11 and Ssk2/22, MAPK kinase Pbs2, MAP kinase SakA and phosphatases Ptp2 and Ptp3. Protein names are based on *S. cerevisiae* except SakA which has been experimentally characterised (Eaton et al. 2008). Important domains and motifs are indicated and include: protein kinase domain (PS50011; kinase), ATP-binding region signature (PS00107; ATP), serine/threonine protein kinases active site signature (PS00108; ASS), sterile α motif (SAM) domain (PS50105), Ras-associating (RA) domain (PS50200), MAP kinase signature (PS01351; MAPK), tyrosine specific protein phosphatases family profile (PS50056; PTP), tyrosine specific protein phosphatases active site signature (PS00383; PASS), and rhodanese domain (PS50206).

Table 5.1 GO annotations for components of the stress-activated MAP kinase pathway

		Biological Process			Molecular Function		
Protein	Organism	Annotation[1]	Description	Code[2]	Annotation[1]	Description	Code[2]
Ssk22p	*S. cerevisiae*	0000168	Activation of MAPK kinase activity involved in osmosensory signalling pathway	TAS	0004709	MAPKK kinase activity	TAS
		0007231	Osmosensory signalling pathway	TAS			
		0006468	Protein amino acid phosphorylation	TAS			
	E. festucae	0006468	Protein amino acid phosphorylation	ISS	0004674	Protein Ser/Thr kinase activity	ISS
					0005524	ATP-binding	ISS
Ste11p	*S. cerevisiae*	0000186	Activation of MAPK kinase activity	IMP	0004709	MAPKK kinase activity	IDA
		0000161	MAPKK kinase cascade involved in osmosensory signalling pathway	IGI, IMP	0032093	SAM domain binding	IDA
		0007232	Osmosensory signalling pathway via Sho1 osmosensor	IGI			
		0006468	Protein amino acid phosphorylation	IMP			
	E. festucae	0007165	Signal transduction	ISS	0004674	Protein Ser/Thr kinase activity	ISS
		0006468	Protein amino acid phosphorylation	ISS	0005524	ATP-binding	ISS
	M. grisea	0000187	Activation of MAP kinase activity	IMP	0004709*	MAPKK kinase activity	IMP
		0052108	Growth or development of symbiont during interaction with host	IMP			
		0009405	Pathogenesis	IMP			
Pbs2p	*S. cerevisiae*	0000169	Activation of MAP kinase activity involved in osmosensory signalling pathway	IMP	0004708	MAPK kinase activity	IMP
		0006972	Hyperosmotic response	IMP			
		0000208	Nuclear transport of MAP kinase involved in osmosensory signalling pathway	IMP			
		0007231	Osmosensory signalling pathway	IMP			
		0006468	Protein amino acid phosphorylation	IMP			
OSM1	*S. cerevisiae*	0006972	Hyperosmotic response	IMP	0004707	MAP kinase activity	IDA
		0007231	Osmosensory signalling pathway	IMP			
		0006468	Protein amino acid phosphorylation	IDA			
		0050790	Regulation of catalytic activity	RCA			
		0046685	Response to arsenic	IGI			
		0006970	Response to osmotic stress	RCA			

	M. grisea	0052108	Growth or development of symbiont during interaction with host	IMP	0004707	MAP kinase activity	IMP
	E. festucae	0033667	Negative regulation of growth or development of symbiont within host	IMP	0004707	MAP kinase activity	IGI
		00757337	Positive regulation of growth or development of symbiont on or near host surface	IMP			
		0051851	Modification by host of symbiont morphology or physiology	IMP			
		0044003	Modification by symbiont of host morphology or physiology	IMP			
		0006970	Response to osmotic stress	IMP			
		0034605	Cellular response to heat	IMP			
		0070301	Cellular response to hydrogen peroxide	IGI			
		0006800	Oxygen and reactive oxygen species metabolic	IMP			
Ptp2p	*S. cerevisiae*	0034605	Cellular response to heat	RCA	0004725	Protein tyrosine phosphatase activity	TAS
		0000173	Inactivation of MAP kinase activity involved in osmosensory signalling pathway	TAS			
		0007231	Osmosensory signalling pathway	TAS			
		0006470	Protein amino acid dephosphorylation	TAS			
	E. festucae	0006470	Protein amino acid dephosphorylation	ISS	0004725	Protein tyrosine phosphatase activity	ISS
Ptp3p	*S. cerevisiae*	0000173	Inactivation of MAP kinase activity involved in osmosensory signalling pathway	IPI	0004725	Protein tyrosine phosphatase activity	IDA
		0006470	Protein amino acid dephosphorylation	IDA			
	E. festucae	0006470	Protein amino acid dephosphorylation	ISS	0004725	Protein tyrosine phosphatase activity	ISS

[1]GO annotation number from the Gene Ontology database (http://amigo.geneontology.org/cgi-bin/amigo/go.cgi).

[2]Evidence code for annotations. Details describing these codes are found at http://www.geneontology.org/GO.evidence.shtml. TAS = traceable author statement, ISS = inferred from sequence similarity, IMP = inferred from mutant phenotype, IGI = inferred from genetic interaction, IDA = inferred direct assay, RCA = reviewed computational analysis. The most reliable evidence sources are IMP, IGI and IDA, which are all experiment-based annotations.

Table 5.2 Amino acid conservation between *E. festucae* MAP kinase pathway components and filamentous fungal homologues

Function	Scaffold protein			Primary kinase			MAPKK kinase			MAPK kinase			MAP kinase			Phosphatase		
Pathway	**Fg**	**Nc**	**Mg**	**Fg**	**Nc**	**Mg**	**Fg**	**Nc**	**Mg**	**Fg**	**Nc**	**Mg**	**Fg**	**Nc**	**Mg**	**Fg**	**Nc**	**Mg**
Stress	-	-	-	-	-	-	77[3]/72[4]	63[3]/65[4]	59[3]/57[4]	63	55	53	95	93	93	52[5]/45[6]	33[5]/24[6]	28[5]/36[6]
Pheromone	68[1]/82[2]	59[1]/69[2]	62[1]/73[2]	68	55	61	72	65	57	80	71	67	98	95	97	52[5]/45[6]/56[7]	33[5]/24[6]/51[7]	28[5]/36[6]/51[7]
Cell integrity	-	-	-	70	65	66	51	46	46	76	68	71	83	70	80	-	-	-

Where multiple components perform the same function in a given pathway, components are represented as follows: [1]Bem1; [2]Ste50; [3]Ssk2/22; [4]Ste11; [5]Ptp2; [6]Ptp3; [7]Msg5. Colour coding is indicative of percentage amino acid identity where: red = 90%+, orange = 80-89%, yellow = 70-79%, green = 60-69%, blue = 50-59%, purple = 40-49%, black = 0-39%. Components that display higher identity between *E. festucae* and *M. grisea* (Mg) than between *E. festucae* and *N. crassa* (Nc) are indicated by shading. Of the three fungi represented in Table 5.2, *E. festucae* is phylogenetically most closely related to *F. graminearum* (Fg), followed by *N. crassa*, then *M. grisea*. Incidences of higher ID to *M. grisea* may reflect adaptation of that component for symbiosis as *F. graminearum* and *M. grisea* are plant symbionts whereas *N. crassa* is a saprobe.

E. festucae homologue with Ssk2p and Ssk22p showed 26% and 28% ID respectively. Given the relatively small difference between these identities it is difficult to determine which yeast gene the *E. festucae* gene is homologous to, although all filamentous fungal sequences examined showed slightly higher identity to Ssk22p. As expected, the predicted *E. festucae* polypeptide contained a protein kinase domain (PS50011) between amino acids 1047-1316 (Hanks and Hunter, 1995). In *S. cerevisiae* this domain is involved in phosphorylation and activation of the downstream MAPK kinase. Within the kinase domain is a protein kinase ATP-binding region signature (PS00107, amino acids 1053-1076) and a serine/threonine protein kinase active site signature (PS00108, amino acids 1167-1179) (Hanks and Hunter, 1995).

5.2.2.2. Ste11p

In addition to Ssk2p and Ssk22p, *S. cerevisiae* contains a third redundant MAPKK kinase for signalling through the Hog1 pathway, Ste11p (EC 2.7.11.25). An *E. festucae* Ste11p homologue was identified, suggesting that in *E. festucae* at least two MAPKK kinases are involved in the stress-activated MAP kinase pathway. The *E. festucae* homologue, A.3.8851, is located on contig 7. As expected the predicted A.3.8851 polypeptide contains a protein kinase domain (amino acids 590-860), with a protein kinase ATP-binding region signature and serine/threonine protein kinases active site signature between amino acids 596-619 and 717-729 respectively. In addition, it is also predicted to contain a sterile α motif (SAM) domain (PS50105) putatively involved in protein interactions (Schultz et al., 1997) between amino acids 28-91, and a Ras-associating (RA) domain (PS50200) between amino acids 209-299 for interaction with Ras and other small GTPases (Ponting and Benjamin, 1996).

5.2.2.3. Pbs2p

In *S. cerevisiae*, one MAPK kinase, Pbs2p (EC 2.7.12.2), acts downstream of the three MAPKK kinases. The *E. festucae PBS2* homologue, A.3.2466, is located on contig 60 and the A.3.2466 polypeptide is predicted to contain a protein kinase domain between amino acids 238-543, and within this a serine/threonine protein kinase active site

signature (amino acids 397-409). In *S. cerevisiae* this domain is involved in phosphorylation and activation of the downstream MAP kinase.

5.2.2.4. OSM1

OSM1 is the *M. grisea* homologue of the *S. cerevisiae* Hog1p MAP kinase (EC 2.7.11.24) and has previously been characterised (Dixon et al., 1999). The *E. festucae* OSM1 homologue is SakA, which is described in Chapter 3. It contains a protein kinase domain between amino acids 20-299. Within this are an ATP-binding region signature, serine/threonine protein kinases active site signature and MAP kinase signature (PS01351) between amino acids 26-50, 137-149, and 55-153 respectively.

5.2.3. Phosphatases

5.2.3.1. Ptp2p

In order for MAP kinase signalling to be dampened, phosphatases act to dephosphorylate the MAP kinase, thereby inactivating it. In *S. cerevisiae*, two phosphatases, Ptp2p and Ptp3p (EC 3.1.3.48), are involved in dampening the stress response mediated by the Hog1 pathway. The *E. festucae PTP2* homologue, A.3.1981, is located on contig 416. Amino acid sequence conservation of filamentous fungal Ptp2p homologues appears considerably lower than that seen for the majority of the protein kinase components of the MAP kinase pathways, with the predicted *E. festucae* Ptp2p homologue showing only 52% amino acid ID to *F. graminearum* FGSG_06297 (Table 5.2). This suggests these proteins may be under less pressure to remain conserved than core components of the MAP kinase cascades. The *E. festucae* Ptp2p homologue is predicted to contain a tyrosine specific protein phosphatases family profile (PS50056) between amino acids 338-425 and within this a tyrosine specific protein phosphatases active site signature (PS00383, amino acids 359-369) (Fischer et al., 1991).

5.2.3.2. Ptp3p

The *E. festucae PTP3* homologue, A.4.2505 is located on contig 644. Similar to the Ptp2p homologue, the predicted A.4.2505 polypeptide shows lower sequence conservation than is displayed for components of the MAP kinase cascade, with only 45% ID to *F. graminearum* FGSG_11979 (Table 5.2). The A.4.2505 polypeptide is predicted to contain a PTP-type protein phosphatase family profile (amino acids 559-927) and within this a tyrosine specific protein phosphatases active site (amino acids 815-825). It is also predicted to contain a Rhodanese domain (PS50206) between amino acids 312-428. In *S. cerevisiae* this domain is involved in catalysing the transfer of the sulphane atom of thiosulphate to cyanide to form sulphite and thiocyanate (Westley, 1981).

5.3. The pheromone response pathway

Components of the *E. festucae* pheromone response pathway are illustrated in Figure 5.3. GO annotations for these components in *S. cerevisiae*, *M. grisea* and *E. festucae* are presented in Table 5.3. Amino acid conservation analyses are summarised in Table 5.2

5.3.1. Primary kinases

5.3.1.1. Bem1p

Although included in the primary kinase section of Figure 3 by Dean et al. (2005), Bem1p is not actually a kinase but rather acts as a scaffold protein, holding Ste5p and Ste20p (MST20) together, as well as performing other functions in the cell. The *E. festucae BEM1* homologue, known as *bemA* (D. Takemoto, unpublished) is located on contig 446 (gene A.24.2117). *E. festucae* BemA is predicted to contain two Src homology 3 (SH3) domains (PS50002) between amino acids 30-93 and 143-205. Although the function of these domains is not fully understood they are thought to mediate assembly of certain protein complexes by binding to proline-rich peptides (Morton and Campbell, 1994). BemA also contains a Phox homology (PX) domain (PS50195) between amino

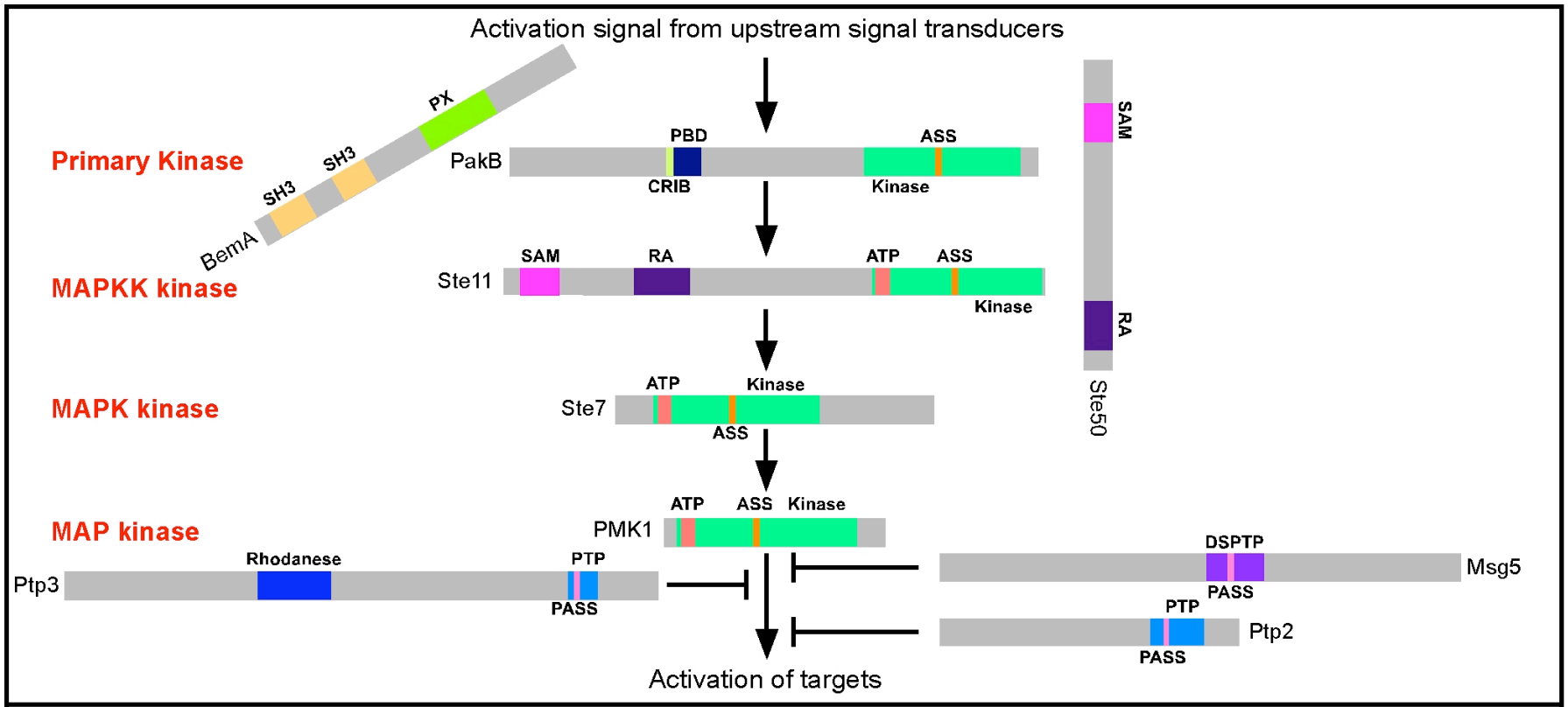

Figure 5.3 The *E. festucae* pheromone response pathway

Schematic illustrating domain structures of key components of the *E. festucae* pheromone response MAP kinase pathway - primary kinase PakB (homologous to *M. grisea* MST20), scaffold proteins BemA and Ste50, MAPKK kinase Ste11, MAPK kinase Ste7, MAP kinase PMK1 and phosphatases Ptp2, Ptp3 and Msg5. Protein names are based on *S. cerevisiae* except PakB (refer Chapter 4), BemA (D. Takemoto, unpublished) and PMK1 (Xu & Hamer, 1996), which have been experimentally characterised. Important domains and motifs are indicated and include: Src homology 3 (SH3) domain (PS50002), Phox homology domain (PS50195; PX), p21-Rho-binding domain (PF00786; PBD), Cdc42-Rac interactive binding motif (PS50108; CRIB) protein kinase domain (PS50011; kinase), ATP-binding region signature (PS00107; ATP), serine/threonine protein kinases active site signature (PS00108; ASS), sterile α motif (SAM) domain (PS50105), Ras-associating (RA) domain (PS50200), tyrosine specific protein phosphatases family profile (PS50056; PTP), tyrosine specific protein phosphatases active site signature (PS00383; PASS), dual specificity protein phosphatase family profile (PS50054; DSPTP) and rhodanese domain (PS50206).

Table 5.3 GO annotations for components of the pheromone response pathway

		Biological Process			Molecular Function		
Protein	Organism	Go no.[1]	Description	Code[2]	Go no.[1]	Description	Code[2]
Bem1p	*S. cerevisiae*	0051301	Cell division	RCA	0032266	Phosphatidylinositol 3-phosphatse binding	IDA
		0016049	Cell growth	RCA	0005515	Protein binding	IDA, IMP
		0000902	Cell morphogenesis	RCA			
		0030010	Establishment of polarity	TAS			
		0007264	Small GTPase mediated signal transduction	RCA			
	E. festucae	0007154	Cell communication	ISS	0005515	Protein binding	ISS
					0035091	Phosphoinositide binding	ISS
MST20	*S. cerevisiae*	0006468	Protein amino acid phosphorylation	IDA	0035174	Histone serine kinase activity	IDA
		0007264	Small GTPase mediated signal transduction	RCA	0008349	MAPKKK kinase activity	IDA
		0007232	Osmosensory signalling pathway via Sho1 osmosensor	IGI			
		0000185	Activation of MAPKK kinase activity	IDA			
		0007266	Rho protein signal transduction	RCA			
	E. festucae	0006468	Protein amino acid phosphorylation	ISS	0004674	Protein Ser/Thr kinase activity	ISS
		0010570	Regulation of filamentous growth	IMP	0005524	ATP-binding	ISS
Ste50p	*S. cerevisiae*	0000161	MAPKK kinase cascade involved in osmosensory signalling pathway	IMP, IPI	0019887	Protein kinase regulator activity	IDA, IPI
		0019236	Response to pheromone	IDA	0032093	SAM domain binding	IDA
	E. festucae	0007165	Signal transduction	ISS			
	M. grisea	0000187	Activation of MAP kinase activity	IMP	0030674	Protein binding, bridging	IMP
		0052108	Growth or development of symbiont during interaction with host	IMP			
		0009405	Pathogenesis	IMP			
Ste11p	*S. cerevisiae*	0000186	Activation of MAPK kinase activity	IMP	0004709	MAPKK kinase activity	IDA
		0000161	MAPKK kinase cascade involved in osmosensory signalling pathway	IGI, IMP	0032093	SAM domain binding	IDA
		0007232	Osmosensory signalling pathway via Sho1 osmosensor	IGI			
		0006468	Protein amino acid phosphorylation	IMP			
	E. festucae	0007165	Signal transduction	ISS	0004674	Protein Ser/Thr kinase activity	ISS
		0006468	Protein amino acid phosphorylation	ISS	0005524	ATP-binding	ISS
	M. grisea	0052108	Growth or development of symbiont during interaction with host	IMP	0004709*	MAPKK kinase activity	IMP
		0000187	Activation of MAP kinase activity	IMP			
		0009405	Pathogenesis	IMP			

Ste7p	*S. cerevisiae*	0006468	Protein amino acid phosphorylation	ISS	0004708	MAPK kinase activity	ISS
					0004674	Protein Ser/Thr kinase activity	TAS
	E. festucae	0006468	Protein amino acid phosphorylation	ISS	0004674	Protein Ser/The kinase activity	ISS
					0005524	ATP-binding	ISS
	M. grisea	0000187	Activation of MAP kinase activity	IMP	0004708	MAPK kinase activity	IMP
		0052108	Growth or development of symbiont during interaction with host	IMP			
		0009405	Pathogenesis	IMP			
PMK1	*M. grisea*	0044408	Growth or development of symbiont on or near host	IMP	0004707	MAP kinase activity	IMP
		0044412	Growth or development of symbiont within host	IMP			
		0009405	Pathogenesis	IMP			
	S. cerevisiae	0006468	Protein amino acid phosphorylation	IDA	0004707	MAP kinase activity	IDA
	E. festucae	0006468	Protein amino acid phosphorylation	ISS	0004674	Protein Ser/Thr kinase activity	ISS
					0005524	ATP-binding	ISS
					0004707	MAP kinase activity	ISS
Ptp2p	*S. cerevisiae*	0034605	Cellular response to heat	RCA	0004725	Protein tyrosine phosphatase activity	TAS
		0000173	Inactivation of MAP kinase activity involved in osmosensory signalling pathway	TAS			
		0007231	Osmosensory signalling pathway	TAS			
		0006470	Protein amino acid dephosphorylation	TAS			
	E. festucae	0006470	Protein amino acid dephosphorylation	ISS	0004725	Protein tyrosine phosphatase activity	ISS
Ptp3p	*S. cerevisiae*	0000173	Inactivation of MAP kinase activity involved in osmosensory signalling pathway	IPI	0004725	Protein tyrosine phosphatase activity	IDA
		0006470	Protein amino acid dephosphorylation	IDA			
	E. festucae	0006470	Protein amino acid dephosphorylation	ISS	0004725	Protein tyrosine phosphatase activity	ISS
Msg5p	*S. cerevisiae*	0006470	Protein amino acid dephosphorylation	IDA	0004727	Prenylated protein tyrosine phosphatase activity	IMP
	E. festucae	0006470	Protein amino acid dephosphorylation	ISS	0004725	Protein tyrosine phosphatase activity	ISS

[1]GO annotation number from the Gene Ontology database (http://amigo.geneontology.org/cgi-bin/amigo/go.cgi).

[2]Evidence code for annotations. Details describing these codes are found at http://www.geneontology.org/GO.evidence.shtml. TAS = traceable author statement, ISS = inferred from sequence similarity, IMP = inferred from mutant phenotype, IGI = inferred from genetic interaction, IPI = inferred from physical interaction, IDA = inferred direct assay, RCA = reviewed computational analysis. The most reliable evidence sources are IMP, IGI, IPI and IDA, which are all experiment-based annotations.

*Changed from GO0008349 as this was likely an annotation error as GO0008349 is MAPKKK kinase activity.

acids 304-425, thought to be involved in binding of phosphoinositides (Song et al., 2001).

5.3.1.2. MST20

MST20 is the *M. grisea* homologue of *S. cerevisiae* Ste20p (EC 2.7.11.1) and has previously been characterised (Li et al., 2004). The *E. festucae* homologue of MST20 is PakB, which is described in Chapter 4. *E. festucae* PakB contains a protein kinase domain between amino acids 567-818, and within this a protein kinase ATP-binding region signature and serine/threonine protein kinases active site signature between amino acids 573-596 and 682-694 respectively. PakB also contains a p21-Rho-binding domain (PBD) (PF00786) between amino acids 251-309 (Burbelo et al., 1995), and within this an N-terminal Cdc42/Rac interactive binding (CRIB) motif (PS50108) between amino acids 252-265, which specifically binds the GTP bound Cdc42 or Rac (Leberer et al., 1997).

5.3.2. The MAP kinase cascade

5.3.2.1. Ste11p

Details for the *E. festucae* Ste11p homologue are presented in Section 5.2.2.2. In addition to its role in the stress-activated MAP kinase pathway, Ste11p acts as the MAPKK kinase for the mating/pheromone response and filamentation/invasion pathways of *S. cerevisiae*. Filamentous fungi do not contain a MAP kinase pathway homologous to the filamentation/invasion pathway.

5.3.2.2. Ste7p

The MAPK kinase acting downstream of Ste11p in both the mating/pheromone response pathway and starvation filamentation/invasion pathway is Ste7p (EC 2.7.12.2). The *E. festucae STE11* homologue, A.4.6254, is located on contig 1102. Similar to the *E. festucae* Pbs2p homologue, the A.4.6254 polypeptide is predicted to contain a protein

kinase domain (amino acids 63-328) and within this a protein kinases ATP-binding region signature and serine/threonine protein kinases active-site signature (amino acids 69-92 and 182-194 respectively).

5.3.2.3. PMK1

PMK1 is the *M. grisea* homologue of *S. cerevisiae* Fus3p, the MAP kinase of the pheromone response pathway (EC 2.7.11.24), and has been previously characterised (Xu and Hamer, 1996). The *E. festucae* homologue of *PMK1* is A.14.7927, located on contig 354. The high sequence identity displayed by filamentous fungal PMK1 homologues (refer Table 5.2) suggests they are under strong pressure to remain unchanged. As expected, the *E. festucae* PMK1 homologue is predicted to contain a protein kinase domain (amino acids 23-311), and within this an ATP-binding region signature, serine/threonine protein kinases active site signature and MAP kinase signature between amino acids 29-53, 143-155 and 57-159 respectively.

5.3.2.4. Ste50p

In *S. cerevisiae* components of the pheromone-signalling pathway are linked together via the adapter protein Ste50p. This protein links Ste20p, which is associated with the G protein Cdc42, to Ste11p in order to facilitate activation of the MAP kinase cascade (Wu et al., 1999). The *E. festucae STE50* homologue, A.6.8820, is located on contig 67. The A.6.8820 polypeptide is predicted to contain a sterile α motif (SAM) domain and Ras-associating (RA) domain between amino acids 69-132 and 385-465 respectively.

5.3.2.5. Ste5p

In *S. cerevisiae* the components of the mating/pheromone response MAP kinase cascade, Ste11p, Ste7p and Fus3p are held together by the Ste5p scaffold protein. However, using Blast analysis no filamentous fungal homologues of Ste5p could be identified. This is consistent with the findings of Dean et al. (2005), and suggest that in filamentous

fungi, components of the pheromone response MAP kinase cascade are either not held together by a scaffold protein or a protein not homologous to Ste5p acts as the scaffold.

5.3.3. Phosphatases

5.3.3.1. Ptp2p

Details for *E. festucae* Ptp2p homologue are presented in Section 5.2.3.1.

5.3.3.2. Ptp3p

Details for *E. festucae* Ptp3p homologue are presented in Section 5.2.3.2.

5.3.3.3. Msg5

The *S. cerevisiae* phosphatase Msg5p is considered a dual-specificity protein phosphatase (EC 3.1.3.48), a sub-class of the protein tyrosine phosphatase gene super-family, and is required for both the pheromone response pathway and cell integrity pathway. The *E. festucae MSG5* homologue, A.19.8369, is located on contig 44, and the A.19.8369 polypeptide is predicted to contain a dual specificity protein phosphatase family profile (PS50054) between amino acids 427-520 (Fischer et al., 1991), and within this a tyrosine specific protein phosphatases active site (amino acids 462-472).

5.4. The cell integrity pathway

Components of the *E. festucae* cell integrity pathway are illustrated in Figure 5.4, and GO annotations for these components from *S. cerevisiae*, *M. grisea* and *E. festucae* are presented in Table 5.4. Amino acid conservation analyses are summarised in Table 5.2.

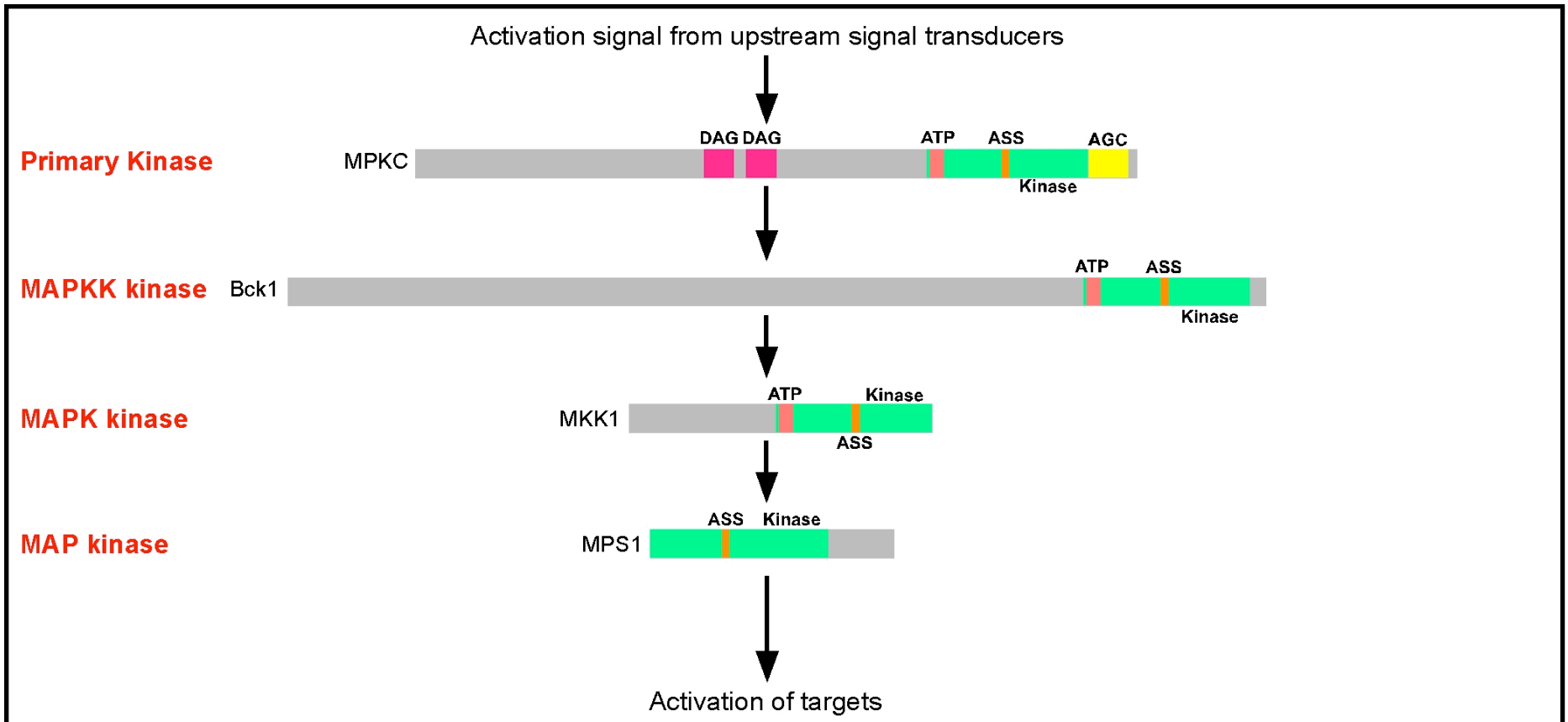

Figure 5.4 The *E. festucae* cell integrity pathway
Schematic illustrating domain structures of key components of the *E. festucae* cell integrity MAP kinase pathway - the primary kinase MPKC, MAPKK kinase Bck1, MAPK kinase Mkk1 and MAP kinase Mps1. Names are based on *M. grisea* with the exception of *S. cerevisiae* Bck1p. Important domains and motifs are indicated and include: protein kinase domain (PS50011; kinase), ATP-binding region signature (PS00107; ATP), serine/threonine protein kinases active site signature (PS00108; ASS), zinc-finger phorbol-ester diacylglycerol (DAG)-type domain (PS00479; DAG) and AGC-kinase C-terminal domain (PS51285).

Table 5.4 GO annotations for components of the cell integrity pathway

		Biological Process			Molecular Function		
Protein	Organism	GO no. [1]	Description	Code[2]	GO no. [1]	Description	Code[2]
MPKC	*S. cerevisiae*	0007165	Signal transduction	IMP	0004697	Protein kinase C activity	IDA
		0007243	Protein kinase cascade	IMP			
		0006468	Protein amino acid phosphorylation	IDA			
		0007047	Cell wall organisation	IMP			
		0000902	Cell morphogenesis	RCA			
		0007015	Actin filament organisation	IGI			
	E. festucae	0006468	Protein amino acid phosphorylation	ISS	0004674	Protein Ser/Thr kinase activity	ISS
		0007165	Signal transduction	ISS	0005524	ATP-binding	ISS
Bck1p	*S. cerevisiae*	0007243	Protein kinase cascade	IMP	0004709	MAPKK kinase activity	IGI
		0006468	Protein amino acid phosphorylation	TAS			
		0030010	Establishment of cell polarity	IMP			
	E. festucae	0006468	Protein amino acid phosphorylation	ISS	0004674	Protein Ser/Thr kinase activity	ISS
					0005524	ATP-binding	ISS
Mkk1	*S. cerevisiae*	0006468	Protein amino acid phosphorylation	ISS	0004708	MAPK kinase activity	ISS
		0007165	Signal transduction	IMP			
	E. festucae	0006468	Protein amino acid phosphorylation	ISS	0004674	Protein Ser/Thr kinase activity	ISS
MPS1	*M. grisea*	0044409	Entry into host	IMP	0004707	MAP kinase activity	IMP
		0044408	Growth or development of symbiont on or near host	IMP			
		0009405	Pathogenesis	IMP			
	S. cerevisiae	0007047	Cell wall organisation	TAS	0004707	MAP kinase activity	ISS
		0006468	Protein amino acid phosphorylation	ISS			
		0008361	Regulation of cell size	IMP			
		0001101	Response to acid	IMP			
		0007165	Signal transduction	IMP			
	E. festucae	0006468	Protein amino acid phosphorylation	ISS	0004674	Protein Ser/Thr kinase activity	ISS
					0005524	ATP-binding	ISS

[1]GO annotation number from the Gene Ontology database (http://amigo.geneontology.org/cgi-bin/amigo/go.cgi).

[2]Evidence code for annotations. Details describing these codes are found at http://www.geneontology.org/GO.evidence.shtml. TAS = traceable author statement, ISS = inferred from sequence similarity, IMP = inferred from mutant phenotype, IGI = inferred from genetic interaction, IDA = inferred direct assay, RCA = reviewed computational analysis. The most reliable evidence sources are IMP, IGI and IDA, which are all experiment-based annotations.

5.4.1. Primary kinases

5.4.1.1. MPKC

MPKC is the *M. grisea* homologue of *S. cerevisiae* Pkc1p (protein kinase C), the primary kinase of the cell integrity MAP kinase pathway (EC 2.7.11.13) and has previously been characterised. The gene encoding the *E. festucae MPKC* homologue is split across two contigs, 559 and 560, with a predicted gap of ~300 nucleotides. Given this gap, it is annotated as two separate genes – A.11.8716 on contig 559 and A.1.8718 on contig 560. The predicted *E. festucae* MPKC homologue contains two zinc finger phorbol-ester DAG-type domains (PS50081) between amino acids 463-511 and 531-581 (Ono et al., 1989). It also contains a protein kinase domain between amino acids 817-1076, and within this a protein kinase ATP-binding region signature and serine/threonine protein kinase active site signature (amino acids 823-846 and 938-950 respectively). In addition it also contains an AGC (cAMP-dependent, cGMP-dependent and protein kinase C)-kinase C-terminal domain profile (PS51285) between amino acids 1077-1142, a domain found in a variety of protein kinases that is characterised by three conserved phosphorylation sites involved in its regulation (Parker and Parkinson, 2001).

5.4.2. The MAP kinase cascade

5.4.2.1. Bck1p

The MAPKK kinase of the *S. cerevisiae* cell integrity pathway is Bck1p (EC 2.7.11.25). The *E. festucae* homologue of *BCK1*, A.4.8813, is located on contig 662. The predicted *E. festucae* Bck1 polypeptide contains a protein kinase domain (amino acids 1269-1583) and within this a protein kinases ATP-binding region signature and serine/threonine protein kinases active-site signature (amino acids 1275-1298 and 1395-1407 respectively).

5.4.2.2. MKK1

The *M. grisea* cell integrity MAPK kinase, MKK1 (EC 2.7.12.2), is homologous to *S. cerevisiae* Mkk1p, and has previously been characterised (Kulkarni and Dean, 2004). The *E. festucae MKK1* homologue, A.9.48 is located on contig 1058. This predicted A.8.48 polypeptide contains a protein kinase domain (amino acids 235-485), and within this a protein kinase ATP-binding region signature and serine/threonine protein kinases active site signature (amino acids 241-264 and 358-370 respectively).

5.4.2.3. MPS1

MPS1 is the *M. grisea* cell integrity pathway MAP kinase that has previously been characterised (Xu et al., 1998), and is homologous to *S. cerevisiae* Slt2p. The *E. festucae MPS1* homologue, A.1.8812, is located on contig 661. The predicted A.1.8812 polypeptide contains a protein kinase domain (amino acids 1-287) and within this a serine/threonine protein kinases active site signature (amino acids 118-130).

5.4.3. Phosphatases

No phosphatases have been detected for the cell integrity MAP kinase pathway.

6. Discussion

6.1. *E. festucae sakA* encodes a functional MAP kinase

6.1.1. *sakA* complements *S. pombe sty1*Δ stress sensitivity and morphology defects

Despite the significant evolutionary distance between *S. pombe* and *E. festucae*, Sty1 and SakA share considerable amino acid identity (81%). For this reason the *S. pombe sty1*Δ mutant was chosen as a model system to test the function of SakA. *sty1*Δ shows increased sensitivity to osmotic (Millar et al., 1995; Shiozaki and Russell, 1995a), oxidative, heat and UV stresses (Degols et al., 1996). Expression of the *sakA* cDNA resulted in survival of *sty1*Δ under both osmotic and oxidative stress conditions, indicating that *sakA* can complement these stress sensitivity defects. *sty1*Δ cells are also elongated due to delayed entry into mitosis (Shiozaki and Russell, 1995b). Expression of *sakA* cDNA resulted in the restoration of wild-type cell length, demonstrating that SakA can also complement the cell cycle function of Sty1. Taken together, these results confirm *sakA* encodes a functional stress-activated MAP kinase orthologous to *S. pombe* Sty1.

The inability of the *sakA* gene containing introns to rescue the *sty1*Δ mutant, due to incorrect splicing of the *E. festucae* introns by *S. pombe*, should perhaps not be surprising given that *S. cerevisiae* appears incapable of correctly splicing transcripts from higher eukaryotes (Langford et al., 1983; Watts et al., 1983). Consistent with this, Kupfer et al. (2004) noted significant differences between introns from yeast and filamentous fungi and speculated that their mechanisms of pre-mRNA splicing may differ.

6.1.2. SakA translocates to the nucleus in response to osmotic stress

In order for stress-activated MAP kinase cascades to alter gene expression, the signal must be transduced into the nucleus. In *S. pombe* this is achieved by relocalisation of activated Sty1 to the nucleus after stress induction (Gaits et al., 1998). Once in the nucleus Sty1 phosphorylates its target transcription factors. Observation of the localisation of a SakA-GFP fusion protein in *S. pombe sty1* under non-stressed and osmotic stress conditions revealed that SakA also rapidly relocalises from the cytoplasm

to the nucleus after stress induction. This suggests that in *E. festucae*, SakA is also likely to mediate responses to stress by translocating to the nucleus and activating target proteins such as transcription factors.

6.2. Loss of *sakA* induces stress sensitivity and fungicide resistance

6.2.1. The Δ*sakA* mutant displays increased stress sensitivity in culture

Deletion analysis of *E. festucae sakA* revealed essential roles for *sakA* in growth under osmotic and temperature stress conditions in culture. This suggests that the *E. festucae* stress-activated MAP kinase pathway is more similar to the *S. pombe* Sty pathway than the *S. cerevisiae* HOG pathway, being able to respond to other stresses in addition to osmotic stress (Banuett, 1998). However, in comparison to the *S. pombe sty1*Δ mutant, the Δ*sakA* mutant showed no increased sensitivity to hydrogen peroxide. Similar to this, *M. grisea* Δ*osm1* mutant conidia are no more sensitive to hydrogen peroxide than wild-type (Dixon et al., 1999), and the *Trichoderma harzianum hog1*-silenced strain shows only slightly increased sensitivity to hydrogen peroxide (Delgado-Jarana et al., 2006). In contrast stress-activated MAP kinase mutants of *B. cinerea* (Segmüller et al., 2007), *B. oryzae* (Moriwaki et al., 2006) and *C. neoformans* serotype A (Bahn et al., 2005) are more like the *S. pombe sty1*Δ mutant, displaying increased sensitivity to hydrogen peroxide. Given *sakA* was able to rescue the *sty1*Δ mutant from sensitivity to oxidative stress, SakA has the potential to transduce oxidative stress signals. However, it appears that in *E. festucae*, an alternative pathway, possibly involving the redox sensitive transcription factor Yap1, is required for the response to oxidative stress mediated by hydrogen peroxide. It is important to note that the lack of increased sensitivity to hydrogen peroxide displayed by the Δ*sakA* mutant does not exclude the possibility that it is sensitive to other oxidative stress agents such as menadione. Temple et al. (2005) emphasise that no one reactive oxidative species is representative of oxidative stress and mutants may be more sensitive to one ROS yet dispensable for the response to another.

6.2.2. *sakA* is required for sensitivity to the phenylpyrrole fungicide fludioxonil

The *sakA* mutant also displays another phenotype characteristic of filamentous fungal stress-activated MAP kinase mutants, resistance to the phenyl-pyrrole fungicide fludioxonil. These fungicides are thought to directly target and hyper-activate the stress-activated MAP kinase pathway. Indeed, in *N. crassa*, treatment with fludioxonil triggers increased intracellular glycerol accumulation, causing conidia and hyphal cells to swell and burst (Zhang et al., 2002). However, this response is not seen in Δ*os-2* mutants suggesting the Os-2 MAP kinase pathway is a target for fludioxonil, although the precise target is unknown. The resistance of the *E. festucae* Δ*sakA* mutant to fludioxonil suggests that in *E. festucae* the SakA MAP kinase is a target for fludioxonil. However, the *E. festucae* stress-activated MAP kinase pathway may not be the only pathway involved in the response to fludioxonil. In *C. neoformans* three pathways are involved in mediating the response to fludioxonil, with the stress-activated MAP kinase pathway promoting sensitivity to fludioxonil and the cell integrity MAP kinase pathway and calcineurin signalling pathway promoting resistance to fludioxonil (Kojima et al., 2006).

6.3. Difficulties in generation and complementation of Δ*sakA*

In planning the targeted disruption of the Δ*sakA* mutant, special consideration was given to the transformation protocol as the Δ*sakA* mutant was predicted to be osmosensitive based on the phenotypes of other filamentous fungal stress-activated MAP kinase mutants (Dixon et al., 1999; Zhang et al., 2002; Kojima et al., 2004; Bahn et al., 2005; Delgado-Jarana et al., 2006; Moriwaki et al., 2006; Igbaria et al., 2008). When generating the *A. nidulans* Δ*sakA* mutant, Kawasaki et al. (2002) employed a conidial electroporation method instead of the normal method of protoplast transformation as this requires the protoplasts to be spread on high osmolarity medium to osmotically stabilise them until their cell wall forms. Unfortunately, conidial electroporation was not an option for generation of the *E. festucae* Δ*sakA* mutant as it would be very difficult to obtain sufficient wild-type conidia for transformation. However, when generating the *M. grisea* Δ*osm1* mutant, Dixon et al. (1999) used a modified protoplast transformation method in which transformed protoplasts were incubated in osmotically-stabilised liquid

medium for 28 h to allow the cell walls to start to regenerate, then the protoplasts were collected by centrifugation and spread onto non-osmotically stabilised medium. Using this approach extended exposure of potentially osmosensitive mutants to high osmolarity medium was prevented. This approach was adopted for generation of the *E. festucae* Δ*sakA* mutant. Transformed protoplasts were incubated in osmotically stabilised RG medium overnight, then the protoplasts collected and spread on non-osmotically stabilised PD medium. However, transformation using this approach yielded no transformants. Transformation using the unmodified method (Itoh et al., 1994), yielded two types of transformants – some that looked like wild-type *E. festucae* growth and some that grew as raised glossy colonies. However, when grown on PD medium, the glossy transformants grew like the wild-type strain suggesting this altered growth was due to the high osmolarity medium. Indeed, all the transformants that displayed this glossy morphology were shown to be osmosensitive Δ*sakA* mutants.

Given the unsuccessful use of the modified transformation method for generation of the Δ*sakA* mutant, Δ*sakA* protoplasts for complementation and generation of an EGFP-expressing Δ*sakA* mutant strain were transformed using the unmodified method (Itoh et al., 1994). Therefore, it was not surprising, given the osmosensitive nature of the Δ*sakA* mutant that very few transformants were obtained from these transformations. Only four transformants were obtained from the EGFP transformation and none of these expressed EGFP. For this reason, plans to generate an EGFP-expressing Δ*sakA* mutant strain were abandoned, as it would likely require disruption of the *sakA* gene with a construct containing both an antibiotic resistance cassette and the EGFP reporter gene. In contrast, all colonies obtained from transformation with pCE1, for complementation of the Δ*sakA* mutant, contained the *sakA* gene. This is likely to be due to the fact that only those transformants that took up the *sakA* construct were able to survive the high osmolarity conditions.

6.4. The Δ*sakA* mutant displays altered morphology in culture

When examined by DIC microscopy, growth of the Δ*sakA* mutant was similar to wild-type, except that branches were frequently observed growing back in towards the body

of the colony. This suggests this mutant may have a defect in maintenance of cell polarity, possibly due to the high levels of delocalised ROS present in this mutant (discussed in Section 6.6.1), as ROS has been implicated in maintenance of hyphal apical dominance (Semighini and Harris, 2008). When grown for extended periods, or on thin layer agar (nutrient stressed conditions), another key difference can be seen between the Δ*sakA* mutant and wild-type strain. Under these conditions wild-type *E. festucae* frequently produces spherical/elliptical structures at the ends of the hyphae, a phenomenon never seen in the Δ*sakA* mutant. These structures are static, indicating that they are not simply burst hyphal tips. In addition, flooding of cultures with media or stain results in these structures detaching from the hyphae and forming clumps, indicating their surface is sticky. When stained with calcofluor white (CFW) the hyphal tips stain intensely and are the same thickness as the rest of the hyphae, indicating these structures are not swollen hyphal tips. CFW staining of these structures is less intense than at the hyphal tip but more intense than staining seen back from the hyphal tip. The possibility that these structures are conidia has been considered. However, these structures are not similar to conidia previously described for other *Epichloë* endophytes, such as the closely related *E. typhina* (Bacon and Hinton, 1991). In addition, these structures arise off the ends of vegetative hyphae rather than being borne on conidiophores. If conidia production by these hyphae is a terminal differentiation step, these hyphae would no longer be able to grow since colonies grow by tip growth (Harris and Momany, 2004). However, these structures are much larger than that of previously reported *E. festucae* conidia (Kuldau et al., 1999). These characteristic *E. festucae* conidia have been observed in the wild-type strain (Y. Rolke, unpublished), but have never been seen in the Δ*sakA* mutant. This apparent absence of conidia in the Δ*sakA* mutant is consistent with results seen for other filamentous fungal stress-activated MAP kinase mutants (Dixon et al., 1999; Park et al., 2004; Segmüller et al., 2007). If the large structures produced by the wild-type strain are indeed conidia they should contain a nucleus. It is therefore of particular interest to examine whether this is the case in the future. Preliminary analysis using DAPI (4', 6-diamidino-2-phenylindole) was unsuccessful as the stain did not appear to enter the cells and no fluorescence was detected. Another possibility is to use Hoechst stain, however, this has been found to rapidly induce the formation of large vacuoles (S. Saikia, unpublished).

Another key difference observed between the wild-type and Δ*sakA* mutant strains was that the Δ*sakA* mutant stained poorly with CFW. In wild-type *E. festucae* the septa and hyphal tip stain strongly with CFW. In comparison, whilst septa of the Δ*sakA* mutant stained normally, the hyphal tips often did not stain or stained very poorly and patches of localised CFW staining were frequently seen. This suggests *sakA* may play a role in regulating cell wall biosynthesis and in particular chitin localisation, as chitin is a major target of CFW staining (Watanabe et al., 2005). This putative reduction in chitin at the hyphal tip is consistent with observations in *C. albicans* where *HOG1* promotes expression of three chitin synthases, and co-stimulation of chitin synthesis by CFW and calcium ions is reduced in the Δ*hog1* mutant compared to the wild-type strain (Munro et al., 2007). In addition, the *A. nidulans SIK1* (Δ*sakA*) mutant has localised chitin deposits throughout the colony (Han and Prade, 2002).

6.5. Loss of *sakA* induces changes associated with increased aging

Deletion of the *E. festucae sakA* gene resulted in a number of changes generally associated with aging. These included loss of aerial hyphae, the presence of dead and dying hyphae within the colony, increased pigmentation and the presence of a halo of exudate around the colony. These features are generally only displayed by wild-type *E. festucae* colonies that have been stored for long periods of time. Similar to the *E. festucae* Δ*sakA* mutant, the *C. heterostrophus* Δ*hog1* mutant also displays phenotypes suggestive of increased aging with colonies abruptly losing viability and becoming darkly pigmented (Igbaria et al., 2008). However, in contrast to the Δ*sakA* mutant colonies from which viable mycelia can be sub-cultured, mycelial plugs from the aged *C. heterostrophus* Δ*hog1* mutant colonies are non-viable. In this respect, the senescence displayed by the *E. festucae* Δ*sakA* mutant is more similar to the crippled growth phenotype of *P. anserina*. Crippled growth is a non-lethal cellular degeneration process characterised by impaired growth, increased senescence and reduced differentiation capability (Silar et al., 1999). The cell integrity MAP kinase cascade has been found to play an integral role in induction of crippled growth in *P. anserina*, with all three kinases (Ask1, Mkk1 and Mpk1) being required for its establishment (Kicka and Silar, 2004; Kicka et al., 2006). Interestingly, the NADPH oxidase subunit PaNox1 also plays a role in regulating crippled growth by acting

upstream of the cell integrity MAP kinase cascade and promoting nuclear localisation of Mpk1 (Malagnac et al., 2004; Jamet-Vierny et al., 2007).

The apparent accelerated aging displayed by the Δ*sakA* mutant may be due to the elevated levels of superoxide and hydrogen peroxide in this mutant. Studies in *S. cerevisiae* have clearly shown a link between ROS and aging, with any changes that result in increased ROS levels, such as deletion of the ROS scavenging superoxide dismutase, leading to reduced lifespan (Wawryn et al., 1999; Nestelbacher et al., 2000; Laun et al., 2001). In also seems reasonable that, given the high levels of ROS in the Δ*sakA* mutant colonies, these colonies would undergo changes to their growth over time due to the well-established damaging effects of ROS on biomolecules (Rodriguez and Redman, 2005).

6.6. Link between *sakA* and ROS signalling

6.6.1. The Δ*sakA* mutant displays increased ROS levels in culture and *in planta*

Levels of reactive oxygen species were found to be elevated both in Δ*sakA* mutant colonies in culture and around Δ*sakA* mutant hyphae growing *in planta*. This elevated ROS may be due to the predicted role of SakA in repression of the Nox complex, as removal of *sakA* would result in derepression (Lara-Ortíz et al., 2003; Eaton et al., 2008). However, in contrast to *A. nidulans sakA* which represses expression of *noxA* (Lara-Ortíz et al., 2003), no differences were seen between the steady state levels of *noxA* and *noxR* transcript produced by the Δ*sakA* mutant in comparison to wild-type. This implies that *sakA* does not regulate *noxA* or *noxR* at the level of transcription. Preliminary results from yeast 2-hybrid analysis has provided some evidence that SakA may interact with NoxR and BemA, a predicted additional component of the fungal Nox complex (Semighini and Harris, 2008). However, this analysis was complicated by SakA and BemA being able to self-activate the reporter genes, resulting in false positives, a common problem encountered in yeast 2-hybrid analyses (Coates and Hall, 2003). Future research will focus on determining whether SakA does interact with components of the fungal Nox

complex, using techniques such as GST pulldowns. Interaction of SakA with components of the Nox complex would not be completely unexpected as in mammalian systems the SakA homologue, p38 MAPK, has been shown to interact with, and phosphorylate the NoxR homologue, p67phox (Dang et al., 2003). This interaction between p38 MAPK and p67phox is proposed to induce a change to an active conformation (Dang et al., 2003), and indeed other studies have demonstrated roles for p38 MAPK in activation of the Nox complex (Brown et al., 2004; Yoo et al., 2008). However, the results of this study and those of Lara-Ortíz et al. (2003) suggest that in fungi the stress-activated MAP kinase may act in the opposite manner to p38 MAPK, repressing the Nox complex. However, there is currently no evidence to support interactions between SakA and BemA in other systems. In *S. cerevisiae*, Bem1 plays an important role in regulating bud morphology, acting as a scaffold to hold cell polarity proteins at the site of polarised growth (Butty et al., 2002). In *A. nidulans*, BemA is a component of the polarisome, the scaffold found at the hyphal tip which links polarity proteins to the cytoskeleton and controls polarised growth (Leeder and Turner, 2008). Based on its domain structure and role in polarised growth BemA has been proposed to be a possible analogue of the mammalian p40phox Nox protein (Semighini and Harris, 2008). The milder phenotypes seen for Δ*bemA* mutants of *A. nidulans* (Semighini and Harris, 2008) and *E. festucae* (D. Takemoto, unpublished) in comparison to Δ*noxR* mutants is consistent with the fact that in mammalian systems p40phox is not essential for Nox activity (Abo et al., 1992). However, in mammalian systems there is no evidence for interactions between p38 MAPK and p40phox, but there is strong evidence showing that p38 MAPK phosphorylates p47phox (Brown et al., 2004; El-Benna et al., 2008). This is particularly interesting given that Semighini and Harris (2008) also suggest that BemA could possibly even be a functional analogue of both p40phox and p47phox.

6.6.2. Other potential sources of ROS

In addition to the possibility that the increase in ROS seen in the Δ*sakA* mutant is due to derepression of the Nox complex, it is important to consider other possible sources of this increased ROS. One such potential source is the peroxidases. These enzymes are best known for their roles as antioxidants due to their ability to remove hydrogen peroxide through dehydrogenation (oxidation) of target substrates (Chen and Schopfer,

1999). However, some peroxidases are also able to function as oxidases and catalyse the NADH-dependent reduction of molecular oxygen to superoxide and hydrogen peroxide, and the production of hydroxyl radicals from hydrogen peroxide (Chen and Schopfer, 1999). The function of these enzymes is well-studied in plant systems where they are generally found in the apoplast, bound to cell wall polymers, and are involved in lignin synthesis via dehydrogenation of substrates (Campa, 1991). However, the role that the ROS producing function of peroxidases plays is still unclear. Interestingly, a ligninase-type peroxidase from the fungus *Arthromyces ramosus* was found to have very high hydroxyl-radical producing activity *in vitro* (Chen and Schopfer, 1999).

Another possible source of ROS is the ferric reductases. These enzymes have a domain structure similar to NADPH oxidases but are generally involved in uptake of iron rather than reduction of molecular oxygen (Roman et al., 1993). However, *A. nidulans* contains at least six ferric reductases homologous to the well-studied Fre1 of *S. cerevisiae* (Dancis et al., 1992; Shatwell et al., 1996), and it has been proposed that at least one of these may be a divergent homologue of the Nox enzymes and able to produce ROS (Semighini and Harris, 2008). In addition, the nitroreductase/ferric reductase DrgA from the bacterium *Synechocystis* is able to catalyse the Fenton reaction, converting hydrogen peroxide into hydroxyl radicals (Takeda et al., 2007).

In addition to these enzymatic sources, ROS are also produced as unintentional by-products of cellular processes, particularly aerobic respiration (Lambeth, 2004). Cells possess a range of ROS scavengers responsible for detoxifying these ROS to prevent cellular damage, including catalases and superoxide dismutases (SODs) that decompose hydrogen peroxide and superoxide respectively. Any decrease in the expression and/or activity of these scavengers would ultimately result in increased levels of these ROS. In many fungi the stress-activated MAP kinase pathway is involved in regulating expression of these ROS scavengers. For example, in *N. crassa, B. oryzae* and *B. cinerea*, the stress-activated MAP kinase regulates catalase expression (Moriwaki et al., 2006; Noguchi et al., 2007; Segmüller et al., 2007). Examination of the regulation of the SOD genes in filamentous fungi will also likely reveal involvement of the stress-activated MAP kinase, as in *S. pombe*, activation of *sod1* expression by oxidative stress requires *sty1* (Mutoh et al., 2002). However, it is unlikely that ROS levels are elevated in the Δ*sakA* mutant simply due to decreased expression/activity of ROS scavengers as SakA is predicted to play

only a minor role, if any, in regulating the ROS scavengers given that the Δ*sakA* mutant does not display increased sensitivity to oxidative stress induced by hydrogen peroxide. Although, this possibility cannot be completely ruled out as SakA is able to rescue the *S. pombe sty1*Δ mutant from oxidative stress sensitivity.

6.7. *sakA* is required for symbiotic maintenance

Maintenance of the mutually beneficial association between *E. festucae* and perennial ryegrass requires signalling between the fungus and its host in order to regulate fungal growth *in planta*. The stress-activated MAP kinase was found to play a crucial role in this signalling, with the Δ*sakA* mutant displaying a drastically altered host interaction phenotype.

6.7.1. The Δ*sakA* mutant has reduced ability to colonise perennial ryegrass

The Δ*sakA* mutant had significantly reduced ability to colonise perennial ryegrass seedlings, resulting in much lower infection rates than was seen for the wild-type strain. Given the manner in which seedlings are inoculated with *E. festucae*, by insertion of hyphae into a slit made across the host shoot apical meristem region, the low infection rate cannot be attributed to reduced ability to infect perennial ryegrass but rather to reduced ability to establish systemic infection from the point of inoculation. Many other filamentous fungal stress-activated MAP kinase mutants also show defects in host infection or virulence. For example, the *B. cinerea* Δ*sak1* mutant is unable to penetrate unwounded plant tissue and can only colonise through wounds (Segmüller et al., 2007), and the *C. heterostrophus* Δ*hog1* mutant shows reduced virulence on corn (Igbaria et al., 2008). Stress-activated MAP kinase mutants of the animal pathogens *C. neoformans* and *C. albicans* also display reduced virulence (Alonso-Monge et al., 1999; Bahn et al., 2005). In addition, the *M. graminicola* Δ*hog1* mutant is also non-pathogenic but this is likely due to an inability to switch from yeast to filamentous growth required for infection (Mehrabi et al., 2006). In contrast, the *M. grisea* Δ*osm1* and *C. lagenarium* Δ*osc1* mutants are fully pathogenic with no defects in penetration or virulence (Dixon et al., 1999;

Kojima et al., 2004). A possible explanation for the reduced colonisation of perennial ryegrass by the Δ*sakA* mutant may be due to the osmotic environment within the plant tissues hampering growth of the osmosensitive Δ*sakA* mutant. The osmolarity of the plant apoplast fluctuates greatly due to its role in the transport of water and nutrients, and solute concentrations can often reach quite high levels (Sattelmacher, 2001). For example, levels of sucrose within the intercellular fluid of sugarcane can reach levels as high as 12% (Dong et al., 1994). Whilst it is unclear exactly what the osmotic environment facing *E. festucae* in the perennial ryegrass apoplast is like, it is likely that solute concentrations will fluctuate to high levels that may hamper growth of the osmosensitive Δ*sakA* mutant.

The reduced colonisation of perennial ryegrass by Δ*sakA* mutant may also be due to increased sensitivity to chemicals produced as part of the host's wounding response. A variety of chemicals will be produced by perennial ryegrass seedlings in response to the wounding imposed during inoculation. These are likely to include toxic insect and herbivore feeding deterrents, as one of the major causes of plant wounding is herbivory by grazing animals and insect pests (Kessler and Baldwin, 2002). Wounding also induces the production of a number of plant hormones including jasmonic acid, ethylene and abscisic acid (León et al., 2001). The production of jasmonic acid is of particular interest as jasmonic acid has been shown to inhibit formation of appressoria by the barley powdery mildew fungus *Erysiphe graminis*, thereby preventing infection (Schweizer et al., 1993). In addition, jasmonic acid produced by wild rice plants (*Oryza officinalis*) was shown to greatly reduce spore germination and production of appressoria by the rice blast fungus *M. grisea* (*Pyricularia oryzae*) (Neto et al., 1991).

The reduced virulence displayed by the *C. albicans* Δ*hog1* mutant has been proposed to be due to the mutant displaying increased sensitivity to oxidative stress and therefore being unable to cope with the host's oxidative burst defense response (Orozco-Cardenas and Ryan, 1999). ROS are also produced as part of the wounding response of plants (Schilmiller and Howe, 2005). However, it is unlikely that the reduced ability of the Δ*sakA* mutant to colonise perennial ryegrass is due to increased sensitivity to this ROS as the mutant is no more sensitive to hydrogen peroxide than the wild-type strain. Although sensitivity of the Δ*sakA* mutant to superoxide generated by addition of menadione has not been examined, it is unlikely that the reduced colonisation of the

Δ*sakA* mutant is due to increased sensitivity to superoxide as this is rapidly dismutated into hydrogen peroxide.

It is important to note that the *E. festucae* Nox complex mutants (Δ*noxA*, Δ*noxR* and Δ*racA*) did not display reduced ability to colonise perennial ryegrass (Takemoto et al., 2006; Tanaka et al., 2006; Tanaka et al., 2008a), suggesting that the cause of this reduced colonisation by the Δ*sakA* mutant is the loss of its role as a stress-activated MAP kinase rather than its potential role as a regulator of the Nox complex.

6.7.2. Loss of *sakA* induces increased tillering

Similar to that seen for the *E. festucae* Nox complex mutants (Takemoto et al., 2006; Tanaka et al., 2006; Tanaka et al., 2008a), infection of perennial ryegrass with the Δ*sakA* mutant resulted in loss of apical dominance, leading to increased tillering and stunting of the host. This increased tillering was likely due to activation of axillary meristems that are normally repressed in wild-type associations. Growth of axillary meristems is controlled by the balance of three main groups of plant hormones - auxin, cytokinins and strigolactones (McSteen, 2009). Auxin (indole-3-acetic acid; IAA) is produced at the apex and is transported to the axillary buds, preventing their outgrowth. Conversely, strigolactones are produced in the roots and are transported up to the axillary buds, where they assist auxin in inhibiting axillary bud outgrowth. In contrast, cytokinins, also produced in the roots, are transported up to the axillary meristems and promote their outgrowth (McSteen, 2009). The increased tillering observed in Δ*sakA* mutant-infected plants may be due to a change in the balance of these hormones. For example, an increase in cytokinin levels or a decrease in auxin or strigolactone levels would result in increased outgrowth from the axillary meristems.

6.7.3. Plants infected with the Δ*sakA* mutant have poor root systems

In contrast to the increase in tillering seen for plants infected with the Δ*sakA* mutant, the root systems in these plants are poorly developed. This raises an important question - why are the root systems of these plants so significantly affected when *E. festucae* does not

colonise the root tissues? A possible explanation for this may also provide an explanation for the increased tillering seen in these plants. In addition to its role in inhibiting axillary bud outgrowth, auxin also plays an important role in promoting lateral root growth (Casimiro et al., 2001). However, the majority of auxin present in the roots is produced in the shoot and translocated to the root (Elliott, 1977). Thus, both the reduction in root growth and increase in tillering can be explained by a decrease in the production of auxin as this would lead to increased axillary bud outgrowth and decreased lateral root growth. However, changes in the levels of other plant hormones involved in root growth cannot be ruled out. For example brassinosteroids also play an important role in promoting lateral root growth and have actually been shown to act synergistically with auxin in promoting lateral root outgrowth (Bao et al., 2004).

In addition to the possibility that the decreased root growth seen in Δ*sakA* mutant-infected plants is due to alterations in the levels of plant hormones, there is also the possibility that the Δ*sakA* mutant may actually colonise the root tissues. Wild-type *E. festucae* is seldom found within root tissues (Schardl, 2001). However, this does not necessarily preclude the Δ*sakA* mutant from colonising the roots as it is able to colonise the host vascular bundles which are seldom colonised in wild-type associations (Christensen et al., 2002). However, hyphae of the *E. festucae* Δ*racA* symbiotic mutant have been seen on the surface of root tissues of infected plants (M. Becker, unpublished). Possible colonisation of host roots by the Δ*sakA* mutant will be examined in the future.

6.7.4. The Δ*sakA* mutant induces host stunting and precocious senescence

Similar to plants infected with the *E. festucae* Nox mutants (Δ*noxA*, Δ*noxR* and Δ*racA*) (Takemoto et al., 2006; Tanaka et al., 2006; Tanaka et al., 2008a), Δ*sakA* mutant-infected plants displayed stunted growth and prematurely senesced around 2-3 months after inoculation. This stunted growth may be a consequence of the poor root system discussed earlier being unable to transport sufficient water and nutrients. However, this is unlikely as when Δ*sakA* mutant-infected plants were grown on water agar in temperature controlled rooms the plants were still stunted. It is also unlikely that the stunting displayed by these plants is simply a consequence of the increased fungal biomass in these Δ*sakA* mutant associations as another group of endophytes, the p-

endophytes, display similar levels of biomass as the Δ*sakA* mutant with similarly deregulated growth, yet the host remains asymptomatic (Christensen et al., 2002). This suggests that the stunting induced by the Δ*sakA* mutant is due to other factors such as alteration of plant hormone levels or disruption of host signalling pathways.

The premature senescence displayed by Δ*sakA* mutant-infected plants may be due to their poorly developed root systems. Observations suggest this is true to a certain extent as infected plants displayed longer survival times during winter months when the environmental stresses were less severe and when grown in temperature controlled rooms. However, even under these conditions the Δ*sakA* mutant-infected plants did eventually senesce, suggesting other factors are also involved. This senescence was not induced by a host defense response as no localised areas of cell death were detected by lactophenol trypan blue staining. Tissue from Δ*sakA* mutant-infected plants did stain more intensely than wild-type infected tissue but this staining was diffuse throughout the tissue. It is likely that this increased staining was caused by the Δ*sakA* mutant-infected tissue being more permeable due to the onset of senescence, as the tissue also cleared more quickly with methanol than wild-type infected tissue. Indeed, leaf senescence has been shown to correlate with increased membrane permeability (Dhindsa et al., 1981).

6.7.5. The Δ*sakA* mutant displays reduced epiphyllous growth

In Δ*sakA* mutant associations epiphyllous hyphal growth is greatly reduced in comparison to wild-type associations. Those epiphyllous hyphae that are seen often contain swellings and have convoluted growth, but in contrast to wild-type do not form coil-like structures. In addition, the manner in which the Δ*sakA* mutant hyphae grew out of the host tissues onto the surface was altered in comparison to wild-type. In wild-type associations hyphae appear to break through the cuticle, possibly via production of an appressorial-like structure, then grow across the leaf surface (M. Becker, unpublished). In contrast, Δ*sakA* mutant hyphae appear unable to break through the cuticle and instead grow out through the host stomatal pores, a phenomenon never seen in wild-type associations. A possible explanation for this inability of the Δ*sakA* mutant to break through the cuticle draws on the suggestion that *E. festucae* produces an appressorial-like structure to break out of the host tissues, analogous to the way in which appressoria of

plant pathogenic fungi gain entry into host tissues (M. Becker, unpublished). The stress-activated MAP kinase has been found to play an important role in appressoria based infection by a number of plant pathogenic fungi. For example, the *B. cinerea* Δ*sak1* mutant is unable to produce appressoria-like structures and is therefore unable to penetrate host tissues (Segmüller et al., 2007). In addition, the *C. heterostrophus* Δ*hog1* mutant produces much smaller appressoria than the wild-type strain and causes greatly reduced disease symptoms in corn (Igbaria et al., 2008). A possible explanation for this arises from the role of the stress-activated MAP kinase in regulating production of the compatible solute glycerol. In *N. crassa* expression of three key genes involved in glycerol biosynthesis is regulated by the Os-2 MAP kinase (Noguchi et al., 2007), and the role of *S. cerevisiae* Hog1p in glycerol production is well-established (Brewster et al., 1993). Thus, if glycerol is required for the generation of turgor in appressoria-like structures and the stress-activated MAP kinase mutants are defective in glycerol production they will be unable to produce functional appressoria. This may explain the phenotype seen for the Δ*sakA* mutant as, to burst through the host cuticle, *E. festucae* may produce an appressoria-like structure that requires glycerol production for the generation of turgor. If glycerol production by the Δ*sakA* mutant is impaired it would be unable to penetrate the cuticle and therefore its only means of exiting the host tissues would be via the stomatal pores. However, it appears that the stress-activated MAP kinase pathway does not regulate glycerol production in all filamentous fungi, as glycerol accumulation is unaltered in the *M. grisea* Δ*osm1* mutant, whereas arabitol accumulation is reduced. Consequently, this mutant was able to produce normal appressoria that were fully pathogenic (Dixon et al., 1999). This implies that for deletion of the stress-activated MAP kinase to affect turgor generation in appressoria-like structures, production of the compatible solute required for turgor generation must be under control of the stress-activated MAP kinase pathway. Future studies will focus on determining whether *E. festucae* does produce appressoria-like structures to break through host tissues. If this were the case it would be interesting to examine whether turgor generation by this structure is through the production of glycerol, and if so whether glycerol production is altered in the Δ*sakA* mutant.

6.7.6. Growth of the Δ*sakA* mutant *in planta* is deregulated

In Δ*sakA* mutant associations hyphal growth is deregulated in comparison to the wild-type strain, and growth appears similar to that of the Nox mutants (Takemoto et al., 2006; Tanaka et al., 2006; Tanaka et al., 2008a). Hyphae of the Δ*sakA* mutant are seldom aligned parallel to the leaf axis and are hyper-branched, resulting in a dramatic increase in fungal biomass in these mutant associations. *Epichloë* endophytes are proposed to grow in a two-step manner in which growth at the base of tillers is predominantly by tip growth (Tan et al., 2001), but then when hyphae enter the leaf primordia and the host cells start to expand, fungal growth switches to intercalary growth and extension (Christensen et al., 2008). This fungal growth pattern mimics that of the host and prevents the hyphae being sheared apart as the leaf elongates. The hyper-branching nature of the Δ*sakA* mutant hyphae *in planta* suggests that the switch to intercalary extension may not have occurred and the hyphae are still growing by tip growth. However, it is unclear how these hyphae escape being sheared apart by the mechanical forces generated during host cell expansion. It would therefore be interesting to pursue this further in the future.

6.7.7. The Δ*sakA* mutant shows altered morphology *in planta*

When examined by transmission electron microscopy (TEM) a number of differences can be seen between Δ*sakA* mutant and wild-type hyphae growing *in planta*. The Δ*sakA* mutant hyphae appear much more irregular in size and shape, similar to the *E. festucae* Nox mutants (Takemoto et al., 2006; Tanaka et al., 2006; Tanaka et al., 2008a). In addition, in comparison to wild-type associations where generally only one or two hyphae are found in any given intercellular space, many Δ*sakA* mutant hyphae often occupy a single intercellular space, distorting the surrounding host cells. Another striking difference to the wild-type strain was the presence of large vacuoles within the Δ*sakA* mutant hyphae, a phenomenon seldom seen in wild-type hyphae *in planta*. Examination of vacuoles in wild-type and the Δ*sakA* mutant in culture revealed that there are no differences in vacuolation between these two strains in culture, suggesting that the differences seen *in planta* are due to conditions within the host. A possible

explanation for this is that the osmotic environment in the host apoplast stresses the osmosensitive Δ*sakA* mutant, causing it to produce large vacuoles. This possibility is particularly important in light of work by Vitalini et al. (2007), who showed that the *N. crassa* stress-activated MAP kinase, Os-2, is regulated by the circadian clock, and this is proposed to prepare *N. crassa* for possible dessication at sunrise. If *E. festucae* SakA is also regulated by the clock it is conceivable that the clock may prepare *E. festucae* for the increase in osmolarity that will occur at sunrise, when photosynthesis commences in the host. Therefore, loss of *sakA* would prevent *E. festucae* from being able to pre-empt the increase in osmolarity that will occur at sunrise, and the osmosensitive mutant will consequently become stressed, leading to increased vacuolation. In support of this, exposure of wild-type *M. grisea* to osmotic stress in culture was found to induce vacuolation (Dixon et al., 1999). It would therefore be interesting to examine whether there would be any differences in vacuolation of the wild-type and Δ*sakA* mutant strains grown under osmotic stress conditions in culture, and to examine whether hyphae in plants grown in the dark prior to sampling also contain large vacuoles. However, the *E. festucae* Nox mutants also contain large vacuoles *in planta*, suggesting that the extensive vacuolation seen in these and the Δ*sakA* mutant may be related to changes in ROS homeostasis (Takemoto et al., 2006; Tanaka et al., 2006; Tanaka et al., 2008a).

6.7.8. Δ*sakA* mutant hyphae are surrounded by an electron dense ECM *in planta*

When examined by TEM, the extra-cellular matrix surrounding the Δ*sakA* mutant hyphae appeared very electron dense in comparison to wild-type associations. It has been proposed that this electron density is due to a defense response being mounted by the host (Koga et al., 1993). In support of this, phenolic compounds produced by bean plants as a response to infection by *Colletotrichum lindemuthianum* give the host cell walls an electron dense appearance (Bolwell et al., 2001). However, as discussed earlier, the Δ*sakA* mutant does not appear to invoke a host defense response, as evidenced by the lack of localised lactophenol trypan blue staining. Alternatively, senescence-associated compounds produced by the host may contribute to the electron density seen in Δ*sakA* mutant associations, as plants used for TEM analysis had already started to senesce.

6.8. Loss of *sakA* induces changes in host development

6.8.1. Δ*sakA* mutant-infected tillers display swollen bases

Plants infected with the Δ*sakA* mutant display drastically altered development in comparison to uninfected plants and those infected with wild-type *E. festucae.* The base of Δ*sakA* mutant-infected tillers appears swollen and bulbous, giving these plants a spring onion or scallion-like appearance. Examination of the swollen region by microscopy revealed that the host cells within this region are disordered and no longer form cell files as in wild-type associations. These cells also appear much more irregular in size and shape than those from the same region in wild-type associations. The swollen region is located below the shoot apical meristem in the region known as the true stem (Langer, 1979). This region is referred to as the true stem as what is generally called the grass stem is actually a tightly rolled collection of leaf blades and sheaths (Langer, 1979). The grass stem arises from the shoot apical meristem and the cells are arranged in linear files due to the manner in which they arise off the meristem (Bowman and Floyd, 2008). The shoot apical meristem also gives rise to axillary meristems (buds), from which new tillers arise (Langer, 1979). Each new tiller therefore contains its own meristem. In adult plants it is difficult to identify the first tiller, which contains the true shoot apical meristem, so although all other tillers grow from axillary meristems they are referred to as apical meristems. A possible explanation for the disorganisation of the host cells seen below the shoot apical meristem in Δ*sakA* mutant associations may be that when new tillers form, the signalling that controls how the cells below the meristem are laid down, is disrupted. However, this is unlikely as examination of the region below very young axillary meristems revealed that these cells are often not disorganised but similar to those seen in wild-type associations. Thus a better explanation is that the cells of the true stem arise normally off the meristem and are laid down in files but then somehow their organisation is disrupted. A possible cause for this may be the increased ROS seen in Δ*sakA* mutant associations. Hydroxyl radicals have been shown to be capable of cleaving cell-wall polysaccharides, leading to cell wall loosening and elongation (Schopfer, 2001; Liszkay et al., 2004). In addition, experimental generation of hydroxyl radicals in maize cell walls was found to increase cell wall extensibility (Schopfer et al., 2002). Expansion

of plant cells is normally prevented by the rigid cell wall. However, once the cell wall is loosened the cells are able to expand through turgor generated by the uptake of water. Since ROS levels surrounding Δ*sakA* mutant hyphae are elevated in comparison to wild-type associations, and ROS has been shown to be able to loosen plant cell walls it is conceivable that the Δ*sakA* mutant could induce expansion of adjacent host cells, leading to disruption of cell file organisation.

6.8.2. Δ*sakA* mutant-infected tillers display a loss of anthocyanin pigmentation

Another major difference observed between plants infected with wild-type *E. festucae* and the Δ*sakA* mutant is the almost complete loss of anthocyanin pigmentation at the base of tillers infected with the Δ*sakA* mutant. Anthocyanins are water-soluble pigments found within plant vacuoles, and range in colour from orange to blue (Tanaka et al., 2008b). The red anthocyanin seen at the base of perennial ryegrass tillers is likely to be cyanidin (Tanaka et al., 2008b). Grasses contain a variety of anthocyanins (Fossen et al., 2002). These pigments are predicted to play a role in photo-protection and their localisation at the base of tillers may protect the shoot apical meristem from photo-damage (Steyn et al., 2002). There are a number of possible explanations for the loss of anthocyanin pigmentation seen Δ*sakA* mutant associations. Perhaps the most simple of these is that the increased ROS seen in Δ*sakA* mutant-infected plants bleaches the anthocyanins. However, if ROS levels were so significantly elevated in Δ*sakA* mutant associations that they bleached the anthocyanin pigmentation, it is likely that the chlorophyll pigmentation would also be bleached. While the base of Δ*sakA* mutant-infected tillers do appear white, it is unclear whether in wild-type infected plants this region contains chlorophyll, as it is masked by the anthocyanins. In addition, if the increased ROS were bleaching the host tissues, it would be expected that the leaf tissues would also appear bleached. Since this is not the case it is unlikely that the loss of anthocyanin pigmentation is due to bleaching. An alternative explanation is that the Δ*sakA* mutant may interfere with the anthocyanin biosynthetic pathway. Anthocyanins are produced in the cytosol from phenylalanine via the phenylpropanoid pathway (Tanaka et al., 2008b). The first committed step in this pathway is catalysed by chalcone synthase (CHS), which converts coumaroyl CoA into a chalcone, from which the flavanone naringenin is derived. A variety of dihydroflavanols can then be generated from

naringenin, with each specific to a particular anthocyanin. Cyanidin, for example, is synthesised from the dihydroflavanol dihydroquercetin via a two-step process where first dihydroquercetin is converted to leucocyanidin via the dihydroflavanol reductase (DFR), then anthocyanidin synthase (ANS) catalyses formation of cyanidin (Tanaka et al., 2008b). The spatial and temporal expression of genes involved in anthocyanin biosynthesis is regulated by a variety of transcription factors (Tanaka et al., 2008b). Any changes in the expression or activity of these biosynthetic enzymes would lead to changes in anthocyanin pigmentation. Thus an explanation for the loss of anthocyanin pigmentation seen in Δ*sakA* mutant-infected plants is that somehow the expression or activity of one or more enzymes of the anthocyanin biosynthetic pathway is reduced or blocked. Alternatively, precursors required for anthocyanin production may be reduced via up-regulation of other enzymes. For example, the phenylpropanoid pathway is also involved in production of lignins, with coumaroyl CoA being a substrate for the hydroxycinnamoyl transferase (HCT) rather than the chalcone synthase (CHS) (Besseau et al., 2007). Up-regulation of HCT would result in more coumaroyl CoA being fed into the lignin biosynthetic pathway, leading to reduced anthocyanin biosynthesis. Another possibility is that naringenin is being diverted into production of phytoalexins for host defense, leading to less naringenin being available for anthocyanin biosynthesis. In rice naringenin is a precursor of the flavanone phytoalexin sakuranetin (Rakwal et al., 1996). Sakuranetin is a plant defense compound and has been shown to be toxic to *M. grisea* (Kuo and Gardner, 2002). This leads to the hypothesis that the Δ*sakA* mutant somehow elicits a defense response from the host, leading to production of sakuranetin thereby reducing available naringenin for anthocyanin production. This may also explain why the Δ*sakA* mutant hyphae contain large vacuoles *in planta* as they could be stressed by the presence of sakuranetin. This may also account for the electron dense extra-cellular matrix seen around Δ*sakA* mutant hyphae as these may also be electron dense similar to phenolics (Bolwell et al., 2001).

It will be of particular interest in the future to determine whether expression of key genes involved in the anthocyanin biosynthetic pathway such as the chalcone synthases and anthocyanidin synthases is altered in Δ*sakA* mutant-infected plants.

6.8.3. Δ*sakA* mutant-infection induces increased branching of host vasculature

Another difference observed between plants infected with wild-type *E. festucae* and those infected with the Δ*sakA* mutant was the increase in branching between vascular bundles in blade and pseudostem tissue. The leaves of monocotyledonous plants contain numerous vascular strands or bundles that generally run parallel to one another (Scarpella and Meijer, 2004). These vascular bundles form in maturing leaf initials as vascular traces that extend down into the stem, interconnect at leaf nodes and fuse with the stem vascular system (Chapman, 1996). In grasses, leaves are arranged in an alternate pattern either side of the stem, with nodes directly beneath each other, allowing for interconnection of the vascular strands. Fescue grasses such as *Lolium perenne* generally contain one median or main vascular strand and six lateral strands (Hitch and Sharman, 1971). These strands are initiated basipetally (from tip to base), and extend down to the leaf axis where they bend and grow down into the stem (Hitch and Sharman, 1971). The vascular strands continue to grow down the stem, passing the vascular strands of the node beneath unhindered, and then at the next node bifurcate. The bifurcated strands then continue down to the next node where they merge with the strands of that node (Chapman, 1996).

In addition to the main parallel vascular bundles characteristic of monocot plants, a number of species have been reported to also contain small transverse bundles or cross veins (commissural veins) that link these parallel bundles (Blackman, 1971). These species include bread wheat (*Triticum aestivum*) (Blackman, 1971), rice (Kaufman, 1959), maize (Arber, 1934), sugarcane (*Saccharum officinarum*) (Moreland and Flint, 1942), and St. Augustine grass (*Stenotaphrum secundatum*) (Arber, 1934). These cross veins are thought to provide alternative routes for solute and water transport in the event of leaf damage (Blackman, 1971). The cross veins are generally spaced at regular intervals between parallel veins, analogous to rungs of a ladder, with the spacing varying between species (Sakaguchi and Fukuda, 2008). Differentiation of these structures is only detected once the metaxylem and xylem vessels of large and small vascular bundles respectively have differentiated. The cross veins arise in both small and large vascular bundles from a circular layer cell that is in contact with a metaxylem vessel and one or more phloem cells (Sakaguchi and Fukuda, 2008). This cell is triggered to differentiate into a procambial progenitor cell. It then signals to an adjacent vascular bundle sheath cell to

differentiate into a procambial progenitor, which in turn induces a cell from the middle layer of the ground meristem to differentiate into a procambial progenitor. This differentiation into procambial progenitors continues across the ground meristem until procambial progenitor cells link two adjacent parallel vascular bundles. These cells then undergo a single periclinal division, generating the final cross vein (Sakaguchi and Fukuda, 2008). It has been proposed that directed auxin transport from the developing metaxylem is the signal that triggers differentiation leading to the formation of cross veins (Sakaguchi and Fukuda, 2008), as the polar transport of auxin has already been shown to play a role in patterning of vasculature (Scarpella et al., 2006).

The increase in the number of cross veins seen in Δ*sakA* mutant infected plants suggests that the signals leading to differentiation of these cross veins is altered in Δ*sakA* mutant associations. This may be due to changes in auxin transport as it has already been predicted that auxin levels are altered in Δ*sakA* mutant associations, evidenced by the increase in tillering and poor root systems displayed by these plants. However, as auxin transport has not unequivocally been shown to be responsible for induction of cross vein formation it is possible that the Δ*sakA* mutant is interfering with other signalling leading to formation of these structures. Regardless of how the Δ*sakA* mutant is altering cross vein formation, its effects appear more significant closer to the base of tillers, as the increased cross vein formation seen in Δ*sakA* mutant-infected plants is most significant close to the leaf sheaths.

6.9. The *sakA* locus displays conserved micro-synteny

This study has revealed significant conservation of micro-synteny at stress-activated MAP kinase loci across the Sordariomycetes, supporting the results of Hamer et al. (2001) who showed conservation of micro-synteny between *M. grisea* and *N. crassa*. The presence of conserved micro-synteny at the *sakA* locus suggests this region provides a selective advantage or barrier to gene rearrangement in order for the gene order and organisation to be maintained throughout evolution. In addition, the high sequence conservation of the two conserved hypothetical proteins (44D6-1 and 44D6-3) across the species examined suggests these genes must perform an important function in order for

them to remain relatively unchanged throughout evolution.

6.10. Sequence analysis of the *E. festucae pak* genes

Analysis of the amino acid conservation displayed by the predicted *E. festucae* PakA and PakB polypeptides revealed that PakA is more highly conserved across the Sordariomycetes than PakB. Amino acid identity between PakA and its homologues from *F. graminearum*, *N. crassa* and *M. grisea* are 78%, 69% and 73% respectively. In comparison, identity between PakB and its homologues from *F. graminearum*, *N. crassa* and *M. grisea* are only 54%, 55% and 59% respectively. This is particularly interesting given that in filamentous fungi, the PakA homologues appear to play more important roles in symbiosis than the PakB homologues. For example, the *M. grisea* PakA homologue CHM1 is required for normal growth, conidiation and virulence, whereas the PakB homologue MST20 is required for aerial hyphae formation and conidiation but is dispensable for pathogenicity (Li et al., 2004). Similar to this, the *U. maydis* PakA homologue, Cla4, is essential for pathogenicity and normal budding (Leveleki et al., 2004), whereas the PakB homologue plays a lesser role in virulence (Smith et al., 2004). The greater amino acid identity displayed between the *E. festucae* paks and their homologues from *M. grisea*, in comparison to the *N. crassa* homologues, may be due to the adaptation of these proteins for roles in symbiosis, resulting in these proteins being more conserved between symbionts than saprobes.

6.11. Paks are required for normal growth in culture

Loss of the *E. festucae* paks was found to induce changes in colony morphology. The Δ*pakA* mutant displayed greatly reduced radial growth in comparison to the wild-type strain, and appeared fluffy due to an increase in aerial hyphae. This phenotype is very similar to that seen for the *E. festucae* Δ*racA* mutant, which displayed greatly reduced radial growth (Tanaka et al., 2008a). This is also similar to the *M. grisea* and *C. purpurea cla4* mutants that also displayed reduced radial growth (Li et al., 2004; Rolke and

Tudzynski, 2008). In contrast, the Δ*pakB* mutant grew at a normal rate, but had a reduction in aerial hyphae that made the colony appear flatter. This is similar to the *M. grisea* Δ*mst20* mutant, which also had reduced aerial hyphae formation (Li et al., 2004).

6.11.1. Paks are required for growth under cell wall-stressing conditions

Examination of the growth of the Δ*pakA* and Δ*pakB* mutants in the presence of the cell wall stress-inducing compounds, SDS and CFW, revealed that the Δ*pakA* mutant displayed increased sensitivity to both these compounds, whereas the Δ*pakB* mutant was only slightly more sensitive to CFW than the wild-type strain, and no more sensitive to SDS. These compounds induce cell wall stress by different modes of action, with CFW directly interfering with assembly of chitin microfibrils in the cell wall, and SDS acting indirectly by perturbing the cell membrane (Ram et al., 2004). While the sensitivity of pak mutants from other filamentous fungi to SDS and CDW has not been examined, the *Candida glabrata* Δ*ste20* mutant was found to display increased sensitivity to both SDS and CFW (Calcagno et al., 2004). The increased sensitivity to SDS and CFW displayed by the *E. festucae* Δ*pakA* mutant suggests this mutant has reduced cell wall integrity. The slightly increased sensitivity of the Δ*pakB* mutant to CFW suggests that this mutant also has mildly reduced cell wall integrity.

6.12. The *E. festucae pak* mutants display altered morphology in culture

6.12.1. The pak mutants display altered branching in culture

Examination of the pak mutants using DIC microscopy revealed major changes in the branching of these mutants in comparison to the wild-type strain. Hyphae of the Δ*pakA* mutant appeared hyper-branched, with frequent tip bifurcations, and were often convoluted, indicative of a loss of cell polarity. This morphology was very similar to that seen for the *E. festucae* Δ*racA* mutant (Tanaka et al., 2008a), suggesting PakA is acting in

the same pathway as RacA. The Δ*pakB* mutant also displayed a loss of cell polarity, with hyphae frequently bifurcated at the tip, branches forming in the middle of cell compartments rather than close to the tip-proximal septa, and branches growing back in towards the body of the colony. Δ*pakB* mutant hyphae also frequently contained swellings, generally located just back from the hyphal tip, and often appeared bent or kinked. In *S. cerevisiae*, both Cla4 and Ste20 play important roles in maintenance of cell polarity through regulation of the polarisome (Goehring et al., 2003). In *C. purpurea* and *U. maydis*, Cla4 homologues were also found to play important roles in maintenance of cell polarity (Leveleki et al., 2004; Rolke and Tudzynski, 2008). In contrast, the *M. grisea cla4* homologue *CHM1* was found to be dispensable for polarised growth, indicating that not all filamentous fungi rely on Cla4 for maintenance of polarity (Li et al., 2004). Interestingly, whilst the *Penicillium marneffei* Ste20 homologue was found to play a role in maintenance of cell polarity, Ste20 homologues from *M. grisea* and *U. maydis* appeared dispensable for polarised growth (Li et al., 2004; Smith et al., 2004; Boyce and Andrianopoulos, 2007).

The altered cell polarity seen in the Δ*pakA* mutant may be due to the elevated ROS levels in this mutant, as ROS have been shown to play an important role in regulating hyphal apical dominance (Semighini and Harris, 2008). However, the fact that the elevated ROS is still highly localised to the hyphal tip in this mutant, combined with the fact that the Δ*pakA* phenotype is very similar to that of the Δ*racA*, which has lower ROS levels than wild-type (Tanaka et al., 2008a), suggests this is unlikely to be the case.

Interestingly, the presence of the spherical/elliptical structures seen at the tips of wild-type *E. festucae* hyphae under conditions of nutrient stress (discussed in Section 6.4) appears altered in the pak mutants. These structures were never observed in the Δ*pakA* mutant, suggesting the pathway leading to their production is blocked in this mutant. In contrast, the Δ*pakB* mutant was found to overproduce these structures, with nearly every hypha having one of these structures under nutrient stressed conditions. These results suggest that PakA is necessary for formation of these structures, whereas PakB represses their formation.

6.12.2. The Δ*pakA* mutant displays altered cell dimensions

Examination of the cell size of the *E. festucae* pak mutants using CFW to stain the septa revealed that the Δ*pakA* mutant cells are significantly shorter and wider than those of wild-type *E. festucae*. This is consistent with what is seen for the *cla4* mutants from *C. purpurea* and *M. grisea* (Li et al., 2004; Rolke and Tudzynski, 2008). This change in cell dimensions is likely due to disorganisation of the cytoskeleton. In *S. cerevisiae*, both Cla4 and Ste20 have been shown to be involved in organisation of the actin cytoskeleton and polarised growth (Cvrcková et al., 1995; Eby et al., 1998). When stained with CFW, it was also observed that the Δ*pakA* mutant had extended CFW staining further back from the hyphal tip than is seen in the wild-type strain. CFW is known to bind to both chitin and β-linked glucans in the cell wall (Maeda and Ishida, 1967). Thus, the increased staining seen in the Δ*pakA* mutant suggests there is altered chitin or β-linked glucan composition in the cell wall.

6.12.3. The Δ*pakA* mutant contains large vacuoles in culture

Unlike the Δ*sakA* mutant (discussed in Section 6.7.7), the Δ*pakA* mutant contained large vacuoles in culture. Vacuoles are highly dynamic organelles that constantly undergo fusion and fission (Peters et al., 2004). Therefore, there are a number of possible explanations for the increased in vacuole size seen in the Δ*pakA* mutant. Firstly, the Δ*pakA* mutant may have an increase in vacuole fusion. Secondly, the Δ*pakA* mutant may be defective in vacuole fission. And thirdly, the increased vacuole size seen in the Δ*pakA* mutant may simply be a consequence of the hyphae being wider, as wider hyphae generally contain larger vacuoles (Shoji et al., 2006). Examination of vacuolation has not been reported for most of the filamentous fungal pak mutants analysed to date, although in the *C. purpurea* Δ*cla4* mutant vacuolation was found to be normal (Rolke and Tudzynski, 2008). Interestingly, in *S. cerevisiae* both Cla4 and Ste20 have been shown to be involved in regulating vacuole inheritance (Bartholomew and Hardy, 2009).

6.13. Loss of *pakA* induces increased ROS levels in culture

Examination of in culture hydrogen peroxide and superoxide levels in the pak mutants revealed that both these species are elevated in the Δ*pakA* mutant. This was unexpected given our hypothesis that a pak is involved in activation of the Nox complex, possibly by triggering release of the small GTPase RacA from RhoGDI. It would be expected that disruption of the pak would lead to less activated RacA and consequently reduced ROS production by the Nox complex. However, this increased ROS should perhaps not be so surprising in light of recent research findings. For example, the *M. grisea* Δ*nox1*Δ*nox2* mutant was found to display increased superoxide levels compared to the wild-type strain, and it was suggested that this was due to up-regulation of an alternative ROS source (Egan et al., 2007). Similar to this, secretion of superoxide and peroxide was found to be elevated in the *P. anserina* Δ*PaNox2* and Δ*PaNox1*Δ*PaNox2* mutants, leading the authors to also suggest there is up-regulation of an alternative source of ROS (Malagnac et al., 2004). Thus, it is possible that the increased ROS seen in the Δ*pakA* mutant is due to up-regulation of an alternative source of ROS, similar to that seen in *M. grisea* and *P. anserina*. Possible alternative sources of ROS were discussed in Section 6.7.3. An alternative hypothesis is that the increase in ROS seen in the Δ*pakA* mutant is due to PakA acting as a repressor of an alternative source of ROS. It is also conceivable that *E. festucae* PakA may act in an opposite fashion to that seen for mammalian Pak1 (DerMardirossian et al., 2004; Martyn et al., 2005), such that rather than activating the fungal Nox complex it represses it. If this were the case, loss of *pakA* would lead to the observed increase in ROS levels. This is possible, given that the *A. nidulans* and *E. festucae* stress-activated MAP kinases (SakA) are predicted to repress the fungal Nox complex (Lara-Ortíz et al., 2003; Eaton et al., 2008), whereas in mammalian systems the homologous p38 MAPK activates the Nox complex (Dang et al., 2003; Brown et al., 2004; Yoo et al., 2008).

It is important to note, that compared to the Δ*sakA* mutant in which ROS levels were elevated and delocalised throughout the colony, the increased ROS seen in the Δ*pakA* mutant were still highly localised to the hyphal tip. This suggests that *sakA* and *pakA* may regulate the Nox complex differently, with *sakA* being required for localisation of ROS

production to the hyphal tip, and *pakA* required for regulating the level of ROS production at the tip. It would be interesting to examine whether ROS levels are also elevated around Δ*pakA* mutant hyphae growing *in planta*. However, due to the very low survival rate of plants inoculated with the Δ*pakA* mutant, and the severe stunting of these plants it would be very difficult to obtain enough plant tissue for this analysis to be performed.

6.14. *pakA* is likely required for symbiotic maintenance

When the pak mutants were inoculated into perennial ryegrass seedlings it was found that the Δ*pakA* mutant drastically decreased the survival rate of the seedlings, with only 40% of seedlings inoculated with the Δ*pakA* mutant surviving to 51 days post planting in comparison to around 80% for the wild-type and Δ*pakB* mutant strains. Plants that were infected with the Δ*pakA* mutant were severely stunted, seldom grew larger than two tillers, and died within eight weeks. It is important to note, however, that these plants likely showed the mildest symptoms of Δ*pakA* infection as all other plants infected with the Δ*pakA* mutant died even earlier, before they were large enough to be screened for infection. The host stunting and premature senescence induced by the Δ*pakA* mutant is the most severe seen for any of the *E. festucae* symbiotic mutants isolated to date (Takemoto et al., 2006; Tanaka et al., 2006; Tanaka et al., 2008a).

The severe host stunting and premature senescence induced by the Δ*pakA* mutant is likely due to extensive colonisation of the host vascular bundles by this mutant. As mentioned earlier, wild-type *E. festucae* seldom colonises the host vascular bundles (Christensen et al., 2002). However, in Δ*pakA* associations, hyphae densely pack the host vascular bundles such that the bundles swell to almost twice their normal size and the host cells appear distorted. It is likely that this extensive colonisation hampers the transport of water and nutrients by the host. This may also account for why seedlings inoculated with the Δ*pakA* mutant survive longer in the greenhouse during periods of cool weather, as the plants would be less stressed.

In contrast to the reduced radial growth displayed by the Δ*pakA* mutant in culture, growth of this mutant *in planta* is deregulated with a substantial increase in fungal biomass. Similar to its growth in culture, hyphae of the Δ*pakA* mutant appear hyper-branched, with frequent tip bifurcations and the formation of hyphal networks. Extensive vacuolation of these mutant hyphae could also be seen both by light microscopy of aniline blue stained tissue and confocal microscopy of the Δ*pakA* mutant constitutively expressing EGFP. This deregulated growth *in planta* is very similar to that seen for the *E. festucae* Nox mutants (Takemoto et al., 2006; Tanaka et al., 2006; Tanaka et al., 2008a), supporting a role for *pakA* in regulation of the Nox complex. Despite not inducing senescence of the host, the Δ*pakB* mutant also displayed mildly deregulated growth *in planta*. In Δ*pakB* mutant associations there was an apparent increase in fungal biomass and the hyphae appeared more branched, with frequent tip bifurcations. However, growth of the Δ*pakB* mutant *in planta* was still much more regulated than that of the Δ*pakA* mutant. This suggests that *pakB* plays only a minor role in regulating fungal growth *in planta* compared to *pakA*, which is likely required for maintenance of the association with perennial ryegrass.

Examination of hyphal morphology *in planta* using transmission electron microscopy (TEM) revealed dramatic changes in morphology of the Δ*pakA* mutant compared to the wild-type strain. Similar to the Δ*sakA* mutant (discussed in Section 6.8.7), the Δ*pakA* mutant hyphae were very irregular in size and shape compared to the relatively uniform hyphae of the wild-type strain. As discussed above, the Δ*pakA* hyphae also contained very large vacuoles, a feature seldom seen in wild-type associations. This should perhaps be expected though, as this mutant contains large vacuoles in culture. However, it is important to note that the *E. festucae* Nox mutants also contain large vacuoles *in planta* (Takemoto et al., 2006; Tanaka et al., 2006; Tanaka et al., 2008a). Similar to the Δ*sakA* mutant (Section 6.8.8), the Δ*pakA* mutant hyphae were also often surrounded by an electron dense extra-cellular matrix not seen in wild-type associations. Possible causes for this are discussed in Section 6.8.8. The increased biomass seen in Δ*pakA* mutant associations was also very apparent from the TEM as individual intercellular spaces contained so many hyphae that the host cells became distorted and the intercellular spaces merged into one another, linked by networks of fungal hyphae. This is dramatically different from the one or two hyphae generally seen in a given intercellular

space in wild-type associations. Although growth of the Δ*pakB* mutant *in planta* was deregulated compared to that of the wild-type strain, the Δ*pakB* mutant hyphae displayed wild-type morphology.

6.15. Inability of *pakA* and *pakB* to complement the altered symbioses

Perhaps the most surprising result of this study was the inability of the defective plant interaction phenotypes of the Δ*pakA* and Δ*pakB* mutants to be complemented by transformation of these mutants with pCE43 and pCE42 respectively. Strains A13, the Δ*pakA* mutant containing pCE43, and B3, the Δ*pakB* mutant containing pCE42, displayed wild-type growth and morphology in culture. However, when inoculated into perennial ryegrass the resulting *in planta* phenotypes appeared possibly even more severe than those of the Δ*pakA* and Δ*pakB* mutants, suggesting that reinsertion of these genes into the mutants may exacerbate the mutant phenotype. However, given this analysis has only been performed once this needs to be repeated to confirm this result.

The possibility that the inability of pCE43 and pCE42 to rescue the host phenotypes of the Δ*pakA* and Δ*pakB* mutants was due to insufficient promoter sequence in the complementation constructs was considered. However, this is unlikely as the *pakA* complementation fragment contained 1.2 kb of sequence upstream of the start codon and the *pakB* complementation fragment contained the entire 3.8 kb intergenic sequence between *pakB* and the gene upstream. In addition, the ability of these fragments to restore wild-type growth in culture suggests this is unlikely. It is possible, however, that there may be plant-specific regulatory elements located outside the regions used in the complementation constructs. If the *pakA* or *pakB* gene needs to be close to these elements to be expressed correctly *in planta* this may explain why these fragments are unable to rescue the pak mutants, as they will be improperly expressed. The *E. festucae* lolitrem genes, for example, are known to be plant regulated as they are much more highly expressed *in planta* than in culture (Young et al., 2006). It will therefore be interesting to examine whether expression of the pak genes is altered *in planta* in comparison with expression in culture.

Another possible explanation for the lack of rescue of the host phenotype in A13 and B3 is position effects. Only single Δ*pakA* and Δ*pakB* strains containing pCE43 and pCE42 respectively were used in these analyses. Depending on where in the genome these complementation fragments inserted, they may be more highly or more lowly expressed than in wild-type. This may not be so important for regulation of growth in culture, given that A13 and B3 appear normal in culture, but may be important for growth *in planta*. In addition, the location of the *pakA* and *pakB* genes at ectopic loci may have altered their spatial and temporal regulation, which may be important for regulation of growth *in planta*. To overcome the problem of position effects, the *in planta* complementation analysis will be repeated with multiple independent Δ*pakA* and Δ*pakB* mutant strains containing pCE43 and pCE42 respectively. Each independent strain will contain the *pakA* or *pakB* gene at a different ectopic locus. If all these strains still display abnormal association with perennial ryegrass, this will rule out the possibility of position effects causing this problem.

Another possibility that needs to be considered is that the *pakA* complementation construct pCE43 may contain polymerase-induced sequence errors. This fragment was prepared by PCR using a proof-reading enzyme and with reduced cycle number (25) to minimise the possibility of polymerase induced errors. The PCR product was then cloned into pCR4-TOPO and DNA from twelve independent clones pooled. It is likely that any polymerase errors would not be in all of the PCR products so by pooling DNA from multiple clones, each is likely to have a different set of errors, if any. Given the obvious phenotype of the Δ*pakA* mutant in culture it was relatively easy to screen for transformants that had wild-type growth. Given strain A13 displayed wild-type growth in culture it was assumed that it was error free. However, it is possible that there may be an error in a region required only for regulating the association with perennial ryegrass but not for growth in culture. Although, the fact that the *pakB* complementation construct, pCE42, which was prepared by restriction digests, also does not complement the Δ*pakB in planta* phenotype suggests there are likely other factors involved for the Δ*pakA* complementation also. Before further *in planta* complementation analysis is performed it will be important to confirm that pCE43 is free of polymerase-induced errors.

The unexpected results obtained for strains A13 and B3 are not the only cases of problematic complementation in *E. festucae*. For example, complementation of the *E. festucae* Δ*proA* mutant has proven difficult, with the complemented strain displaying a similar *in planta* phenotype to the Δ*proA* mutant (A. Tanaka and S. Saikia, unpublished). Complementation also does not always fully restore the wild-type phenotype. For example, complementation of the *E. festucae* Δ*lpsB* mutant restored ergovaline production but only to very low levels in comparison to the wild-type strain (Fleetwood et al., 2007).

6.16. The pak loci display conserved synteny and gene rearrangement

The results of this study have revealed a rearrangement of gene order at the *pakA* locus in the lineage leading to *F. graminearum* and *E. festucae*. In the *N. crassa* and *M. grisea* lineage the *pakA* homologue displays conserved micro-synteny with five other genes. In *F. graminearum* and *E. festucae* this synteny has been split, with three genes relocated to a different chromosome, but with retention of the gene order and orientation. Interestingly, the *pakA* homologue and the two genes that remained linked to it in *F. graminearum* and *E. festucae* appear to have been under stronger selection pressure than the other three genes, as evidenced by their much higher E-values when compared using BLASTp. The function of the two genes adjacent to *pakA* may also explain their highly conserved nature as one is predicted to encode an RNA-binding protein and the other is predicted to encode a tRNA synthetase.

In contrast to the rearrangement seen at the *pakA* locus, the *pakB* locus displays considerable conservation of micro-synteny. Comparison of the *pakB* locus from *E. festucae* and *F. graminearum* identified thirteen genes that likely show conserved synteny between these species. The term likely is used as in *E. festucae* strain 2368, these genes are found on three separate contigs. However, in the Fl1 strain, two of these contigs are linked by the *perA* gene, which is inactive in strain 2368 and flanked by a transposon relic. These transposon relics make linkage of contigs difficult due to their repetitive nature. It is likely that the third contig found in *E. festucae* is also linked to *pakB* as the gene order and orientation is the same as is seen in *F. graminearum* and the ends of this

contig also appear to contain transposon relics. Six of the genes found at the *pakB* locus in *F. graminearum* remain linked in *N. crassa* and another five of these genes remain linked to each other but have relocated elsewhere in the genome. The *pakB* locus has undergone considerable rearrangement in *M. grisea*, with only two genes remaining linked to the *pakB* homologue. However, the same five genes that are linked in *N. crassa* remain linked in *M. grisea*, suggesting the rearrangement of these genes from the *pakB* locus occurred in the lineage leading to *N. crassa* and *M. grisea*. Interestingly, *N. crassa* and *M. grisea* contain no homologue of the *E. festucae* gene A.7.2646. This gene encodes a conserved hypothetical protein and is also found in *F. graminearum* (FGSG_09496). However, the E-value obtained by BLASTp suggests low conservation between the *E. festucae* and *F. graminearum* homologues. It is possible that this gene may be mis-annotated and either be a pseudogene or not actually exist, given it is not predicted in the well-annotated *N. crassa* and *M. grisea* genomes.

6.17. Features of the *E. festucae* MAP kinase pathways

This study has resulted in identification of the key components of the three MAP kinase pathways from *E. festucae*. When these three MAP kinase pathways are compared in terms of amino acid conservation of the various components, a number of key features are identified. Firstly, all three MAP kinases display the highest level of amino acid identity of any of the components examined. This suggests the MAP kinase genes are under strong selection pressure to remain unchanged. This should perhaps be expected, as it is the MAP kinase that translates the activating signal, which has been transmitted through the MAP kinase pathway, into changes in gene expression via targeting of specific transcription factors (Banuett, 1998). In comparison, the phosphatases involved in dampening of the MAP kinase signalling, display the lowest amino acid identity of the various components examined, suggesting they are under less stringent selection pressure.

Another key feature is that many of the *E. festucae* pheromone response and cell integrity pathway components display greater amino acid identity to the more distantly related plant symbiont *M. grisea* than the closely related saprobe *N. crassa*. Whether this is due to

a role for these proteins in symbiosis is not clear. However, it is interesting that in *M. grisea*, both the pheromone response and cell wall integrity pathways are required for processes involved in host infection and colonisation (Dean et al., 2005), whereas the stress-activated pathway is not involved in symbiosis.

6.18. Conclusions

To understand how plants and fungi communicate with each other during symbiosis has long been the subject of intense research. This study adds to the body of research in this area by demonstrating a role for the stress-activated MAP kinase, *sakA*, and p21-activated kinase, *pakA*, in maintenance of the mutually beneficial association between *E. festucae* and perennial ryegrass. This study has also demonstrated a minor role for the p21-activated kinase, *pakB,* in regulation of fungal growth *in planta*. Preliminary evidence from analysis of ROS levels in Δ*sakA* and Δ*pakA* mutants suggests SakA and PakA may exert their symbiotic regulation via interaction with the fungal Nox complex. This study, therefore, paves the way for future molecular analysis of the mechanisms by which SakA and PakA regulate the association with perennial ryegrass, including potential interactions with the Nox complex.

Analysis of the effects that loss of *sakA* had on the association with perennial ryegrass also revealed an important role for *sakA* in the development of its host. Plants infected with the Δ*sakA* mutant displayed loss of anthocyanin pigmentation and disorganisation of host cells below the shoot apical meristem, resulting in a swollen appearance. Given that infection of perennial ryegrass with *E. festucae* is not required for normal development, this finding illustrates that disruption of an *E. festucae* gene can have dramatic effects on host processes not normally influenced by the endophyte.

This study has also aided in annotation of the recently released *E. festucae* genome via identification and sequence characterisation of major components of the three MAP kinase pathways encoded in the *E. festucae* genome. The observation that some genes, but not others, display conserved micro-synteny is an interesting question for future study.

The results of this study have provided insight into how communication between *E. festucae* and perennial ryegrass maintains this highly tuned association. It has also highlighted how finely balanced this communication is, with disruption of one gene being able to completely switch the association from mutualism to antagonism.

7. Appendices

7.1. Multiple sequence alignments

7.1.1. Alignment of pak sequences for primer design

Partial alignment of Cla4- and Ste20-type paks from *F. graminearum* (Fg), *Trichoderma reesei* (Tr), *Nectria haematococca* (Nh), *N. crassa* (Nc) and *M. grisea* (Chm1 and Mst20) showing the regions to which degenerate primers pak1a and pak1b were designed.

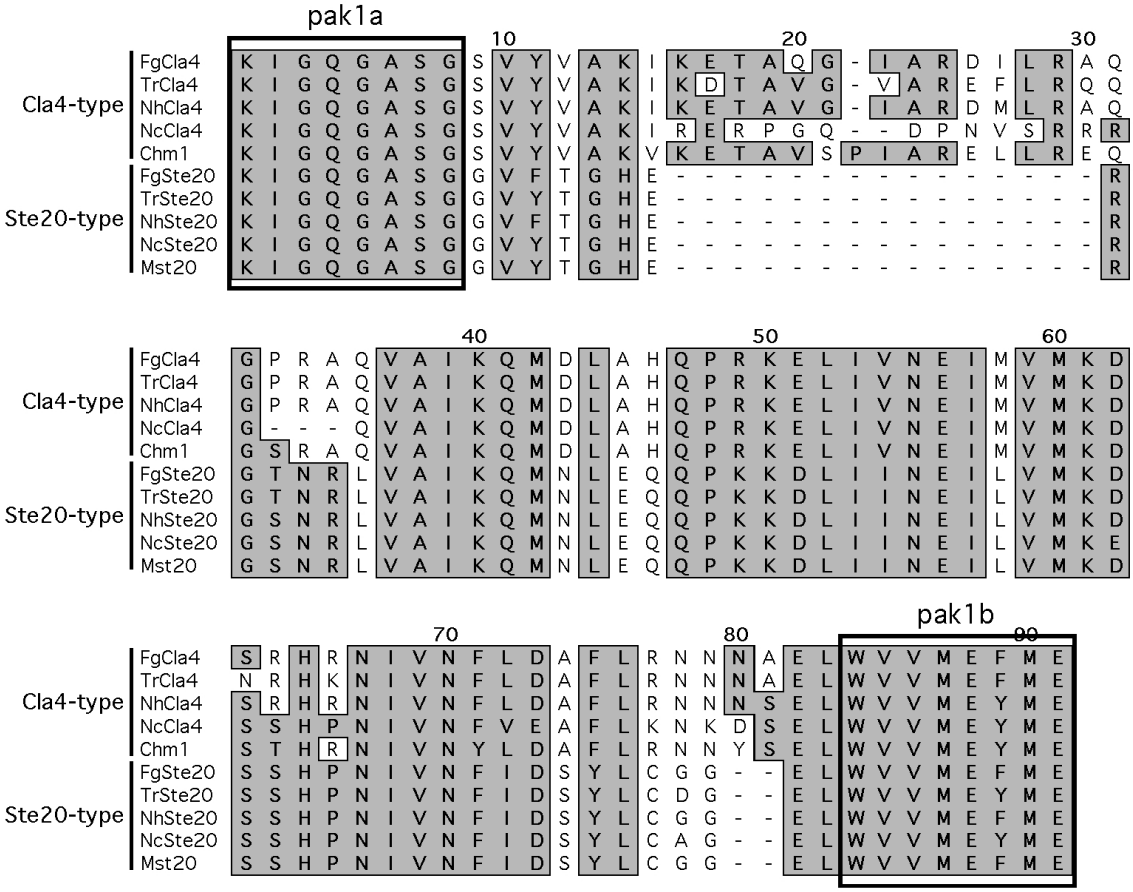

7.2. Vector and construct maps

Maps of vectors routinely used in this study and constructs prepared during this study are presented below.

7.2.1. pGEM®-T Easy (Promega)

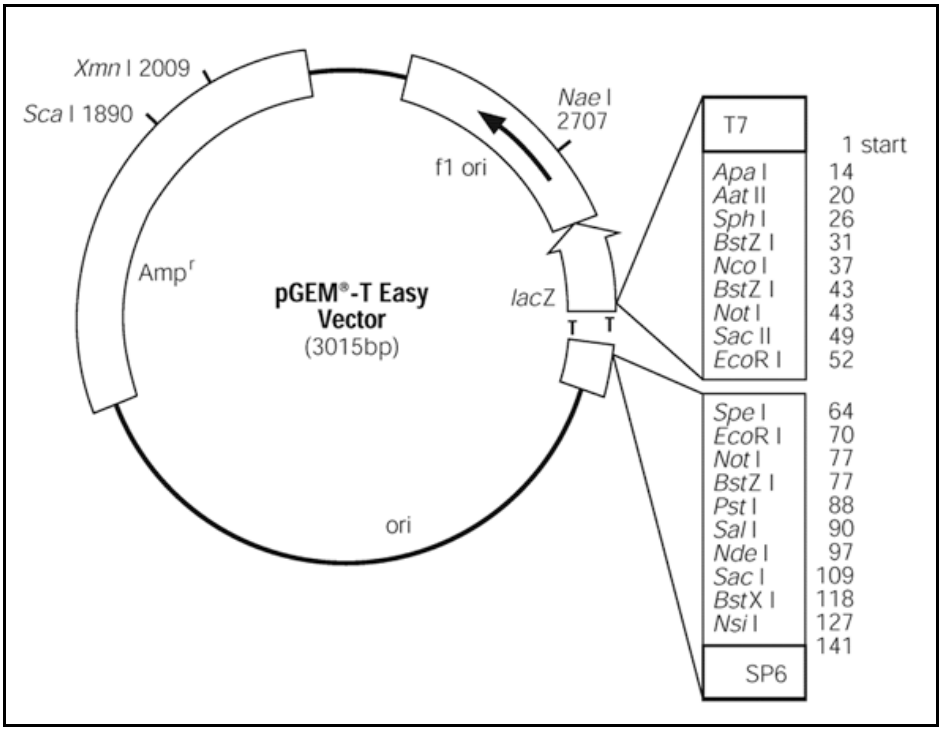

7.2.2. pUC118

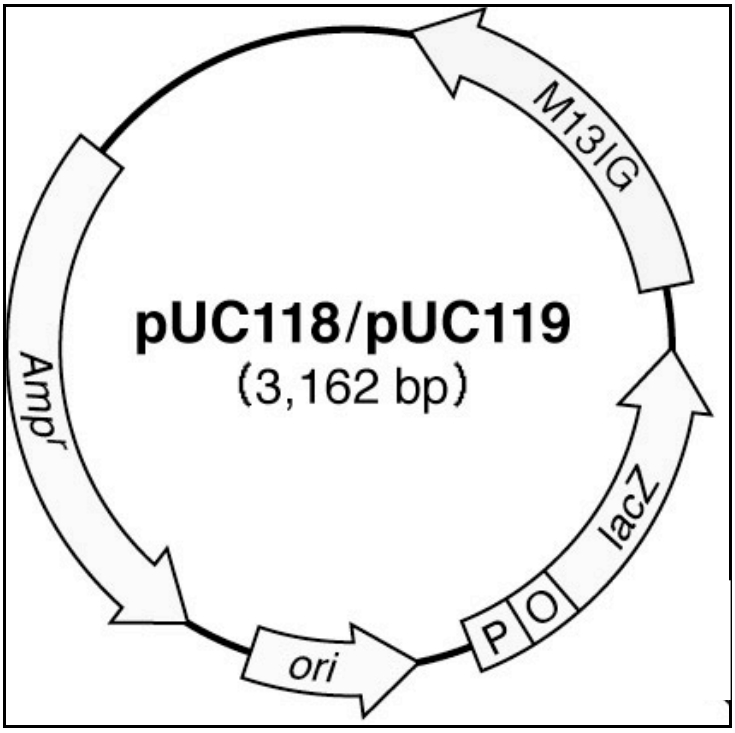

7.2.3. pPN83

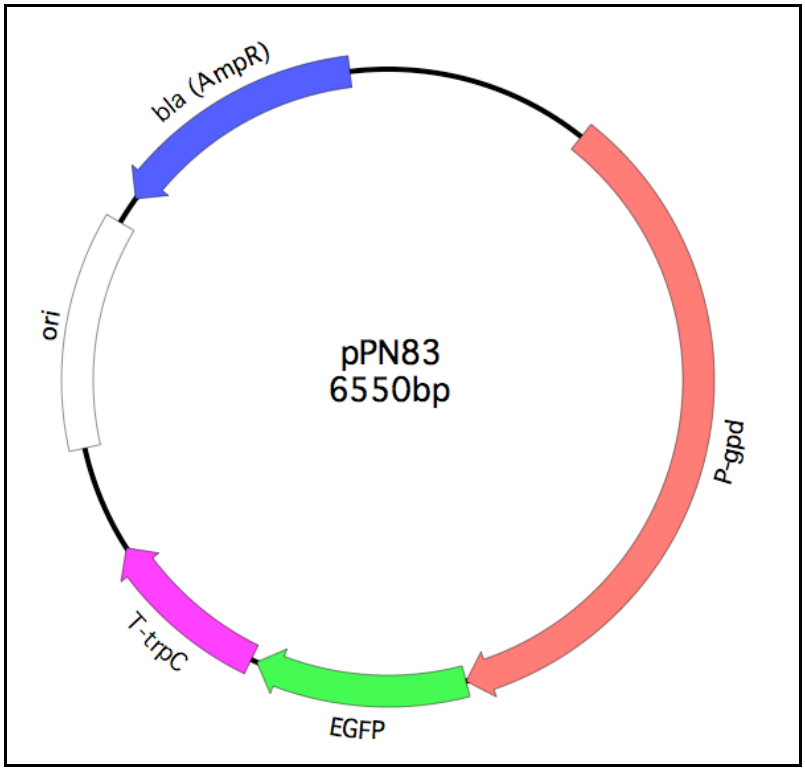

7.2.4. pII99

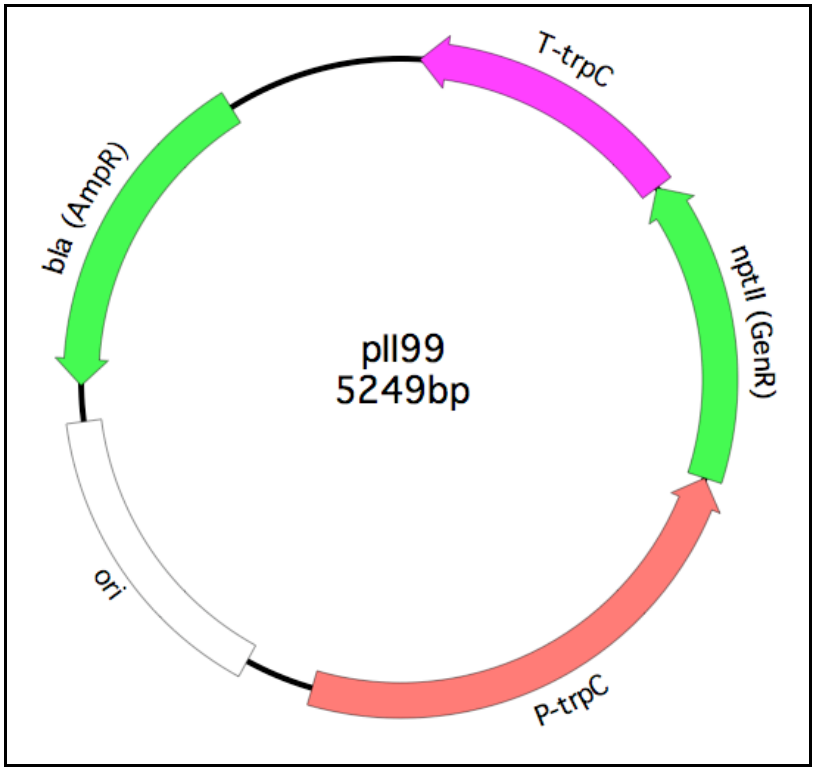

7.2.5. pCR4-TOPO

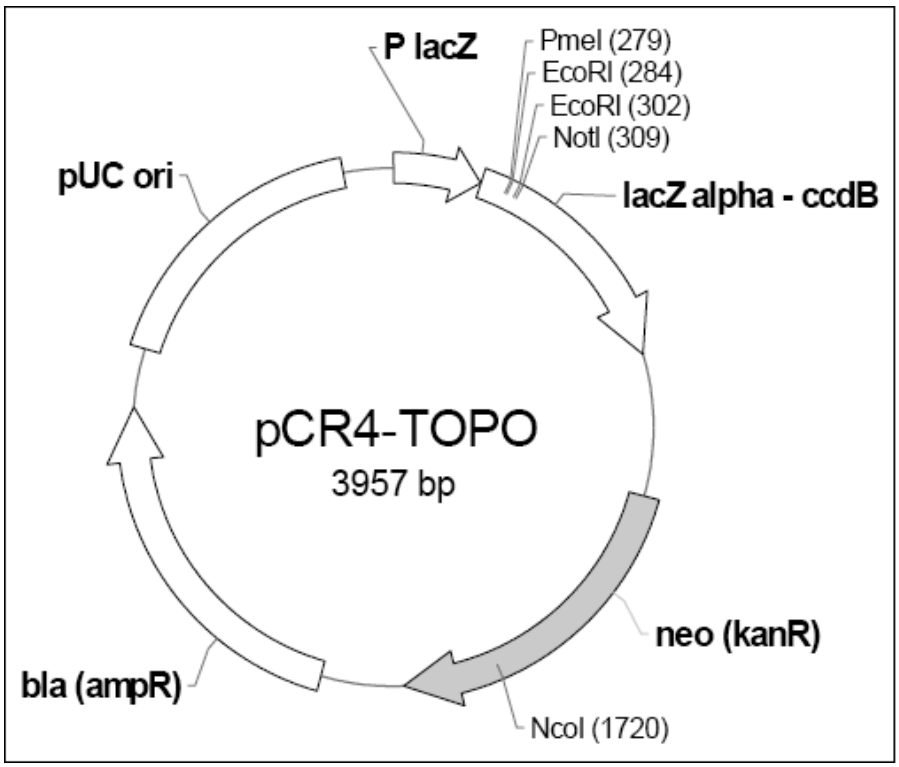

7.2.6. pCE1 (*sakA* complementation construct)

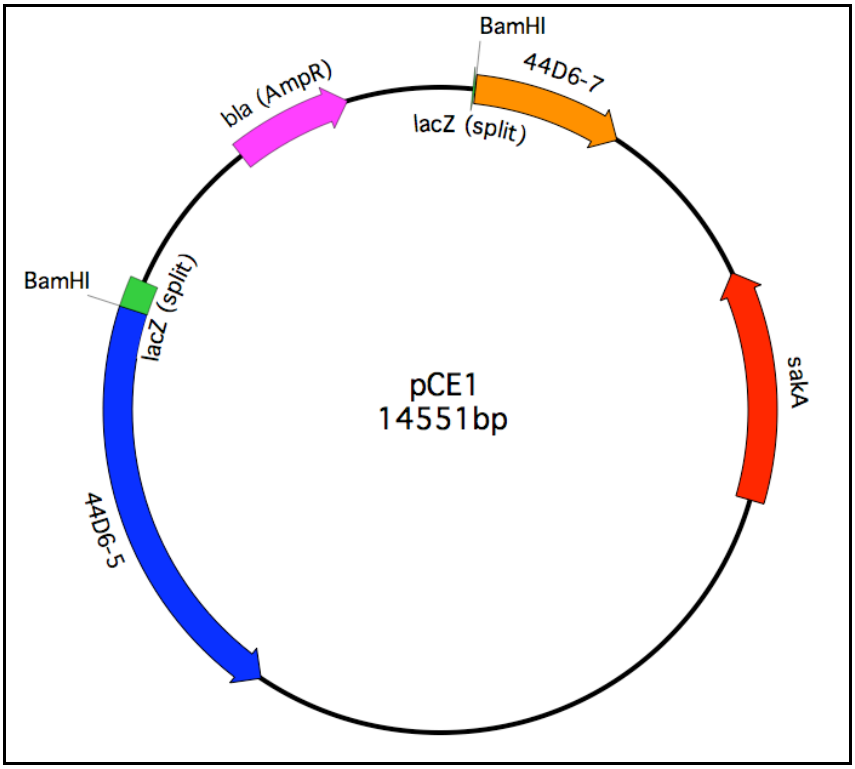

7.2.7. pCE12 (*sakA* replacement construct)

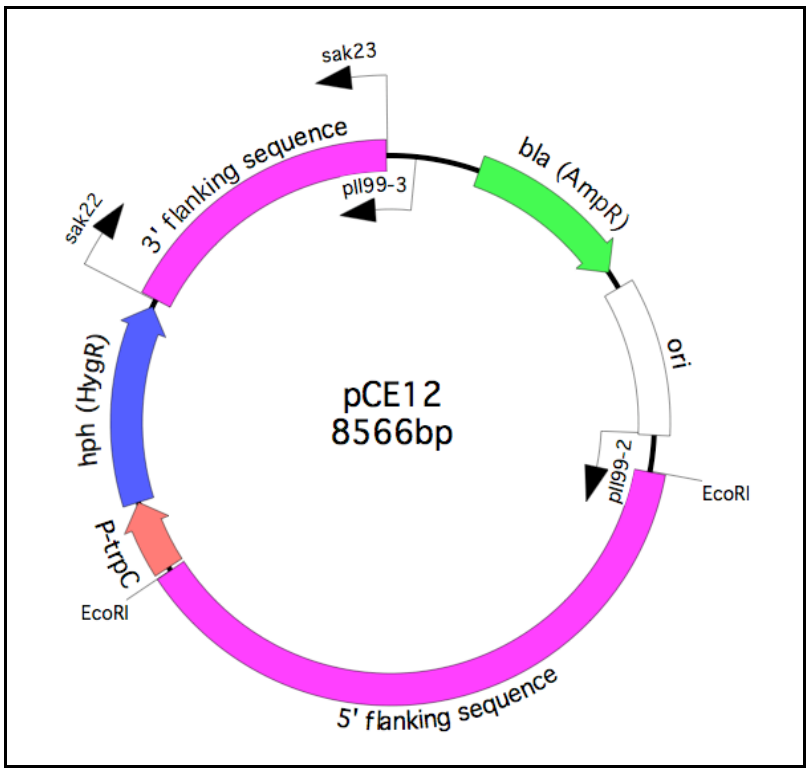

7.2.8. pCE22 (*S. pombe* gDNA complementation construct)

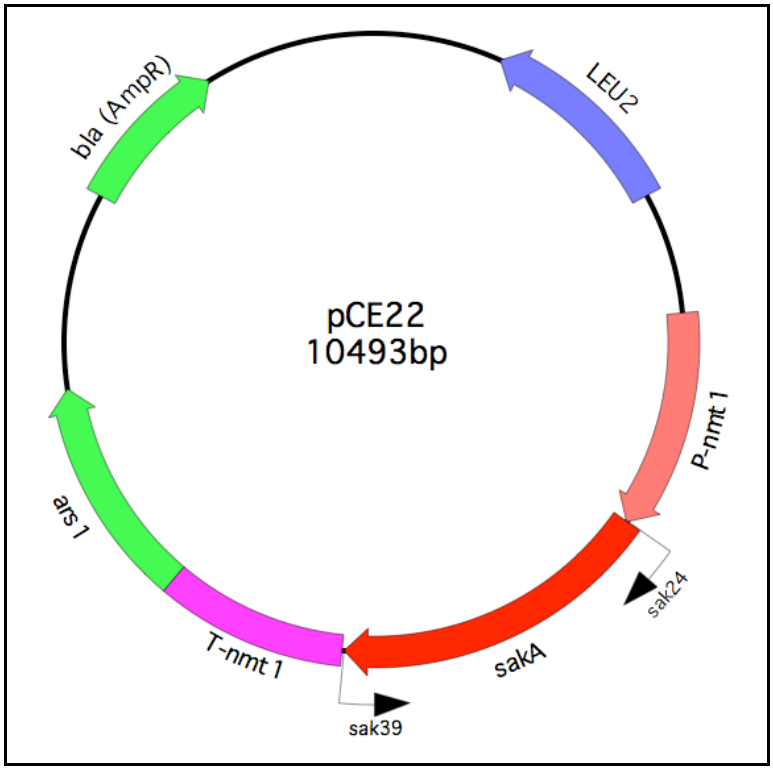

7.2.9. pCE23 (*S. pombe* cDNA complementation construct)

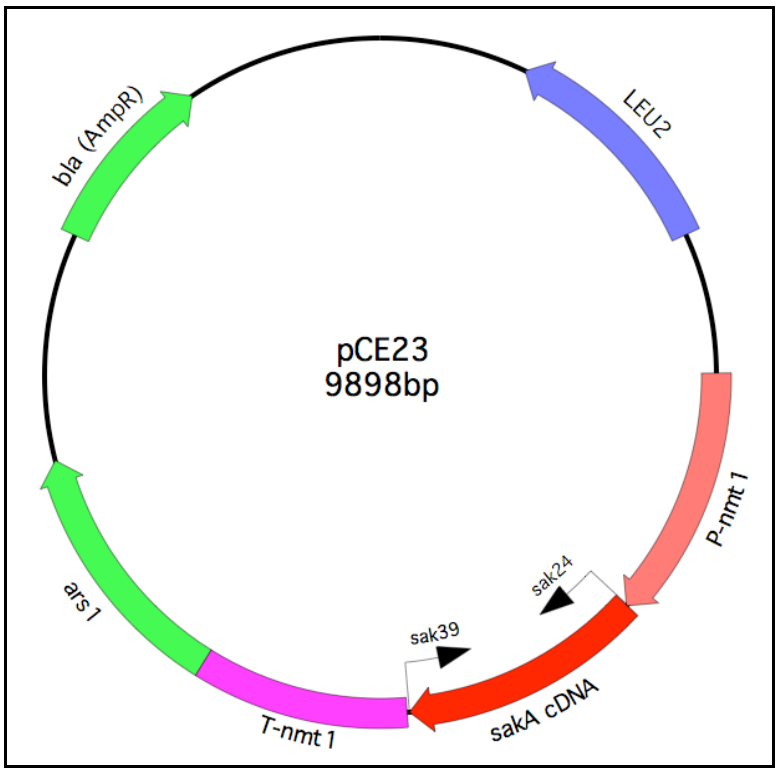

7.2.10. pCE36 (*pakA* replacement construct)

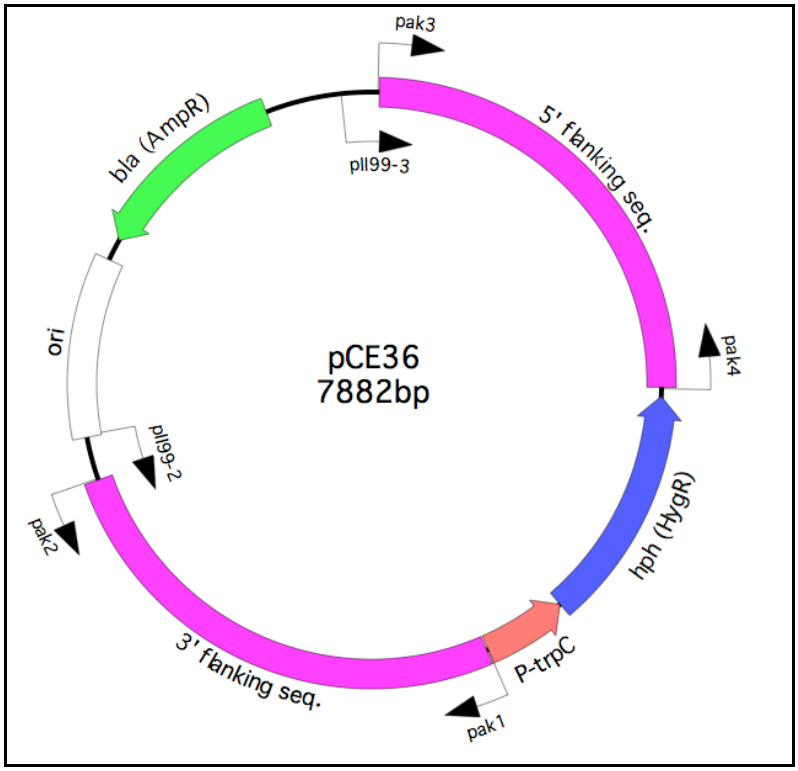

7.2.11. pCE38 (*pakB* replacement construct)

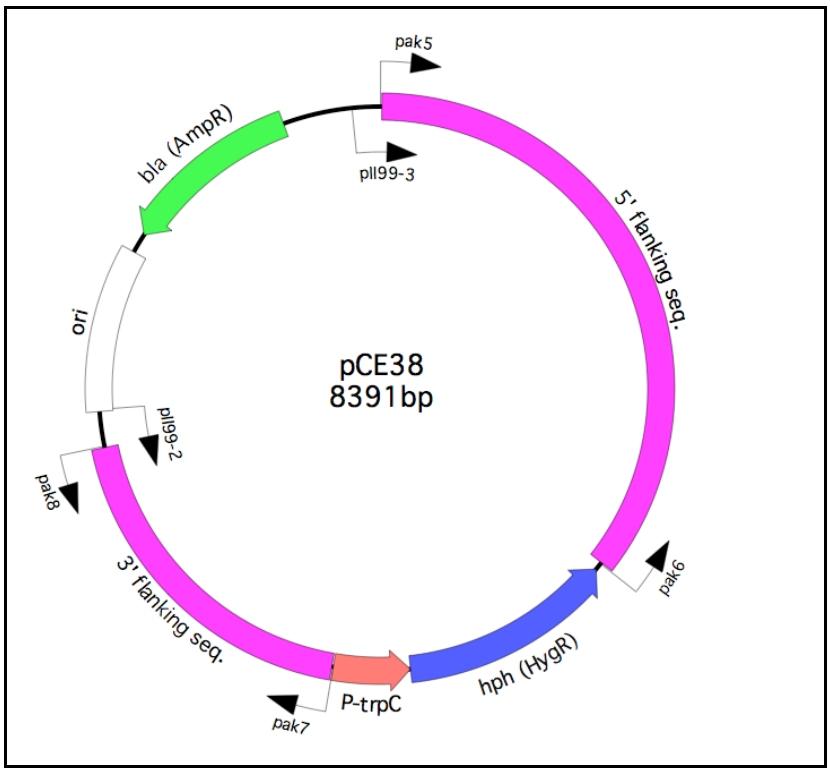

7.2.12. pCE42 (*pakB* complementation construct)

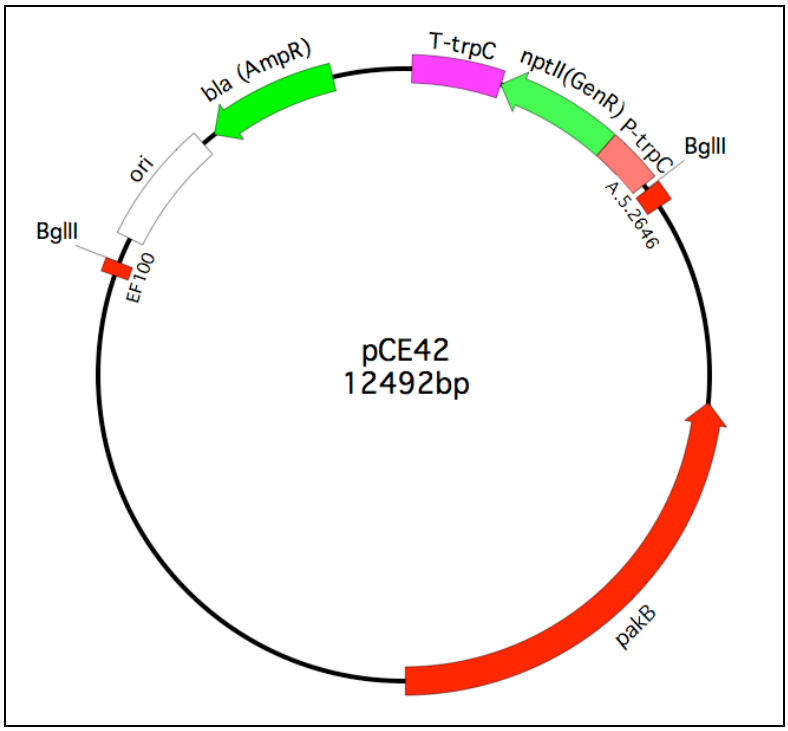

7.2.13. pCE43 (*pakA* complementation construct)

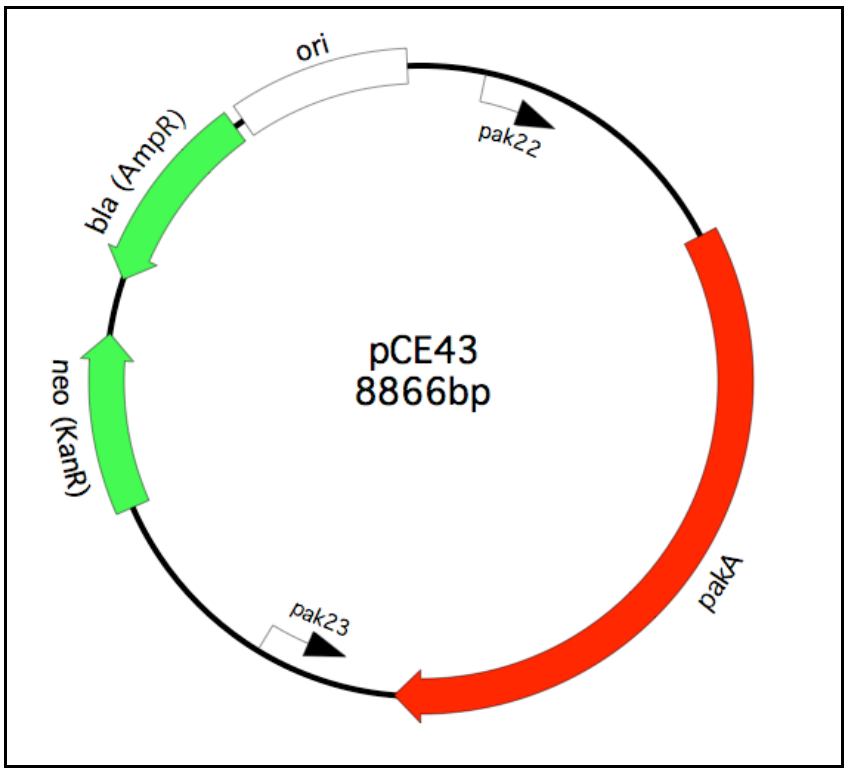

7.3. Sequence Data

Nucleotide and amino acid sequences for *E. festucae sakA*, *pakA* and *pakB*; and nucleotide sequences for *E. festucae sakA*, *pakA* and *pakB* loci used in synteny analysis are appended in FASTA and MacVector™ format on the CD attached to the back cover of this thesis.

7.4. Statistical Analysis

Results of the Student's *t*-test analyses are presented below. Statistical significance is deemed as a p-value < 0.05.

Reference	Comparison	Test	df	*t*-value	*p*-value
Fig. 3.15A	Δ*sakA* vs WT	one-tailed	1.01	4.47	0.070^{ns}
	WT vs comp	two-tailed	1.43	0.99	0.46^{ns}
	Δ*sakA* vs comp	one-tailed	1.02	-7.06	0.043*
Fig. 3.15B (blade)	Δ*sakA* vs WT	one-tailed	1.47	-17.44	0.0055**
	WT vs comp	two-tailed	1.91	-4.53	0.050*
	Δ*sakA* vs comp	one-tailed	1.31	-20.80	0.0065**
Fig. 3.15B (sheath)	Δ*sakA* vs WT	one-tailed	1.13	-29.35	0.0073**
	WT vs comp	two-tailed	1.97	-6.23	0.026*
	Δ*sakA* vs comp	one-tailed	1.10	-34.38	0.0067**
Fig. 3.15C	WT vs Δ*sakA*	one-tailed	1.01	-3.77	0.082^{ns}
	WT vs comp	two-tailed	1.27	-0.98	0.48^{ns}
	Comp vs Δ*sakA*	one-tailed	1.05	-3.57	0.082^{ns}
Fig. 3.20C	WT b1 vs Δ*sakA* b1	one-tailed	1.43	-3.74	0.053^{ns}
	WT b2 vs Δ*sakA* b2	one-tailed	1.36	-9.27	0.017*
	WT b3 vs Δ*sakA* b3	one-tailed	1.79	-2.01	0.098^{ns}
Fig. 4.10B	Δ*pakA* vs WT	one-tailed	1.81	-8.80	0.0085**
	WT vs A13	two-tailed	1.40	-0.17	0.89^{ns}
	Δ*pakA* vs A13	one-tailed	1.21	-4.85	0.049*
	Δ*pakB* vs WT	one-tailed	1.04	-2.98	0.099^{ns}
	WT vs B3	two-tailed	1.93	-0.19	0.87^{ns}
	Δ*pakB* vs B3	one-tailed	1.03	-2.71	0.11^{ns}
Fig. 4.10C	Δ*pakA* vs WT	one-tailed	1.50	-5.29	0.030*
	WT vs A13	two-tailed	1.25	-1.01	0.47^{ns}
	Δ*pakA* vs A13	one-tailed	1.07	-5.32	0.053^{ns}
	Δ*pakB* vs WT	one-tailed	1.09	2.03	0.86^{ns}
	WT vs B3	two-tailed	1.59	0	1.00^{ns}
	Δ*pakB* vs B3	one-tailed	1.28	-3.39	0.067^{ns}

df = degrees of freedom, * = *p*-value 0.05-0.01, ** = *p*-value 0.01-0.001, ns = non-significant.

Bibliography

Abo, A., Boyhan, A., West, I., Thrasher, A.J., and Segal, A.W. (1992). Reconstitution of neutrophil NADPH oxidase activity in the cell-free system by four components: p67-phox, p47-phox, p21rac1, and cytochrome b-245. J Biol Chem **267,** 16767-16770.

Abo, A., Pick, E., Hall, A., Totty, N., Teahan, C.G., and Segal, A.W. (1991). Activation of the NADPH oxidase involves the small GTP-binding protein p21rac1. Nature **353,** 668-670.

Alonso-Monge, R., Navarro-García, F., Román, E., Negredo, A.I., Eisman, B., Nombela, C., and Pla, J. (2003). The Hog1 mitogen-activated protein kinase is essential in the oxidative stress response and chlamydospore formation in *Candida albicans*. Eukaryot Cell **2,** 351-361.

Alonso-Monge, R., Navarro-García, F., Molero, G., Diez-Orejas, R., Gustin, M., Pla, J., Sánchez, M., and Nombela, C. (1999). Role of the mitogen-activated protein kinase Hog1p in morphogenesis and virulence of *Candida albicans*. J Bacteriol **181,** 3058-3068.

Altschul, S.F., Madden, T.L., Schaffer, A.A., Zhang, J., Zhang, Z., Miller, W., and Lipman, D.J. (1997). Gapped BLAST and PSI-BLAST: a new generation of protein database search programs. Nucleic Acids Res **25,** 3389-3402.

Arber, A. (1934). The Gramineae - a study of cereal, bamboo and grass. (Cambridge: Cambridge University Press).

Arechavaleta, M., Bacon, C.W., Hoveland, C.S., and Radcliffe, D.E. (1989). Effect of the tall fescue endophyte on plant response to environmental stress. Agron J **81**.

Ayad-Durieux, Y., Knechtle, P., Goff, S., Dietrich, F., and Philippsen, P. (2000). A PAK-like protein kinase is required for maturation of young hyphae and septation in the filamentous ascomycete *Ashbya gossypii*. J Cell Sci **113 Pt 24,** 4563-4575.

Bacon, C.W., and Hinton, D.M. (1991). Microcyclic conidiation cycles in *Epichloë typhina*. Mycologia **83,** 743-751.

Bacon, C.W., Lyons, P.C., Porter, J.K., and Robbins, J.D. (1986). Ergot toxicity from endophyte-infected grasses: a review. Agron J **78,** 106-116.

Bahn, Y.S., Kojima, K., Cox, G.M., and Heitman, J. (2005). Specialization of the HOG pathway and its impact on differentiation and virulence of *Cryptococcus neoformans*. Mol Biol Cell **16,** 2285-2300.

Banuett, F. (1998). Signalling in the yeasts: an informational cascade with links to the filamentous fungi. Microbiol Mol Biol Rev **62,** 249-274.

Bao, F., Shen, J., Brady, S.R., Muday, G.K., Asami, T., and Yang, Z. (2004). Brassinosteroids interact with auxin to promote lateral root development in Arabidopsis. Plant Physiol **134,** 1624-1631.

Bartholomew, C.R., and Hardy, C.F. (2009). p21-activated kinases Cla4 and Ste20 regulate vacuole inheritance in *Saccharomyces cerevisiae*. Eukaryot Cell **8,** 560-572.

Basi, G., Schmid, E., and Maundrell, K. (1993). TATA box mutations in the *Schizosaccharomyces pombe nmt1* promoter affect transcription efficiency but not the transcription start point or thiamine repressibility. Gene **123,** 131-136.

Bedard, K., and Krause, K.H. (2007). The NOX family of ROS-generating NADPH oxidases: physiology and pathophysiology. Physiol Rev **87,** 245-313.

Besseau, S., Hoffmann, L., Geoffroy, P., Lapierre, C., Pollet, B., and Legrand, M. (2007). Flavonoid accumulation in *Arabidopsis* repressed in lignin synthesis affects auxin transport and plant growth. Plant Cell **19,** 148-162.

Bestwick, C.S., Brown, I.R., Bennett, M.H., and Mansfield, J.W. (1997). Localization of hydrogen peroxide accumulation during the hypersensitive reaction of lettuce cells to Pseudomonas syringae pv phaseolicola. Plant Cell **9,** 209-221.

Blackman, E. (1971). Morphology and development of cross veins in leaves of bread wheat (*Triticum aestivum* L.). Ann Bot **35,** 653-665.

Bokoch, G.M. (2003). Biology of the p21-activated kinases. Annu Rev Biochem **72,** 743-781.

Bolwell, P.P., Page, A., Pislewska, M., and Wojtaszek, P. (2001). Pathogenic infection and the oxidative defences in plant apoplast. Protoplasma **217,** 20-32.

Bowman, J.L., and Floyd, S.K. (2008). Patterning and polarity in seed plant shoots. Annu Rev Plant Biol **59,** 67-88.

Boyce, K.J., and Andrianopoulos, A. (2007). A p21-activated kinase is required for conidial germination in *Penicillium marneffei*. PLoS Pathog **3,** 1556-1569.

Bradford, M.M. (1976). A rapid and sensitive method for the quantitation of microgram quantities of protein utilizing the principle of protein-dye binding. Anal Biochem **72,** 248-254.

Brewster, J.L., de Valoir, T., Dwyer, N.D., Winter, E., and Gustin, M.C. (1993). An osmosensing signal transduction pathway in yeast. Science **259,** 1760-1763.

Briggs, R.T., Drath, D.B., Karnovsky, M.L., and Karnovsky, M.J. (1975). Localization of NADH oxidase on the surface of human polymorphonuclear leukocytes by a new cytochemical method. J Cell Biol **67,** 566-586.

Brown, G.E., Stewart, M.Q., Bissonnette, S.A., Elia, A.E., Wilker, E., and Yaffe, M.B. (2004). Distinct ligand-dependent roles for p38 MAPK in priming and activation of the neutrophil NADPH oxidase. J Biol Chem **279,** 27059-27068.

Bullock, W., Fernandez, J., and Short, J. (1987). XL1-Blue: a high efficiency plasmid transforming *recA Escherichia coli* strain with beta-galactosidase selection. BioTechniques **5,** 376-378.

Bultman, T.L., White, J.F., Bowdish, T.I., Welch, A.M., and Johnston, J. (1995). Mutualistic transfer of *Epichloe* spermatia by Phorbia flies. Mycologia **87,** 182-189.

Burbelo, P.D., Drechsel, D., and Hall, A. (1995). A conserved binding motif defines numerous candidate target proteins for both Cdc42 and Rac GTPases. J Biol Chem **270,** 29071-29074.

Butty, A.C., Perrinjaquet, N., Petit, A., Jaquenoud, M., Segall, J.E., Hofmann, K., Zwahlen, C., and Peter, M. (2002). A positive feedback loop stabilizes the guanine-nucleotide exchange factor Cdc24 at sites of polarization. EMBO J **21,** 1565-1576.

Byrd, A.D., Schardl, C.L., Songlin, P.J., Mogen, K.L., and Siegel, M.R. (1990). The beta-tubulin gene of *Epichloë typhina* from perennial ryegrass (*Lolium perenne*). Curr Genet **18,** 347-354.

Calcagno, A.M., Bignell, E., Rogers, T.R., Canedo, M., Muhlschlegel, F.A., and Haynes, K. (2004). *Candida glabrata* Ste20 is involved in maintaining cell wall integrity and adaptation to hypertonic stress, and is required for wild-type levels of virulence. Yeast **21,** 557-568.

Campa, A. (1991). Biological roles of plant peroxidases: known and potential function. (Boca Raton: CRC Press).

Casimiro, I., Marchant, A., Bhalerao, R.P., Beeckman, T., Dhooge, S., Swarup, R., Graham, N., Inzé, D., Sandberg, G., Casero, P.J., and Bennett, M. (2001). Auxin transport promotes Arabidopsis lateral root initiation. Plant Cell **13,** 843-852.

Chapman, G.P. (1996). The biology of grasses. (Oxon: CAB International).

Chen, S.X., and Schopfer, P. (1999). Hydroxyl-radical production in physiological reactions. A novel function of peroxidase. Eur J Biochem **260,** 726-735.

Chong, C., Tan, L., Lim, L., and Manser, E. (2001). The mechanism of PAK activation. Autophosphorylation events in both regulatory and kinase domains control activity. J Biol Chem **276,** 17347-17353.

Choquer, M., Fournier, E., Kunz, C., Levis, C., Pradier, J.M., Simon, A., and Viaud, M. (2007). *Botrytis cinerea* virulence factors: new insights into a necrotrophic and polyphageous pathogen. FEMS Microbiol Lett **277,** 1-10.

Christensen, M.J., Bennett, R.J., and Schmid, J. (2002). Growth of *Epichloë/Neotyphodium* and p-endophytes in leaves of *Lolium* and *Festuca* grasses. Mycol Res **106,** 93-106.

Christensen, M.J., Ball, O.J.-P., Bennett, R.J., and Schardl, C.L. (1997). Fungal and host genotype effects on compatibility and vascular colonization by *Epichloë festucae*. Mycol Res **101,** 493-501.

Christensen, M.J., Bennett, R.J., Ansari, H.A., Koga, H., Johnson, R.D., Bryan, G.T., Simpson, W.R., Koolaard, J.P., Nickless, E.M., and Voisey, C.R. (2008). *Epichloë* endophytes grow by intercalary hyphal extension in elongating grass leaves. Fungal Genet Biol **45,** 84-93.

Coates, P.J., and Hall, P.A. (2003). The yeast two-hybrid system for identifying protein-protein interactions. J Pathol **199,** 4-7.

Cooper, J.E. (2007). Early interactions between legumes and rhizobia: disclosing complexity in a molecular dialogue. J Appl Microbiol **103,** 1355-13565.

Cvrcková, F., De Virgilio, C., Manser, E., Pringle, J.R., and Nasmyth, K. (1995). Ste20-like protein kinases are required for normal localization of cell growth and for cytokinesis in budding yeast. Genes Dev **9,** 1817-1830.

Daga, R.R., Bolaños, P., and Moreno, S. (2003). Regulated mRNA stability of the Cdk inhibitor Rum1 links nutrient status to cell cycle progression. Curr Biol **13,** 2015-2024.

Dancis, A., Roman, D.G., Anderson, G.J., Hinnebusch, A.G., and Klausner, R.D. (1992). Ferric reductase of *Saccharomyces cerevisiae*: molecular characterization, role in iron uptake, and transcriptional control by iron. Proc Natl Acad Sci USA **89,** 3869-3873.

Dang, P.M., Morel, F., Gougerot-Pocidalo, M.A., and Benna, J.E. (2003). Phosphorylation of the NADPH oxidase component p67(PHOX) by ERK2 and P38MAPK: selectivity of phosphorylated sites and existence of an intramolecular regulatory domain in the tetratricopeptide-rich region. Biochemistry **42,** 4520-4526.

Daniels, R.H., and Bokoch, G.M. (1999). p21-activated protein kinase: a crucial component of morphological signaling? Trends Biochem Sci **24,** 350-355.

Dean, R.A., Talbot, N.J., Ebbole, D.J., Farman, M.L., Mitchell, T.K., Orbach, M.J., Thon, M., Kulkarni, R., Xu, J.R., Pan, H., Read, N.D., Lee, Y.H., Carbone, I., Brown, D., Oh, Y.Y., Donofrio, N., Jeong, J.S., Soanes, D.M., Djonovic, S., Kolomiets, E., Rehmeyer, C., Li, W., Harding, M., Kim, S., Lebrun, M.H., Bohnert, H., Coughlan, S., Butler, J., Calvo, S., Ma, L.J., Nicol, R., Purcell, S., Nusbaum, C., Galagan, J.E., and Birren, B.W. (2005). The genome sequence of the rice blast fungus *Magnaporthe grisea*. Nature **434,** 980-986.

Degols, G., Shiozaki, K., and Russell, P. (1996). Activation and regulation of the Spc1 stress-activated protein kinase in *Schizosaccharomyces pombe*. Mol Cell Biol **16,** 2870-2877.

Delgado-Jarana, J., Sousa, S., González, F., Rey, M., and Llobell, A. (2006). ThHog1 controls the hyperosmotic stress response in *Trichoderma harzianum*. Microbiology **152,** 1687-1700.

DerMardirossian, C., and Bokoch, G.M. (2005). GDIs: central regulatory molecules in Rho GTPase activation. Trends Cell Biol **15,** 356-363.

DerMardirossian, C., Schnelzer, A., and Bokoch, G.M. (2004). Phosphorylation of RhoGDI by Pak1 mediates dissociation of Rac GTPase. Mol Cell **15,** 117-127.

Dhindsa, R.S., Plumb-Dhindsa, P., and Thorpe, T.A. (1981). Leaf senescence: correlated with increased levels of membrane permeability and lipid peroxidation, and decreased levels of superoxide dismutase and catalase. J Exp Bot **32,** 93-101.

Dixon, K.P., Xu, J.R., Smirnoff, N., and Talbot, N.J. (1999). Independent signaling pathways regulate cellular turgor during hyperosmotic stress and appressorium-mediated plant infection by *Magnaporthe grisea*. Plant Cell **11,** 2045-2058.

Dong, Z., Canny, M.J., McCully, M.E., Roboredo, M.R., Cabadilla, C.F., Ortega, E., and Rodés, R. (1994). A Nitrogen-Fixing Endophyte of Sugarcane Stems (A New Role for the Apoplast). Plant Physiol **105,** 1139-1147.

Dower, W.J., Miller, J.F., and Ragsdale, C.W. (1988). High efficiency transformation of *E. coli* by high voltage electroporation. Nucleic Acids Res **16,** 6127-6145.

Dransart, E., Olofsson, B., and Cherfils, J. (2005). RhoGDIs revisited: novel roles in Rho regulation. Traffic **6,** 957-966.

Eaton, C.J. (2005). Cloning and functional analysis of a stress-activated protein kinase (SAPK) in *Epichloë festucae*. In Institute of Molecular BioSciences. Palmerston North: Massey University.

Eaton, C.J., Jourdain, I., Foster, S.J., Hyams, J.S., and Scott, B. (2008). Functional analysis of a fungal endophyte stress-activated MAP kinase. Curr Genet **53,** 163-174.

Eby, J.J., Holly, S.P., van Drogen, F., Grishin, A.V., Peter, M., Drubin, D.G., and Blumer, K.J. (1998). Actin cytoskeleton organization regulated by the PAK family of protein kinases. Curr Biol **8,** 967-970.

Egan, M.J., Wang, Z.Y., Jones, M.A., Smirnoff, N., and Talbot, N.J. (2007). Generation of reactive oxygen species by fungal NADPH oxidases is required for rice blast disease. Proc Natl Acad Sci USA **104,** 11772-11777.

El Benna, J., Faust, R.P., Johnson, J.L., and Babior, B.M. (1996). Phosphorylation of the respiratory burst oxidase subunit p47phox as determined by two-dimensional phosphopeptide mapping. Phosphorylation by protein kinase C, protein kinase A, and a mitogen-activated protein kinase. J Biol Chem **271,** 6374-6378.

El-Benna, J., Dang, P.M., and Gougerot-Pocidalo, M.A. (2008). Priming of the neutrophil NADPH oxidase activation: role of p47phox phosphorylation and NOX2 mobilization to the plasma membrane. Semin Immunopathol **30,** 279-289.

Elliott, M.C. (1977). Auxins and the regulation of root growth. In Plant growth regulation, P.E. Pilet, ed (Berlin: Springer-Verlag.

Fischer, E.H., Charbonneau, H., and Tonks, N.K. (1991). Protein tyrosine phosphatases: a diverse family of intracellular and transmembrane enzymes. Science **253,** 401-406.

Fleetwood, D.J., Scott, B., Lane, G.A., Tanaka, A., and Johnson, R.D. (2007). A complex ergovaline gene cluster in epichloë endophytes of grasses. Appl Environ Microbiol **73,** 2571-2579.

Fossen, T., Slimestad, R., Øvstedal, D.O., and Andersen, Ø.M. (2002). Anthocyanins of grasses. Biochem Syst Ecol **30,** 855-864.

Gaits, F., Degols, G., Shiozaki, K., and Russell, P. (1998). Phosphorylation and association with the transcription factor Atf1 regulate localization of Spc1/Sty1 stress-activated kinase in fission yeast. Genes Dev **12,** 1464-1473.

Gallagher, R.T., Hawkes, A.D., Steyn, P.S., and Vleggaar, R. (1984). Tremorgenic neurotoxins from perennial ryegrass causing ryegrass staggers disorder of livestock: Structure elucidation of lolitrem B. J Chem Soc Chem Comm **1984,** 614-616.

Gehmann, K., Nyfeler, R., Leadbeater, A.J., Nevill, D., and Sozzi, D. (1990). CGA 173506: a new phenylpyrrole fungicide for broad-spectrum disease control. Brighton Crop Prot Conf Pests Dis **2,** 399-406.

Giesbert, S., Schürg, T., Scheele, S., and Tudzynski, P. (2008). The NADPH oxidase Cpnox1 is required for full pathogenicity of the ergot fungus *Claviceps purpurea*. Mol Plant Pathol **9,** 317-327.

Gietz, R.D., and Woods, R.A. (2002). Transformation of yeast by lithium acetate/single-stranded carrier DNA/polyethylene glycol method. Methods Enzymol **350,** 87-96.

Glenn, A.E., Bacon, C.W., Price, R., and Hanlin, R.T. (1996). Molecular phylogeny of *Acremonium* and its taxonomic implications. Mycologia **88,** 369-383.

Goehring, A.S., Mitchell, D.A., Tong, A.H., Keniry, M.E., Boone, C., and Sprague, G.F., Jr. (2003). Synthetic lethal analysis implicates Ste20p, a p21-activated potein kinase, in polarisome activation. Mol Biol Cell **14,** 1501-1516.

Groemping, Y., and Rittinger, K. (2005). Activation and assembly of the NADPH oxidase: a structural perspective. Biochem J **386,** 401-416.

Gustin, M.C., Albertyn, J., Alexander, M., and Davenport, K. (1998). MAP kinase pathways in the yeast *Saccharomyces cerevisiae*. Microbiol Mol Biol Rev **62,** 1264-1300.

Hahn, H., McManus, M.T., Warnstorff, K., Monahan, B.J., Young, C.A., Davies, E., Tapper, B.A., and Scott, B. (2008). *Neotyphodium* fungal endophytes

confer physiological protection to perennial ryegrass (*Lolium perenne* L.) subjected to a water deficit. Environ Exp Bot **63,** 183-199.

Hamer, L., Pan, H., Adachi, K., Orbach, M.J., Page, A., Ramamurthy, L., and Woessner, J.P. (2001). Regions of microsynteny in *Magnaporthe grisea* and *Neurospora crassa*. Fungal Genet Biol **33,** 137-143.

Han, C.H., Freeman, J.L., Lee, T., Motalebi, S.A., and Lambeth, J.D. (1998). Regulation of the neutrophil respiratory burst oxidase. Identification of an activation domain in p67(phox). J Biol Chem **273,** 16663-16668.

Han, K.H., and Prade, R.A. (2002). Osmotic stress-coupled maintenance of polar growth in *Aspergillus nidulans*. Mol Microbiol **43,** 1065-1078.

Hanks, S.K., and Hunter, T. (1995). Protein kinases 6. The eukaryotic protein kinase superfamily: kinase (catalytic) domain structure and classification. FASEB J **9,** 576-596.

Harris, S.D., and Momany, M. (2004). Polarity in filamentous fungi: moving beyond the yeast paradigm. Fungal Genet Biol **41,** 391-400.

Hitch, P.A., and Sharman, B.C. (1971). The vascular pattern of festucoid grass axes, with particular reference to nodal plexi. Bot Gaz **132,** 38-56.

Hofmann, C., Shepelev, M., and Chernoff, J. (2004). The genetics of Pak. J Cell Sci **117,** 4343-4354.

Igbaria, A., Lev, S., Rose, M.S., Lee, B.N., Hadar, R., Degani, O., and Horwitz, B.A. (2008). Distinct and combined roles of the MAP kinases of *Cochliobolus heterostrophus* in virulence and stress responses. Mol Plant Microbe Interact **21,** 769-780.

Irmler, S., Rogniaux, H., Hess, D., and Pillonel, C. (2006). Induction of OS-2 phosphorylation in *Neurospora crassa* by treatment with phenylpyrrole fungicides and osmotic stress. Pestic Biochem Phys **84,** 25-37.

Itoh, Y., Johnson, R., and Scott, B. (1994). Integrative transformation of the mycotoxin-producing fungus, *Penicillium paxilli*. Curr Genet **25,** 508-513.

Jamet-Vierny, C., Debuchy, R., Prigent, M., and Silar, P. (2007). IDC1, a pezizomycotina-specific gene that belongs to the PaMpk1 MAP kinase transduction cascade of the filamentous fungus *Podospora anserina*. Fungal Genet Biol **44,** 1219-1230.

Jespers, A.B.K., and De Waard, M.A. (1995). Effect of fenpiclonil on phosphorylation of glucose in *Fusarium sulphureum*. Pestic Sci **44,** 167-175.

Jespers, A.B.K., Davidse, L.C., and De Waard, M.A. (1993). Biochemical effects of the phenylpyrrole fungicide fenpiclonil in *Fusarium sulphureum* (Schlecht). Pestic Biochem Phys **45,** 116-129.

Kato, T., Jr., Okazaki, K., Murakami, H., Stettler, S., Fantes, P.A., and Okayama, H. (1996). Stress signal, mediated by a Hog1-like MAP kinase, controls sexual development in fission yeast. FEBS Lett **378,** 207-212.

Kaufman, P.B. (1959). Development of the shoot of *Oryza sativa* L. II. Leaf histogenesis. Phytomorphology **9,** 227-311.

Kawasaki, L., Sánchez, O., Shiozaki, K., and Aguirre, J. (2002). SakA MAP kinase is involved in stress signal transduction, sexual development and spore viability in *Aspergillus nidulans*. Mol Microbiol **45,** 1153-1163.

Kessler, A., and Baldwin, I.T. (2002). Plant responses to insect herbivory: the emerging molecular analysis. Annu Rev Plant Biol **53,** 299-328.

Kicka, S., and Silar, P. (2004). PaASK1, a mitogen-activated protein kinase kinase kinase that controls cell degeneration and cell differentiation in *Podospora anserina*. Genetics **166,** 1241-1252.

Kicka, S., Bonnet, C., Sobering, A.K., Ganesan, L.P., and Silar, P. (2006). A mitotically inheritable unit containing a MAP kinase module. Proc Natl Acad Sci USA **103,** 13445-13450.

Kobayashi, T., Abe, K., Asai, K., Gomi, K., Juvvadi, P.R., Kato, M., Kitamoto, K., Takeuchi, M., and Machida, M. (2007). Genomics of *Aspergillus oryzae*. Biosci Biotechnol Biochem **71,** 646-670.

Koch, E., and Slusarenko, A. (1990). Arabidopsis is susceptible to infection by a downy mildew fungus. Plant Cell **2,** 437-445.

Koga, H., Christensen, M.J., and Bennett, R.J. (1993). Incompatibility of some grass-Acremonium endophyte associations. Mycol Res **97,** 1237-1244.

Kojima, K., Bahn, Y.S., and Heitman, J. (2006). Calcineurin, Mpk1 and Hog1 MAPK pathways independently control fludioxonil antifungal sensitivity in *Cryptococcus neoformans*. Microbiology **152,** 591-604.

Kojima, K., Takano, Y., Yoshimi, A., Tanaka, C., Kikuchi, T., and Okuno, T. (2004). Fungicide activity through activation of a fungal signalling pathway. Mol Microbiol **53,** 1785-1796.

Kuldau, G.A., Tsai, H.-F., and Schardl, C.L. (1999). Genome sizes of *Epichloë* species and anamorphic hybrids. Mycologia **91,** 776-782.

Kulkarni, R.D., and Dean, R.A. (2004). Identification of proteins that interact with two regulators of appressorium development, adenylate cyclase and cAMP-dependent protein kinase A, in the rice blast fungus *Magnaporthe grisea*. Mol Genet Genomics **270,** 497-508.

Kuo, T.M., and Gardner, H.W. (2002). Lipid biotechnology. (Boca Raton: CRC Press).

Kupfer, D.M., Drabenstot, S.D., Buchanan, K.L., Lai, H., Zhu, H., Dyer, D.W., Roe, B.A., and Murphy, J.W. (2004). Introns and splicing elements of five diverse fungi. Eukaryot Cell **3,** 1088-1100.

Lambeth, J.D. (2004). NOX enzymes and the biology of reactive oxygen. Nat Rev Immunol **4,** 181-189.

Langer, R.H.M. (1979). How grasses grow. (Southhampton: Edward Arnold Ltd).

Langford, C., Nellen, W., Niessing, J., and Gallwitz, D. (1983). Yeast is unable to excise foreign intervening sequences from hybrid gene transcripts. Proc Natl Acad Sci USA **80,** 1496-1500.

Lara-Ortíz, T., Riveros-Rosas, H., and Aguirre, J. (2003). Reactive oxygen species generated by microbial NADPH oxidase NoxA regulate sexual development in *Aspergillus nidulans*. Mol Microbiol **50,** 1241-1255.

Latch, G.C.M., and Christensen, M.J. (1985). Artificial infection of grasses with endophytes. Ann Appl Biol **107,** 17-24.

Laun, P., Pichova, A., Madeo, F., Fuchs, J., Ellinger, A., Kohlwein, S., Dawes, I., Fröhlich, K.U., and Breitenbach, M. (2001). Aged mother cells of *Saccharomyces cerevisiae* show markers of oxidative stress and apoptosis. Mol Microbiol **39,** 1166-1173.

Leberer, E., Wu, C., Leeuw, T., Fourest-Lieuvin, A., Segall, J.E., and Thomas, D.Y. (1997). Functional characterization of the Cdc42p binding domain of yeast Ste20p protein kinase. EMBO J **16,** 83-97.

Leeder, A.C., and Turner, G. (2008). Characterisation of *Aspergillus nidulans* polarisome component BemA. Fungal Genet Biol **45,** 897-911.

Lei, M., Lu, W., Meng, W., Parrini, M.C., Eck, M.J., Mayer, B.J., and Harrison, S.C. (2000). Structure of PAK1 in an autoinhibited conformation reveals a multistage activation switch. Cell **102,** 387-397.

Lemmon, M.A., Falasca, M., Schlessinger, J., and Ferguson, K. (1997). Regulatory recruitment of signalling molecules to the cell membrane by pleckstrin homology domains. Trends Cell Biol **7,** 237-242.

León, J., Rojo, E., and Sánchez-Serrano, J.J. (2001). Wound signalling in plants. J Exp Bot **52,** 1-9.

Leveleki, L., Mahlert, M., Sandrock, B., and Bölker, M. (2004). The PAK family kinase Cla4 is required for budding and morphogenesis in *Ustilago maydis*. Mol Microbiol **54,** 396-406.

Li, L., Xue, C., Bruno, K., Nishimura, M., and Xu, J.R. (2004). Two PAK kinase genes, CHM1 and MST20, have distinct functions in *Magnaporthe grisea*. Mol Plant Microbe Interact **17,** 547-556.

Lin, Q., Fuji, R.N., Yang, W., and Cerione, R.A. (2003). RhoGDI is required for Cdc42-mediated cellular transformation. Curr Biol **13,** 1469-1479.

Liszkay, A., van der Zalm, E., and Schopfer, P. (2004). Production of reactive oxygen intermediates ($O_2^{\cdot-}$, H_2O_2, and $^{\cdot}OH$) by maize roots and their role in wall loosening and elongation growth. Plant Physiol **136,** 3114-3123.

Liu, W., Leroux, P., and Fillinger, S. (2008). The HOG1-like MAP kinase Sak1 of *Botrytis cinerea* is negatively regulated by the upstream histidine kinase Bos1 and is not involved in dicarboximide- and phenylpyrrole-resistance. Fungal Genet Biol **45,** 1062-1074.

Maeda, H., and Ishida, N. (1967). Specificity of binding of hexopyranosyl polysaccharides with fluorescent brightener. J Biochem **62,** 276-278.

Malagnac, F., Lalucque, H., Lepère, G., and Silar, P. (2004). Two NADPH oxidase isoforms are required for sexual reproduction and ascospore germination in the filamentous fungus *Podospora anserina*. Fungal Genet Biol **41,** 982-997.

Malinowski, D.P., and Belesky, D.P. (1999). *Neotyphodium coenophialum*-endophyte infection affects the ability of tall fescue to use sparingly available phosphorus. J Plant Nutr **222,** 835-853.

Manser, E., Leung, T., Salihuddin, H., Zhao, Z.S., and Lim, L. (1994). A brain serine/threonine protein kinase activated by Cdc42 and Rac1. Nature **367,** 40-46.

Marcus, S., Polverino, A., Chang, E., Robbins, D., Cobb, M.H., and Wigler, M.H. (1995). Shk1, a homolog of the *Saccharomyces cerevisiae* Ste20 and mammalian p65PAK protein kinases, is a component of a Ras/Cdc42 signaling

module in the fission yeast *Schizosaccharomyces pombe*. Proc Natl Acad Sci USA **92,** 6180-6184.

Martin, H., Mendoza, A., Rodríguez-Pachón, J.M., Molina, M., and Nombela, C. (1997). Characterization of SKM1, a *Saccharomyces cerevisiae* gene encoding a novel Ste20/PAK-like protein kinase. Mol Microbiol **23,** 431-444.

Martyn, K.D., Kim, M.J., Quinn, M.T., Dinauer, M.C., and Knaus, U.G. (2005). p21-activated kinase (Pak) regulates NADPH oxidase activation in human neutrophils. Blood **106,** 3962-3969.

McSteen, P. (2009). Hormonal regulation of branching in grasses. Plant Physiol **149,** 46-55.

Mehrabi, R., Zwiers, L.H., de Waard, M.A., and Kema, G.H. (2006). MgHog1 regulates dimorphism and pathogenicity in the fungal wheat pathogen *Mycosphaerella graminicola*. Mol Plant Microbe Interact **19,** 1262-1269.

Menotta, M., Amicucci, A., Basili, G., Polidori, E., Stocchi, V., and Rivero, F. (2008). Molecular and functional characterization of a Rho GDP dissociation inhibitor in the filamentous fungus *Tuber borchii*. BMC Microbiol **8,** 57.

Millar, J.B., Buck, V., and Wilkinson, M.G. (1995). Pyp1 and Pyp2 PTPases dephosphorylate an osmosensing MAP kinase controlling cell size at division in fission yeast. Genes Dev **9,** 2117-2130.

Miller, J. (1972). Experiments in molecular genetics. Cold Spring Harbor Laboratory Press, New York.

Miskei, M., Karányi, Z., and Pócsi, I. (2009). Annotation of stress-response proteins in the aspergilli. Fungal Genet Biol **46 Suppl 1,** S105-120.

Moreland, C.F., and Flint, L.H. (1942). The development of vascular connections in the leaf sheath of sugar cane. Am J Bot **29,** 360-362.

Moriwaki, A., Kubo, E., Arase, S., and Kihara, J. (2006). Disruption of *SRM1*, a mitogen-activated protein kinase gene, affects sensitivity to osmotic and ultraviolet stressors in the phytopathogenic fungus *Bipolaris oryzae*. FEMS Microbiol Lett **257,** 253-261.

Morrow, C.A., and Fraser, J.A. (2009). Sexual reproduction and dimorphism in the pathogenic basidiomycetes. FEMS Yeast Res **9,** 161-177.

Morton, C.J., and Campbell, I.D. (1994). SH3 domains. Molecular 'Velcro'. Curr Biol **4,** 615-617.

Moy, M., Belanger, F., Duncan, R., Freehoff, A., Leary, C., Meyer, W., Sullivan, R., and White, J.F. (2000). Identification of epiphyllous mycelial nets on leaves of grasses infected by clavicipitaceous endophytes. Symbiosis **28,** 291-302.

Munro, C.A., Selvaggini, S., de Bruijn, I., Walker, L., Lenardon, M.D., Gerssen, B., Milne, S., Brown, A.J., and Gow, N.A. (2007). The PKC, HOG and Ca2+ signalling pathways co-ordinately regulate chitin synthesis in *Candida albicans*. Mol Microbiol **63,** 1399-1413.

Mutoh, N., Nakagawa, C.W., and Yamada, K. (2002). Characterization of Cu, Zn-superoxide dismutase-deficient mutant of fission yeast *Schizosaccharomyces pombe*. Curr Genet **41,** 82-88.

Namiki, F., Matsunaga, M., Okuda, M., Inoue, I., Nishi, K., Fujita, Y., and Tsuge, T. (2001). Mutation of an arginine biosynthesis gene causes reduced pathogenicity in *Fusarium oxysporum* f. sp. *melonis*. Mol Plant Microbe Interact **14,** 580-584.

Nestelbacher, R., Laun, P., Vondráková, D., Pichová, A., Schüller, C., and Breitenbach, M. (2000). The influence of oxygen toxicity on yeast mother cell-specific aging. Exp Gerontol **35,** 63-70.

Neto, G.C., Kono, Y., Hyakutake, H., Watanabe, M., Suzuki, Y., and Sakurai, A. (1991). Isolation and indentification of (-)-jasmonic acid from wild rice, *Oryza officinalis*, as an antifungal substance. Agric Biol Chem **55,** 3097-3098.

Nevill, D., Nyfeler, R., and Sozzi, D. (1988). CGA142705: a novel fungicide for seed treatment. Proc Brighton Crop Prot Conf Pests Dis **1,** 65-72.

Nichols, C.B., Fraser, J.A., and Heitman, J. (2004). PAK kinases Ste20 and Pak1 govern cell polarity at different stages of mating in *Cryptococcus neoformans*. Mol Biol Cell **15,** 4476-4489.

Noguchi, R., Banno, S., Ichikawa, R., Fukumori, F., Ichiishi, A., Kimura, M., Yamaguchi, I., and Fujimura, M. (2007). Identification of OS-2 MAP kinase-dependent genes induced in response to osmotic stress, antifungal agent fludioxonil, and heat shock in *Neurospora crassa*. Fungal Genet Biol **44,** 208-218.

Ono, Y., Fujii, T., Igarashi, K., Kuno, T., Tanaka, C., Kikkawa, U., and Nishizuka, Y. (1989). Phorbol ester binding to protein kinase C requires a cysteine-rich zinc-finger-like sequence. Proc Natl Acad Sci USA **86,** 4868-4871.

Orozco-Cardenas, M., and Ryan, C.A. (1999). Hydrogen peroxide is generated systemically in plant leaves by wounding and systemin via the octadecanoid pathway. Proc Natl Acad Sci USA **96,** 6553-6557.

Park, S.M., Choi, E.S., Kim, M.J., Cha, B.J., Yang, M.S., and Kim, D.H. (2004). Characterization of HOG1 homologue, CpMK1, from *Cryphonectria parasitica* and evidence for hypovirus-mediated perturbation of its phosphorylation in response to hypertonic stress. Mol Microbiol **51,** 1267-1277.

Parker, P.J., and Parkinson, S.J. (2001). AGC protein kinase phosphorylation and protein kinase C. Biochem Soc Trans **29,** 860-863.

Parniske, M. (2008). Arbuscular mycorrhiza: the mother of plant root endosymbioses. Nat Rev Microbiol **6,** 763-775.

Peters, C., Baars, T.L., Buhler, S., and Mayer, A. (2004). Mutual control of membrane fission and fusion proteins. Cell **119,** 667-678.

Ponting, C.P., and Benjamin, D.R. (1996). A novel family of Ras-binding domains. Trends Biochem Sci **21,** 422-425.

Punt, P.J., Oliver, R.P., Dingemanse, M.A., Pouwels, P.H., and van den Hondel, C.A. (1987). Transformation of *Aspergillus* based on the hygromycin B resistance marker from *Escherichia coli*. Gene **56,** 117-124.

Qyang, Y., Yang, P., Du, H., Lai, H., Kim, H., and Marcus, S. (2002). The p21-activated kinase, Shk1, is required for proper regulation of microtubule dynamics in the fission yeast, *Schizosaccharomyces pombe*. Mol Microbiol **44,** 325-334.

R Development Core Team. (2009). R: A language and environment for statistical computing. R Foundation for Statistical Computing, Vienna, Austria.

Rakwal, R., Hasegawa, M., and Kodama, O. (1996). A methyltransferase for synthesis of the flavanone phytoalexin sakuranetin in rice leaves. Biochem Biophys Res Commun **222,** 732-735.

Ram, A.F., Arentshorst, M., Damveld, R.A., vanKuyk, P.A., Klis, F.M., and van den Hondel, C.A. (2004). The cell wall stress response in *Aspergillus niger* involves increased expression of the glutamine : fructose-6-phosphate amidotransferase-encoding gene (*gfaA*) and increased deposition of chitin in the cell wall. Microbiology **150,** 3315-3326.

Regier, D.S., Greene, D.G., Sergeant, S., Jesaitis, A.J., and McPhail, L.C. (2000). Phosphorylation of p22phox is mediated by phospholipase D-dependent and -

independent mechanisms. Correlation of NADPH oxidase activity and p22phox phosphorylation. J Biol Chem **275,** 28406-28412.

Reyes, G., Romans, A., Nguyen, C.K., and May, G.S. (2006). Novel mitogen-activated protein kinase MpkC of *Aspergillus fumigatus* is required for utilization of polyalcohol sugars. Eukaryot Cell **5,** 1934-1940.

Rispail, N., Soanes, D.M., Ant, C., Czajkowski, R., Grünler, A., Huguet, R., Perez-Nadales, E., Poli, A., Sartorel, E., Valiante, V., Yang, M., Beffa, R., Brakhage, A.A., Gow, N.A., Kahmann, R., Lebrun, M., Lenasi, H., Perez-Martin, J., Talbot, N.J., Wendland, J., and Di Pietro, A. (2009). Comparative genomics of MAP kinase and calcium-calcineurin signalling components in plant and human pathogenic fungi. Fungal Genet Biol **46,** 287-298.

Rodriguez, R., and Redman, R. (2005). Balancing the generation and elimination of reactive oxygen species. Proc Natl Acad Sci USA **102,** 3175-3176.

Rolke, Y., and Tudzynski, P. (2008). The small GTPase Rac and the p21-activated kinase Cla4 in *Claviceps purpurea*: interaction and impact on polarity, development and pathogenicity. Mol Microbiol **68,** 405-423.

Roman, D.G., Dancis, A., Anderson, G.J., and Klausner, R.D. (1993). The fission yeast ferric reductase gene *frp1+* is required for ferric iron uptake and encodes a protein that is homologous to the gp91-phox subunit of the human NADPH phagocyte oxidoreductase. Mol Cell Biol **13,** 4342-4350.

Román, E., Arana, D.M., Nombela, C., Alonso-Monge, R., and Pla, J. (2007). MAP kinase pathways as regulators of fungal virulence. Trends Microbiol **15,** 181-190.

Sakaguchi, J., and Fukuda, H. (2008). Cell differentiation in the longitudinal veins and formation of commissural veins in rice (*Oryza sativa*) and maize (*Zea mays*). J Plant Res **121,** 593-602.

Sattelmacher, B. (2001). The apoplast and its significance for plant mineral nutrition. New Phytol **149,** 167-192.

Scarpella, E., and Meijer, A.H. (2004). Pattern formation in the vascular system of monocot and dicot plant species New Phytol **164,** 209-242.

Scarpella, E., Marcos, D., Friml, J., and Berleth, T. (2006). Control of leaf vascular patterning by polar auxin transport. Genes Dev **20,** 1015-1027.

Schardl, C.L. (2001). *Epichloë festucae* and related mutualistic symbionts of grasses. Fungal Genet Biol **33,** 69-82.

Schardl, C.L., Leuchtmann, A., and Spiering, M.J. (2004). Symbioses of grasses with seedborne fungal endophytes. Annu Rev Plant Biol **55,** 315-340.

Schardl, C.L., Craven, K.D., Speakman, S., Stromberg, A., Lindstrom, A., and Yoshida, R. (2008). A novel test for host-symbiont codivergence indicates ancient origin of fungal endophytes in grasses. Syst Biol **57,** 483-498.

Schilmiller, A.L., and Howe, G.A. (2005). Systemic signaling in the wound response. Curr Opin Plant Biol **8,** 369-377.

Schopfer, P. (2001). Hydroxyl radical-induced cell-wall loosening in vitro and in vivo: implications for the control of elongation growth. Plant J **28,** 679-688.

Schopfer, P., Liszkay, A., Bechtold, M., Frahry, G., and Wagner, A. (2002). Evidence that hydroxyl radicals mediate auxin-induced extension growth. Planta **214,** 821-828.

Schultz, J., Ponting, C.P., Hofmann, K., and Bork, P. (1997). SAM as a protein interaction domain involved in developmental regulation. Protein Sci **6,** 249-253.

Schweizer, P., Gees, R., and Mösinger, E. (1993). Effect of Jasmonic Acid on the Interaction of Barley (*Hordeum vulgare* L.) with the Powdery Mildew *Erysiphe graminis* f.sp. *hordei*. Plant Physiol **102,** 503-511.

Scott, B., and Eaton, C.J. (2008). Role of reactive oxygen species in fungal cellular differentiations. Curr Opin Microbiol **11,** 488-493.

Scott, B., Takemoto, D., Tanaka, A., Young, C.A., Bryant, M.K., and May, K.J. (2007). Functional analysis of the *Epichloë festucae*-perennial ryegrass symbiosis. In 6th International Symposium on Fungal Endophytes of Grasses, A.J. Popay and E.R. Thom, eds (NZ Grassland Association), pp. 443-441.

Segmüller, N., Ellendorf, U., Tudzynski, B., and Tudzynski, P. (2007). BcSAK1, a stress-activated mitogen-activated protein kinase, is involved in vegetative differentiation and pathogenicity in *Botrytis cinerea*. Eukaryot Cell **6,** 211-221.

Segmüller, N., Kokkelink, L., Giesbert, S., Odinius, D., van Kan, J., and Tudzynski, P. (2008). NADPH oxidases are involved in differentiation and pathogenicity in *Botrytis cinerea*. Mol Plant Microbe Interact **21,** 808-819.

Sells, M.A., Barratt, J.T., Caviston, J., Ottilie, S., Leberer, E., and Chernoff, J. (1998). Characterization of Pak2p, a pleckstrin homology domain-containing, p21-activated protein kinase from fission yeast. J Biol Chem **273,** 18490-18498.

Semighini, C.P., and Harris, S.D. (2008). Regulation of apical dominance in *Aspergillus nidulans* hyphae by reactive oxygen species. Genetics **179,** 1919-1932.

Shatwell, K.P., Dancis, A., Cross, A.R., Klausner, R.D., and Segal, A.W. (1996). The FRE1 ferric reductase of *Saccharomyces cerevisiae* is a cytochrome b similar to that of NADPH oxidase. J Biol Chem **271,** 14240-14244.

Shiozaki, K., and Russell, P. (1995a). Counteractive roles of protein phosphatase 2C (PP2C) and a MAP kinase kinase homolog in the osmoregulation of fission yeast. EMBO J **14,** 492-502.

Shiozaki, K., and Russell, P. (1995b). Cell-cycle control linked to extracellular environment by MAP kinase pathway in fission yeast. Nature **378,** 739-743.

Shoji, J.Y., Arioka, M., and Kitamoto, K. (2006). Possible involvement of pleiomorphic vacuolar networks in nutrient recycling in filamentous fungi. Autophagy **2,** 226-227.

Silar, P., Haedens, V., Rossignol, M., and Lalucque, H. (1999). Propagation of a novel cytoplasmic, infectious and deleterious determinant is controlled by translational accuracy in *Podospora anserina*. Genetics **151,** 87-95.

Smith, D.G., Garcia-Pedrajas, M.D., Hong, W., Yu, Z., Gold, S.E., and Perlin, M.H. (2004). An ste20 homologue in *Ustilago maydis* plays a role in mating and pathogenicity. Eukaryot Cell **3,** 180-189.

Song, X., Xu, W., Zhang, A., Huang, G., Liang, X., Virbasius, J.V., Czech, M.P., and Zhou, G.W. (2001). Phox homology domains specifically bind phosphatidylinositol phosphates. Biochemistry **40,** 8940-8944.

Southern, E.M. (1975). Detection of specific sequences among DNA fragments separated by gel electrophoresis. J Mol Biol **98,** 503-517.

Spiering, M.J., Moon, C.D., Wilkinson, H.H., and Schardl, C.L. (2005). Gene clusters for insecticidal loline alkaloids in the grass-endophytic fungus *Neotyphodium uncinatum*. Genetics **169,** 1403-1414.

Spiers, A.G., and Hopcroft, D.H. (1993). Black canker and leaf spot of *Salix* in New Zealand caused by *Glomerella miyabeana* (*Colletotrichum gloeosporioides*). Eur J Forest Pathol **23,** 92-102.

Steyn, W.J., Wand, S.J.E., Holcroft, D.M., and Jacobs, G. (2002). Anthocyanins in vegetative tissues: a proposed function in photoprotection. New Phytol **155,** 349-361.

Sumimoto, H., Miyano, K., and Takeya, R. (2005). Molecular composition and regulation of the Nox family NAD(P)H oxidases. Biochem Biophys Res Commun **338,** 677-686.

Sumimoto, H., Sakamoto, N., Nozaki, M., Sakaki, Y., Takeshige, K., and Minakami, S. (1992). Cytochrome b558, a component of the phagocyte NADPH oxidase, is a flavoprotein. Biochem Biophys Res Commun **186,** 1368-1375.

Takeda, K., Iizuka, M., Watanabe, T., Nakagawa, J., Kawasaki, S., and Niimura, Y. (2007). *Synechocystis* DrgA protein functioning as nitroreductase and ferric reductase is capable of catalyzing the Fenton reaction. Febs J **274,** 1318-1327.

Takemoto, D., Tanaka, A., and Scott, B. (2006). A p67Phox-like regulator is recruited to control hyphal branching in a fungal-grass mutualistic symbiosis. Plant Cell **18,** 2807-2821.

Takemoto, D., Tanaka, A., and Scott, B. (2007). NADPH oxidases in fungi: diverse roles of reactive oxygen species in fungal cellular differentiation. Fungal Genet Biol **44,** 1065-1076.

Tan, Y.Y., Spiering, M.J., Christensen, M.J., Saunders, K., and Schmid, J. (1997). *In planta* metabolic state of *Neotyphodium* mycelium assessed through use of the Gus reporter gene in combination with hyphal enumeration. In *Neotyphodium*/Grass Interactions C.W. Bacon and N.S. Hill, eds (New York: Plenum Press), pp. 85-87.

Tan, Y.Y., Spiering, M.J., Scott, V., Lane, G.A., Christensen, M.J., and Schmid, J. (2001). *In planta* regulation of extension of an endophytic fungus and maintenance of high metabolic rates in its mycelium in the absence of apical extension. Appl Environ Microbiol **67,** 5377-5383.

Tanaka, A., Tapper, B.A., Popay, A., Parker, E.J., and Scott, B. (2005). A symbiosis expressed non-ribosomal peptide synthetase from a mutualistic fungal endophyte of perennial ryegrass confers protection to the symbiotum from insect herbivory. Mol Microbiol **57,** 1036-1050.

Tanaka, A., Christensen, M.J., Takemoto, D., Park, P., and Scott, B. (2006). Reactive oxygen species play a role in regulating a fungus-perennial ryegrass mutualistic interaction. Plant Cell **18,** 1052-1066.

Tanaka, A., Takemoto, D., Hyon, G.S., Park, P., and Scott, B. (2008a). NoxA activation by the small GTPase RacA is required to maintain a mutualistic

symbiotic association between *Epichloë festucae* and perennial ryegrass. Mol Microbiol **68,** 1165-1178.

Tanaka, Y., Sasaki, N., and Ohmiya, A. (2008b). Biosynthesis of plant pigments: anthocyanins, betalains and carotenoids. Plant J **54,** 733-749.

Temple, M.D., Perrone, G.G., and Dawes, I.W. (2005). Complex cellular responses to reactive oxygen species. Trends Cell Biol **15,** 319-326.

Tiedje, C., Sakwa, I., Just, U., and Höfken, T. (2008). The Rho GDI Rdi1 regulates Rho GTPases by distinct mechanisms. Mol Biol Cell **19,** 2885-2896.

Vieira, J., and Messing, J. (1987). Production of single-stranded plasmid DNA. Methods Enzymol **153,** 3-11.

Vignais, P.V. (2002). The superoxide-generating NADPH oxidase: structural aspects and activation mechanism. Cell Mol Life Sci **59,** 1428-1459.

Vitalini, M.W., de Paula, R.M., Goldsmith, C.S., Jones, C.A., Borkovich, K.A., and Bell-Pedersen, D. (2007). Circadian rhythmicity mediated by temporal regulation of the activity of p38 MAPK. Proc Natl Acad Sci USA **104,** 18223-18228.

Wang, P., Nichols, C.B., Lengeler, K.B., Cardenas, M.E., Cox, G.M., Perfect, J.R., and Heitman, J. (2002). Mating-type-specific and nonspecific PAK kinases play shared and divergent roles in *Cryptococcus neoformans*. Eukaryot Cell **1,** 257-272.

Watanabe, H., Azuma, M., Igarashi, K., and Ooshima, H. (2005). Analysis of chitin at the hyphal tip of *Candida albicans* using calcofluor white. Biosci Biotechnol Biochem **69,** 1798-1801.

Watts, F., Castle, C., and Beggs, J. (1983). Aberrant splicing of *Drosophila* alcohol dehydrogenase transcripts in *Saccharomyces cerevisiae*. EMBO J **2,** 2085-2091.

Wawryn, J., Krzepilko, A., Myszka, A., and Bilinski, T. (1999). Deficiency in superoxide dismutases shortens life span of yeast cells. Acta Biochim Pol **46,** 249-253.

Westley, J. (1981). Thiosulfate: cyanide sulfurtransferase (rhodanese). Methods Enzymol **77,** 285-291.

Wilson, R.A., and Talbot, N.J. (2009). Under pressure: investigating the biology of plant infection by *Magnaporthe oryzae*. Nat Rev Microbiol **7,** 185-195.

Winters, M.J., and Pryciak, P.M. (2005). Interaction with the SH3 domain protein Bem1 regulates signaling by the *Saccharomyces cerevisiae* p21-activated kinase Ste20. Mol Cell Biol **25,** 2177-2190.

Wu, C., Leberer, E., Thomas, D.Y., and Whiteway, M. (1999). Functional characterization of the interaction of Ste50p with Ste11p MAPKKK in Saccharomyces cerevisiae. Mol Biol Cell **10,** 2425-2440.

Xu, J.R., and Hamer, J.E. (1996). MAP kinase and cAMP signaling regulate infection structure formation and pathogenic growth in the rice blast fungus *Magnaporthe grisea*. Genes Dev **10,** 2696-2706.

Xu, J.R., Staiger, C.J., and Hamer, J.E. (1998). Inactivation of the mitogen-activated protein kinase Mps1 from the rice blast fungus prevents penetration of host cells but allows activation of plant defense responses. Proc Natl Acad Sci USA **95,** 12713-12718.

Xue, T., Nguyen, C.K., Romans, A., and May, G.S. (2004). A mitogen-activated protein kinase that senses nitrogen regulates conidial germination and growth in *Aspergillus fumigatus*. Eukaryot Cell **3,** 557-560.

Yang, P., Kansra, S., Pimental, R.A., Gilbreth, M., and Marcus, S. (1998). Cloning and characterization of shk2, a gene encoding a novel p21-activated protein kinase from fission yeast. J Biol Chem **273,** 18481-18489.

Yoo, B.K., Choi, J.W., Shin, C.Y., Jeon, S.J., Park, S.J., Cheong, J.H., Han, S.Y., Ryu, J.R., Song, M.R., and Ko, K.H. (2008). Activation of p38 MAPK induced peroxynitrite generation in LPS plus IFN-gamma-stimulated rat primary astrocytes via activation of iNOS and NADPH oxidase. Neurochem Int **52,** 1188-1197.

Young, C.A., Bryant, M.K., Christensen, M.J., Tapper, B.A., Bryan, G.T., and Scott, B. (2005). Molecular cloning and genetic analysis of a symbiosis-expressed gene cluster for lolitrem biosynthesis from a mutualistic endophyte of perennial ryegrass. Mol Genet Genomics **274,** 13-29.

Young, C.A., Felitti, S., Shields, K., Spangenberg, G., Johnson, R.D., Bryan, G.T., Saikia, S., and Scott, B. (2006). A complex gene cluster for indole-diterpene biosynthesis in the grass endophyte *Neotyphodium lolii*. Fungal Genet Biol **43,** 679-693.

Zhang, Y., Lamm, R., Pillonel, C., Lam, S., and Xu, J.R. (2002). Osmoregulation and fungicide resistance: the *Neurospora crassa os-2* gene encodes a HOG1

mitogen-activated protein kinase homologue. Appl Environ Microbiol **68,** 532-538.